Sliding wear and fretting behaviour of electrodeposited γ-phase zinc-nickel coatings as a replacement for electrodeposited cadmium coatings

Lisa Lee

Department of Mining and Materials Engineering
McGill University, Montreal

A thesis submitted to McGill University in partial fulfilment of the requirements for the degree of Doctor of Philosophy

Contents

Abstract i

Résumé iii

Acknowledgements v

Preface vii

Chapter 1: Introduction

1.1 General background 1

1.2 Organization of Thesis 3

Chapter 2: Literature Review

2.1 Zn-Ni Coatings 6

2.2 Selected Review on Tribology 7

2.2.1 Friction and wear 7

2.2.2 Third body approach 8

2.2.3 Particle detachment mechanisms 9

2.2.4 Velocity accommodation mechanisms 11

2.2.5 Hertzian Contact 13

2.3 Fretting and reciprocating sliding 14

2.4 Tribology of Zn-Ni coatings 16

2.4.1 Effects of roughness in tribology of Zn-Ni 17

2.4.2 Effects of humidity in tribology of Zn-Ni 18

2.5 Tribology of Cd coatings 19

2.6 Summary 20

Chapter 3: **Experimental Techniques**

3.1 Material Characterization 21
  3.1.1 Microscopy 21
  3.1.2 Nanoindentation 22
  3.1.3 Raman spectroscopy 24
3.2 Fretting 24
  3.2.1 Test set-up 24
  3.2.2 Choosing test parameters 26
  3.2.3 Characterization 27
3.3 Sliding wear tests 28
  3.3.1 Test set-up 28
  3.3.2 Characterization 29
3.4 Material Properties 31

Chapter 4: **Fretting wear behavior of Zn-Ni alloy coatings**

Abstract 34
4.1 Introduction 35
4.2 Methods 36
  4.2.1 Coating deposition 36
  4.2.2 Characterization 37
  4.2.3 Fretting wear test 38
4.3 Results 39
  4.3.1 Coating characterization 39
  4.3.2 Fretting wear test 41
  4.3.3 Ex situ wear scar analysis 45

4.4 Discussion 52

4.5 Conclusion 53

Acknowledgments 54

Chapter 5: Comparison of fretting behavior of electrodeposited Zn-Ni and Cd coatings

Abstract 55

5.1 Introduction 55

5.2 Background information 56

5.3 Methods 60

- 5.3.1 Coating deposition 60
- 5.3.2 Characterization 61
- 5.3.3 Fretting wear test 61

5.4 Results 62

- 5.4.1 Coating characterization 62
- 5.4.2 Energy ratio 64
- 5.4.3 Ex situ wear scar analysis 68

5.5 Discussion 73

5.6 Conclusion 77

Acknowledgements 77

Chapter 6: The effect of contact stress on the sliding wear behaviour of Zn-Ni electrodeposited coatings

Abstract 78

6.1 Introduction 79

6.2 Methods 81

- 6.2.1 Coating Process 81
- 6.2.2 Characterization 81

6.2.3 Wear Test 82

6.3 Results 83

6.3.1 Characterization 83

6.3.2 Adhesion testing 85

6.3.3 Wear Test 87

6.3.4 Wear Rate 90

6.3.5 Chemical analysis of wear track 94

6.3.6 Counterface 98

6.4 Discussion 99

6.5 Conclusion 105

Acknowledgement 105

Chapter 7: Effects of humidity on the sliding wear properties of Zn-Ni alloy coatings

Abstract 106

7.1 Introduction 106

7.2 Methods 109

7.2.1 Coating Process 109

7.2.2 Characterization 109

7.2.3 Wear Tests 109

7.3 Results 111

7.3.1 Characterization 111

7.3.2 Wear Test 111

7.3.3 Wear Rate 116

7.3.4 Raman Spectroscopy 117

7.3.5 Transmission Electron Microscopy: Selective Area Electron Diffraction 119

7.4 Discussion 121

7.5 Conclusion 121

Acknowledgements 124

Chapter 8: Additional Discussion on Sliding Wear

8.1 Comparison of the effect on humidity on the sliding wear behaviour of B-ZnNi and cadmium coatings 125

8.1.1 Test Parameters 125

8.1.2 Comparison of the as-plated samples 126

8.1.3 Comparison of humidity effects 127

8.2 General discussion of the effects of humidity on Zn-Ni and cadmium coatings 130

Chapter 9: Synopsis

9.1 Summary and conclusions 132

9.2 Suggestion for future work 134

9.3 Contributions to original knowledge 135

References 137

Appendix A: Matlab code for calculation of energy ratio, friction and fretting log 154

Appendix B: Fretting logs 160

Appendix C: TEM SAED patterns 166

Abstract

Electrodeposited Zn-Ni coatings is used as a sacrificial corrosion protective coating for steel in the automotive industry. Recently, the aerospace industry has taken an interest in these coatings due to the increasing restrictions on cadmium. Many studies have been made on improving the plating process and corrosion properties of Zn-Ni coatings. Although these coatings encounter tribological situations, there is still an information gap on their tribological behaviour. Therefore, the tribological behaviour of Zn-Ni coatings are studied in terms of fretting and sliding wear in this work and are compared with cadmium.

Tribological studies of the fretting and sliding wear behaviour on Zn-Ni and Cd coatings were conducted. For Zn-Ni coating, studies showed that the surface morphology had a strong effect on the velocity accommodation mechanisms. In the stick or partial slip regime, the smoother and dense coating formed cracks on the surface in order to accommodate wear, whereas for the rougher coating, only asperities of the coating were deformed, as the morphology of the coating allowed some degree of elastic deformation. In the mixed slip and the gross slip regimes, shearing of the third bodies accommodated the velocity in both cases. When slipping occurred, the rougher coating also showed higher wear, as the morphology of the coating allowed easier detachment, as cracks and through thickness defects were present where the agglomerates of the coating meets. When compared with Cd coatings, the material properties affected the fretting behaviour strongly. Cadmium coating remained in the partial slip regime despite changing the displacement amplitude, due to the mechanical properties and crystal structure of cadmium. Plastic flow of the coating material accommodated the velocity for cadmium coating, as cadmium has a hexagonal crystal structure and is very ductile. Although cadmium remained in the stick and partial slip regime, increasing the displacement amplitude increased the friction and wear of the coating. When a high displacement amplitude was used, cadmium coating was removed from the center of the contact and the substrate was exposed.

Sliding wear studies of the effect of normal load, surface morphology and humidity for Zn-Ni coatings were conducted and the results were compared with Cd. Formation of an oxide layer appeared to have a strong effect on the sliding wear behaviour, the smoother and dense coating was subjected to test performed in various humidity conditions. At high humidity, a continuous nanocrystalline ZnO film was formed on the surface of the wear track, which helped mitigate wear and stabilize the friction. This is because velocity was accommodated through shearing of the nanocrystalline film. In contrast, at zero humidity level, a prow formed due to adhesive wear behaviour. Velocity was accommodated by ploughing of the wear track and shearing of the particles. When tests were performed in high humidity, increasing the normal load caused breaking of the oxide layer that was formed on the wear track, which resulted in more adhesive wear. At low normal loads, the rougher coating showed more wear than the smoother coating. At the highest normal load, the wear of the smoother coating became more severe as the lack of a continuous oxide film caused more adhesive wear. The rougher coating was less sensitive to increase of initial Hertzian contact stress, as the surface morphology of the coating allowed some degree of elastic and plastic deformation. When compared to Cd, humidity also affected the sliding wear behaviour of Cd due to change in the composition of the third bodies. Decreasing the humidity was beneficial to cadmium but detrimental to Zn-Ni. Due to material properties, a lower CoF was observed for cadmium, while a higher wear resistance was observed in Zn-Ni coating.

Résumé

Des revêtements de Zn-Ni déposés par électrolyse sont utilisés par l'industrie automobile en tant que revêtements sacrificiels pour l'acier. Récemment, l'industrie aérospatiale a manifesté un intérêt pour ces revêtements, car les restrictions deviennent plus en plus rigoureuses pour le Cd. La plupart des recherches examinant le Zn-Ni sont faites sur le procédé de placage et de corrosion. Tandis qu'il y a peu de recherche effectuée sur la tribologie de ces revêtements, bien qu'ils sont souvent assujettis à des situations de tribologie. Donc, la tribologie des revêtements de Zn-Ni et de Cd est comparée dans cette étude.

Des études de tribologie ont été menées sur le comportement d'usure par glissement et par fretting des revêtements de Zn-Ni et de Cd. Pour les études sur l'usure par fretting des revêtements de Zn-Ni, le mécanisme d'accommodation de vitesses était fortement influencé par la morphologie de la surface. Dans le régime d'adhérence, le Zn-Ni plus dense et lisse a formé des fissures pour accommoder la vitesse. Par contre, pour le Zn-Ni plus rugueux et poreux, les aspérités étaient déformées plastiquement. De plus, la morphologie du revêtement a permis un certain degré de déformation élastique. Dans le régime mixte ainsi que dans le régime de glissement, la vitesse était accommodée par le cisaillement du troisième corps dans les deux cas. Quand il y a eu du glissement dans le contact, le revêtement plus rugueux présentait une usure plus agressive, car des fissures et des défauts qui sont présentes où les agglomérés du revêtement se rencontrent permettaient le détachement du revêtement plus facile. Par contre, en comparaison avec les revêtements de Cd, les propriétés des matériaux ont influencé les caractéristiques d'usure par fretting. Malgré les changements de l'amplitude du déplacement, le Cd présente un comportement de glissement partiel à cause des propriétés mécaniques et de la structure cristalline du matériau. La vitesse était accommodée par l'écoulement plastique du revêtement de Cd, car le Cd a une structure cristalline hexagonale très ductile. Même si le comportement de contact avec le Cd reste dans le régime de glissement partiel, l’augmentation de l’amplitude de déplacement a augmenté la friction et l’usure du revêtement. Quand l’amplitude de déplacement était haute, le revêtement de Cd a été retiré du centre du contact exposant le substrat.

Des études sur l’usure par glissement ont été effectuées pour analyser l’effet de la force normale, la morphologie de la surface et l’humidité sur les revêtements de Zn-Ni. Les résultats sont comparés avec les revêtements de Cd. La formation d’une couche d’oxyde a fortement influencé le comportement de l’usure par glissement. Le revêtement de Zn-Ni plus dense et lisse a été sujet à différents niveaux d’humidité. Quand le niveau d’humidité était élevé, une couche continue nanocristalline de ZnO a été formée sur la surface de la trace. Cette couche a atténué l’usure et stabilisé la friction. La vitesse était accommodée par le cisaillement de la couche de ZnO nanocristalline. Par contre, quand le niveau d’humidité était presque zéro, l’usure adhésive a causé la formation d’un bourrelet. La vitesse était accommodée par la déformation plastique de la trace et le cisaillement des particules dans la trace. D’autres tests ont été effectués sur les niveaux d’humidité élevés, mais avec différentes forces normales. Quand la force normale était faible, les revêtements plus rugueux présentaient plus d’usure que les revêtements plus lisses. En revanche, quand la force normale était élevée, l’usure des revêtements plus lisses était plus agressive puisque la couche de ZnO cristalline continue est fracturée causante plus d’usure adhésive. Le revêtement plus rugueux était moins susceptible à l’effet d’augmentation de la force normale, car la morphologie de la surface a permis un certain degré de déformation élastique et plastique. En comparaison avec les revêtements de Cd, l’humidité avait aussi affecté le comportement d’usure par glissement en raison du changement de la composition du troisième corps. La réduction du niveau d’humidité était avantageuse pour le Cd, mais désavantageuse pour le Zn-Ni. La friction pour le Cd était plus basse que pour le Zn-Ni, lorsque le Zn-Ni avait une résistance d’usure plus haute.

Acknowledgements

First and foremost, I would like to thank my supervisor Prof. Richard Chromik for offering me the opportunity to work in this project, the point in which this journey began. For teaching and guiding me throughout the years, and providing endless support when I was lost, for which I am deeply grateful. Thank you for giving me the privilege to explore my ideas and learning from mistakes. Thank you for finding my shortcomings and guiding me to be better. His expertise and patience has made this a wonderful learning experience.

I must also give a heartfelt thank you to Dr. Sriraman Rajagopalan. He has helped and guided me throughout this project. Thank you for all the exchanges of ideas and teaching me how to use the equipment. Thank you for making sure I had what I needed throughout this journey, whether it was an idea, a skill or a sample. He has made this stay a much enjoyable one.

I would also like to give a special thanks to Dr. Sylvie Descartes for guiding and supporting me on my fretting wear tests at INSA. Thank you for making my stay at INSA enjoyable, for making my stay easy and for making sure I got home every night. Her expertise and kindness has made the stay fruitful and delightful.

I am also thankful to Dr. Salim Brahimi for managing and coordinating everything in the project. Thank you for arranging all the meetings with the industrial partners and exposing me to the industrial side of the project. Thank you for always keeping the big picture in mind. His expertise and industrial insight has provided invaluable dimension to the project.

I also thank my co-supervisor Prof. Stephen Yue for providing his expertise and support throughout the project and for asking simple yet challenging questions.

Thanks are also due to many people from McGill whom have helped make this possible and made an impression in my life including Priyadarshi, Evelin, Holger, Yinyin, Praveena, Dina, Michael, and many others. You guys are amazing!

I would also like to thank and acknowledge the technical support at McGill including Monique Riendeau for letting me use the AAS, Line Mongeon and David Liu for preparing FIB samples and TEM imaging, and Florence Paray for SEM and light optical microscope support. I would also like to acknowledge Edouard Régis from LaMCoS for providing support for all the tests I did for fretting wear and Thomas Schmitt from École Polytechnique Montreal for letting me use the scratch tester.

I would also like to express my gratitude towards Natural Science and Engineering Research Center (NSERC), Boeing Canada, Pratt & Whitney Canada, Héroux Devtek, Canadian Fastener Institute and Safran for their financial support. I would also like to thank the Bourse de maîtrise Hydro-Quebec Génie, McGill Engineering Doctoral Award (MEDA) and the Vadasz family and Gail de Belle for funding the named fellowship I received and the Graduate Excellence Fellowship for providing personal financial support. I would also like to thank Boeing, Coventya and Dipsol Inc. for providing specimens for the tests.

Last but never the least, I would like to thank my family and friends. Especially my parents, because without you there won`t be me.

Preface

The thesis is a manuscript-based thesis containing one publication and four manuscripts that are about to be submitted to journals. The manuscripts contain work completed from September 2012 to December 2016 under the supervision of Prof. Richard R. Chromik. Sliding wear tests and corrosion test, along with the characterization work were performed in McGill University. Fretting tests and their post-test analysis were performed in Lyon, France at LaMCoS, INSA-Lyon during a visit from March 2014 to May 2014, in which the work was performed under the supervision of Dr. Sylvie Descartes. Details of the contribution of each author of the manuscripts are listed below according to the chapter in which they appear.

Chapter 4: Lee L, Régis É, Descartes S, Chromik RR. Fretting wear behavior of Zn–Ni alloy coatings. Wear. 2015;330–331:112-21.

In this article, Lisa Lee as the first author did most of the fretting wear tests, performed pre-test and post-test characterization and analysis, and also wrote the manuscript. Edouard Régis (from LaMCoS, INSA-Lyon) performed some of the fretting tests. Sylvie Descartes (from LaMCoS, INSA-Lyon) and Richard R. Chromik supervised the project and edited the manuscript and provided valuable input and ideas for this manuscript.

Chapter 5: A comparison of the fretting behaviour of electrodeposited Zn-Ni alloy coatings and LHE Cd coating. Intended for publication

In this manuscript, Lisa Lee performed all the fretting tests, pre-test and post-test characterization and analysis, and wrote the manuscript. Sylvie Descartes and Richard R. Chromik supervised the project and edited the manuscript and provided valuable input and ideas for this manuscript.

Chapter 6: The effect of contact stress on the sliding wear behaviour of Zn-Ni electrodeposited coatings. To be submitted

In this manuscript, Lisa Lee performed all the sliding wear tests, adhesion tests, pre-test and post-test characterization and analysis, and wrote the manuscript. Experimental conditions were selected in collaboration with Priyadarshi Behera and Sriraman Rajagopalan. Sriraman Rajagopalan also edited the manuscript and provided valuable input and ideas to the manuscript. Richard R. Chromik supervised the project, edited the manuscript and provided valuable input and ideas to the manuscript.

Chapter 7: Effects of humidity on the dry sliding wear properties of Zn-Ni alloy coatings. To be submitted

In this manuscript, Lisa Lee performed all sliding wear tests, pre-test and post test characterization and analysis, and wrote the manuscript. Experimental conditions were selected in collaboration with Priyadarshi Behera and Sriraman Rajagopalan. Sriraman Rajagopalan also edited the manuscript and provided valuable input and ideas to the manuscript. Richard R. Chromik supervised the project, edited the manuscript and provided valuable input and ideas to the manuscript.

Chapter 8: Additional discussion

In this chapter, Lisa Lee performed all experiments and analyses for Zn-Ni coatings as well as wrote the chapter. Information for cadmium coating was referenced from the work of Priyadarshi Behera. Comparisons discussions were made by Lisa Lee.

Chapter 1

Introduction

1.1 General background

Electrodeposited Zn-Ni alloy coatings were developed in the 1980`s for the automotive industry to replace pure zinc coating, which were used as a sacrificial coating for steel [1]. This is because Zn-Ni coatings have better corrosion properties and hydrogen embrittlement properties than pure zinc and other Zn-alloy coatings [1]. Recently, Zn-Ni alloy coating has caught the attention of the aerospace industry, as the sacrificial corrosion protection coating for steel that is used in the aerospace industry, cadmium, is carcinogenic and toxic. Also, some plating baths used for Cd plating contain cyanide, which is toxic [2-5]. Generally, sacrificial corrosion protective coating for steel is used for applications such as steel fasteners or landing gear components in the aerospace industry. Although the main use of these coatings is for corrosion protection, Zn-Ni has different properties than cadmium, which can either improve or worsen the behaviour of the sacrificial coatings for the intended applications, such as corrosion and tribological behaviour of these applications.

Zn-Ni is an intermetallic, therefore the bonds between the atoms in its crystal structure is not purely metallic, but a combination of metallic, covalent and ionic bonding [6, 7]. This generally translates to a mechanical properties to somewhere between metals and ceramics [6, 7]. Generally, intermetallics are harder, stiffer and have higher melting temperature and oxidation resistance than their pure metal counterparts. However, they are also more brittle and less ductile [6, 7]. Zn-Ni coatings have a few intermetallic phases, however, cubic γ-ZnNi coatings, usually found in coatings with 12-15 wt% Ni, have been found to have the highest corrosion resistance when compared to other intermetallic phases [1, 8, 9]. All Zn-Ni coatings used for the work were γ-phase Zn-Ni coatings due to their superior corrosion resistance, and for the purpose of the thesis, γ-phase Zn-Ni will be referred to simply Zn-Ni from here on.

As result of Zn-Ni being an intermetallic, a higher hardness is imparted as one of the major difference between Zn-Ni and Cd. This may result in different tribological behaviour, as softer coatings can act as a solid lubricant due to their low shear strength, however is less wear resistant. [10, 11] A harder coating, on the other hand, is more wear resistant as it prevents macroscopic and microscopic scale ploughing and has a smaller area of contact [10, 11]. However, hard coatings generally have a high friction due to their high shear strength [10, 11]. Hard and soft coatings both have different advantages and disadvantages. Replacing cadmium (a soft coating) with Zn-Ni (a harder coating) may open up new applications for these coatings.

Furthermore, as these coatings are electrodeposited, varying the deposition parameters can incur differences in the surface morphologies, which can further alter their behaviour [12]. In terms of tribological properties, surface morphology has a strong effect on the friction and wear behaviour of the system, especially during the initial run-in period, where asperities are flattened [13]. A higher surface roughness leads to a smaller contact area, which lowers the adhesion, friction and wear [14]. However, a higher roughness is also correlated to higher wear [13, 15-17]. In terms of corrosion,

The objective of this thesis is largely dedicated to studying the effects of the surface morphology of Zn-Ni coatings on the tribological behaviour. In order to explore this, two Zn-Ni coatings with different surface morphologies, one rough and porous, while the other is smooth and dense, were studied in terms of fretting and sliding wear. Although both coatings are γ-phase Zn-Ni with similar hardness, considerable difference was observed in their tribological and corrosion behaviours due to their morphological differences.

A second objective of this thesis will also be dedicated to compare the tribological properties of Zn-Ni and Cd coatings.

1.2 Organization of Thesis

The thesis is divided into ten chapters. The current chapter gives a general background and objectives of the thesis. The following chapters are organized as follows:

Chapter 2 provides an in depth literature review and is divided into five sections. The first section will give a general review and uses of Zn-Ni alloy coatings and why they are of interests. The second section will present basic principles on tribology as well as third body concepts, velocity accommodation and the Hertzian contact. The third section reviews fretting and reciprocating sliding wear. The fourth section will give a review of the tribological work done on Zn-Ni coatings in the open literature in order to understand what have been done on Zn-Ni coatings in terms of tribology, particularly focusing on the effects of humidity and contact stress. The final section will briefly discuss the tribology of cadmium coatings.

Chapter 3 discusses the experimental details that might not be present in the manuscripts, due to the limited length required and interests of the audience. This includes details of sample preparation for characterization, SEM working conditions, details of the characterization steps such as details of the nanoindenter used to characterize hardness, how the hardness was calculated from the measurements, details of the Raman spectroscope and experiment conditions. Details of the fretting test set up is also discussed, such as how the samples were prepared, details of the custom built tribometer, data acquisition parameters, how test parameters were chosen, details of the post-test analysis etc. Similarly, such details were also discussed with the sliding wear tests, for example, test set-up, wear rate calculations, counterface wear calculations, etc.

Chapter 4 and 5 look at the fretting wear behaviour of Zn-Ni coatings with regards to how coating morphology will affect the stick slip behaviour and a comparison will be made between Cd and Zn-Ni coatings.

Chapter 4 focusses on the effects of the morphology of Zn-Ni coatings on their stick slip behaviour during fretting. Two coatings, one rough and porous, the other dense and smooth, were subjected to fretting against an AISI 440C steel counterface under 133 N and 447 N. Fretting in the stick, mixed slip and gross slip regimes were obtained by imposing displacements of ± 70, 100 and 150 μm respectively. Stick slip behaviour was discussed through comparing the energy ratios and post-test characterizations of the wear scar. Differences in the fretting behaviour are discussed in terms of velocity accommodation mechanisms due to differences in surface morphologies.

Chapter 5 compares the fretting behaviour of Zn-Ni with cadmium coatings at similar loads and calculated initial Hertzian contact stresses. Both coatings have a porous and rough morphology. Again, displacements of ± 70, 100 and 150 μm were imposed in order to obtain the stick, mixed slip and gross slip regimes respectively for Zn-Ni coatings. Comparisons with cadmium coatings are made in terms of energy ratio, wear scar morphology and wear volume. In comparison to Zn-Ni coatings, cadmium showed a partial slip behaviour as cadmium is easier to shear and deform than Zn-Ni coatings due to different material properties and crystal structure.

Chapter 6 and 7 discuss the sliding wear behaviour of Zn-Ni coatings in terms of variation of normal load and humidity. Comparison with Cd will be supplemented at the end of Chapter 7 due to the division of work in the project, tribological work on cadmium coatings was done by another student.

Chapter 6 discusses the sliding wear behaviour and how the contact stress may affect the sliding wear behaviour. In this study, Zn-Ni with two different coating morphologies, one porous and rough, the other dense and smooth. The coatings were subjected to normal loads of 3.5, 7 and 12 N. Increasing the normal load increased the CoF for both coatings. Wear behaviour between the coatings differed due to the different surface morphologies. Wear rate of the rougher coating, although slightly higher than the smoother coating, remained the same for all three loads. However, for the smoother coatings, although at loads 3.5 and 7 N the wear rate remained low, at 12 N the increased in load cause a sudden increase in wear due to delamination, showing that coating morphology does have an influence on the tribological behaviour.

Chapter 7 further looks at the dense and smoother coating in order to understand why the coating behaved so differently. The coating was subjected to 3.5 N normal load, however the humidity was varied at 0, 20, 40 and 60 relative humidity. It was found that at high humidity levels, a nanocrystalline ZnO film was formed at tribolayer, effectively lubricating the contact. However, when the humidity decreased, the ZnO nanocrystalline layer was not formed, resulting in higher wear. Formation of the ZnO nanocrystalline layer was found to mitigate wear and stabilize the CoF.

Chapter 8 compares the sliding wear behaviour of Zn-Ni coating with cadmium coating. The effect of humidity on the sliding wear behaviour of the two coatings were discussed, and a decrease in humidity was found to benefit cadmium coatings, while the reverse is true for Zn-Ni coatings. Mechanical and material property differences between the two coatings also affected the tribological behaviour, as cadmium had lower CoF while Zn-Ni showed better wear resistance.

Chapter 2

Literature Review

2.1 Zn-Ni Coatings

Zinc is one of the most effective coating used to protect steel from corrosion. Combining zinc with transition metals, such as iron, nickel, cobalt, manganese or tin, can help increase its corrosion resistance [1, 18]. Addition of nickel to zinc has shown better corrosion resistance over zinc and its other alloys [1]. Zn-Ni was commercially adopted in the 1980's and was mainly used for the automotive industry. As these coatings were mostly used for corrosion, many corrosion tests were performed on these coatings, such as those found in [1, 8, 9, 19-30]. It is reported that Zn-Ni with 10-15% Ni has optimized corrosion properties in sodium chloride [1]. This is due to the formation of an intermetallic γ-phase Zn-Ni [8, 9, 30]. Recently, Zn-Ni has caught the attention of the aerospace industry as it is one of the primary candidates to replace cadmium coatings as a corrosion protective coating for steel.

Cadmium is used in the aerospace industry as protective coatings for fasteners and landing gear components. Cadmium is carcinogenic and toxic and there is a desire to replace these coatings due to health and regulation reasons [2-5]. Many studies have been done on comparing Zn-Ni coatings to cadmium in order to see how Zn-Ni compares with cadmium, such as those found in [3-5, 9, 19, 21, 22, 28, 29, 31]. It is found that in terms of corrosion, Zn-Ni has comparable corrosion resistant to cadmium coatings [9, 21, 22, 27-29]. This makes Zn-Ni an attractive replacement for cadmium coatings. However, corrosion is not the only important feature, especially in aerospace application, where regulations and safety is much more stringent.

Although many studies have been conducted on Zn-Ni coatings, among these literature, very little focuses on the tribological behaviours of these coatings although their applications have tribological requirements. In the past five years, over a hundred articles were written for Zn-Ni coatings. However, over half of these papers focusses on plating parameters and additives [12, 32-81] and how these will affect the microstructure and corrosion properties of these coatings [23, 82-95]. Another forty articles were dedicated to improving these coatings by adding a third metal [96-114], such as Co, Mn and Mo, or adding ceramic particles [115-131], such as Al_2O_3, TiO_2 and SiO_2 in order to improve mechanical and corrosion properties of these coatings. Less than ten articles were written for the tribological studies of these coatings [3, 12, 28, 49, 50, 132].

2.2 Selected Review on Tribology

2.2.1 Friction and wear

Tribology is defined as the "science and technology of interacting surfaces in relative motion and of related subjects and practices" [133]. It comes from the Greek word *tribos*, meaning "to rub" [134]. , it is the study of friction, wear and lubrication of interacting surfaces. Friction is defined as the resistance force tangential to the direction of motion and is characterized through the coefficient of friction (CoF), μ, given in Equation (2.1) [135]. Wear, on the other hand, is defined as the removal of material of one or both of the surfaces in contact and relative motion [135]. Commonly, wear is quantified by the wear coefficient, K, which was introduced by Archard and Hirst [136] shown in Equation (2.2). Siniawski *et al.* [137] presents another way quantify wear called "universal wear law for abrasion". This method takes into account the effects of abrasion on wear. This method gives a simple equation (Equation (2.3)) for wear quantification, which gives a good prediction of wear across multiple systems. One major attraction to this equation is it considers the time-dependence of the wear rate using β. In most systems, when $-1 < \beta < 0$, most of the wear occurs near the beginning of the wear cycles, whereas $\beta = 0$ indicates the wear rate is constant. When $\beta > 1$, the wear rate increases with time. Sriraman *et al.* [3] compared the tribological behaviours of Zn-Ni and cadmium and used this method to compare their wear properties. Both cadmium and zinc nickel had negative β values, but cadmium coatings had a more negative β value than zinc nickel. Thus, it is postulated that zinc nickel coatings are more resistant to adhesive wear and material loss when compared to cadmium coatings [3].

$$\mu = \frac{Friction\ Force}{Normal\ Load} \tag{2.1}$$

$$K = \frac{Volume\ of\ wear}{(Normal\ Load) \times (Distance)} \tag{2.2}$$

$$A(n) = \frac{V_n}{d} = A_1 n^{\beta} \tag{2.3}$$

Where
$A(n)$ = average abrasion rate for n cycles
A_1 = abrasion rate of first cycle
n = number of cycles
β = time dependent constant
V_n = Average volume of wear for n cycles
d = sliding distance for n cycles

2.2.2 Third body approach

Another important concept in tribology is the “third body” concept. Many studies treat friction and wear as a two body system and only report the coefficient of friction [138]. This is often seen in general comparisons between cadmium and Zn-Ni coating, where only a friction coefficient value is reported while other aspects, such as wear and velocity accommodation mechanisms are often ignored [18, 21, 139]. In the third body concept, the counterface and surface are referred to as the two first bodies, while the third bodies refer to the material that is in a zone between the first bodies, where the material is chemically and/or mechanically different from the first bodies [138, 140]. In sliding without lubrication, third bodies often arise through the wearing of the first bodies, which causes particle detachment [138, 140]. Differences could be due to mechanical strain, chemical reaction. Third bodies have a strong influence on the wear and velocity accommodation mechanisms (section 2.2.4). In terms of wear, the third bodies are relatively looser than the asperities of the first bodies which are locked in place, thereby can cause less damage than the first bodies rubbing against each other [140]. This is especially true in the case of fretting, where when a debris bed separates the first bodies, decrease wear is observed [140]. In terms of velocity accommodation, on the onset of motion, third bodies change the location of sliding from the two first bodies, to between a first body and a third body, or between two third bodies. This significantly influences the velocity accommodation modes and mechanisms.

2.2.3 Particle detachment mechanisms

The wear process can be divided into three steps [11, 140, 141]: (i) particle is detached through wear mechanisms, such as adhesion, abrasion, corrosion, fatigue, etc. (ii) the particle becomes a third body, where it is trapped in the contact, it which it can transfer from one surface to another, or recirculated between the two surface. At this point, the particle becomes morphologically and chemically different from the parent material due to mechanical strain and reaction to the environment. (iii) the particle is ejected from the contact and becomes a "true" wear particle. The mechanisms in which the particles are detached are well known classical wear mechanisms and selected particle detachment mechanisms are described below.

Adhesive wear occurs due to attractive forces between two surfaces. When two surfaces are in close contact, bonds form between the atoms of the two surfaces creating adhesive junctions. Surfaces that are plastically deformed or clean favours adhesive wear, as the junction size is larger due to the larger contact area [142]. Adhesive wear occurs when the two surfaces are put in relative motion. Junctions that were formed when the surfaces were put into contact are sheared. This results in transfer of material from one surface to the other, thus causing a detached particle as shown in Figure 2.1. [135]

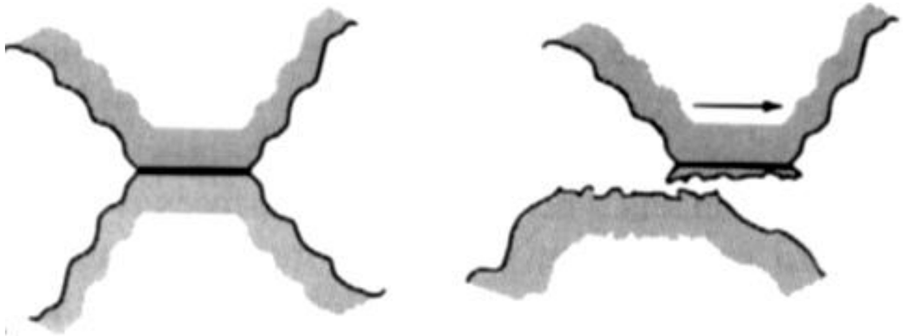

Figure 2.1 Schematic of adhesive wear [135]. Material is transferred from one surface to the other through adhesion

Fatigue and delamination wear occurs through repeating loading and unloading of a surface at stress levels in the material where the load cannot be sustained for multiple loadings. Wear debris are formed when fatigue cracks cause liberation of the surface material (see Figure 2.2a). In sliding wear, cracks are nucleated below the surface and propagate due to repeated loading and unloading. Crack propagation tends to be parallel to the surface, causing plate like wear debris (see Figure 2.2b). Fatigue and delamination wear is usually found in pitting and spalling failure modes. [135]

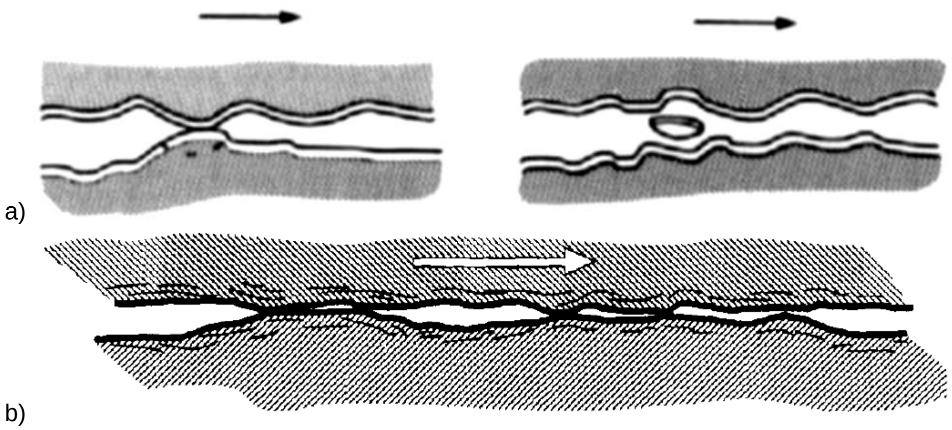

Figure 2.2 Schematic of (a) fatigue and (b) delamination wear [135]. Particles is detached through fatigue and delamination.

Abrasive wear occurs when one of the two contacting materials is significantly harder than the other, or when a third media, which is harder than both contacting material is introduced to the contact. Asperities or wear debris from the harder material causes ploughing, micro cutting or wedge formation in the softer material [143]. Thereby inducing wear in the softer material. A schematic of the process is shown in Figure 2.3.

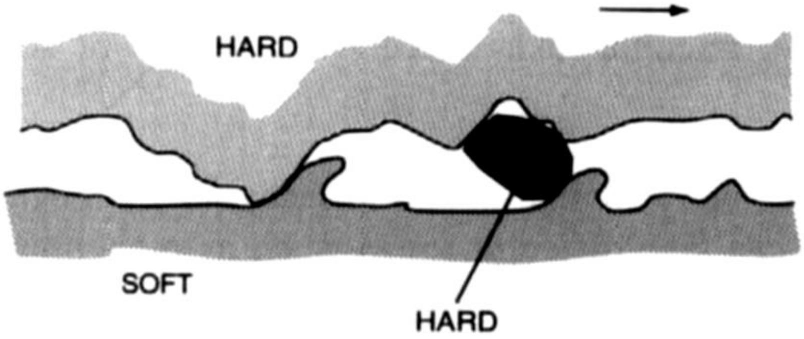

Figure 2.3 Schematic of abrasive wear [135]. Harder particle in the contact causes ploughing, micro cutting or wedge formation on softer material.

Chemical wear refers to the synergetic effect of detrimental chemical reaction coupled with mechanical loading at the contact surface. The coupled phenomenon causes material removal and wear debris formation (see Figure 2.4). Rubbing also causes surface crack formation, which results in a chemical attack of greater severity. A form of chemical wear is oxidative wear, where surface oxides are formed. Continuous rubbing of the oxide layer removes the surface oxide layer, and exposure of the fresh surface to an oxygen rich environment reforms the layer. [135]

Figure 2.4 Schematic of chemical wear [135]. Oxide particles are removed from the surface. The oxide layer is then reformed and removed again.

2.2.4 Velocity accommodation mechanisms

Velocity can be accommodated in a number of sites through different mechanisms in a tribological system. Berthier [144] separated the tribological system into five location, where S_1 and S_5 refers to the two first bodies, S_2 and S_4 refers to the screen between the first body and third bodies, and S_3 as the third bodies. Later articles [145] also added S_0, which refers to the working device, or the tribological instrument. Within these sites, four different velocity accommodation modes can occur, where M_1 refers to the plastic mode, M_2 the fracture mode, M_3 the shearing mode and M_4 the rolling mode [144, 146]. M_0 qualifies “false fretting” and is the elastic mode [145, 146]. A schematic of the sites and modes in the tribological system is shown in Figure 2.5. A combination of these sites and modes makes up the velocity accommodation mechanisms, and the most common combinations are shown in Figure 2.6 [145, 146]. In practice, the mechanisms can coexist in the same contact [145].

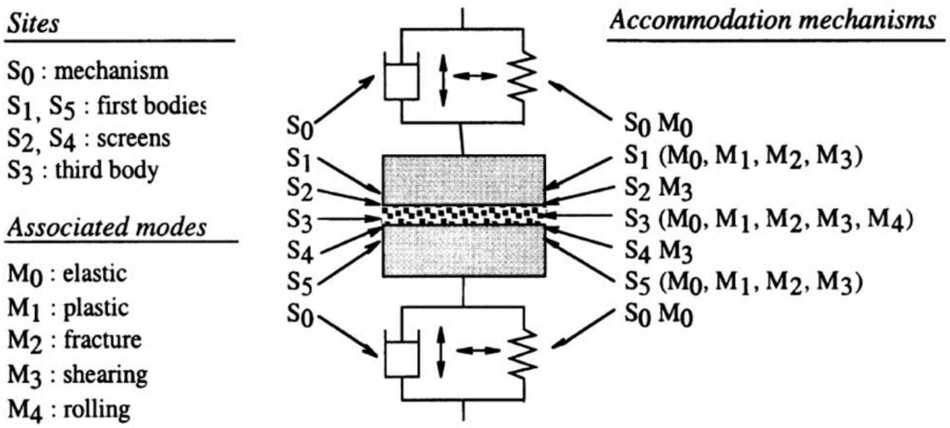

Figure 2.5 Mechanisms of velocity accommodation in the tribological system from [145]

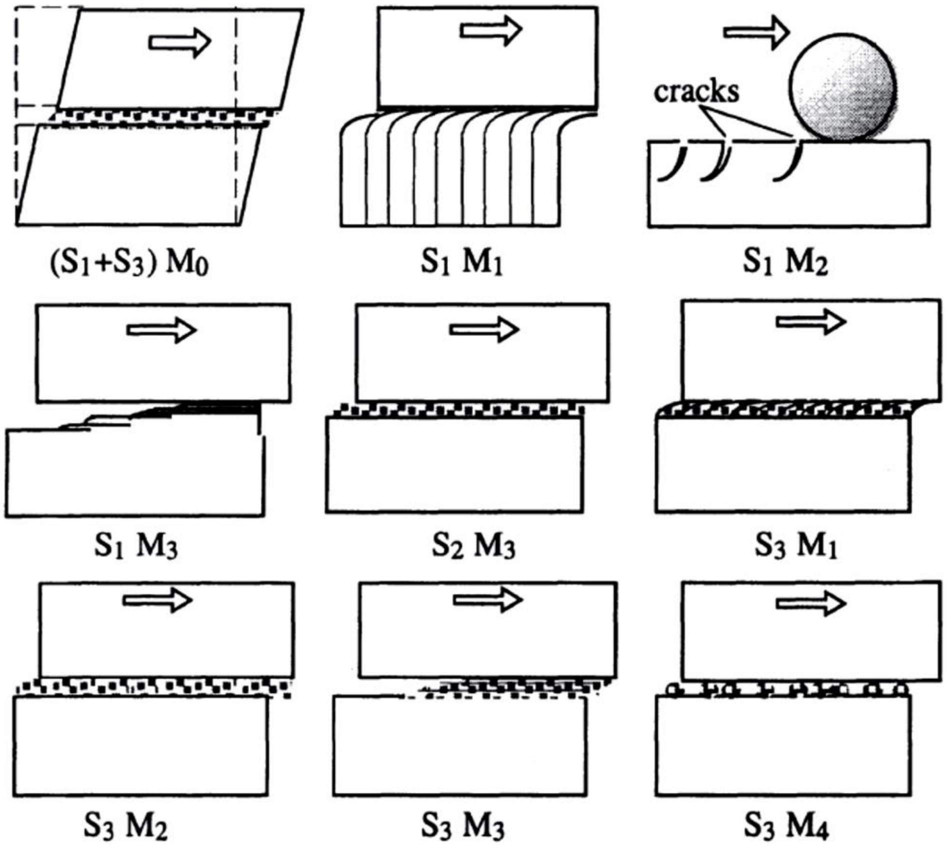

Figure 2.6 Elementary accommodation mechanism for a sliding system from [145]

2.2.5 Hertzian Contact

Another important concept in tribology is the Hertzian contact. A Hertzian contact refers to the deformation and pressure of two elastic bodies [147]. Hertzian analysis are made based on the assumptions that the surfaces are continuous, smooth and non-conforming; strain within the contact is small; as the contact is small compared to the elastic bodies, the elastic bodies are considered as elastic half-spaces; and the surfaces are frictionless [147]. For a sphere on plane contact, the average Hertzian contact stress (P_{avg}) is shown in Equation (2.4). The maximum Hertzian contact stress (P_{max}) is 3/2 times P_{avg} (Equation (2.5)). The radius of the contact (a) can be calculated using Equation (2.6).

$$P_{avg} = \frac{F_n}{\pi a^2} \tag{2.4}$$

$$P_{max} = \frac{3}{2} P_{avg} \tag{2.5}$$

$$a = \left(\frac{3F_n R}{4E_r}\right)^{1/3} \tag{2.6}$$

$$\frac{1}{E_r} = \frac{1-\nu_1^2}{E_1} + \frac{1-\nu_2^2}{E_2} \tag{2.7}$$

Where
F_n is the normal force
a is the contact radius
R is the radius of the sphere
E_r is the reduced modulus
E_1 and E_2 are the modulus of the sphere and flat
ν_1 and ν_2 are the Poisson's ratio of the sphere and flat

The Hertzian contact typically serves as an approximation, as surfaces are not smooth and are in contact in discrete contact points within the calculated contact area due to asperities. Thus the true area of contact is smaller than the calculated area of contact. From the assumptions made for the calculations, analysis is only valid at the beginning of the test, where no sliding has occurred yet. Contact stress during sliding is more complex and difficult to predict.

2.3 Fretting and reciprocating sliding

When considering fretting, it is often difficult to distinguish when to consider it reciprocating sliding and when to consider it fretting. To distinguish these two regimes, a ratio of the displacement amplitude to the contact radius, *e*, was proposed [148]. When $e > 1$, it is considered regular reciprocating sliding, whereas when $e < 1$, fretting is considered (Figure 2.7) [148]. One of the key difference between fretting and reciprocating sliding is that in fretting, a portion of the contact area will always remain unexposed to the environment due to the small displacements, whereas for reciprocation sliding, every point on the wear scar will be exposed to the environment at one point [148].

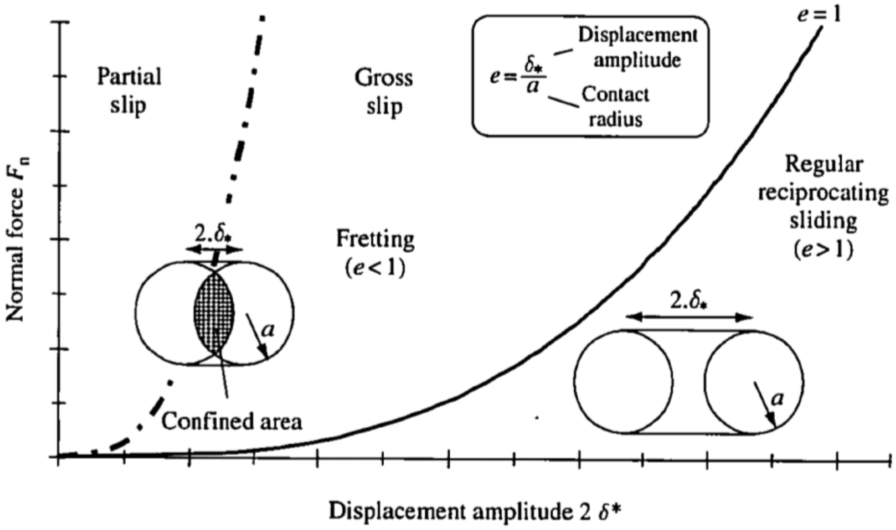

Figure 2.7 Distinguishing regular reciprocating sliding from fretting, from [148]

Fretting is defined as a small amplitude oscillatory motion between two surfaces [148]. By increasing the displacement from zero to $e = 1$, different contact conditions are often observed: stick, partial slip and gross slip [149]. Sticking occurs when motion does not occur within the contact [149]. It is often referred to as “false fretting” as the motion is completely taken up through elastic deformation of the bulk of the first body, the machine or the support [141, 146]. In this case, little to no surface damage is observed [149]. Partial slip on the other occurs when some parts of the contact is stuck together (usually the central region), while motion occurs in other parts of the contact (usually the annular region) [148, 149]. Gross slip occurs when motion occurs throughout the contact. In this case there is severe surface damage due to wear [148-150]. To define these different contact conditions, the tangential force can be plotted against the displacement in order to produce a fretting or hysteresis loop during one cycle of fretting. A completely closed loop indicates stick behaviour, a partially open loop or elliptical loop indicates partial slip behaviour, while a completely open loop or quasi rectangular loop indicates gross slip behaviour (Figure 2.8) [148-150]. Further distinction of the partial slip and gross slip behaviour can be obtained by the energy ratio, A, which is the dissipated energy (indicative of the area within the loop) over the total energy (indicative of the rectangle which encompasses the loop) [148-150]. An energy ratio is below 0.2 indicates partial slip behaviour, while above 0.2 indicates gross slip behaviour [150]. An energy ratio of zero indicates stick behaviour. By looking at the evolution of these fretting loops with time, the fretting behaviour can be separated into three regimes: stick or partial slip regime, mixed slip regime and gross slip regime [148-150]. The stick or partial slip regime is characterized by stick or partial slip behaviour throughout the test [148-150]. The mixed slip regime is characterized by a combination of stick, partial slip or gross slip behaviours[148-150]. The gross slip regime is characterized by gross slip behaviour throughout the test [148-150]. Examples of these fretting logs is found in Figure 2.9.

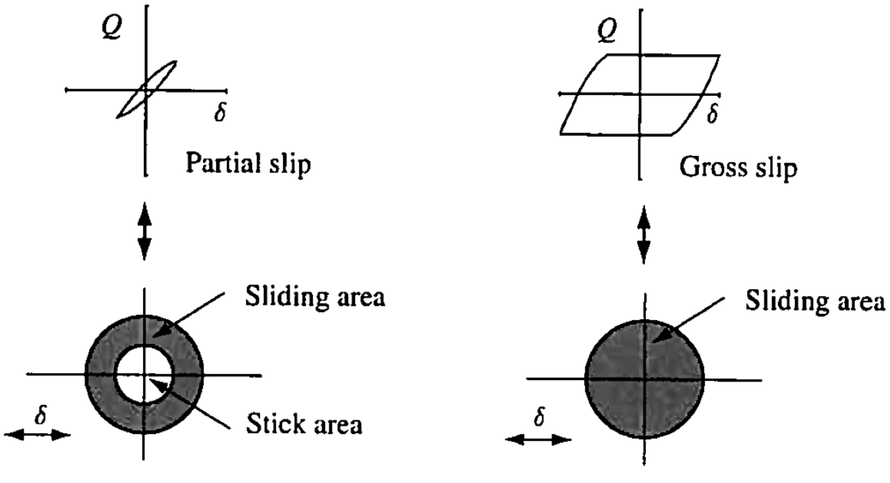

Figure 2.8. Partial slip and gross slip, fretting loop and contact [148]

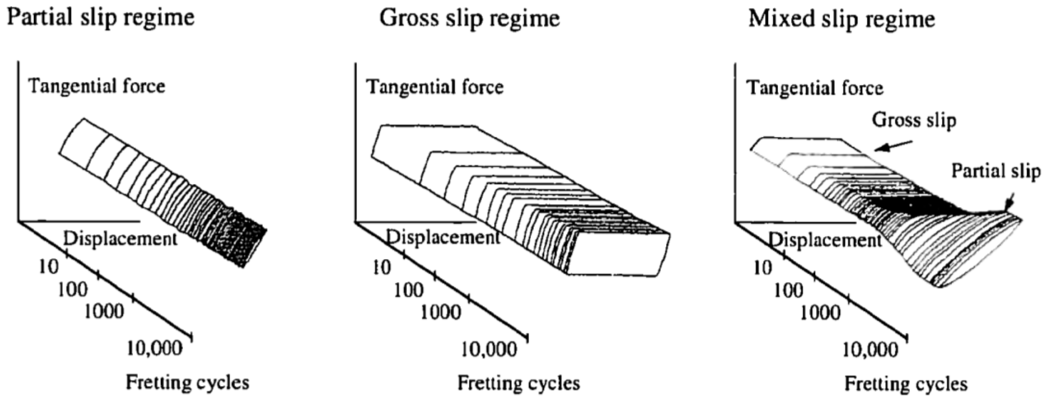

Figure 2.9. Fretting logs of the partial slip, gross slip and mixed slip regimes [148]

2.4 Tribology of Zn-Ni coatings

Although Zn-Ni coatings are also found in tribological applications, only a few studies on the tribological properties are present in the open literature. Recent studies that have been conducted regarding the tribological properties of these coatings have been conducted by Feng *et al.* [47, 50], Ghaziof and Gao [12], Sriraman *et al.* [3, 28] and Panagopoulos *et al.* [151]. Feng *et al.* [47, 50] studied the effects of additives on the properties of the coatings which produced a dull coating (without additives) and a bright coating (with additives) which was much smoother and fined grained than the dull coating. Examination of the tribological properties and found that the bright coating had a slightly lower and stable CoF than the dull coating [47, 50]. Ghaziof and Gao [12] also looked at the effects plating parameters on the tribological properties of Zn-Ni coatings. Coatings with Zn-rich η-phase and two different Ni_5Zn_{21} γ-phase coatings. γ-phase coatings showed better wear resistance and lower CoF than η-phase coatings due to higher hardness [12]. A rougher and smoother coating containing γ-ZnNi were also produced and coatings which were smoother showed better friction and wear properties [12]. Sriraman *et al.* compared Zn-14%-Ni alloy with cadmium, Cd-Ti and zinc with a reciprocating pin on flat tribometer under dry sliding conditions using *in situ* methods [3] and the effect of wear on corrosion [28]. Using *in situ* tribology, under the same test conditions, Zn-14%-Ni alloy was found to be more wear resistant than the other tested coatings and the wear mechanism for Zn-14%-Ni alloy is mild adhesion followed by delamination [3]. Sriraman et al. also found that when submersed in a 3.5% NaCl solution during wear, Zn-14%-Ni alloy performed better than Cd, Cd-Ti and Zn in terms of corrosion resistance and nickel surface enrichment on the coatings were found after the tribocorrosion test [28]. Panagopoulos et al. investigated the effects of the normal load on tribological properties of Zn-Ni alloy coatings with two different counterfaces: steel and alumina [151]. It was found that the stable friction coefficient for Zn-Ni alloy against alumina pins was higher than the friction coefficient for Zn-Ni alloy against steel pins and the highest load used showed a lower friction coefficient in both cases [151]. Although studies of these coatings are in the open literature, it is very few and the studies do not give a complete picture of the tribological properties of Zn-14%-Ni alloy coatings, such as a systematic testing of Zn-14%-Ni alloy coatings with baseline coatings (Cd and Zn coatings) where there is a change in contact conditions, including the change in normal loads, track lengths, counterface material, test environment, etc.

2.4.1 Effects of roughness in tribology of Zn-Ni

Surface roughness has a strong effect on the tribological properties of the system as the initial contact area is affected. When the roughness is increased, the contact area also decreases, as the area of the discrete contact points is decreased [14]. Deformation (elastic or plastic) occurs at these discrete points of contact. Generally, minimizing the contact area minimizes adhesion, friction and wear [14]. The effect normal load of the system is also stronger for surfaces that are rougher, as the contact area is proportional to the square root of the normal force. Thus the contact stress at the discreet contact point is much higher if the contact area is smaller due to higher roughness. At low loads, for rough surfaces, the wear is delayed until the original asperities are worn, whereas for smooth surfaces, wear starts at the beginning of sliding [13]. At high loads, wear of the original asperities of rougher surfaces occurs much faster and sooner [13]. In the case of Zn-Ni, Feng et al. [50] compared the friction and wear behaviour against a steel ball of two γ-phase Zn-Ni coatings with very different roughness. Smoother coatings exhibited a lower and more stable CoF of friction [50]. The smoother coating also exhibited much better wear properties than the rougher coating [50]. It was found that the surface morphology and grain size of the coatings played a significant role on the differences [50]. Ghaziof and Gao [12] also looked at two different γ-phase Zn-Ni coating with different roughness and grain size due to plating parameters [12]. Again, the smoother coating exhibited better friction and wear properties than the rougher coating. They attributed the improved properties to the smoother and more uniform surface morphology and higher hardness of the coating [12]. Although previous studies have shown that surface morphology and roughness play a significant role in the tribological behaviour of the system, the wear and velocity accommodation mechanisms can still be further discussed. Also the synergistic effects of contact stress and surface morphology are not discussed in previous studies. The effects of surface morphology and contact stress on the tribological properties are further discussed in this research.

2.4.2 Effects of humidity in tribology of Zn-Ni

Humidity has a prominent role in tribology, especially in metals tribology. Metals easily form a contamination film when exposed to the ambient environment [152]. The contamination film is made up of adsorbed gas particles or an oxide layer for metals [152]. Experiments performed in ambient environment and vacuum chamber showed vastly different results, as a higher friction was observed on the test performed in vacuum due to the absence of the contamination film [152]. Baker et al. [153] studied the effects of oxygen and water vapor by cycling the test chamber with humid air and dry nitrogen. By changing the environment, the friction of the coating reverted back and forth between the two environments [153]. In terms of Zn-Ni coating, not many studies have been made regarding the effect of humidity on their tribological properties, although their applications encounter many different environments which could cause critical damage. Feng *et al.* [50] performed chemical analysis post wear test to see the effect of the ambient environment and found the formation of ZnO on the wear track. Although oxides in bulk form do not perform well at low temperatures, as they have high friction and their debris can cause abrasive wear [154], studies have shown that some pulse laser deposited zinc oxide film shows a lubricious property [154-156]. This is due to the nanoscale structure and oxygen deficiency which can cause room temperature ductility through diffusional creep along the grain boundaries and anion vacancies [154-156]. Formation of ZnO in the contact during sliding could potentially affect the tribological behaviour of Zn-Ni coatings. Although studies on the tribological properties of ZnO and chemical analysis of the wear tracks of Zn-Ni coatings have been previously made, the relationship between the two has yet to be discussed. Also, the effects of humidity on the formation of third bodies has not been discussed. The effects of humidity on the tribological behaviour of Zn-Ni coatings will be discussed in this work.

2.5 Tribology of Cd coatings

Many studies have been made comparing cadmium with other potential alternative coatings. A large part of those studies focuses on the corrosion characteristics, torque-tension characteristics and hydrogen embrittlement. Very few have focused on sliding wear properties. Ruggeri *et al.* [157] studied the friction and wear of cadmium coatings using a pin on ring geometry at various loads and sliding speeds. However, to avoid diffusion of cadmium into the steel substrate, nickel and copper was plated beneath the cadmium coating. Therefore, the sliding behaviour of cadmium may be affected by those underlying layers although the layers are only 1 micron thick each. At high loads and low sliding speeds, the cadmium layer was completely worn through. However, this study does show the lubricating abilities of cadmium. They found that during sliding, a composite metallic film formed between the coating and steel pin, which had a low melting temperature, thus became a semi fluid mass at high load and high sliding speed due to the temperature increase, which contributed to the low COF observed.

Sriraman *et al.* [3] compared the COF, wear rate and rheology (movement of the films and third bodies at the interface) of cadmium, zinc and zinc nickel using a reciprocal tribometer fitted with an alumina pin. During the run-in period, a high COF was observed for cadmium, which quickly lowered after a substantial transfer film formation, which remained stable by recirculation of the transfer film and the COF remained constant. When the transfer film became unstable and the pin was in direct contact with the coating, the COF increased. Compared to zinc nickel coatings, cadmium has a high wear rate due to rapid transfer film formation and coating wear through severe adhesive wear mechanisms. At approximately 400 cycles, the cadmium coating failed, resulting in direct contact between the pin and substrate, whereas zinc nickel coatings remained throughout the test, ensuing a longer coating lifetime of zinc nickel in terms of wear.

Direct comparison of cadmium and Zn-Ni coatings were made by Sriraman *et al.* [3]. This work is partially a continuation of the previous work. However, this work will be focused on using a steel counterface instead an alumina counterface, and more aspects, such as the effect of surface morphology, humidity and contact stress are taken into consideration.

2.6 Summary

Zn-Ni is an effective coating for corrosion protection of steel coatings. As regulation on cadmium becomes more stringent, the aerospace industry is looking towards replacing cadmium coatings with Zn-Ni. Although the applications of these coating can encounter tribological situations, a gap in the tribological characterization of these materials exists, resulting from the majority of the research dedicated to plating parameters and corrosion aspects of these coatings. Selected tribological phenomena were reviewed and emphasis was put on the third body approach, velocity accommodation mechanism, fretting and sliding wear. A review of the tribology of Zn-Ni coatings and Cd was also made, and although studies have been performed on the tribological behaviour of these coatings, there is still deficiencies and gaps in this area that can be filled. A few examples are studies of the effect of humidity on these coatings, better understanding of the wear mechanisms and comparison of the previous two with cadmium coatings under the same test conditions.

Chapter 3

Experimental Techniques

3.1 Material Characterization

3.1.1 Microscopy

Surface morphologies and cross sections of the as received coatings were imaged using a scanning electron microscope (SEM) using secondary electrons (SE). Imaging was performed using an FEI F50 microscope with 20 keV accelerating voltage and a working distance around 10 mm. Cross sections of the coatings were obtained by sectioning with a diamond saw, mounting the samples and preparing them metallographically. Samples that were baked were hot mounted with resin with carbon filler. Samples that were not baked were cold mounted in resin with copper filler. Mounted samples were then prepared metallographically by fine grinding using 400, 600 and 800 grit size SiC paper in ethanol and polishing using 0.5 and 0.3 µm 10 wt% alumina powder suspended in isopropanol. Final polishing in 0.05 µm 10 wt% alumina powder suspended in pentanol vibratory polishing for 8 hours was done to samples where an extremely fine surface is needed. All metallographic preparation was performed in alcohol (iso-propanol for grinding and pentanol for polishing) to prevent corrosion of the coating. Electron probe micro analysis (EPMA) was performed on coatings where a ZnS sample was used as a standard for Zn content and Ni metal was used as the standard for Ni content.

3.1.2 Nanoindentation

In order to obtain the mechanical properties of the coatings only, nanoindentation was used due to the small thickness of the coatings. Nanoindentation was performed on the cross section of the coatings to obtain the hardness of the coatings due to the high roughness. A Hysitron Ubi3 was used to perform nanoindentation measurements. For precise placement, a tandem piezoelectric ceramic scanning tube, where the top half consists of 4 quarter cylinders which controls the x and y axes, and the bottom half is a single cylinder which controls the z-axis. A three plate capacitive force/displacement transducer design (Figure 3.1) provides high sensitivity measurements. The three plate capacitive transducer has two fixed outer plates, the drive plates, and a center plate that is held by springs with known spring constant. The drive plates are driven by AC signals which are equal in magnitude but 180° out of phase. This results in a maximized electric field potential at the drive plates, zero at the center between the drive plates and linear dependence between the drive plates. The center plate assumes the potential at its position, allowing the measurement of displacement. In order to indent on the sample, a large DC bias is applied to the bottom plate to create an attractive force between the central plate and bottom plate to pull the central plate down. The force and displacement can be determined from the magnitude of the applied voltage and position of the center plate. [158]

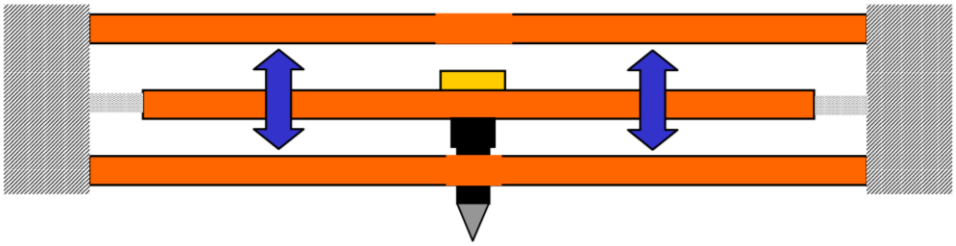

Figure 3.1 Schematic of three plate capacitive transducer from [158]

Indentation was performed using a Berkovich tip and a 5 second loading time, 2 second hold at maximum load and 5 second unloading time function at a constant loading and unloading rate. The load-displacement curve is analyzed using the Oliver-Pharr method [159] to calculate the hardness and modulus. The stiffness of the curve, S, is determined by fitting a line to the initial portion of the unloading curve, which is then used to calculate the reduced modulus E_r as shown in Eq. (3.1. The projected area, A, is approximated using the contact depth, h_c, as shown in Eq. (3.2, where 24.5 is the coefficient for a perfect Berkovich tip shape, and the subsequent constants accounts for imperfections on the tip, such as tip wear. The area function is calculated by indenting on fused quartz, which has a known modulus, at various loads and fitting the area function up to 3-4 polynomial orders [158]. The area function was recalibrated periodically in order to compensate for tip wear.

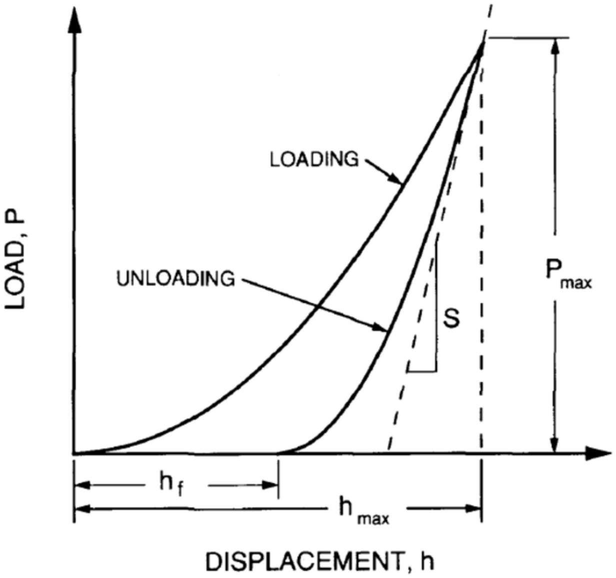

Figure 3.2 Typical load displacement curve [159]

$$S = \frac{2}{\sqrt{\pi}} E_r \sqrt{A} \tag{3.1}$$

$$A(h_c) = 24.5{h_c}^2 + C_1 h_c + C_2 {h_c}^{1/2} + C_3 {h_c}^{1/4} + \cdots \tag{3.2}$$

where,

$$h_c = h_{max} - 0.75 \frac{P_{max}}{S} \tag{3.3}$$

where h_{max} is the maximum depth of the indent and P_{max} is the maximum load. The Young's modulus and hardness are calculated according to Eq. (3.4 and (3.5. The $\nu_{indenter}$ is 0.07 and $E_{indenter}$ is 1140 GPa [158] while for Zn-Ni the Poisson's ratio is 0.23 [160].

$$\frac{1}{E_r} = \frac{1 - \nu_{sample}^2}{E_{sample}} + \frac{1 - \nu_{indenter}^2}{E_{indenter}} \tag{3.4}$$

$$H = \frac{P_{max}}{A} \tag{3.5}$$

As the coating was only around 15 μm in thickness, in order to obtain indents within the coating layer, *in situ* SPM images were taken before indentation to ensure the indentation area is within the coating, and after indentation to ensure good indentations were obtained. A 5 mN load was used for the indentations and reported values are averaged over 10 or more indentation results.

3.1.3 Raman spectroscopy

Raman spectroscopy was used to characterize chemical changes on the wear track. A Renishaw inVia Raman microscope fitted with a 514.5 nm Ar^+ laser as the excitation source. To avoid damaging the specimen, neutral density filters were used to decrease the intensity of the laser to around 2.5 mW. In order to acquire good signal, longer acquisition times, 60 s, and multiple acquisitions of the same spot were averaged together. The data were analyzed with Renishaw's WiRe program in order to get peak position. In some cases, the data were smoothed and levelled. For Raman spectral maps, spot analysis were taken 1 μm apart with a shorter acquisition time (10 s) and lower laser power, 0.5 mW was used to avoid sample damage. To obtain the maps, the intensity of the spectra at between 490 and 600 cm^{-1} was integrated to the baseline in order to obtain a contrast.

3.2 Fretting

3.2.1 Test set-up

Fretting counterface samples machined to the specifications shown in Figure 3.3 using AISI 440C steel. The hole present in the center of the sample is used for inserting a thermal couple to monitor the temperature during high temperature fretting, which was not performed in this work. However, it is noted that although tests were performed at ambient temperature and humidity (23-25°C, 35-40% RH), a slightly higher temperature (27-28°C) was measured by the thermal couple. Prior to the test, the samples were cleaned in an ultrasonic bath of ethanol for around 10 minutes to remove contamination. Flat samples were cut from a larger coated low carbon steel sheet (SAE 1006) of 0.8 mm thickness using a diamond saw, then grinded to the dimensions shown in Figure 3.4. The samples were then cleaned in an ultrasonic bath of ethanol then glued onto 12 x 8 x 5 mm AISI 440C stubs in order to comply to sample specifications for the fretting tests.

The Impact II, a custom built tribometer at Laboratoire de Méchanque des Contacts et des Structures (LaMCoS, INSA-Lyon, Lyon, France) was used to perform fretting wear test. Counterface and flat samples were mounted on the upper and lower ceramic pieces using vices, then aligned as shown in Figure 3.5. The normal force was applied by bringing the samples together and loading the counterface to the desired force. During the test, the normal force is regulated using a piezo. A tolerance of 5 N was used for the normal force regulation. When the normal force changed beyond the limits of the piezo due to the change in the z-displacement (D_z) during the test, the force was adjusted manually to maintain a constant normal force. In terms of the applied tangential displacement (D_y), an initial value was set before the test started, then adjusted accordingly to get the desired measured displacement value. During the test, the displacement was adjusted such that the displacement value maintained constant.

In terms of data acquisition, 1000 data points were recorded for every 1 second acquisition with 15 seconds between acquisition points. The total time (related to the total number of cycles) of the test was set slightly longer than the desired time due to time needed to reach desired parameters, usually 10-20 seconds is required.

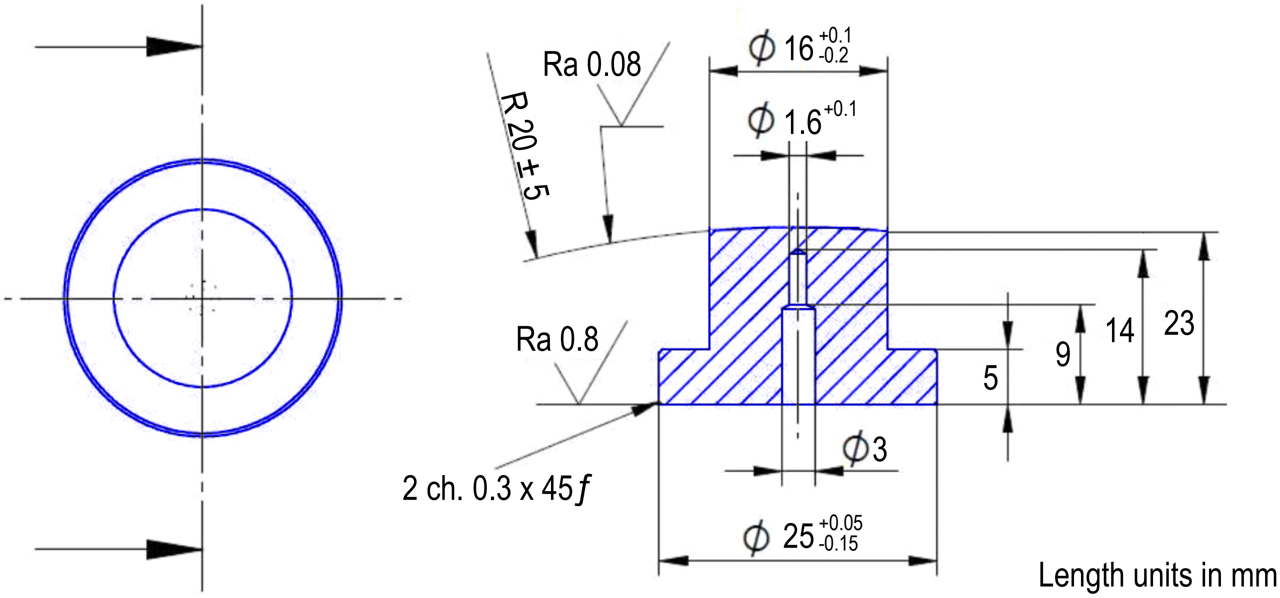

Figure 3.3 Counterface sample used for fretting tests. Top view and cross sectional view.

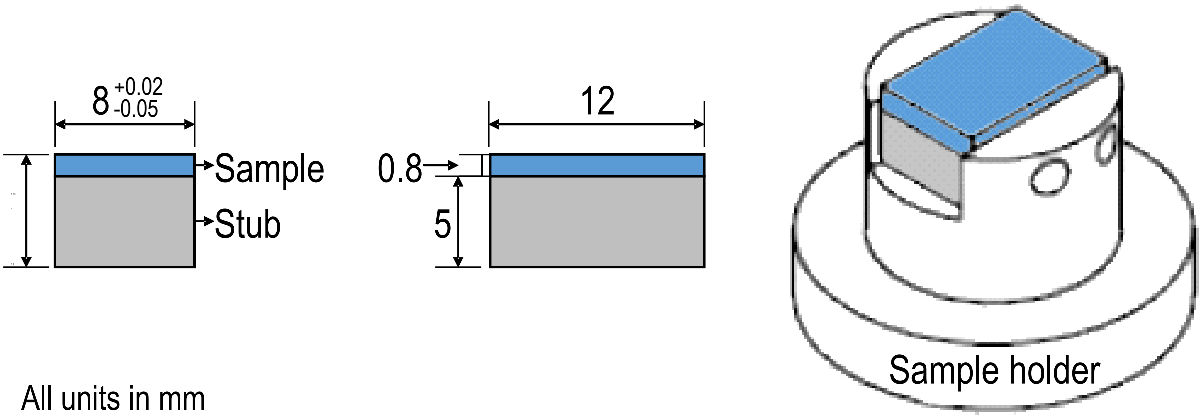

Figure 3.4 Dimensions of flat sample

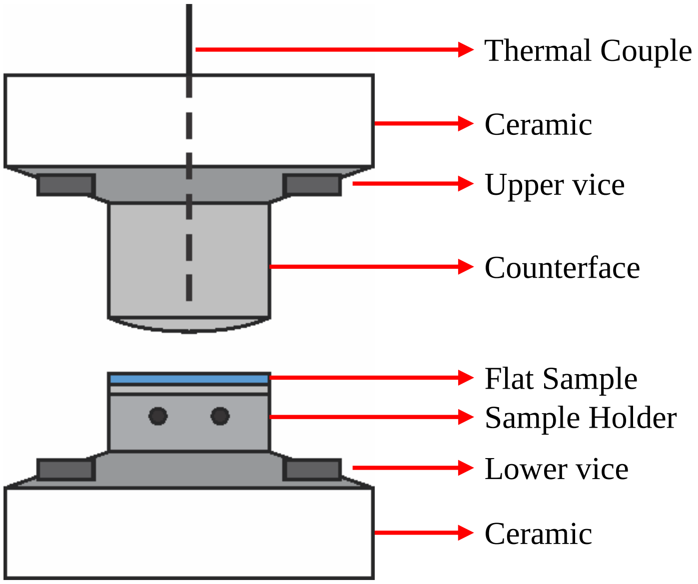

Figure 3.5 Counterface and flat sample mounted and aligned on Impact II, ready for experiment

3.2.2 Choosing test parameters

In order to evaluate how the coatings would fair in a fastener application, test parameters were chosen according to the stress experienced at the head of an M12 x 1.75 fastener when they are fastened to 75% tensile strength. Using the tensile strength of SAE 4340 steel [161], a typical steel used for fasteners, an estimated stress at the bolt head of an M12 x 1.75 fastener is calculated to be around 740 MPa. The displacement amplitudes were selected based on the clearances of fasteners used in the aerospace industry [162-164]. The chosen parameters resulted in tests lying in the stick, partial slip and gross slip regimes for Zn-Ni coatings. A summary of the fretting test parameters is shown in Table 3.1.

Table 3.1 Fretting test parameters

Coating	Cadmium	Zinc Nickel
Coating Properties		
E (GPa)	50	118
Poisson Ratio, ν	0.3	0.23
Test Counterface		
Geometry	Sphere	
Material	AISI 440C	
Counterface Radius (mm)	20	
Test Environment		
Temperature	Ambient Temperature	
Humidity	Ambient Humidity	
Test Parameters		
Frequency (Hz)	15	
Displacement Amplitude (µm)	70, 100 and 150	
# Cycles	10 000	
Test Type 1		
Max Hertzian Contact Stress (MPa)	740	
Average Hertzian Contact Stress (MPa)	493	
Normal Load (N)	434	133
Test Type 2		
Max Hertzian Contact Stress (MPa)	1110	
Average Hertzian Contact Stress (MPa)	740	
Normal Load (N)	1463	447

3.2.3 Characterization

Subsequent wear scars and counterfaces where imaged using a FEI Quanta 600 scanning electron microscope (SEM). The morphologies of the wear scars and counterfaces were studied using secondary electron (SE) images and energy dispersive x-ray (EDX) was used to characterize chemical differences. An accelerating voltage of 20 keV and a working distance of 10 mm were used for obtaining both SE images and EDX spectra.

Profiles of the wear scars and counterfaces were obtained using a confocal profilometry (Altisurf 500) and Mountains© surface imaging and metrology software was used to level the data and measure the depth of the wear scars. An example of wear scar depth measurement is shown in Figure 3.6.

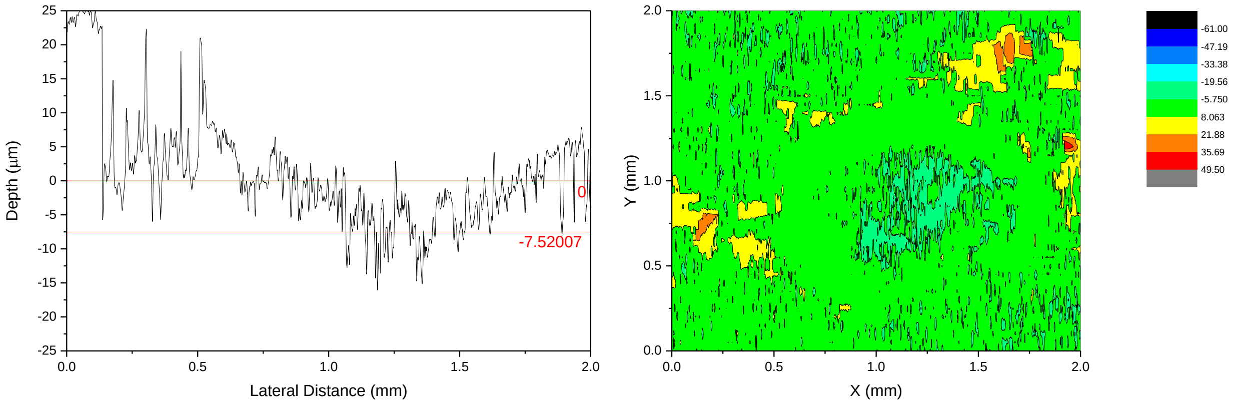

Figure 3.6 Example of wear scar depth measurement

3.3 Sliding wear tests

3.3.1 Test set-up

A custom built tribometer was used to perform reciprocating pin on disk sliding wear test (Figure 3.7). Details of the custom built tribometer can be found in [165]. Reciprocating motion was imposed using a motorized stage, while the pin remained motionless. A piezoelectric sensor was used to measure the lateral force and was sampled at a rate of 800 Hz. The average CoF is obtained through averaging the instantaneous CoF along the whole track in the forward and reverse directions. A sample of a friction loop is shown in Figure 3.8. CoF data at the end of the wear tracks are not considered, due to acceleration at the end of the wear track due to the reciprocating motion. Different weights were used to adjust and apply the normal loads of 3.5, 7 and 12 N. For all tests, a sliding speed of 14 mm/s was used. The tribometer arm and stage were enclosed in a plastic bag in order to control the humidity of the test. The humidity and temperature were monitored using a thermohygrometer. For high humidity tests, bottled dry air was flowed through distilled water in order to obtain humidity levels of 20, 40 and 60% relative humidity. For a relative humidity of 0%, compressed air was flowed through a filter regulator and then through a tube of desiccant to dry the air. At high humidity conditions tolerance of ± 5 % was maintained while for

0% RH, the humidity was maintained below 1 % RH. All tests were performed at room temperature of 22-25°C. AISI 440C steel spheres of 6.35 mm diameter was used to perform the tests.

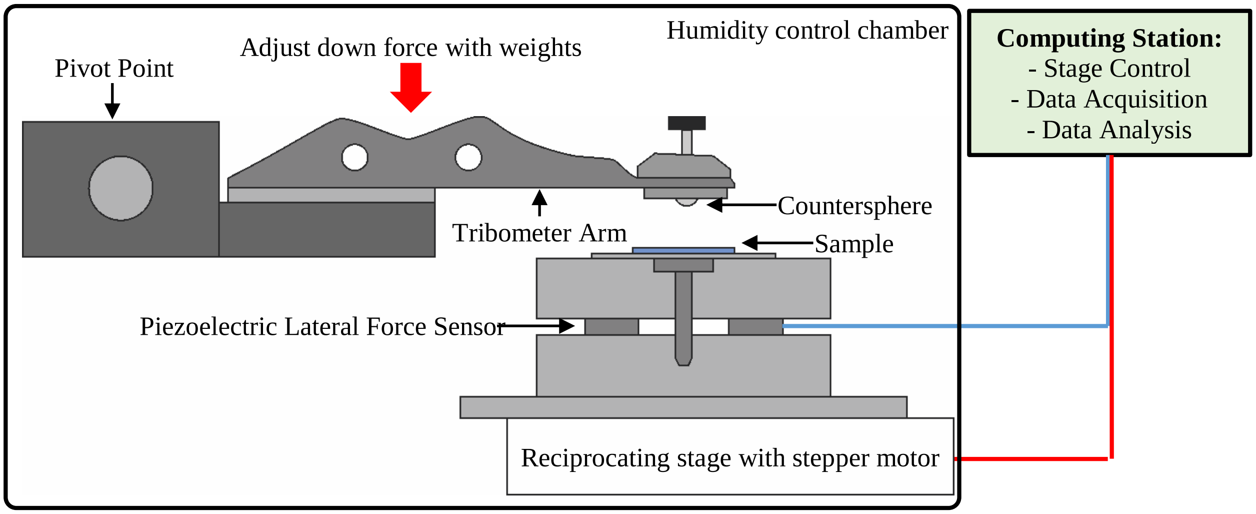

Figure 3.7 Tribometer set-up. Adapted from [166]

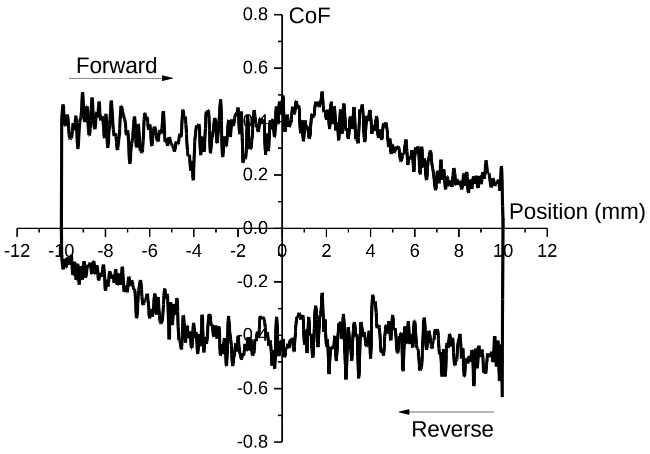

Figure 3.8 Friction loop

3.3.2 Characterization

After the sliding wear tests, the counterspheres and flat samples were separated to perform post-test characterization. SEM was used to characterize the morphologies of the wear track surface and counterspheres using secondary electrons (SE). EDX was also use to determine chemical changes on the wear track. In both cases, an accelerating voltage of 20 keV and working distance of 10 mm was used. 3D profiles of the wear tracks were obtained using an optical interferometer (Wyko NT8000) and an open source scanning probe microscopy analysis software Gwyddion v2.35 was used to process the data. Data drop-out points were interpolated using Laplace equation (Figure 3.9) and the surface was levelled by fitting through a plane using 3 points and bringing the levelled surface to zero. 2D profiles were obtained along the wear track (Figure 3.10), which were then imported to OriginPro 9.1 to calculate the wear area by integrating the area below the average surface. The wear areas were then averaged and multiplied by the track length and divided by sliding distance and normal force, resulting in a wear rate with units of mm^3/Nm.

3D profiles where the countersphere was in contact with the wear track were obtained using an optical interferometer (Zygo Newview) and analyzed using MX software. The data was levelled by fitting a sphere with a diameter of 6.35 mm on unworn portions of the countersphere (Figure 3.11). The unworn portions of the counterface were taken as the zero plane and the volume below the reference plane in the contact area was taken as sphere wear. Height parameters were measured by averaging an area either at the top of the transfer film or at the bottom of the wear scar.

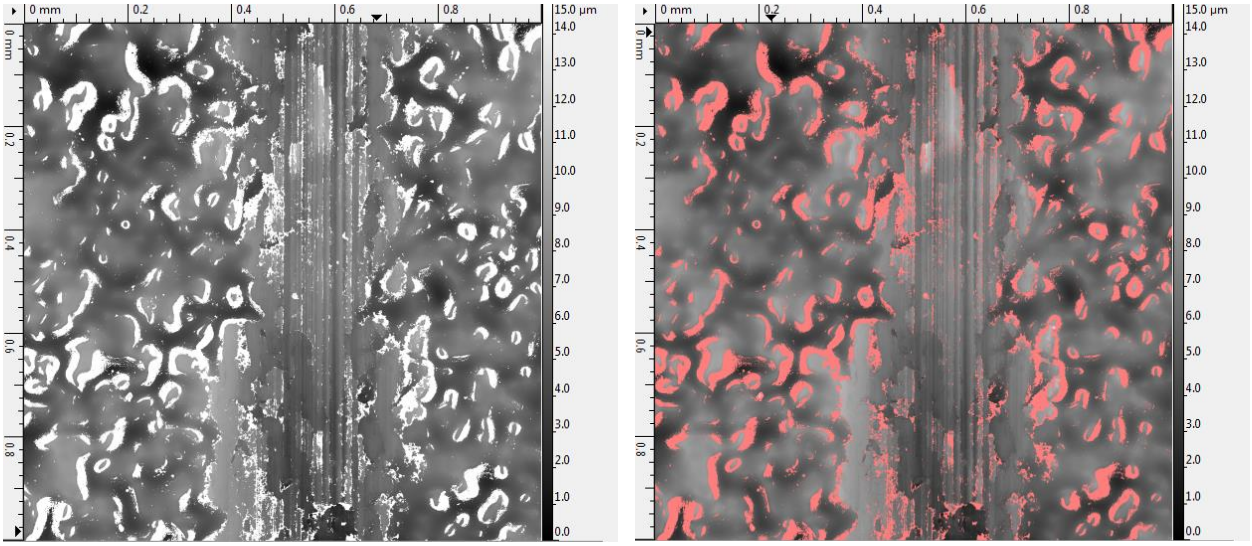

Figure 3.9 Example of data interpolation using Laplace equation

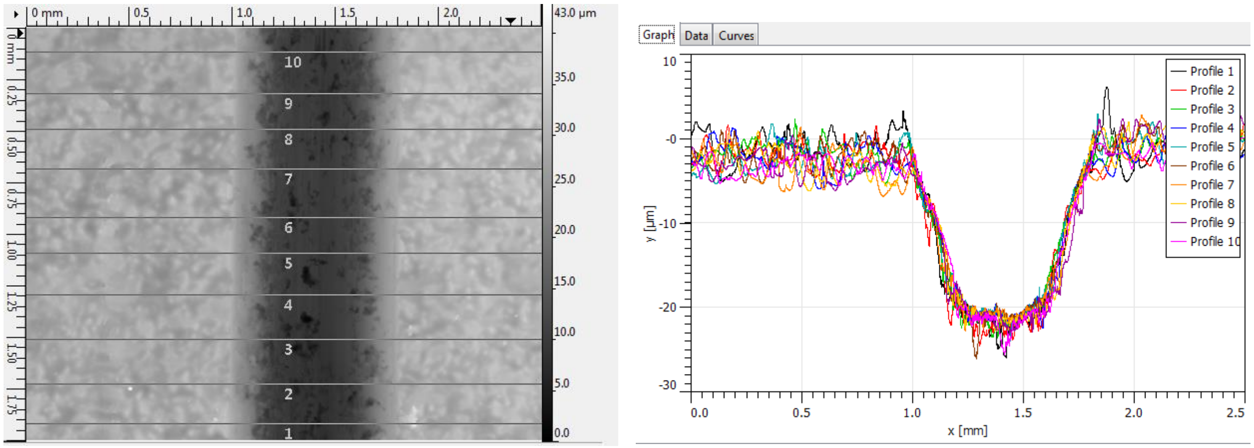

Figure 3.10 Example of 2D profile extraction

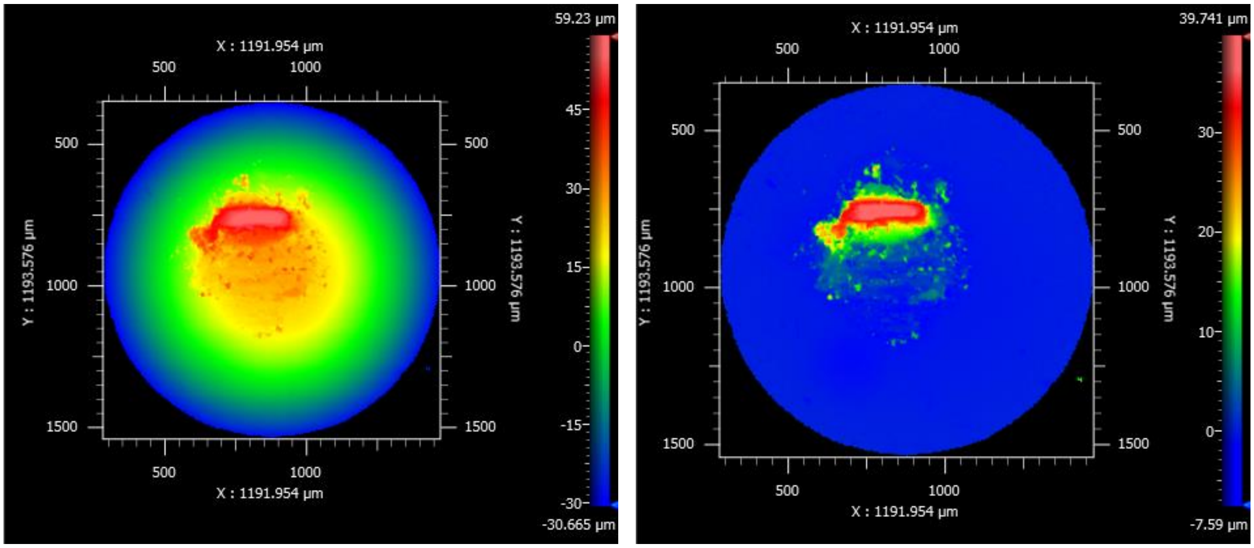

Figure 3.11 Example of data levelling by fitting a sphere

3.4 Material Properties

The tribological studies were conducted using three different Zn-Ni coatings that were commercially plated on low carbon steel plates (SAE 1006) of dimensions 100 x 160 x 0.8 mm^3. The differences of the plating parameters, such as current density, resulted in the variation of the coating morphology. XRD of the coatings showed that the coatings were single γ-phase Zn-Ni and is shown in Figure 3.12. EPMA were also performed on the coatings and showed Ni content ranging from 13-15 wt% and are report in Table 3.2. Reduced modulus and hardness were measured through nanoindentation using a peak load of 5 mN and are reported in Table 3.2.

Examples of the load-displacement curves and SPM images of the indents are shown in Figure 3.13-3.15. Coating thickness and roughness from profilometry are also report in Table 3.2.

Table 3.2 Zn-Ni and Cd sample coating measured properties and appearance in

Sample	Wt% Ni	Reduced Modulus (E_r, GPa)	Hardness (H, GPa)	Coating thickness (µm)	Roughness (R_a, µm)	Chapter
B-ZnNi	13.21 ± 0.28	144 ± 14	4.9 ± 0.7	14 ± 2	2.3 ± 0.3	5, 8
C-ZnNi	14.63 ± 0.05	127 ± 15	5.2 ± 0.3	13 ± 1	1.4 ± 0.2	4, 6, 7
D-ZnNi	15.65 ± 0.05	137 ± 12	6.6 ± 0.3	19 ± 4	2.9 ± 0.4	4, 6
LHE Cd [167]	--	60 ± 10	0.4 ± 0.1	11 ± 2	3.9 ± 0.4	5, 8

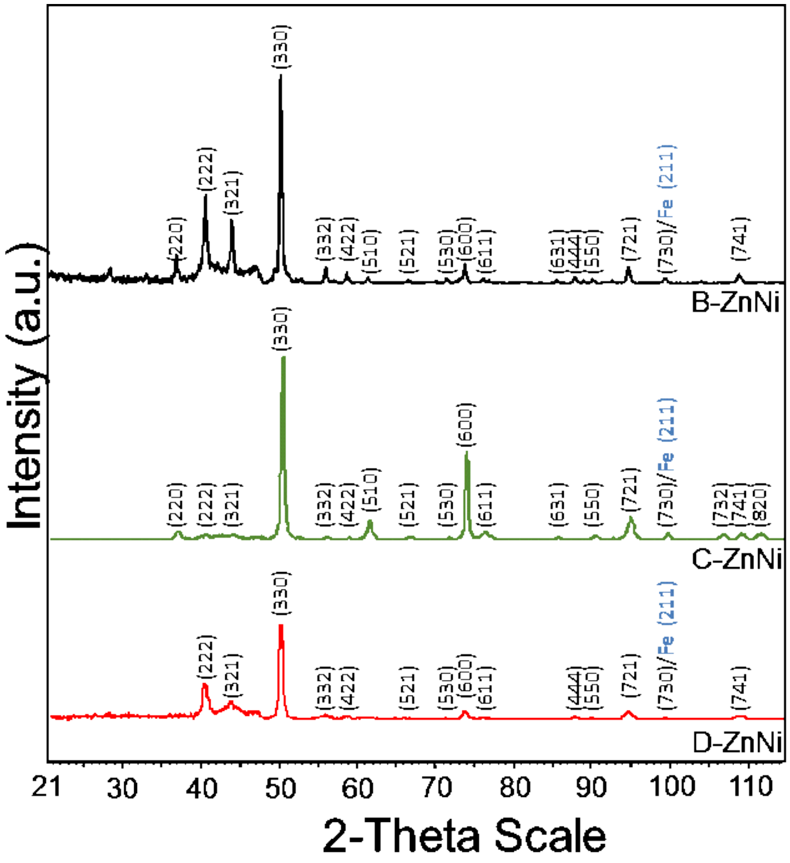

Figure 3.12 X-ray diffraction pattern of Zn-Ni coating samples

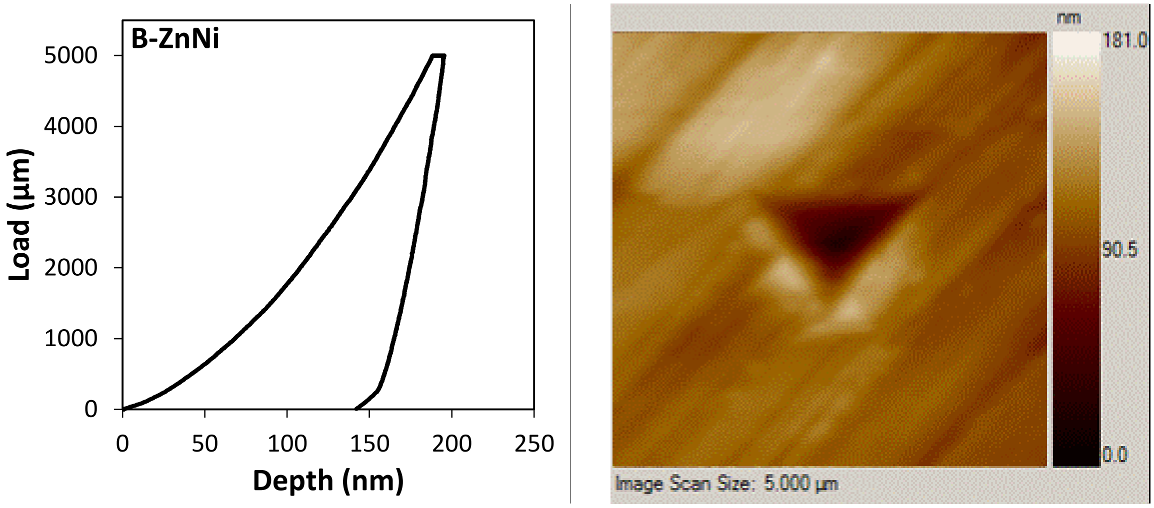

Figure 3.13 Example of load-displacement curve (left) and SPM image of indent (right) for B-ZnNi coating

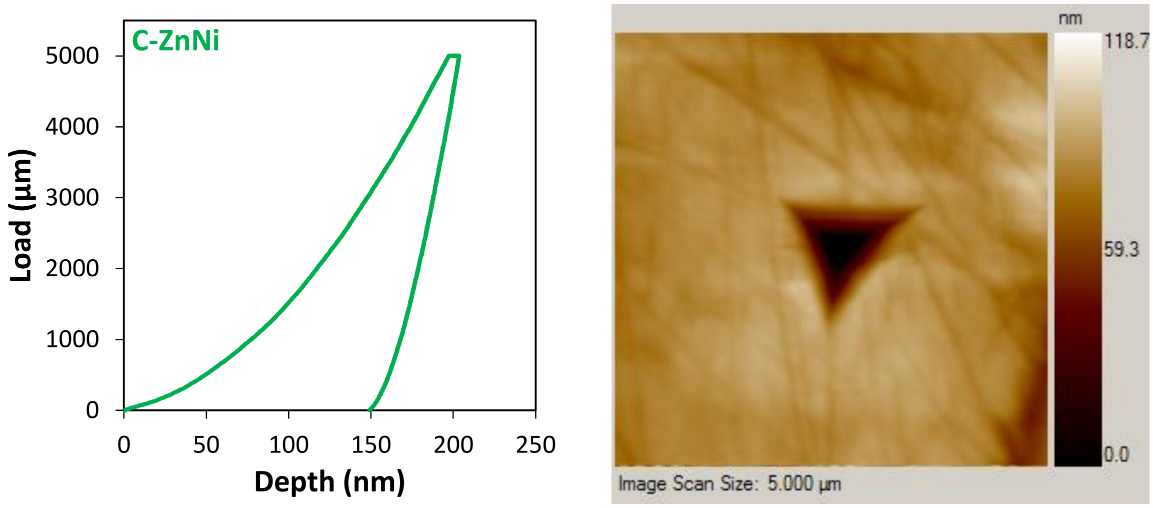

Figure 3.14 Example of load-displacement curve (left) and SPM image of indent (right) for C-ZnNi coating

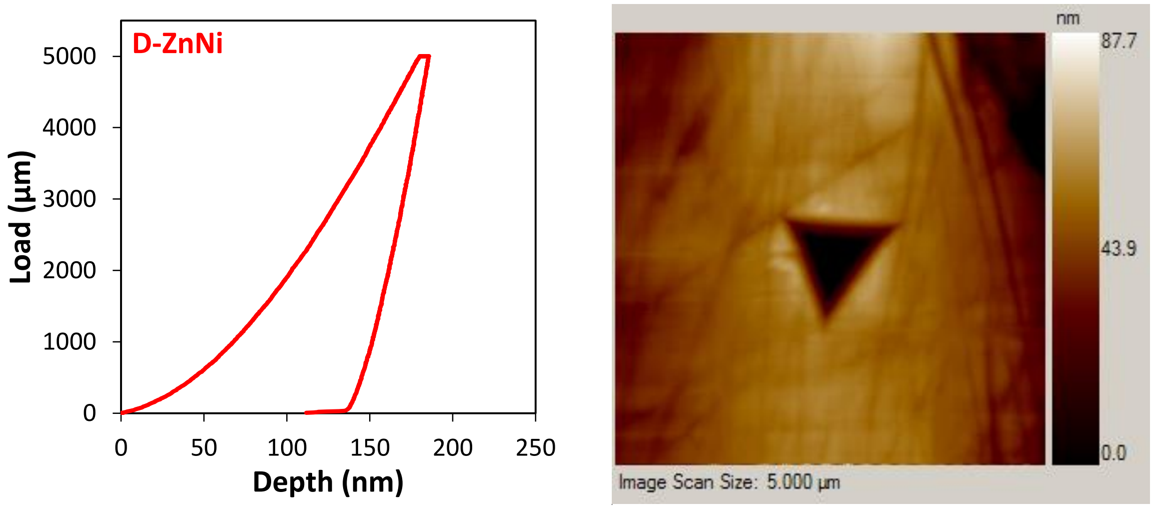

Figure 3.15 Example of load-displacement curve (left) and SPM image of indent (right) for D-ZnNi coating

Chapter 4

Fretting wear behavior of Zn-Ni alloy coatings

L. Lee, É. Régis, S. Descartes & R. R. Chromik*

Adapted from a paper of the same title published in *Wear*, 2015. **330–331**(0): p. 112-121

Abstract

Cadmium coatings are used in the aerospace industry primarily as a corrosion resistant plating, but also in applications where tribological properties are also important. Due to the carcinogenic nature of Cd, many coatings have been proposed as replacements, with Zn-Ni being the leading candidate. In this study, we examine two Zn-Ni coatings with differences in their surface roughness and their content of through thickness defects, including pores and cracks. The morphological differences between the coatings had a noticeable effect on their fretting wear behavior.

A customized tribometer, with a reciprocating rounded pin (AISI 440C steel) on flat (Zn-Ni) geometry, was used to perform fretting wear tests. The two morphologically different Zn-Ni coatings were tested at room temperature using ±70, 100 and 150 μm displacements and 133 N and 447 N constant normal loads. The surface of the wear scar was analyzed using scanning electron microscopy coupled with energy dispersive X-ray spectroscopy for changes in morphology and chemistry. Wear scar depth was measured from surface profiles obtained using confocal microscopy.

Hysteresis fretting loops of the tests showed that for both coatings, at ±70 μm displacement remains in no slip condition, at ±100 μm in the mixed slip condition, and at ±150 μm displacement remains in gross slip condition. Although the coatings had similar stick-slip behavior, the smoother coating has a slower progression of wear from the no slip to gross slip conditions than the rougher coatings. Also, differences in the wear scar morphologies are attributed to the differences in the coating morphologies, which resulted in different wear and velocity accommodation mechanisms.

4.1 Introduction

Zn-Ni alloy coatings are used in the aerospace and automotive industry for corrosion protection coatings of steel. They were developed in the 1980's as a replacement for cadmium coatings due to the carcinogenic and toxic nature of cadmium [1, 4, 168]. There are numerous corrosion properties studies of Zn-Ni coatings in the open literature, such as those found in [1, 8, 9, 21, 28, 29, 31]. However, these coatings are also used where tribological properties are critical to the performance, such as landing gear components and steel fasteners. Research on the tribological properties are fewer and focus on the sliding wear properties [3, 12, 28, 151]. Fretting wear properties of Zn-Ni coatings are also not widely studied although damages due to fretting are observed in aerospace assemblies, especially in joints, fasteners and tight fitting assemblies.

Fretting occurs when two surfaces are in relative oscillatory motion at very small amplitudes [169]. Vingsbo [149] divided fretting into three different regimes (1) stick, (2) mixed stick-slip and (3) gross slip. The stick regime can be obtained through fretting at very low displacement amplitudes and is characterized by mild asperity wear with unworn material between the contact junctions. The mixed stick-slip regime is characterized by a central area mildly worn area due to sticking of the counterface, which is surrounded by a highly worn area where slipping of the counterface occurs. The gross slip regime can be obtained through fretting at relatively large displacement amplitudes and is characterized by severe wear and sliding wear marks are observed. Ramalho *et al.* [170] compared the fretting fatigue behavior of electrodeposited zinc coated steel with uncoated steel. They found that zinc coatings markedly improved the wear resistance and fretting fatigue life of steel and observed much less adhesive wear and oxidation in the wear scars in the coated samples. Gao *et al.* [171] observed the fretting fatigue properties of Ni-P coated steel, and found that Ni-P coatings improved the fretting fatigue resistance of mild strength steels by modifying the tribological behavior of the substrates due to the high hardness of Ni-P coatings.

Tribological properties are not intrinsic to a material, but rather are dependent on many conditions such as coupled materials, surface roughness, temperature, humidity, etc. Commercially available Zn-Ni alloy coatings are mostly electrodeposited on the substrates and depending on the electrodeposition conditions, the surface morphology can differ for similar coating compositions. With other test and material parameters kept similar (normal load, humidity, material composition, etc.), surface morphology and roughness can have a strong effect on the tribological properties. In early studies of fretting wear by Waterhouse [17], the effects of roughness on the surface damage due to wear showed that a rougher surface suffered less fretting damage than a better surface finish. This was attributed to two mechanisms: a rough surface is able to “take-up more tangential movement” due to a higher plasticity index and work hardening of asperities, and also wear debris, which can contribute to higher wear rate, can be removed from the contact by falling into the hollows of the surfaces [17]. More recently, Kubiak *et al.* [15] studied the effects of surface roughness on the fretting behavior of AISI 1034 steel and Ti-6Al-4V and found that with rougher surfaces, the CoF is lower and the wear rate is higher in both material systems.

In this study, two Zn-Ni alloy coatings from different commercially available sources with different surface morphologies were subjected to fretting in order to evaluate the effects of surface morphology. By varying the displacement amplitude, contact conditions under the stick, mixed slip and gross slip regimes were achieved. The coatings were tested under the three regimes in order to compare their fretting wear behaviors by observations of the fretting loops and wear scars through SEM imaging and profilometry.

4.2 Methods

4.2.1 Coating deposition

Two commercially available zinc-nickel alloy coatings were used for this study. Zinc-nickel alloy coating was deposited on 100 x 160 mm^2, 0.8 mm thick low carbon steel (SAE 1006). The coatings were deposited using 2 commercially available plating processes in an industrial pilot plating tank as follows:

For C-ZnNi, an alkaline NaOH (120-135 g/L) based plating solution which contains zinc (7-10 g/L) and nickel (1-1.8 g/L) was used. The plating operation was performed at 21-25 °C with a current density of 10 mA/cm^2. The as plated samples were then passivated using a blue trivalent chrome passivate and then baked at 200 °C for 24 hours [172, 173].

For D-ZnNi, an alkaline NaOH (135 g/L) solution was used with Zn and Ni metal concentration maintained at 10-11:1 ratio and the pH maintained at 12-13.5. The plating operation was performed at 25 °C with a current density of 50 mA/cm^2. The substrates were plated for 20 minutes in order to obtain a coating thickness between 15-20 μm. Prior to plating, the substrates were grit blasted and acid pickled using HCl. The plated samples were passivated using a blue trivalent conversion coating and baked at 200 °C for 24 hours [29].

An electron probe micro-analyzer (EPMA) test was performed on the coatings in order to assess the coating composition, and C-ZnNi contained 14.63wt% ±0.05 Ni and D-ZnNi contained 15.65wt% ±0.58 Ni. Standards of zinc and zinc sulfide were used to assess the content of zinc and standards of nickel and nickel oxide were used to assess nickel content. The higher standard deviation in D-ZnNi coatings is due to higher surface roughness.

4.2.2 Characterization

The morphologies of the coatings were observed using scanning electron microscopy (SEM) in their as received and post-wear states. Chemical composition of the wear scars and transfer films were obtained through energy dispersive X-ray spectroscopy (EDX). SEM and EDX were performed using a FEI Quanta 600 microscope with a tungsten filament source. An accelerating voltage of 20kV was used. Selected specimens were observed in cross section and were cut with a diamond blade and prepared metallographically.

X-ray diffraction (XRD) was used to confirm the phase of the coating. A Bruker Discover D8-2D, fitted with a Co-Kα source, was used in the standard θ-2θ mode on the unworn coatings.

Profilometry was performed on the wear scars. An Altisurf 500 confocal microscope coupled with Phénix 2 software was used to obtain the profile maps.

Mechanical properties of the coatings were determined using nanoindentation with a Ubi3 nanoindenter (Hysitron Incorporated, Minneapolis, MN, USA) and a diamond Berkovich tip. Indentation was carried out on cross sections of the coatings with a peak load of 5 mN, a loading/unloading rate of 1 mN/s and 2 second hold time at peak load. Hardness and elastic modulus were calculated using the Oliver and Pharr method [159].

4.2.3 Fretting wear test

Fretting wear tests were performed using a custom built tribometer at Laboratoire de Mécanique des Contacts et des Structures (LaMCoS, INSA, Lyon, France). An AISI 440C steel counterface with a 20 mm curvature was used. Two initial loads were used to evaluate the coating: 133 N and 447 N. Using Young's Modulus of 118 GPa and Poisson's Ratio of 0.23 for Zn-Ni [174, 175], this corresponds to an initial Hertzian contact stress of 740 MPa and 1110 MPa and a Hertzian contact radius of 292 μm and 439 μm, respectively. In order to evaluate the stick-slip behaviors, tests were run with frequency of 15 Hz and displacement amplitudes of ±70, 100 and 150 μm. In doing so, the degree of exposure of the contact area to the environment will be different (Figure 4.1). As some of the motion can be taken up by the first bodies and structure, the imposed displacement amplitudes will not be the same as the actual slip in the contact [141]. The tests were performed in ambient temperature (23-25 °C) and humidity (35-40% relative humidity). Measurements of the tangential force, normal force and displacement were recorded throughout the test.

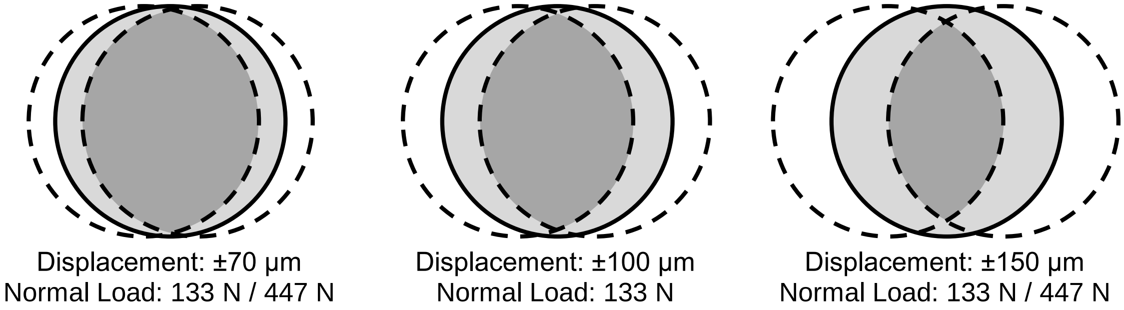

Figure 4.1 Schematic of theoretical contact exposure to environment
Light gray = original contact area, dark gray = unexposed area

4.3 Results

4.3.1 Coating characterization

SEM micrographs of the two different types of coatings for the surface morphology and cross section morphology are shown in Figure 4.2. From the surface morphology, C-ZnNi coatings shows a smooth surface formed through fine platelets, with gradual rises and falls. No through thickness porosity is evident on the surface morphology. However, in the cross section, although the coating appears well adhered to the substrate, through thickness cracks and small porosities are observed. D-ZnNi coatings are formed through agglomeration of platelets in hemispherical shapes, which forms hills and valleys with steep slopes, causing large through thickness porosities from the surfaces. Cross sections of the coating shows good adhesion of the coating to the substrate. Small porosities and cracks along the agglomerations are observed. The differences of the surface morphologies has an effect on the surface roughness. C-ZnNi has the lower roughness (1.35μm ± 0.19 R_a) while D-ZnNi has the higher roughness (2.90μm ± 0.35 R_a). In both coatings, through thickness defects are observed which allows trapped hydrogen from the electrodeposition process to escape from the substrate to the environment during a subsequent baking process at 200 °C, making it less susceptible to hydrogen embrittlement [31, 176].

XRD was performed on the as received coatings in the standard θ-2θ mode, and both diffraction patterns are shown in Figure 4.3. Both coatings show peaks corresponding to γ-ZnNi despite the differences in the intensities of the peaks. The discrepancies in the intensities of the peaks may be due to differences in surface morphology and crystallographic orientation.

Nanoindentation on the cross sections of the coatings showed small differences between the mechanical properties. The reduced elastic moduli were similar, $E_r = 127 \pm 15$ GPa for C-ZnNi and 137 ± 12 GPa for D-ZnNi. However, the hardness of the C-ZnNi coating ($H = 5.2 \pm 0.3$ GPa) was smaller than that for the D-ZnNi coating ($H = 6.6 \pm 0.3$ GPa). The differences in hardness may be attributed to the slightly higher Ni content in D-ZnNi coatings, but may also be related to differences in the crystallographic orientation.

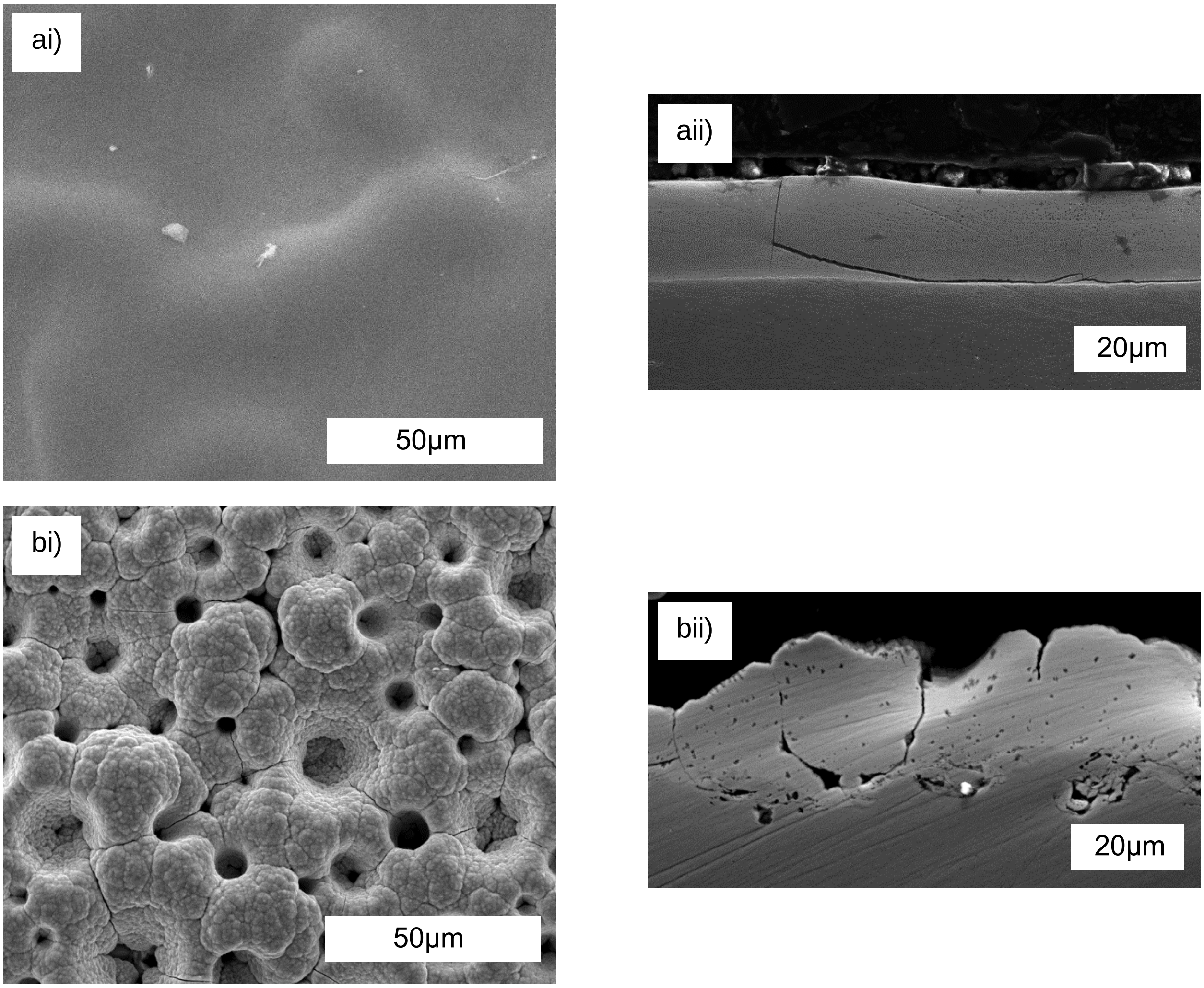

Figure 4.2 (a) C-ZnNi and (b) D-ZnNi SEM images of i) surface morphology ii) cross section

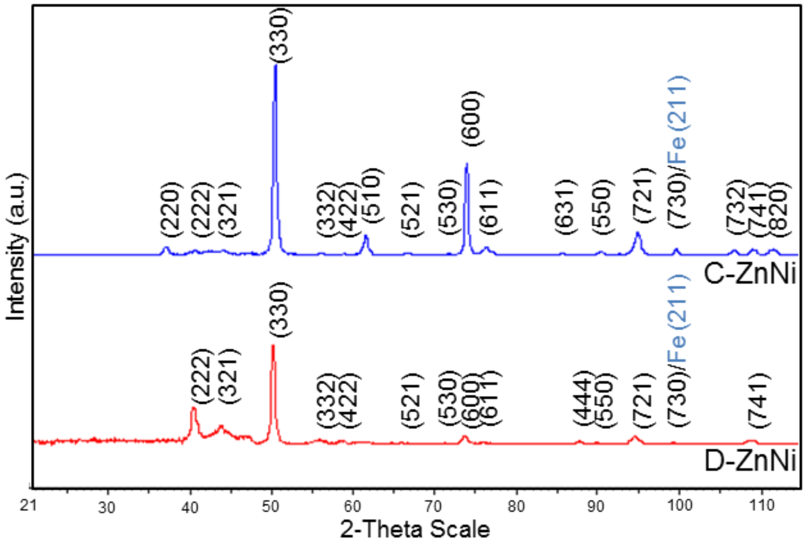

Figure 4.3 Diffraction patterns of C-ZnNi and D-ZnNi

4.3.2 Fretting wear test

Plotting the tangential force versus the tangential displacement gives the fretting wear hysteresis loop, which provides information on the stick-slip phenomena. The area enclosed by the loop (Figure 4.4) is indicative of the dissipated energy due heat, noise, material structure transformation, chemical reactions and third body behavior [177, 178]. Fretting hysteresis loops for stick regime shows a closed loop indicating very little wear occurs in this regime as little energy is lost. For the gross slip regime, a trapezoidal loop is observed due to the large amount of energy dissipated often associated with wear [169, 177, 178].

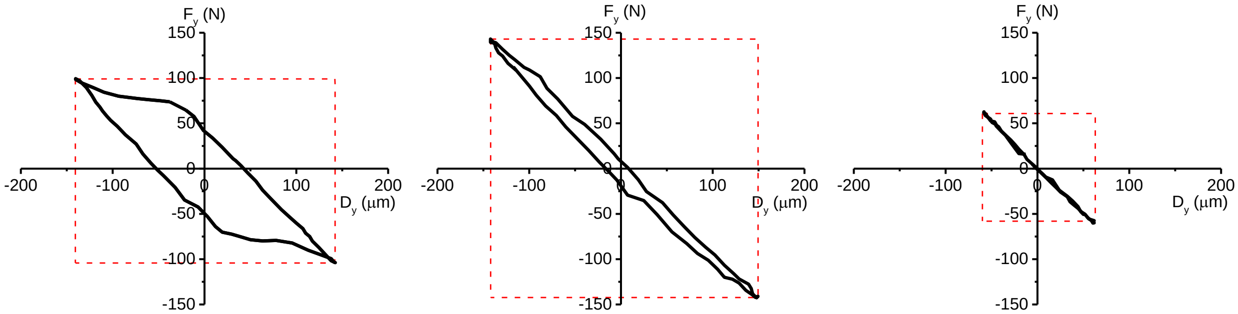

Figure 4.4 Typical shapes of (a) trapezoidal, (b) elliptical and (c) closed fretting loops from tests

Figure 4.4 shows examples of trapezoidal, elliptical and closed fretting loops from typical data obtained from the tests. The energy ratio is defined as the dissipated energy (E_d) over the total energy (E_t) from the fretting loops [150]. The energy ratio (E_d/E_t) of the tests are plotted versus the number of cycles in order to observe the evolution of the fretting wear regimes over time for every 225 cycles (see Figure 4.5). When the energy ratio lies below 0.2, the fretting wear regime is defined as the stick regime, whereas above 0.2 is the gross slip regime [150]. For a normal load of 133 N and a displacement amplitude of ±70 µm, D-ZnNi coatings shows an energy ratio below 0.2 and closed fretting loops throughout the tests (Figure 4.5a), indicating stick behavior at the contact at these conditions. In contrast, for C-ZnNi coatings, the energy ratio went slightly above 0.2 in the initial cycles, and fretting loops were open and trapezoidal in shape. However the energy ratio quickly stabilized after 2000 cycles to values below 0.2 and the fretting loops became closed (Figure 4.5a). This indicates that in the initial 2000 cycles C-ZnNi showed slip behavior and after 2000 cycles exhibited stick behavior until the end of the test. Looking at the wear scar depths shown in Figure 4.6, both coatings showed shallow wear scar depths, indicating mild amount of wear.

The energy ratio and fretting loops for tests performed with displacement amplitude of ±100 μm and 133 N normal load are shown in Figure 4.5b. In both coatings, the energy ratio starts above 0.2 and with an open trapezoidal fretting loop and transitions to an energy ratio below 0.2 with a closed fretting loop, indicating mixed slip behavior. The transition time for C-ZnNi is earlier than D-ZnNi. C-ZnNi also shows a gradual transition to the stick behavior whereas for D-ZnNi the transition is much more abrupt and also shows a more erratic behavior in the earlier cycles with multiple transitions between the sticking and slipping behavior, which is indicated by the opening and closing of the fretting loops and fluctuating energy ratios. Figure 4.6 of the wear scar depth also shows a deeper wear scar with D-ZnNi than with C-ZnNi, indicating that moderate wear occurred with D-ZnNi, whereas for C-ZnNi only mild wear occurred.

At ±150 μm displacement amplitude and 133 N normal load tests, a high energy ratio and open trapezoidal fretting load prevails throughout the tests for the 2 coatings, shown in Figure 4.5c. This indicates a gross slip regime throughout the tests. A drop in the energy ratio due to closed fretting loop is observed in D-ZnNi at around 3000 cycles, whereas for C-ZnNi, the evolution of the energy ratio and fretting loop shapes are more constant. From the wear scar depth shown in Figure 4.6, although the wear depths are large for both coatings, D-ZnNi shows a larger wear depth than C-ZnNi.

For the normal load of 447 N in both ZnNi coatings, tests with displacement amplitudes of ±70 μm fretting loops were closed throughout the test, resulting in an energy ratio well below 0.2 and in the stick regime. Increasing displacement amplitudes to ±150 μm showed elliptical fretting loops and a higher energy ratio (C-ZnNi 0.063 ± 0.004, D-ZnNi 0.069 ± 0.001) indicating partial slip behavior. Shallow wear scar depths were observed for displacement amplitudes of ±70 μm and ±150 μm for both coatings, indicating mild amounts of wear.

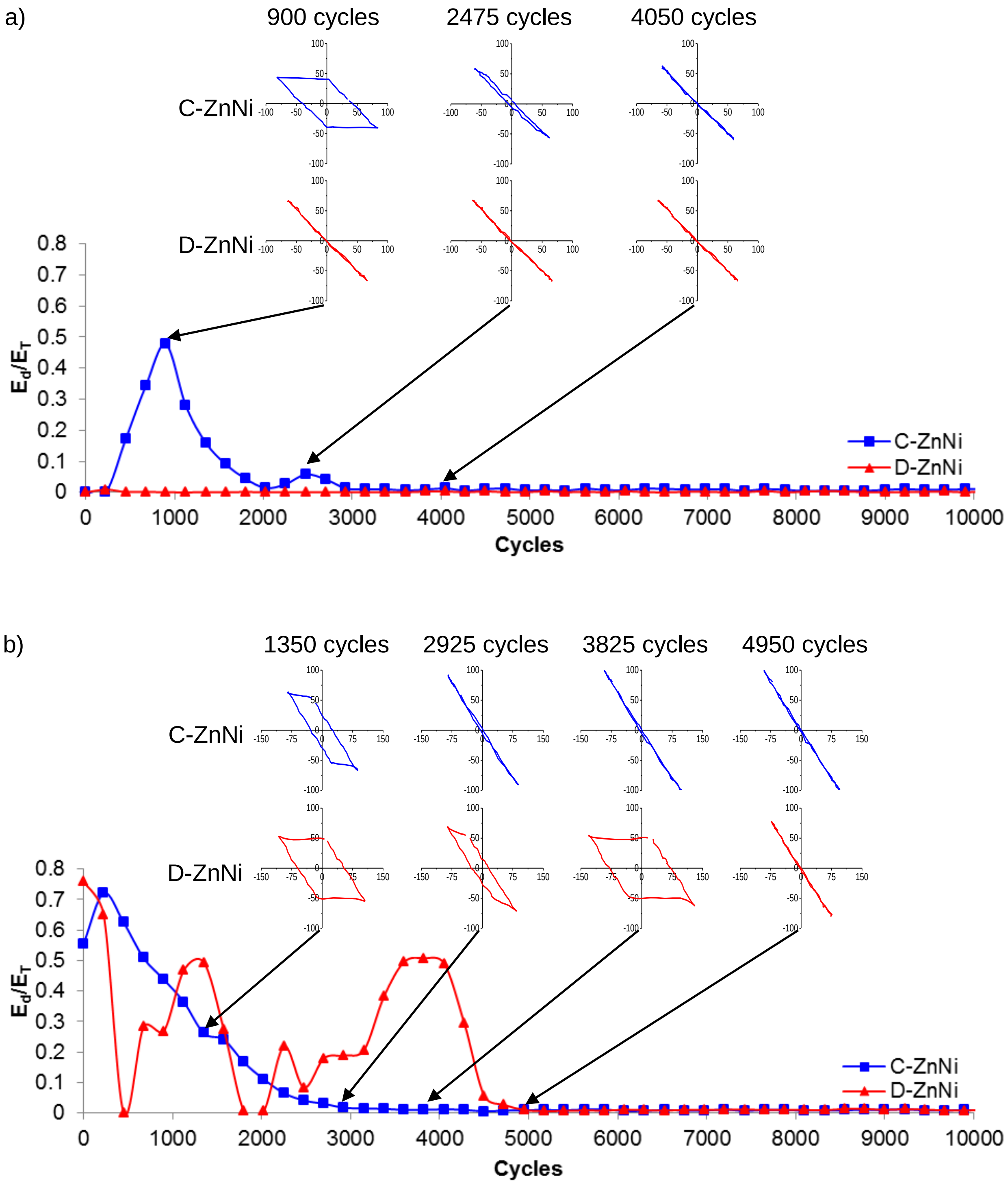
a)
900 cycles
2475 cycles
4050 cycles
C-ZnNi
D-ZnNi
E_d/E_T
0.8
0.7
0.6
0.5
0.4
0.3
0.2
0.1
0
0
1000
2000
3000
4000
5000
6000
7000
8000
9000
10000
Cycles
C-ZnNi
D-ZnNi
b)
1350 cycles
2925 cycles
3825 cycles
4950 cycles
C-ZnNi
D-ZnNi
E_d/E_T
0.8
0.7
0.6
0.5
0.4
0.3
0.2
0.1
0
0
1000
2000
3000
4000
5000
6000
7000
8000
9000
10000
Cycles
C-ZnNi
D-ZnNi

c)

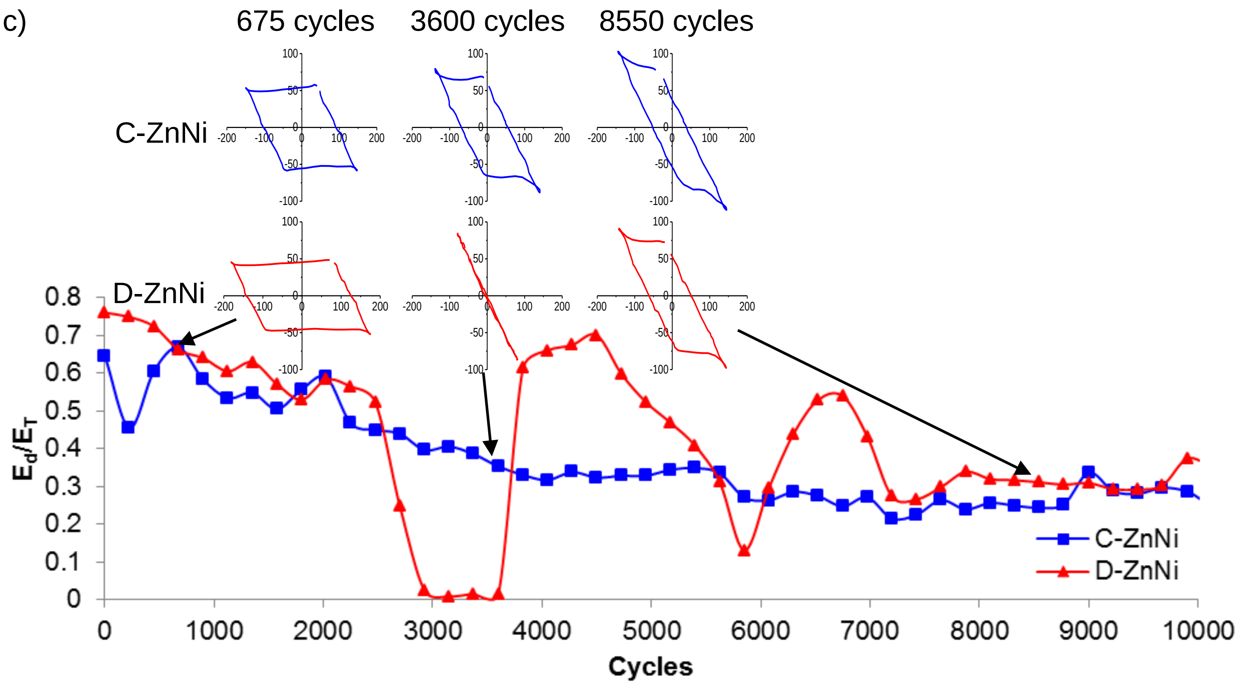
675 cycles
3600 cycles
8550 cycles
C-ZnNi
D-ZnNi
100
50
0
-50
-100
-200
-100
0
100
200
0.8
0.7
0.6
0.5
0.4
0.3
0.2
0.1
0
E_d/E_T
0
1000
2000
3000
4000
5000
6000
7000
8000
9000
10000
Cycles
C-ZnNi
D-ZnNi

d)

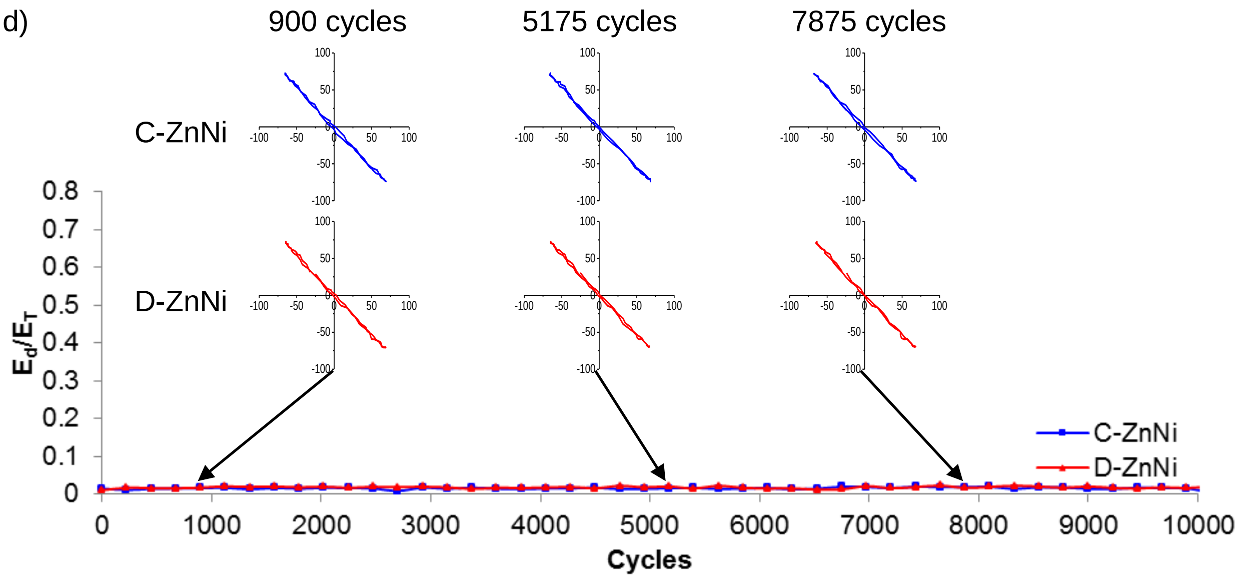
900 cycles
5175 cycles
7875 cycles
C-ZnNi
D-ZnNi
100
50
0
-50
-100
-100
-50
0
50
100
0.8
0.7
0.6
0.5
0.4
0.3
0.2
0.1
0
E_d/E_T
0
1000
2000
3000
4000
5000
6000
7000
8000
9000
10000
Cycles
C-ZnNi
D-ZnNi

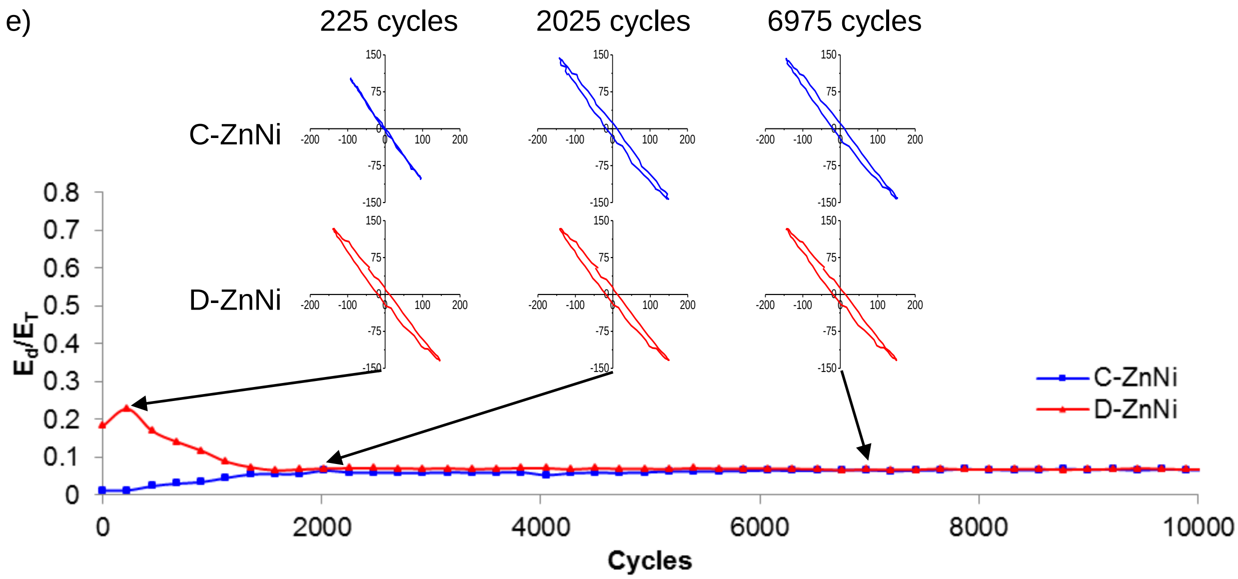

Figure 4.5 Energy ratio evolution of C-ZnNi and D-ZnNi at (a) ± 70 µm (b) ± 100 µm and (c) ± 150 µm displacement amplitude and 133 N normal load and (d) ± 70 µm and (e) ± 150 µm displacement amplitude and 447 N normal load for 10,000 cycles

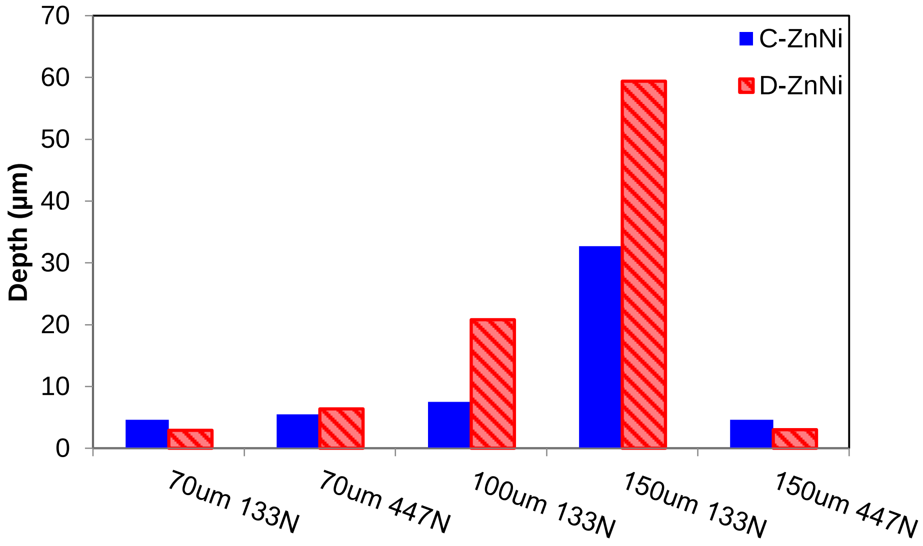

Figure 4.6 Fretting wear scar depths of C-ZnNi and D-ZnNi after 10,000 cycles of wear

4.3.3 Ex situ wear scar analysis

SEM images of the wear scars were obtained post-fretting wear test and are shown in Figure 4.7-12. Tests with displacement amplitude of ±70 µm and 133 N normal load after 10,000 cycles are shown in Figure 4.7, where only mild wear occurred in both coatings. C-ZnNi coatings (Figure 4.7a) show more wear particles at this condition. This may be due to slip occurring at the beginning of the test where the energy ratio rises above 0.2 before stabilizing to near zero values (Figure 4.5a). The wear scar is characterized by plastic flow and small regions of unworn coating in a central region, delamination and oxidized wear particles at the edge of the contact and periphery. The counterface of the C-ZnNi coating shows transferred material at the center and oxidized wear debris adhering to the sides. D-ZnNi coatings (Figure 4.7b) show less wear debris compared to C-ZnNi. Slight deformation of the asperities is observed and small oxidized wear particles are observed at the hollows of the coating. This is in agreement with the near zero energy ratio and closed fretting loops throughout the test observed in Figure 4.5a. Wear debris are not observed on the counterface of D-ZnNi coatings test and instead gouges are observed.

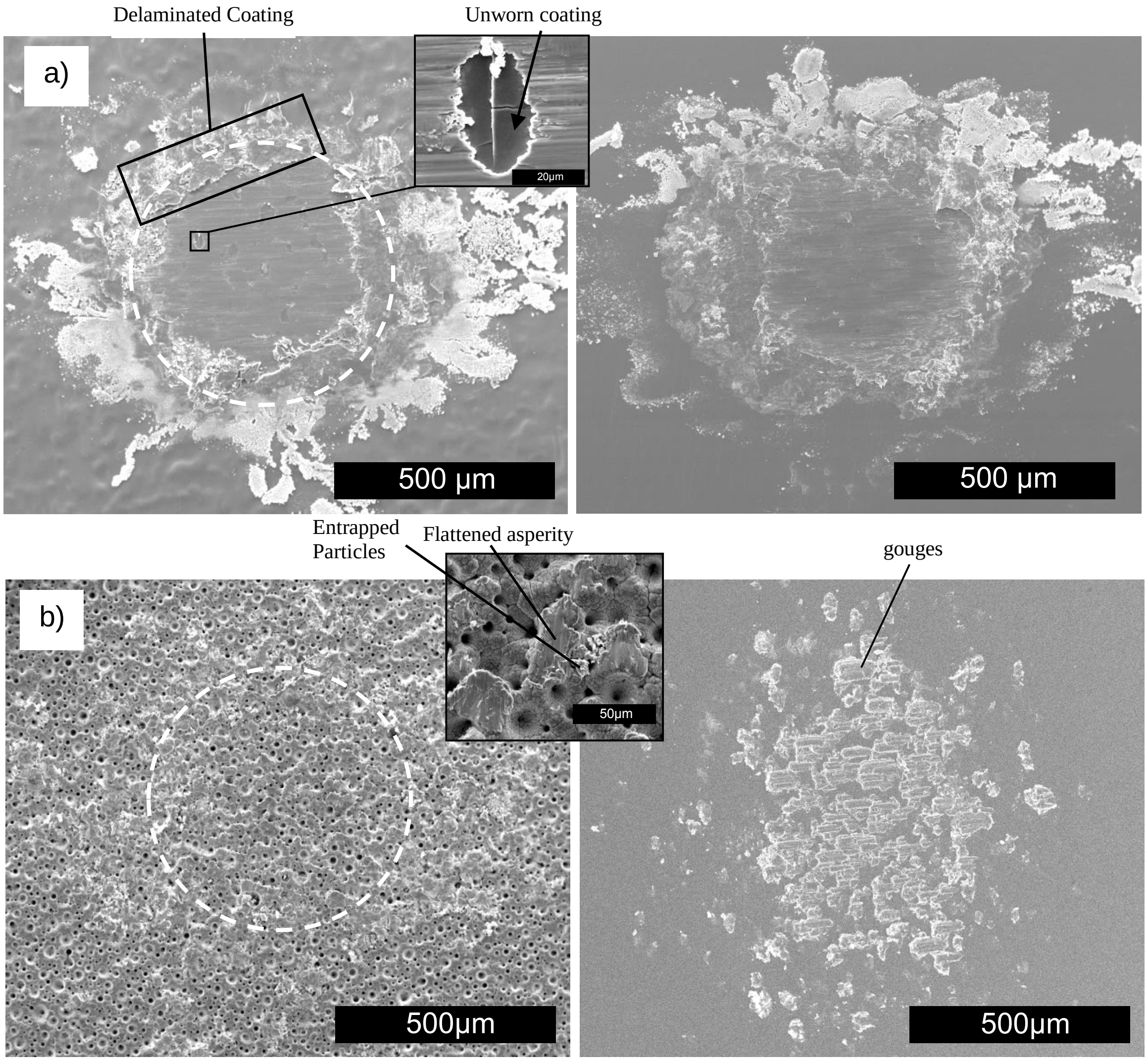

Figure 4.7 Fretting wear scar (left) and counterface (right) at contact condition of 133 N normal load and ±70 µm displacement amplitude after 10,000 cycles (a) C-ZnNi and (b) D-ZnNi. Sliding direction ↔

Figure 4.8 shows the tests performed at ±70 μm displacement amplitude and 447 N normal load. After 10,000 cycles, minimal wear and only slight wearing of the asperities are observed for both coatings. For C-ZnNi coatings (Figure 4.8a), cracks formed in the contact area. Junctions where the coating and counterface meet appear to be worn off and small oxide particles reside within the worn junctions. Some sliding marks are also observed inside the wear scar, indicating plastic flow of material. At the edge of the contact area, more wear particles are observed than at the central region of the wear scar. Smearing occurred on the counterface where it was in contact with the C-ZnNi coatings. D-ZnNi coatings (Figure 4.8b) underwent asperity wear through plastic deformation. Wear particles are also observed in the hollows of the coating. There also appears to have re-deposited wear particles on the worn asperities. Oxidized small wear particles were observed in the edge of the contact area. Similar wear scar morphologies but slightly more severe wear and larger oxide particles at the edge of the wear scar were observed when increasing the displacement amplitude to ±150 μm. Gouges formed on the counterface where the asperities of D-ZnNi coatings were in contact with the counterface.

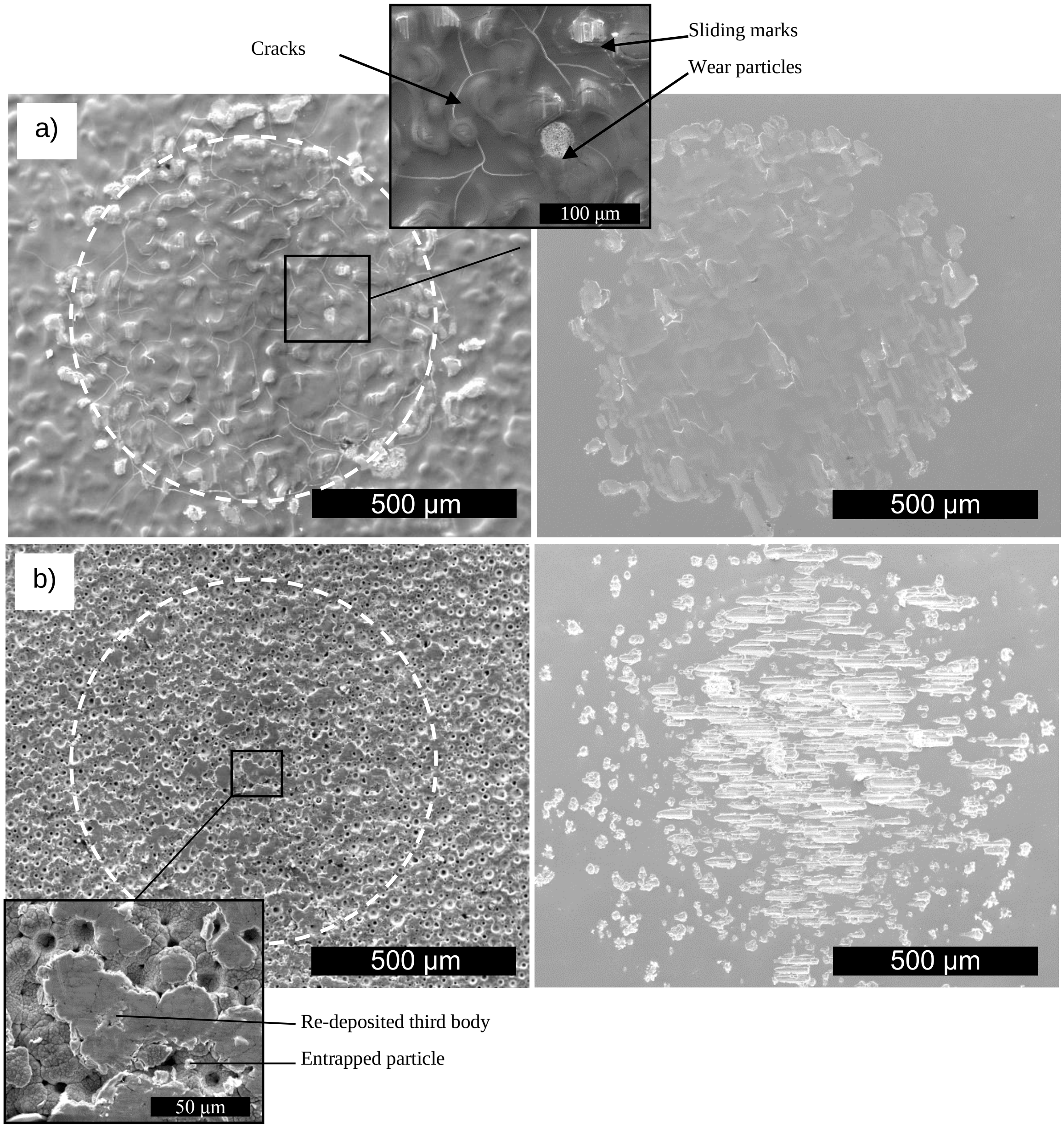

Figure 4.8 Fretting wear scar (left) and counterface (right) at contact conditions of 447 N normal load and ±70 µm displacement amplitude after 10,000 cycles (a) C-ZnNi and (b) D-ZnNi. Sliding direction ↔

Increasing the displacement amplitude from ±70 µm to ±100 µm at a normal load of 133 N caused an increase in wear for both coatings, as seen by observation of the wear scars in Figure 4.9-10. After 10,000 cycles, C-ZnNi (Figure 4.9a) and D-ZnNi (Figure 4.10a) coatings both showed plastically deformed material at the central region of the wear scar surrounded by chunks of detached material and oxidized wear particles in the annular area around the central region (Figures 9b2 and 10b1.

Difference between the C-ZnNi and D-ZnNi coatings for ±100 μm and 133 N load was the shape of the extruded wear particles, as with C-ZnNi coatings, flatter flake-like compacted oxides formed, while with D-ZnNi coatings, thin flakes-like compacted oxides were formed (Figures 9b1 and 10b2). At the center of the wear scar for C-ZnNi coatings, EDX showed no iron peaks (Figure 4.9c), indicating a layer of coating material is still present. D-ZnNi coatings have a larger wear scar and EDX at the center shows presence of iron but not chromium, which may indicate substrate exposure rather than sources of iron from the counterface. These observations are consistent with the wear scar depths (Figure 4.6). D-ZnNi shows a higher wear depth which is slightly larger than the coating thickness, whereas C-ZnNi shows a moderate wear depth which is lower than the coating thickness. Thus substrate exposure is more likely for D-ZnNi than C-ZnNi.

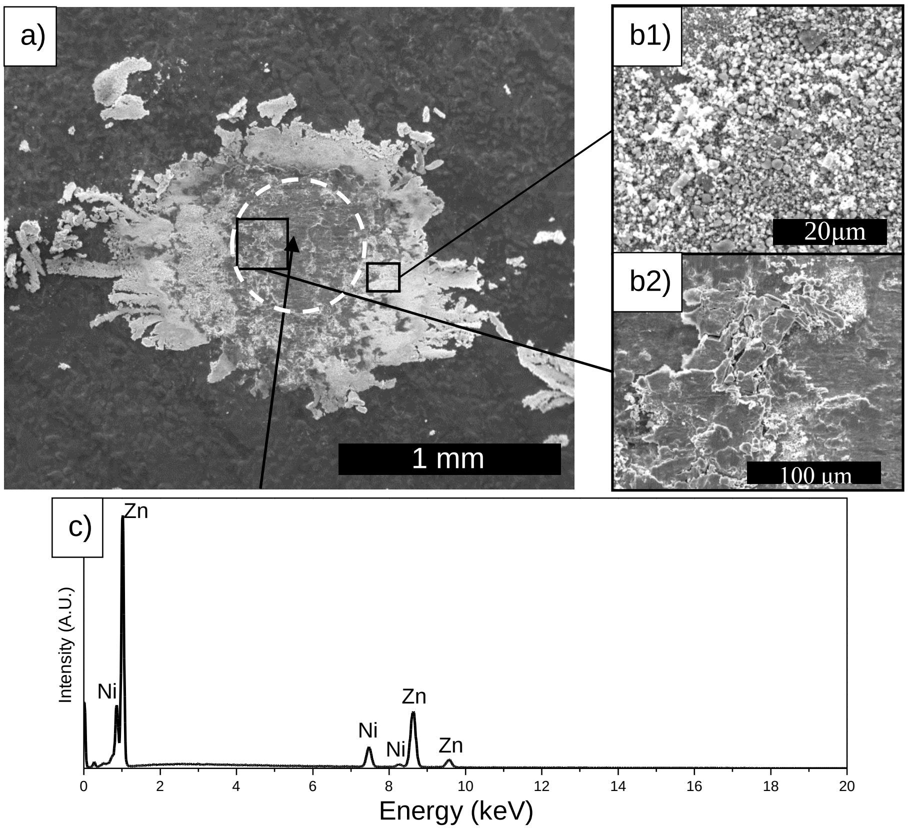

Figure 4.9 (a) Fretting wear scar, (b) third body morphology and (c) EDX spectrum of center area of C-ZnNi coating at contact conditions 133 N normal load and ±100 μm displacement amplitude after 10,000 cycles. Sliding direction ↔

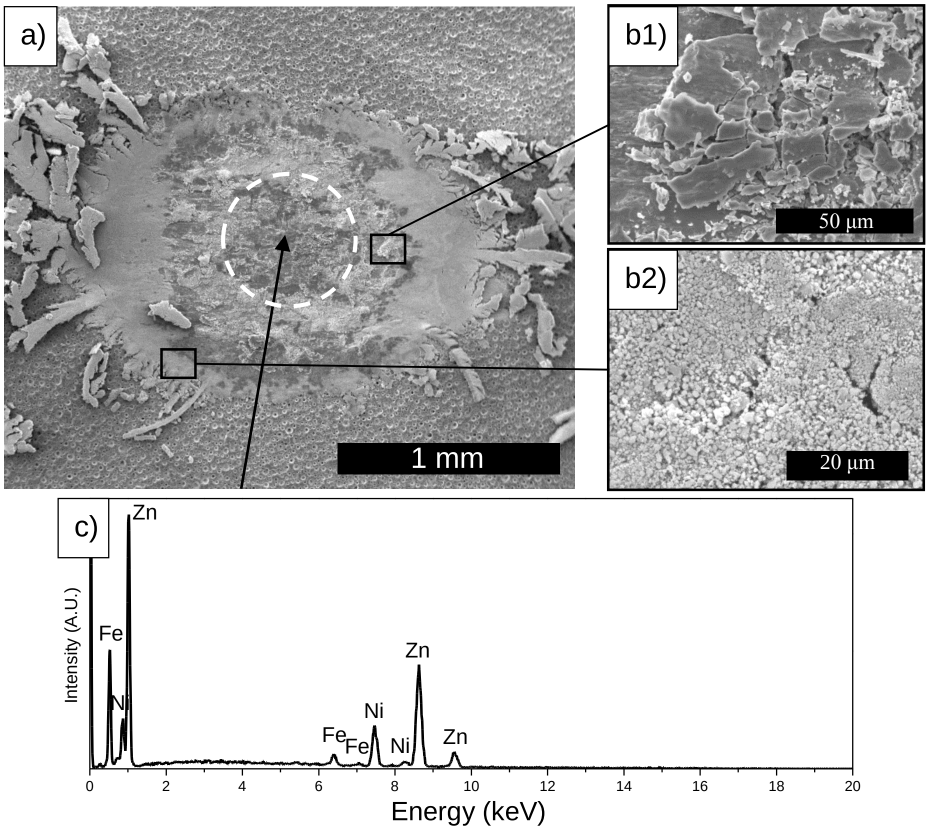

Figure 4.10 (a) Fretting wear scar, (b) third body morphology and (c) EDX spectrum of center area of D-ZnNi coating at contact conditions 133 N normal load and ±100 µm displacement amplitude after 10,000 cycles. Sliding direction ↔

Tests performed at ±150 µm displacement amplitude and 133 N normal load showed severe wear in all cases after 10,000 cycles (Figure 4.11-4.12). Oxide particles are present throughout the contact except for small patches of areas where plastic flow of material is observed. In the patches, C-ZnNi coatings (Figure 4.11a) show plastic flow of material. Chunks of detached material and re-deposited third bodies are also observed near the edge of the patch area shown in the inset image. For D-ZnNi coating, deformation due to sliding is observed in the patch, with re-deposition of third bodies. A substantial amount of wear debris was extruded out of the wear scar. Extruded wear debris from D-ZnNi coatings shows small particles compacted into thin flake-like shapes and are more abundant, whereas for C-ZnNi coatings, extruded debris are flat and more flake-like. For both coatings at this condition, intense iron peaks were found at the center of the wear scars (Figure 4.11-4.12b) with EDX. This indicates substrate exposure and is in agreement with the wear scar depth (Figure 4.6), which was much higher than the coating thickness. C-ZnNi coatings showed small intensity zinc and nickel peaks, indicating that some coating material remained in the center of the contact, whereas D-ZnNi coating showed no zinc and nickel peaks, indicating complete removal of the coating. The abundance of wear particles and sliding marks in the central region indicate that both coatings were in the gross slip regime.

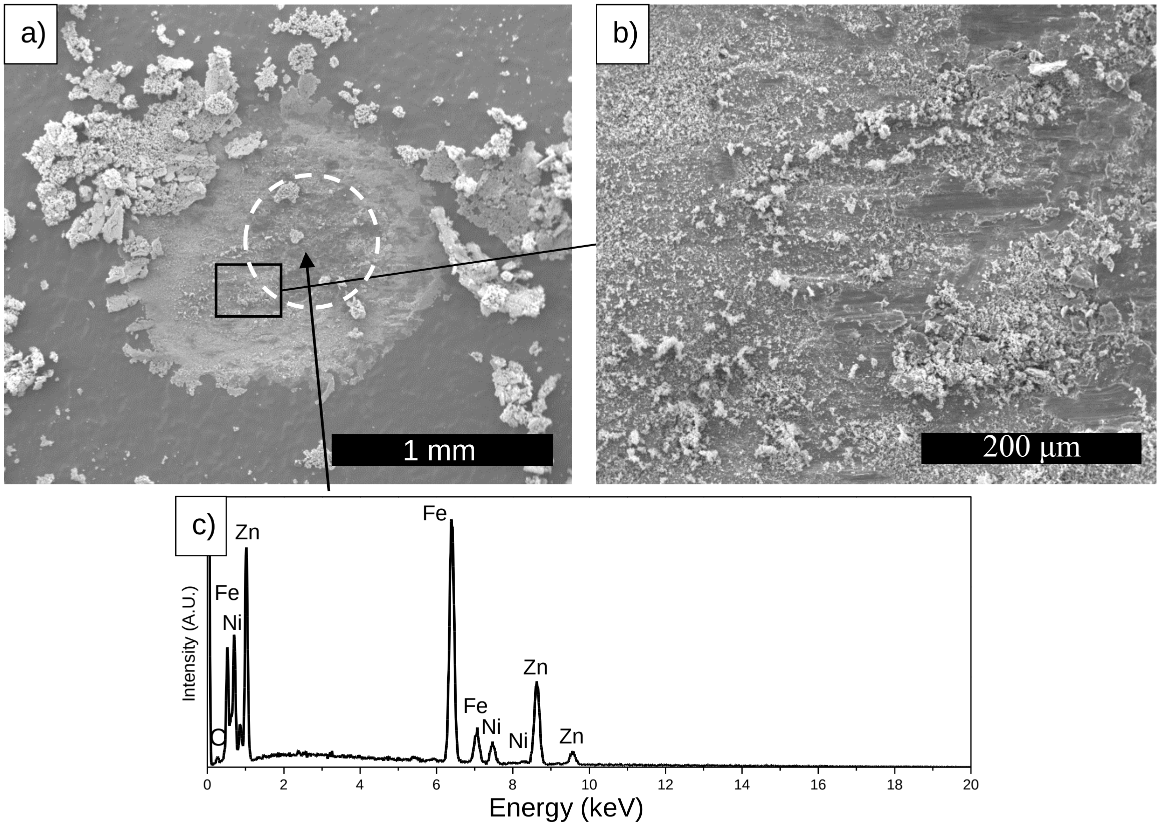

Figure 4.11 (a) Fretting wear scar (b) third body morphology and (c) EDX spectrum of center area of C-ZnNi coating at contact conditions 133 N normal load and ±150 µm displacement amplitude after 10,000 cycles. Sliding direction ↔

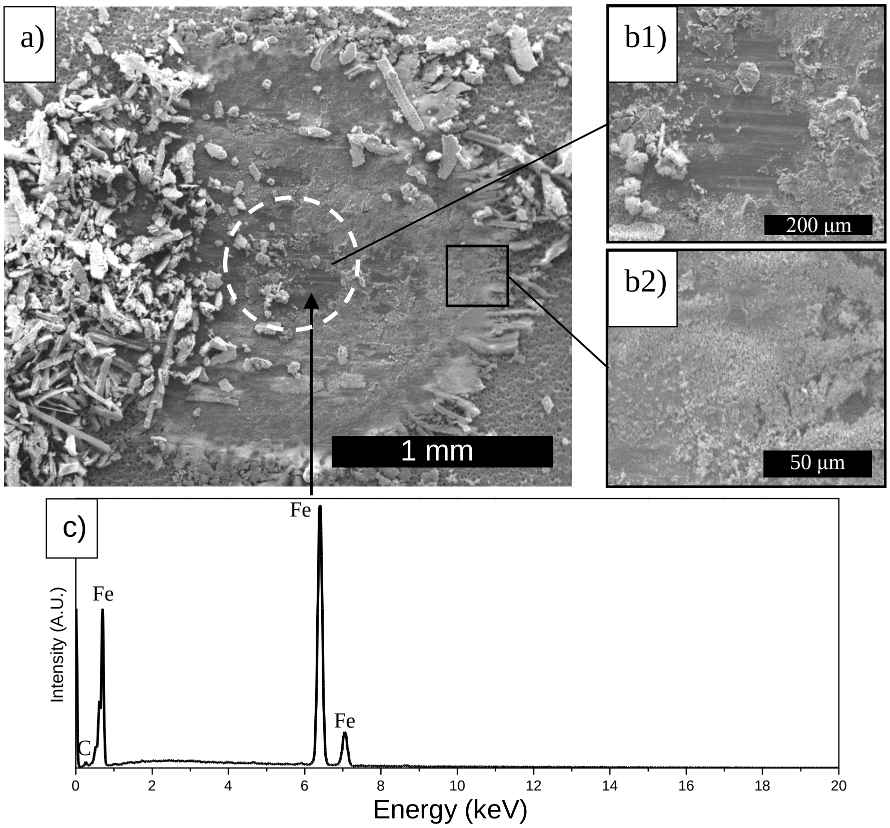

Figure 4.12 (a) Fretting wear scar (b) third body morphology and (c) EDX spectrum of center area of D-ZnNi coating at contact conditions 133 N normal load and ±150 µm displacement amplitude after 10,000 cycles. Sliding direction ↔

4.4 Discussion

The fretting wear behavior of two Zn-Ni coatings with different surface morphologies was studied under various contact conditions including the stick, mixed slip and gross slip. In the stick regime, cracks formed in C-ZnNi as a method of velocity accommodation, where through-thickness cracks formed columns in the smooth, compact coating, making it easier to flex [146]. In contrast, D-ZnNi did not form any cracks and the coating's nodular surface morphology allowed for velocity accommodation easier than a smooth, compact coating (e.g. C-ZnNi). Plastic deformation at the tops of the nodules was observed, similar to the wear behavior of rough surfaces discussed by Waterhouse [17]. Zn and Ni were present in patches on the counterface and indicated adhesion between the top of the nodules and the steel counterface. This adhesive process was identified by Berthier as a velocity accommodation mechanism through plastic deformation of asperities [146].

In the gross slip regime, despite a higher coating hardness, more severe wear occurred for D-ZnNi than C-ZnNi although increase in hardness improves fretting wear favourably [179-181]. Higher wear in D-ZnNi than C-ZnNi may be attributed to the difference in surface morphology and roughness of the coatings. Kubiak *et al.* [15] found that in the gross slip regime, a higher roughness is associated with a higher wear rate. Also both Zn-Ni coatings had through thickness defects, but defects for C-ZnNi were more vertical cracks, whereas defects in D-ZnNi, small porosities and cracks along the platelet agglomerations. Although the morphology in D-ZnNi coatings facilitates tangential motion in the stick regime, it also facilitated asperity detachment during sliding, which led to the larger wear scar depth and greater amount of wear debris found around the wear scar.

In the mixed slip regime, crack formation and particle detachment competed to accommodate motion [182]. Substantial amount of wear debris in both coatings in the mixed slip regime (Figure 4.9a &10a) indicates particle detachment [182]. Patches of deformed material at the center of the wear scar indicates that plastic flow of material occurred where the counterface was stuck to the wear scar. Both coatings transition from gross slip to stick (Figure 4.5b). Traversing from gross slip to stick indicates that particle detachment occurs before plastic deformation as velocity accommodation mechanisms. Higher wear rate of D-ZnNi coating is observed as the morphology of the coating facilitates particle detachment during sliding.

4.5 Conclusion

Differences in surface morphology contributed to a difference in fretting wear behavior between two Zn-Ni coatings. C-ZnNi coatings had a much smoother surface with gradual sloped peaks and low surface roughness, whereas D-ZnNi had a much rougher surface with steep sloped peaks and large through thickness pores. Through thickness cracks were observed in both coatings, but cracks in D-ZnNi appeared to go along the platelet agglomerates, making them easier to detach during sliding. In high load tests, although both coatings remained in the stick regime, the morphologies of the wear scars were different due to differences in their wear and velocity accommodation mechanisms, which were directly tied to differences in the surface morphologies of the coatings. Cracks and plastic deformation at the junctions were observed for C-ZnNi. In contrast, with D-ZnNi, due to large surface porosities, plastic deformation and asperity detachment was observed in the junctions between the counterface and the coating. Wear particles were also observed in the hollows of the coating. At low loads and small displacement amplitudes, the both coatings remained in the stick regime, but wear scar morphology was completely different from one coating to the other. For C-ZnNi, small oxidized wear particles were extruded out of the wear scars and mild delamination occurred. For D-ZnNi, wear was similar to that observed at high loads. Low loads and high displacement amplitudes allowed slipping between the contacts. D-ZnNi coatings had a much deeper wear scar and more oxidized wear particles than C-ZnNi coatings, which may be attributed to the surface morphology of D-ZnNi coatings, as the agglomerates are easier to remove than the compact C-ZnNi coating.

Acknowledgments

The authors would like to thank Dr. Sriraman Rajagopalan, Priyadarshi Behera, Salim Brahimi and Professor Stephen Yue for their continual support and inputs throughout the experiments. We would also like to thank the Natural Science and Engineering Research Center (NSERC), Boeing Canada, Pratt & Whitney Canada, Héroux Devtek, Canadian Fastener Institute and Messier-Bugatti-Dowty for their financial support. We would also like to thank Boeing, Coventya and Dipsol Inc. for providing specimens.

Chapter 5

Comparison of fretting behavior of electrodeposited Zn-Ni and Cd coatings

L. Lee, S. Descartes & R. R. Chromik

This chapter is a manuscript intended to be submitted. Chapter 4 discusses the effects of the Zn-Ni coating morphology on the fretting behaviour. It was found that the coating with high roughness, in the stick regime the motion was accommodated by flexing the columns of the coating, while for the smoother coating, cracks were induced to accommodate motion. In contrast when motion occurred, coating material was easier to detach due to the surface defects and roughness or the rougher coating. In this chapter, a Zn-Ni coating with a roughness value in between the smoother and rougher coatings is compared with Cd coatings. As these coatings are intended to replace cadmium, comparisons with the fretting behaviour of cadmium are made, in this case with the Zn-Ni coating with a intermediate surface morphology, as the rough and porous coating and the smooth and dense coating is discussed in the previous chapter.

Abstract

Cadmium is used in the aerospace industry as a corrosion protection coating for steels in applications such as fasteners and landing gear components. However, as cadmium is carcinogenic and toxic, replacements such as Zn-Ni are developed. Although Zn-Ni is a primary replacement candidate, tribological behaviours of these coatings are not well understood, despite being an important factor in these applications. This study compares the fretting behaviour of commercially available Zn-Ni and cadmium coating by comparing the contact conditions and velocity accommodation mechanisms using the third body approach. Tests are performed under similar contact stress and normal loads due to the large difference in mechanical properties of these coatings. It was found that at similar contact stresses, gross slip occurred in Zn-Ni coating when the displacement amplitude was increased, while cadmium remained in a partial slip regime. As such, when gross slip occurred in Zn-Ni coating, severe fretting damage occurred. For cadmium, as the displacement amplitude was increased, the ejection of the coating material in the contact region through plastic flow became more severe. When a similar normal load was used (which translated to a higher initial Hertzian contact stress for Zn-Ni), the contact condition remained in the stick and partial slip regime. Little wear was observed at the contact, which could be attributed to the morphology of the coating.

5.1 Introduction

Zn-Ni was developed in the 1980’s as a replacement for cadmium as a corrosion protective coating in the automotive industry due to the carcinogenic and toxic nature of cadmium [1-5, 21, 168]. As requirements for cadmium becomes more stringent, there is an increasing interest for Zn-Ni coatings in the aerospace industry. In the aerospace industry, cadmium is mainly used as a corrosion protective coating for steel applications, such as fasteners and landing gear components. Fretting, due to small oscillatory motions, such as vibration is an issue in these application.

Fretting occurs when there are small oscillatory motions that have amplitudes smaller than the contact radius. In practice, the displacement amplitude does not equal to the actual displacement, as some of the motion can be accommodated through elastic deformation of the test set-up or the bulk of the sample [146]. It is also known that increasing the displacement amplitude can change the contact conditions, which can be separated into different fretting regimes: stick or partial slip regime, mixed slip regime and gross slip regime [149, 150, 183]. The sticking occurs when there is no motion in the contact and is characterized by very limited surface damage [149, 150]. Partial slip occurs when there is a region in the contact where the surfaces are stuck together, usually in the center of the contact, and a location in the contact where sliding occurs, usually in the annular region [150, 183]. Gross slip occurs when the entire contact is slipping and is characterized by severe surface damage by wear [149, 150, 183]. The stick or partial slip regime is characterized by sticking or partial slip contact conditions mostly prevails, whereas the gross slip regime is described by gross slip contact conditions prevails throughout the test. Mixed slip regime occurs when a combination of other two contact conditions occur [150, 183]. Another method of distinguishing these regimes is through dynamic force versus displacement characterization, such as fretting loops or hysteresis loops [149, 150, 183]. Generally, a closed loop indicates stick behaviour, a partially open or elliptical loop indicates partial slip, and an open or quasi rectangular loop indicates gross slip behaviour [146, 149, 150, 183]. A ratio of the dissipated energy (E_d), which is the area enclosed by the loop, over the total energy (E_t) can give an idea of the contact conditions, as an energy ratio below 0.2 indicates of partial slip behaviour and above 0.2 indicates gross slip behaviour [150, 183]. The evolution of the energy ratio helps define the three fretting regimes [150, 183].

The third body approach is used to analyze the fretting test [140, 144, 145]. In this approach, the two original contacting surfaces are called the “first bodies”, and the zone where the material is chemically or mechanically different from the parent material is called the “third body” [140]. Velocity accommodation between the moving component and the stationary component can be separated into five different sites and four different modes. Velocity accommodation mechanisms can be characterized by combining these sites and modes [144, 145].

Vincent *et al.* [182] summarized the fretting regimes and velocity accommodation mechanism. During the stick or partial slip regime, velocity is usually accommodated through elastic or plastic deformation, or crack initiation followed by crack arrest or propagation [182]. Where as for gross slip regime is associated with shear and/or formation of a tribological transformed structure, followed by particle detachment [182]. When the particles are detached, low wear occurs when the particles are entrapped and forms a debris bed, whereas when the particles are ejected, high wear occurs, as new detached particles are formed [182]. For the mixed slip regime, either can occur [182].

Few studies are found in the literature on the fretting behaviour of Cd and Zn-Ni coatings despite its importance. For cadmium, previous fretting studies by Carton *et al*. [184, 185] found that although no cracks were initiated in the coating and Cd greatly improved the running conditions during fretting, the coating was removed from the contact rapidly during the gross slip regime due to the viscous nature of the coating, and counterface to substrate contact is observed at the central part of the contact. Long lamellae of coating material was also pushed to the side of the contact, parallel to the sliding direction [185]. With regards to Zn-Ni, previous studies by the author [186] found a change in fretting behaviour when the surface morphology of the coating was changed. Coatings that were smooth and dense cracked during the stick regime, while for coatings that were porous and irregular, the tops of the asperities were flattened and deformed elastically to accommodate the velocity.

In this study, the fretting behaviour of commercially available Zn-Ni and Cd coatings are compared. The coatings are subjected to fretting at different displacement amplitude that changes the contact conditions to the stick, mixed ship and gross slip regimes for Zn-Ni coatings. As the mechanical properties of Cd and Zn-Ni are immensely different, tests conditions with similar contact stresses and with similar normal loads were compared. Comparisons were made through characterizing the contact conditions and velocity accommodation mechanisms.

5.2 Background information

Berthier and coworkers did substantial work on defining velocity accommodation mechanisms in a sliding contact. There are five sites that can accommodate the velocity: the two first bodies, the two screens third body screens, and the third bodies bulk (Figure 5.1) [144]. The first bodies refer to the two rubbing specimens [144]. The third body screens refer to the screens that separates the first and third body bulks [144]. The third body bulk refers to the central part of the third bodies [144]. There are also five modes: elastic, plastic, fracture, shearing and rolling, only the elastic mode is reversible [144, 145]. Combination of a site and a mode gives an accommodation mechanism [144, 145]. Velocity can be also accommodated by the machine through elastic deformation, which is designated S_0M_0 which can cause false fretting [145]. A few examples of velocity accommodation modes that are relevant to this paper is shown below.

S_1M_0: occurs when the bulk of the first bodies take up the motion through elastic deformation. Usually, total adhesion occurs at the contact points [145]. An example is when cracks form on a surface due to high shear stresses, creating short columns, which can bend elastically to accommodate the velocity [146].

S_1M_1: shallow or deep plastic deformation in first body (including coating). It should be noted that material is not loss [145].

S_1M_3: superficial shear, usually characterized by sliding cards morphology, which leads to particle detachment [145].

S_3M_1: third bodies that are within the contact under goes plastic deformation [145]

S_3M_3: third bodies within the contact under goes shear [145]. It should be noted that shear planes are not always parallel to the direction of rubbing [144].

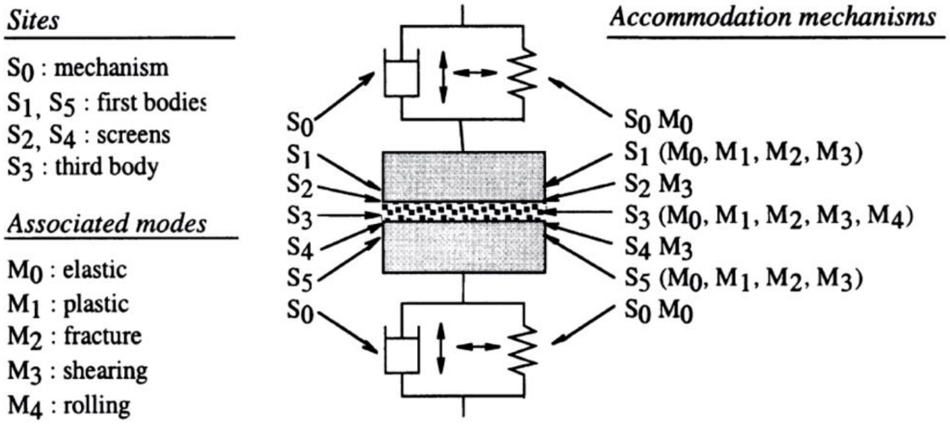

Figure 5.1 Schematic of sites, modes and mechanisms of velocity accommodation in the tribological system [145]

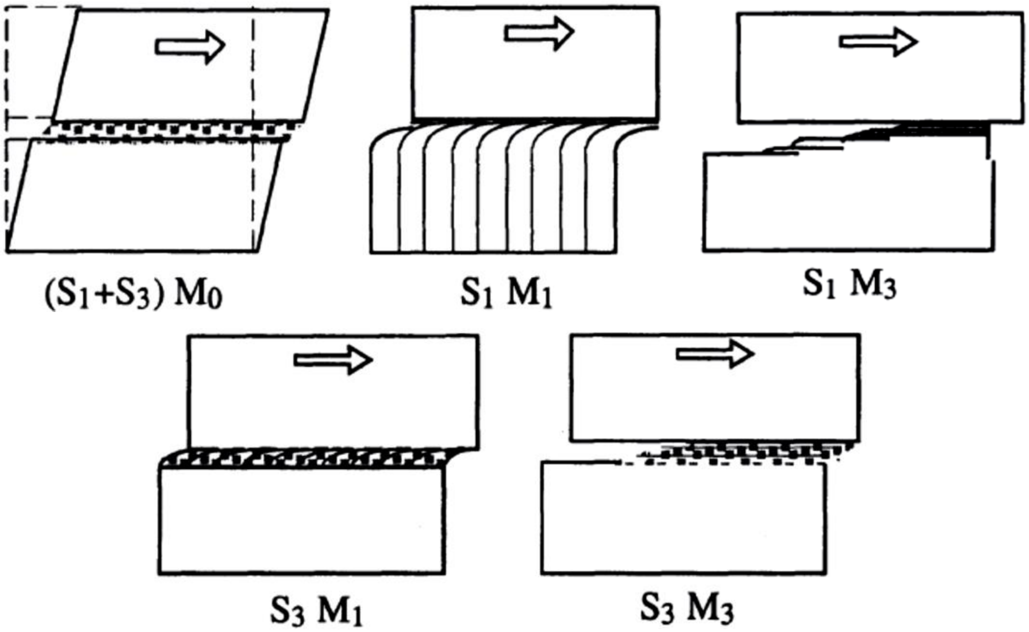

Figure 5.2 Schematic of velocity accommodation mechanisms [145]

5.3 Methods

5.3.1 Coating deposition

Coatings were commercially deposited using industrial pilot plating tanks onto low carbon steel sheets (SAE 1006) of dimensions 100 x 160 x 0.8 mm^3.

B-ZnNi: Coatings were plated using NaOH (135 g/L) and Na_2CO_3 (60 g/L) alkaline based plating solution. The plating solution contained 9-11 g/L of zinc and 0.8-1.2 g/L nickel which were maintained at a ratio of 10-11:1. The pH of the solution was kept at 12-13.5 and plating was performed at 20-25 °C and a current density of 48 mA/cm^2. Prior to plating, the substrates were aqueous degreased, abrasive grit blasted and pickled in HCl. The plated samples were passivated using a blue trivalent conversion coating [187].

LHE Cd: Coatings were plated using an alkaline cyanide (NaOH 11-30 g/L, NaCN 90-181 g/L, Na_2CO_3 0-60 g/L) based plating solution containing 20-30 g/L CdO. The plating temperature was maintained at 15-30 °C and a current density of 118-120 mA/cm^2 was used. Prior to plating, the substrates were solvent degreased, grit blasted then acid pickled. The plated samples were then passivated using a chromate passivation [188].

Both types of samples were mechanically sheared to 40 x 25 mm^2 samples, then cut using a diamond saw and grinded with SiC paper to 8 x 12 mm^2 samples. Samples were then baked at 200 °C for 24 hours to removed entrapped hydrogen.

5.3.2 Characterization

Morphologies of coatings were observed using a FEI Quanta 600 scanning electron microscope (SEM), which uses a tungsten filament source. Cross sections of the coatings were obtained by cutting the samples with a diamond saw, and preparing them metallographically. Grinding and polishing the samples were performed in isopropanol to avoid corrosion. Energy dispersive spectrometry (EDS) was used to study the chemical changes in the wear scars.

X-ray diffraction (XRD) was performed in the standard θ-2θ mode on the as-received coatings in order to confirm the phases present in the Cd and B-ZnNi coatings. A Bruker Discover D8-2D (USA) with a Co-Kα source was used.

Profilometry of the wear scars were obtained using a Newview (Zygo, USA) white light interferometer. Wear scar depths were measured using the companion MX software (Zygo, USA).

Hardness of the coatings were obtained using nanoindentation using a Ubi3 nanoindenter (Hysitron, USA). Due to the small thickness of the cross section of the coatings (~ 15 µm), a diamond Berkovich tip was used and test were performed on the cross section of the coating with 5mN load using a 5 second loading time, 2 second hold time and 5 second unloading time. The elastic modulus and hardness were calculated using the Oliver and Pharr method [159].

5.3.3 Fretting wear test

Fretting wear tests were performed using a custom built tribometer at Laboratoire de Méchanique des Contacts et des Structures (LaMCoS, INSA, Lyon, France). Samples were mounted onto AISI 440C steel blocks using super glue and mounted into the specimen holder. AISI 440C steel counterfaces with 20 mm radius of curvature were used. For B-ZnNi coating, initial normal loads of 133 and 447 N were used. This corresponds to a maximum initial Hertzian contact stress of 740 MPa and 1110 MPa and a Hertzian contact radius of 292 μm and 439 μm respectively when a Young`s Modulus of 118 GPa and Poisson’s Ratio of 0.23 [174, 175] were used for the calculations. For Cd coating, a normal load of 434 N was used, which corresponds to a maximum initial Hertzian contact stress of 740 MPa and a contact radius of 529 μm when a Young’s Modulus of 50 GPa and Poisson’s Ratio of 0.3 were used [189]. Displacements of ±70, 100 and 150 µm were imposed at a frequency of 15 Hz in order to evaluate the stick-slip behaviours of the coatings. It should be noted that as some of the motion can be taken up by the first bodies and structure, the imposed displacement is not always the actual displacement at the contact [141]. From a previous study [186], this corresponds to stick, mixed-slip and gross slip regimes for Zn-Ni coatings. The tests were performed at ambient temperature (23-25 °C) and relative humidity (35-40% RH). The imposed displacement and normal force was kept constant throughout the test, while the normal force, tangential force and displacement values were measured and recorded.

5.4 Results

5.4.1 Coating characterization

SE images of the as received coatings are shown in Figure 5.3. Both coating has a nodular structure composed of platelets agglomerated into hemispherical shapes. Agglomerates from B-ZnNi has small features on the surface, while the surface of the agglomerates of Cd coating is smoother. Through coating thickness porosity is also larger in B-ZnNi coating than Cd coating. Through thickness defects such as through coating pores and cracks are observed in the cross sections of the coatings (Figure 5.4) and are present throughout the coating. Through coating thickness defects are present to ease the escape of hydrogen during the baking process [31, 176]. Cross sections of the coatings also show good adhesion to the substrates, and are shown in Figure 5.4 for B-ZnNi and [190] for cadmium coatings. Roughness measurements (Table 5.1) also show that the cadmium coating is slightly rougher than the B-ZnNi coating.

XRD and hardness measurements of the cadmium coating were previously reported in a tribological study of the coating [190]. XRD patterns for the cadmium coatings shows a single cadmium phase, which has a hexagonal crystal structure. XRD was also performed on the B-ZnNi coating to observe the phases present in the coating and results are shown in Figure 5.5. Diffraction patterns of the B-ZnNi coating shows peaks corresponding to the γ-ZnNi which has a cubic crystal structure. Hardness of the coatings were obtained through nanoindentation of the cross section of the coating and results are shown in Table 5.1. B-ZnNi shows a much higher hardness and reduced modulus than cadmium coating.

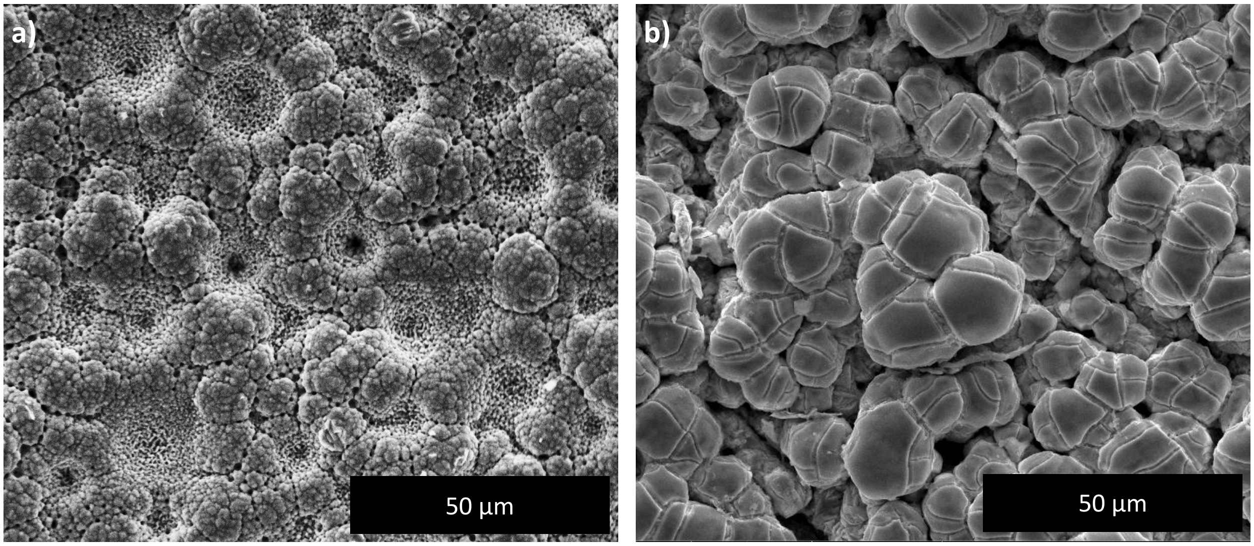

Figure 5.3 SE images of as received coating morphologies (a) B-ZnNi and (b) Cd

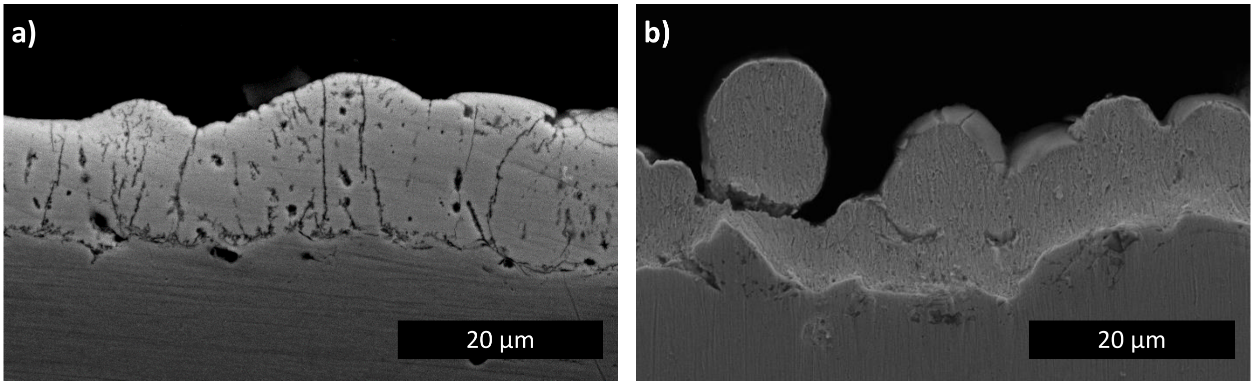

Figure 5.4 Cross section of (a) B-ZnNi and (b) Cd coatings

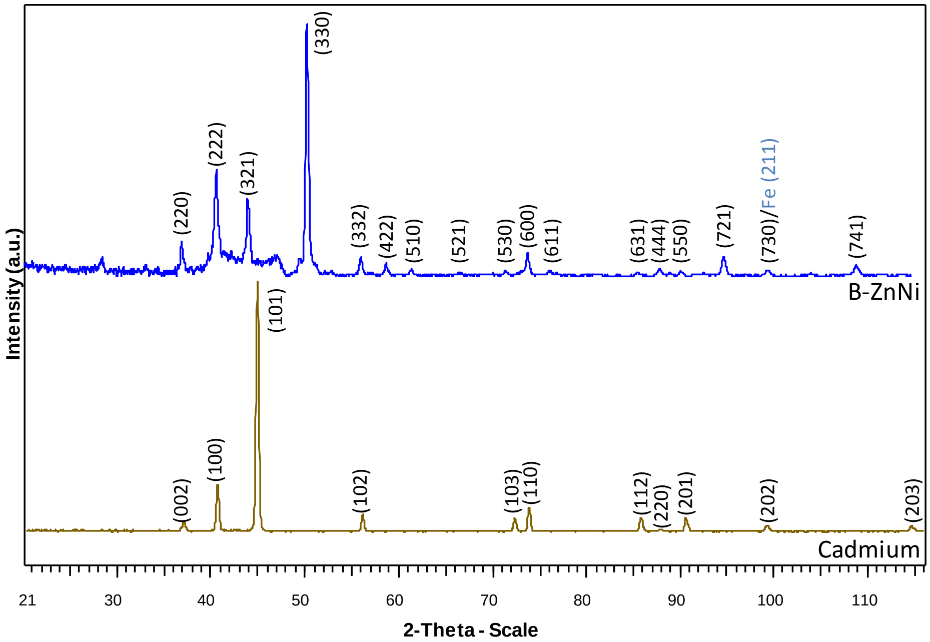

Figure 5.5 X-ray diffraction pattern of B-ZnNi and Cd coatings

Table 5.1 Selected Coating Properties

	B-ZnNi	**Cd**
Roughness (R_a, μm)	2.3 ± 0.3	3.9 ± 0.4
Hardness (H, GPa)	4.9 ± 0.7	0.42 ± 0.09 [190]
Reduced Modulus (E_r, GPa)	144 ± 14	60 ± 10 [190]
Thickness (μm)	14 ± 2	11 ± 2 [190]

5.4.2 Energy ratio

Hysteresis loops, obtained through plotting the tangential force against the displacement, can be used to characterize the stick slip behaviour. A completely closed loop is indicative of a stick behaviour, while a completely opened loop of gross slip behaviour. A partially open or elliptical loop is indicative of a partial slip behaviour. The area enclosed by the loop characterizes the dissipated energy (E_d). An energy ratio can be obtained by dividing the dissipated energy by the total energy. Examples of the hysteresis loops are shown in Figure 5.6 for B-ZnNi under 133 N normal load, Figure 5.7 for B-ZnNi under 447 N normal load and Figure 5.8 for Cd under 434 N normal load. The energy ratios of the tests as a function of cycles are shown in Figure 5.9. At displacement amplitude of ±70 μm, the fretting loops of the three tests remain closed, which is characteristic of the stick regime [149, 150]. This is also observed through the near zero energy ratios. The steady state CoF is also reached early in the test, but interestingly, at a lower load, the

CoF of B-ZnNi coatings take longer to stabilize (~500 cycles) and is higher (~0.3) than tests performed at higher loads for B-ZnNi and Cd. Tests for B-ZnNi at 447 N and Cd at 434 N exhibits the same steady state CoF at around 0.1.

When the displacement amplitude is increased to ±100 µm (Figure 5.9b), B-ZnNi coating under 133 N normal load has a mixed slip behaviour, where the beginning of the test, for ~4000 cycles, a gross slip behaviour is observed since the fretting loops exhibits an open trapezoidal shape. The energy ratio is also high and unstable. The CoF (Figure 5.10b) of this portion of the test is also unstable. After around 4000 cycles, a stick behaviour is observed, as the hysteresis loops are closed and the energy ratio is near zero. The CoF of this portion also stabilizes to ~0.4 after 5000 cycles. At ±100 µm displacement amplitude, cadmium exhibits a partial slip behaviour, as the hysteresis loops are slightly opened and elliptical. This is also reflected in the energy ratio plot where the energy ratio is slightly above zero (~0.05). The CoF (Figure 5.10b) also stabilizes to ~0.15 after ~1000 cycles.

At displacement amplitudes of ±150 µm (Figure 5.9c), for B-ZnNi under 133 N, a gross slip behaviour is observed, as the hysteresis loops remain open trapezoidal shapes throughout the test. This is also reflected in the high energy ratio. The energy ratio is also very erratic in the first 5000 cycles, which is reflected in the CoF (Figure 5.10c). After 5000 cycles, the energy ratio stabilizes. The CoF for this portion of the test doesn't really become stable, but rather increases until the end of the test. In contrast, the tests performed at higher loads for B-ZnNi and Cd are in the partial slip regime, as the loops are elliptical and the energy ratio remains stable and below 0.2 [150] at ~0.1. A similar steady state CoF of around 0.2 is also observed for both coatings.

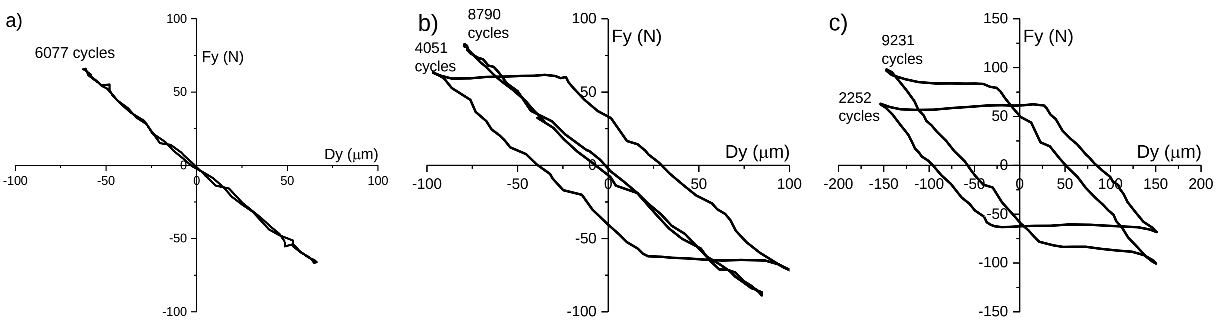

Figure 5.6 Hysteresis loops for B-ZnNi coatings under 133 N normal load at (a) ±70, (b) ±100 and (c) ±150 µm displacement amplitudes

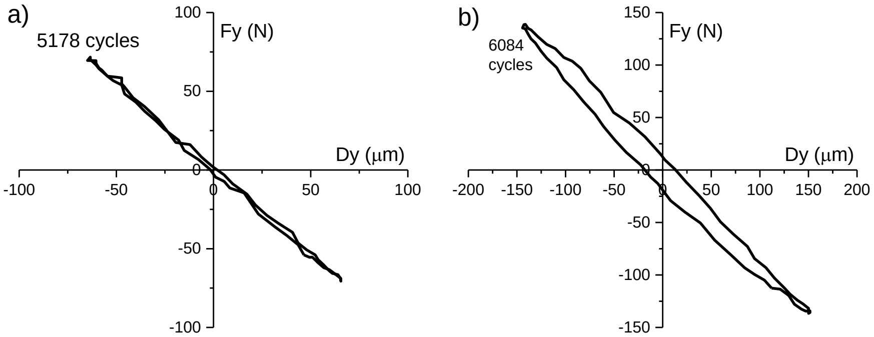

Figure 5.7 Hysteresis loops for B-ZnNi coatings under 447 N normal load at (a) ±70 and (b) ±150 µm displacement amplitudes

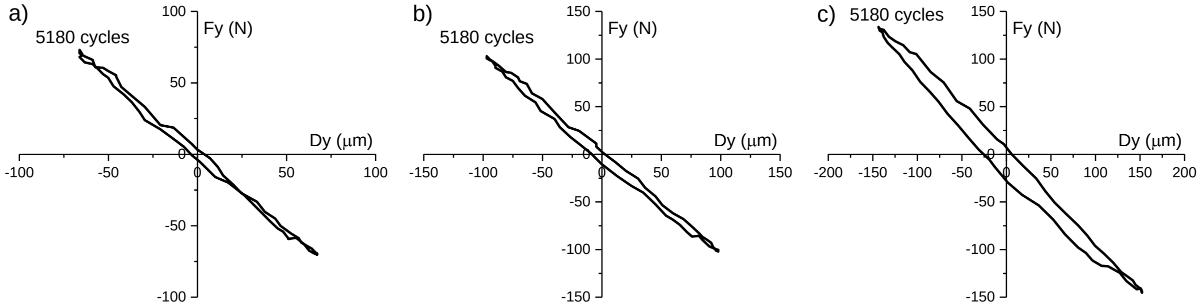

Figure 5.8 Hysteresis loops for Cd coatings under 434 N normal load at (a) ±70, (b) ±100 and (c) ±150 µm displacement amplitudes

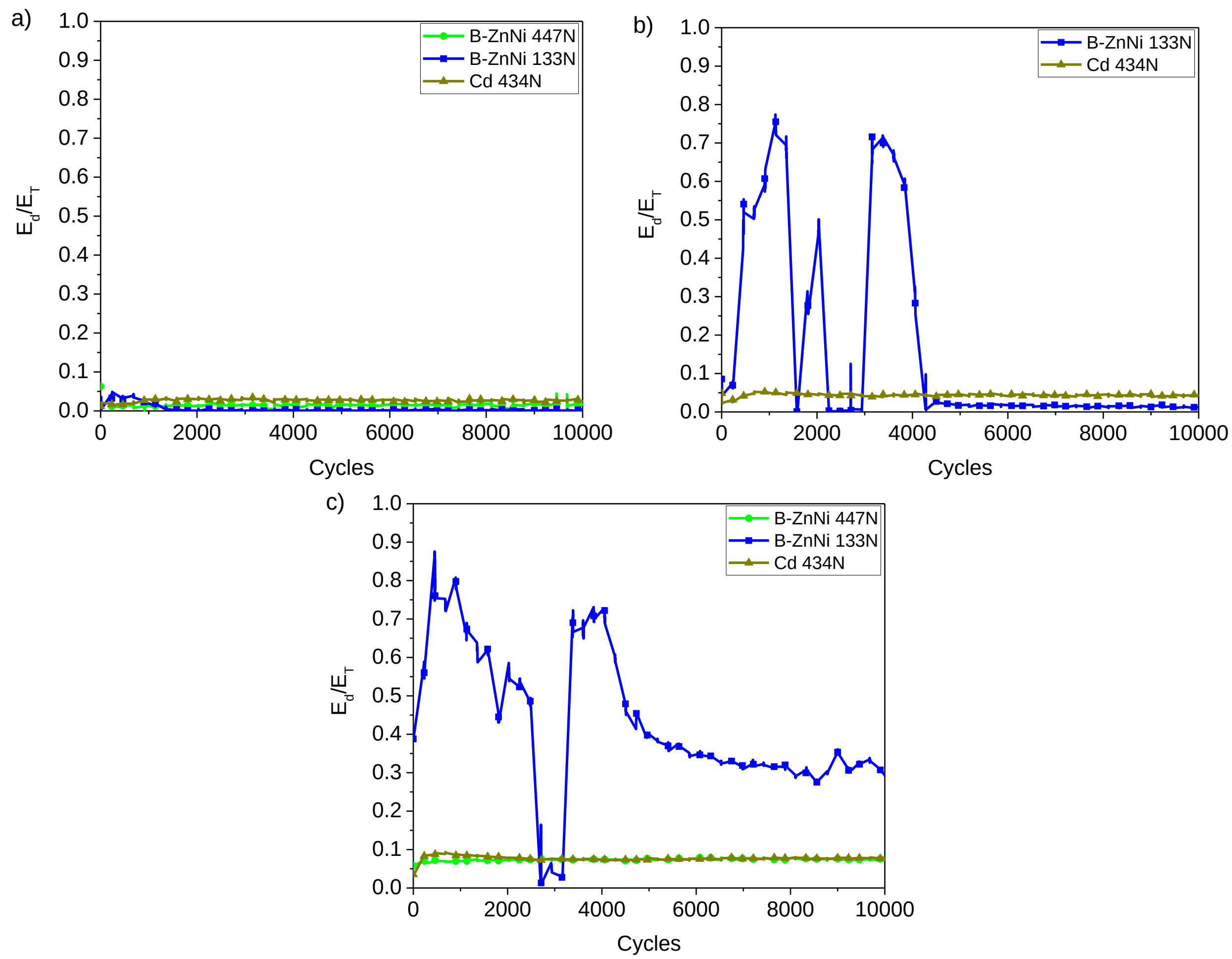

Figure 5.9 Energy ratio at displacement amplitudes of (a) ±70μm, (b) ±100μm and (c) ±150μm

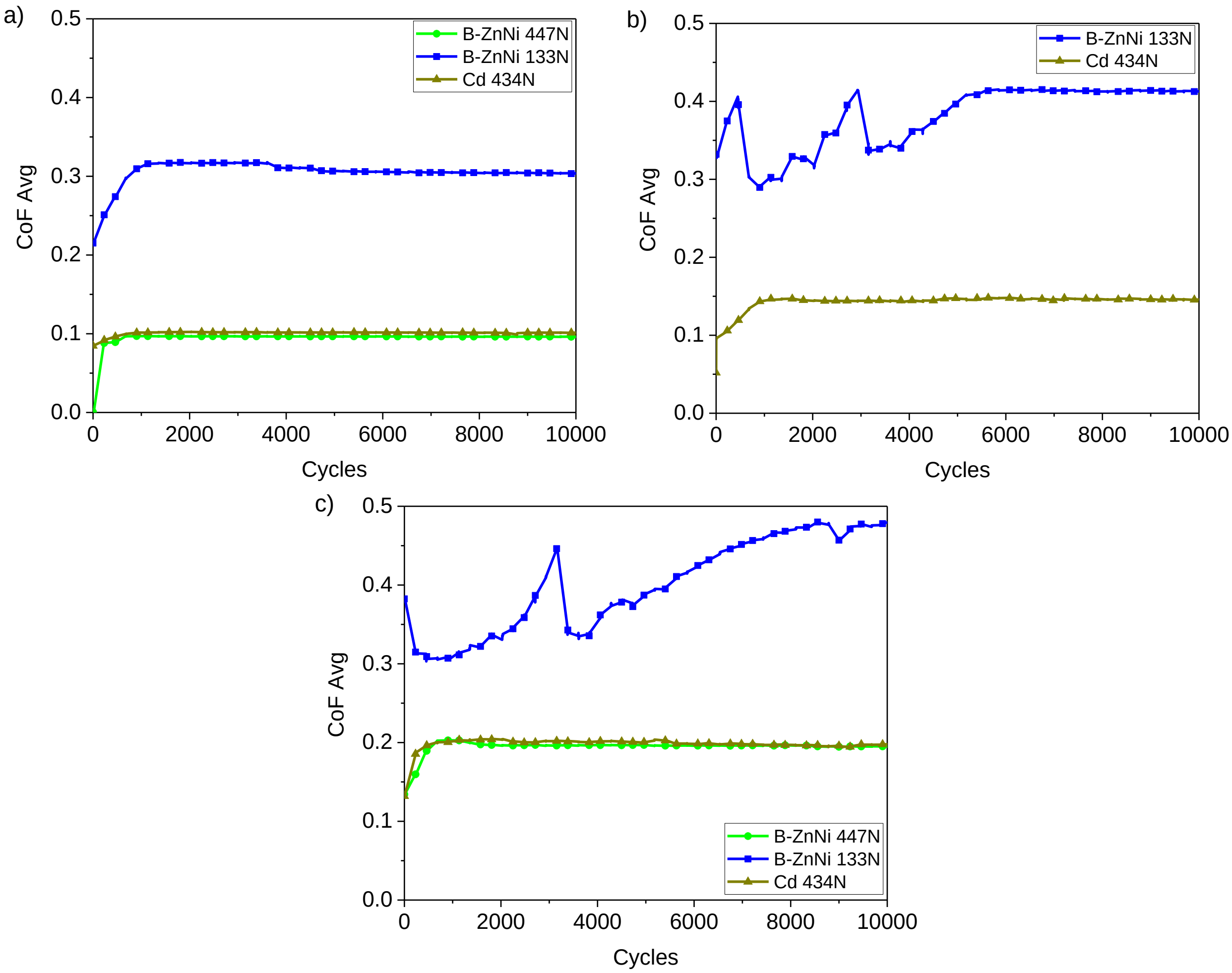

Figure 5.10 Coefficient of friction evolution at displacement amplitudes of (a) ±70 µm, (b) ±100 µm and (c) ±150 µm

5.4.3 Ex situ wear scar analysis

SE images of the wear scars are shown in Figure 5.11-5.13. The calculated contact area is circled in white. At ±70 µm displacement amplitude, for B-ZnNi at 133 N normal load (Figure 5.11a & b), mostly the tops of the agglomerates are sheared and deformed plastically. This caused the agglomerates to merge together and form large areas of flattened asperities. Plastically deformed particles, detached from the coating due to severe plastic deformation, are also found in the hollows of the coating. The area of deformed asperities also matches with the calculated area of contact, indicating that little to no sliding motion has occurred. At 447 N normal load (Figure 5.11c & d), only the tips of the asperities are deformed, as the motions remain in the stick regime. Particles are produced through severe plastic deformation of the asperities and fell into the hollows of the coating. The area where the asperities are flattened also matches the calculated area of contact due to no sliding motion. For Cd coating (Figure 5.11e & f), although the fretting loops suggests a stick regime, the asperities of the coating were plastically deformed and flattened such that the through coating thickness porosities were closed. EDX was performed on the different phases present and Cr and Cd was detected on the darker phase while the lighter phase only contained Cd. As the passivating coating contains Cr, the passivating coating may have broken down during fretting and caused patches where the passivating coating is embedded. Some of the coating material from the contact area also appears to be pushed to the side of the wear track through plastic flow of material.

When the displacement amplitude is increased to ±100 µm, B-ZnNi under 133 N load appears to be in the mixed slip regime as the energy ratio transitions from gross slip to stick regimes. From Figure 5.12a, the worn area is much larger than the calculated contact area. A significant amount of wear debris is also ejected from the contact area, creating a debris bed in the annular region, while the central region, mostly large flakes of material is observed. EDX of the wear debris also shows a strong iron peak, which may be from the substrate or wear of the counterface. For Cd coating, similar to the smaller amplitude, the agglomerates appears to be plastically deformed and flattened to fill in the through coating thickness pores, resulting the agglomerates to flow together. Again, the central region shows a darker phase which contains the passivating layer, and a lighter phase which contains only Cd. The bulk of the coating material under the contact area also appears to be pushed to the side through plastic deformation.

SE images of the wear scars when the displacement amplitude is increased to ±150 µm are shown in Figure 5.13. For B-ZnNi under 133 N normal load, the worn area is much larger than the calculated initial contact area, due to gross slip behaviour. Substantial amount of debris are ejected from the contact, and little amount of debris remain within the contact to act as a debris bed. Shearing is also observed where the counterface was directly in contact with the coating or substrate. EDX results also show strong iron peaks, indicating that the substrate is exposed. For B-ZnNi coatings, under 447 N normal load, the asperities in the contact region is flattened through plastic deformation and some wear particles were produced and fell into the hollow of the coatings and ejected from the contact area, although not a lot of wear is observed as the contact conditions remain in the stick regime. For Cd, the coating appears to be plastically deformed and pushed to the side of the wear scar. The dual phase due to the passivating layer embedment seen in previous conditions is not observed in this condition. EDX on the darker patches shows Fe peaks, indicating that the coating material may be pushed out of the contact and the substrate may be exposed.

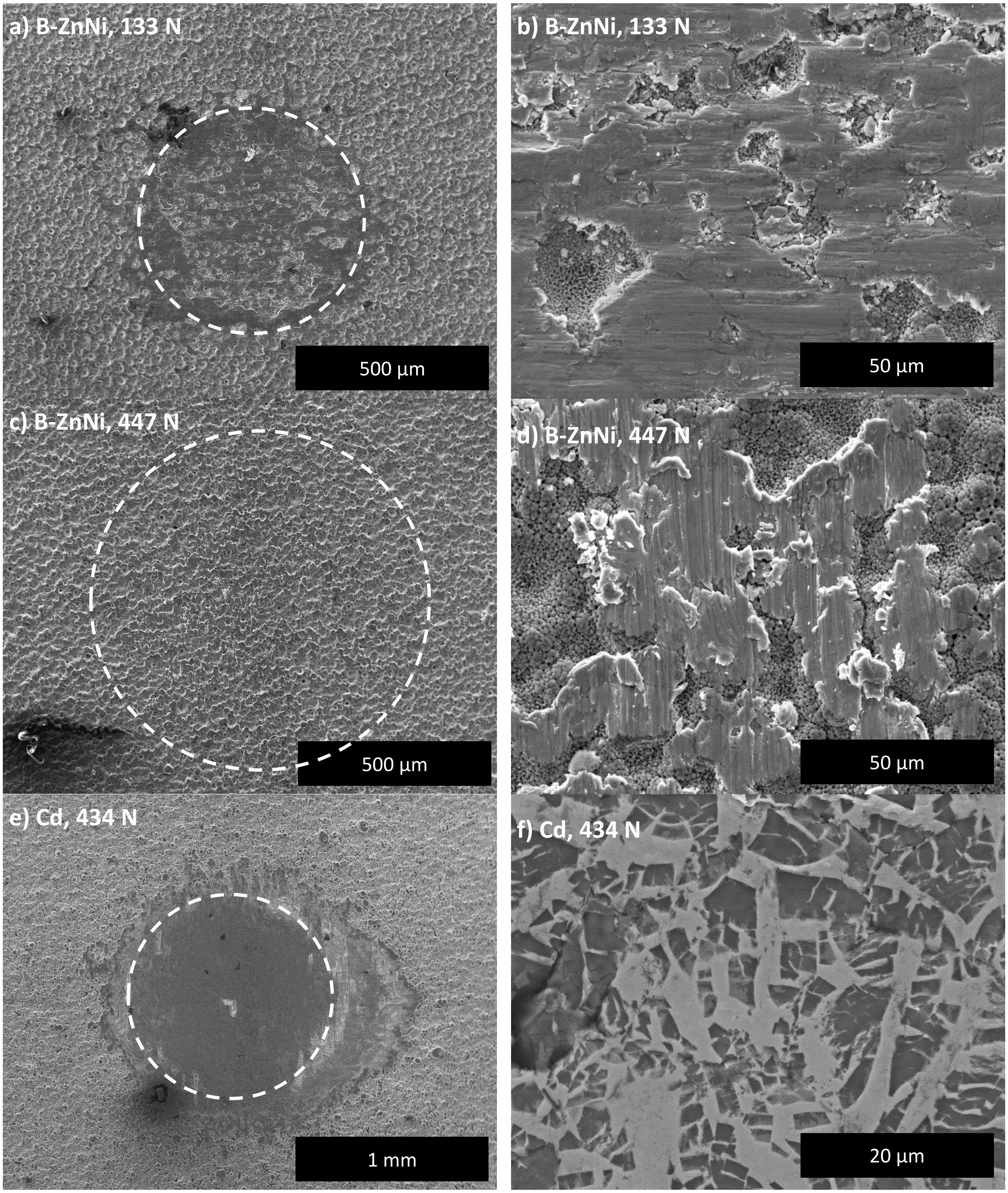

Figure 5.11 SE images of fretting scars for B-ZnNi at (a-b) 133 N and (c-d) 447 N normal loads and (e-f) Cd at 434 N using ±70 µm displacement amplitude after 10,000 cycles. ↔ Sliding direction

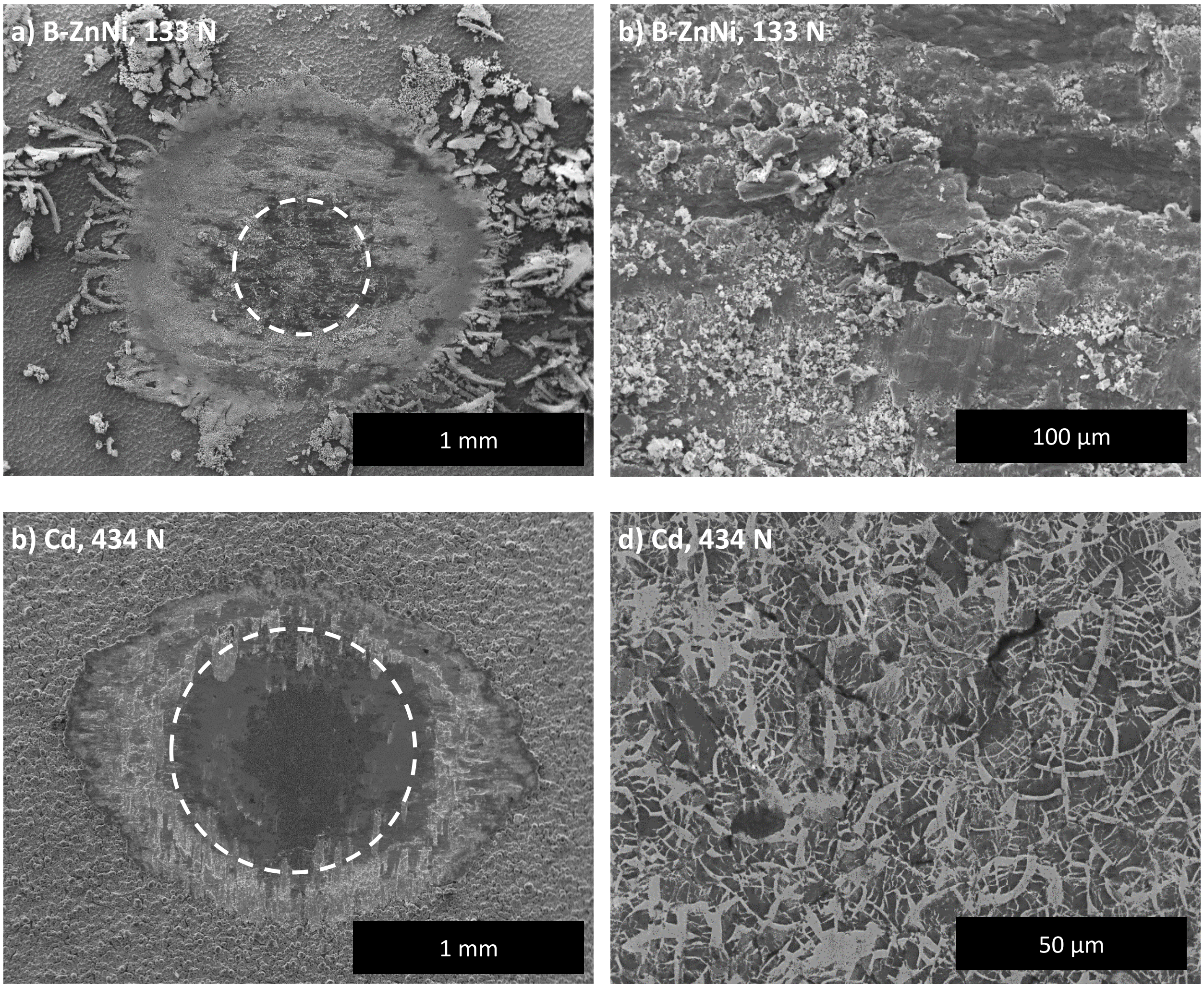

Figure 5.12 SE images of fretting scars for (a-b) B-ZnNi at 133 N and (c-d) Cd at 434 N using ±100 µm displacement amplitude after 10,000 cycles. ↔ Sliding direction

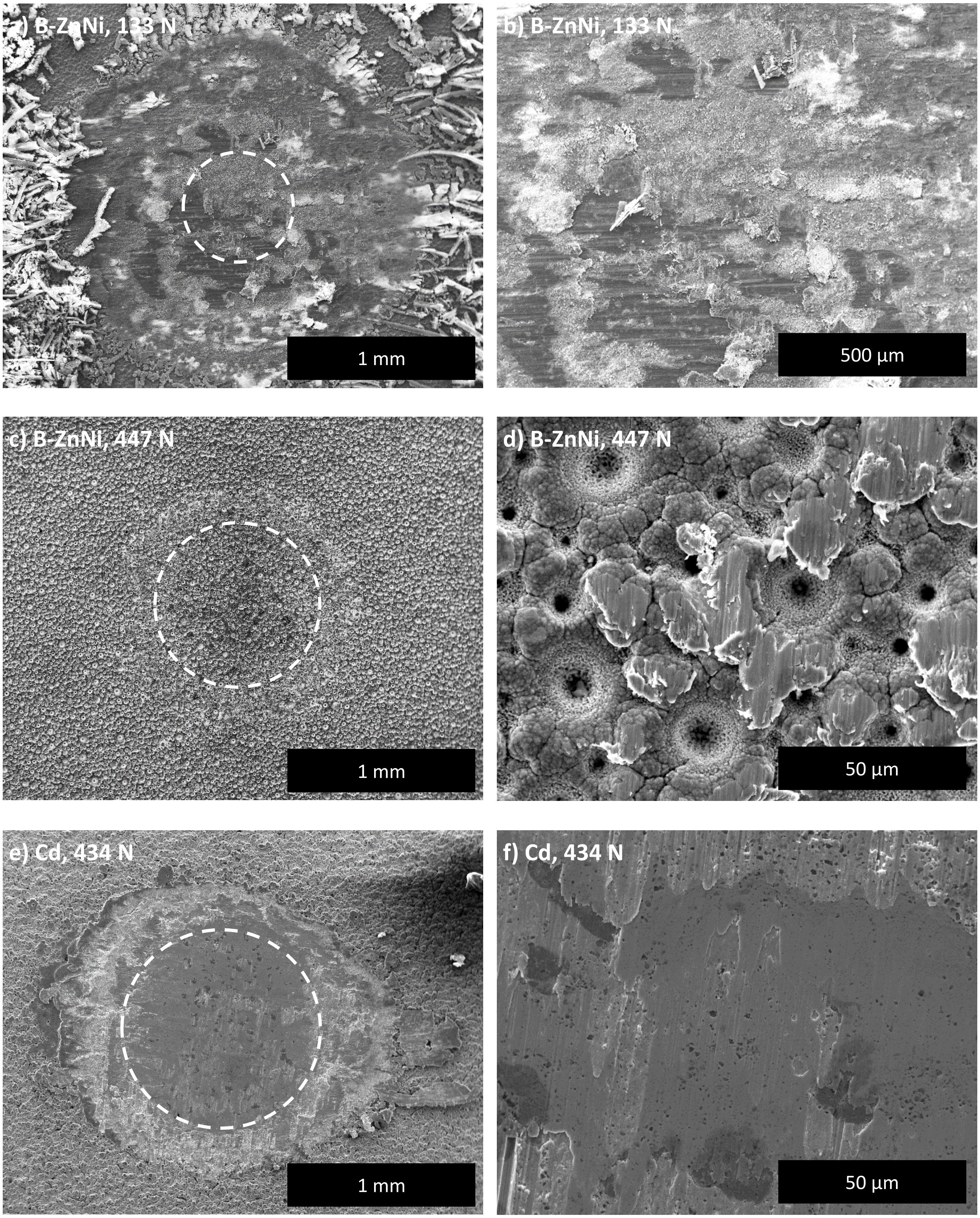

Figure 5.13 SE images of fretting scars for B-ZnNi at (a-b) 133 N and (c-d) 447 N normal loads and (e-f) Cd at 434 N using ±150 µm displacement amplitude after 10,000 cycles. ↔ Sliding direction

Analysis of the wear scar depth is shown in Figure 5.14. As the displacement amplitude increased, the depth of the wear scars increased. At ±70 µm, cadmium coating has the deepest wear scar, followed by B-ZnNi under 133 N load, then B-ZnNi under 447 N load. As the displacement amplitude is increased, the wear scar depth of B-ZnNi under 133 N load increases substantially. The wear scar depth of B-ZnNi under 447 N remain the lowest of the 3 conditions.

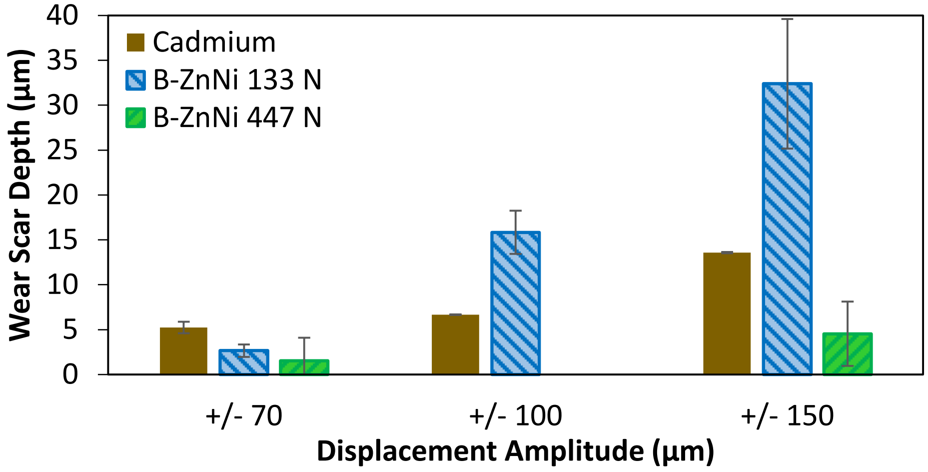

Figure 5.14 Wear Scar Depth Comparison

5.5 Discussion

The fretting behaviour of cadmium and Zn-Ni coatings were studied. As both coating has very different properties and crystal structures, the fretting behaviour was also different. A sensitivity to load is observed for B-ZnNi coating. At 133 N normal load, stick, mixed slip, and gross slip regimes are observed when the displacement amplitude is increased from ± 70, 100 and 150 µm respectively. However, for tests conducted at 447 N, the contact condition remains in the stick regime due to higher adhesion between the coating and counterface. A higher CoF and wear scar depth is also observed for tests conducted at 133 N, which may be attributed to the material removal of the coating at 133 N load is observed, where velocity is mostly accommodated through shearing of the third bodies, coating material and/or substrate. In contrast, for tests conducted at 447N, most of the velocity is accommodated through elastic deformation of the coating and plastic deformation of the tops of the asperities.

Comparison of the fretting behaviour can be made for Cd and B-ZnNi coatings for when the same initial Hertzian contact stress (Cd under 434 N and B-ZnNi under 133 N normal load) is used and when a similar load (Cd under 434 N and B-ZnNi under 447 N normal load) is used. When the same initial Hertzian contact stress was used for Cd and Zn-Ni coatings (Cd under 434 N and B-ZnNi under 133 N normal load) different behaviours were observed. At ±70 µm, although both conditions remain in the stick regime, B-ZnNi has a higher CoF (Figure 5.10) and a smaller wear depth (Figure 5.14). As cadmium is a much softer coating, velocity is accommodated through the plastic deformation of the coating (S_1M_1 [145]) (Figure 5.15a).There also appears to be an ejection flow of material, as coating material from the contact appears to be pushed to the sides of the wear scar, which could lead to the higher wear observed. This phenomena is also observed by Carton *et al*, [185]. In contrast, the velocity accommodation for B-ZnNi is through plastic deformation and shearing of the tops of the asperities of the coating (S_1M_1 & S_1M_3 [145]) and plastically deformed particles fall in the hollows of the coating (Figure 5.15b). Due to the columnar structure of the coating, much less wear occurred for this coating, as elastic deformation can occur by flexing the columns [17, 141], rather than the flow of material, as in the case for Cd. The ejection flow occurred in the form of particles to the sides of the wear scar and is also lower, as there is less wear occurring. As the displacement amplitude is increased, B-ZnNi has a mixed slip and gross slip behaviour, while Cd remains in the partial slip regime. The CoF also increases for both coating, but is less stable for B-ZnNi. Slipping also caused more severe wear for B-ZnNi than Cd. For Cd, the velocity accommodation remains as deformation of the coating (S_1M_1 [145]), although as the displacement amplitude increases, the ejection flow also increases, resulting in more severe wear. B-ZnNi, on the other hand, shows signs of deformation and shearing of the third bodies (S_3M_1 & S_3M_3 [145]) as evidence of the large flat flakes and particulate bed of wear debris. As the displacement amplitude increases, the ejection flow also increases, resulting in a high amount of wear. It should also be noted that the wear scar depth is also much larger than the coating thickness, which could be due to substrate wear or substrate deformation or a combination of both.

When similar normal loads are used (Cd at 434 N and B-ZnNi at 447 N), fretting behaviour is very similar, where both coatings remain in the stick regime when the displacement amplitude is small, and as the displacement amplitude is increased, both coating are within the partial slip regime. The CoF of both coatings are also similar. However, the wear behaviour of both coatings are different.

At high load, the wear of B-ZnNi remains low, while the wear of Cd increases, as evidence in the SE images and wear scar depth. The velocity accommodated for B-ZnNi coating is through plastic deformation of the asperities and elastic deformation of the columns of the coating (S_1M_0 and S_1M_1 [145]) by flexing of the columns (Figure 5.15c) [17, 141]. At this increased load, slipping is more difficult compared to the low load test [186]. As sliding motion did not occur, wear also remained low. In contrast with Cd coating, although similar loads were used, Zn-Ni is also a much harder and stiffer coating, which discourages plastic flow of the material. The yield stress of the coatings were estimated with Equation (5.1) [191]. The maximum principle shear stress before sliding ($(\tau_1)_{max}$) can be estimated by Equation (5.2). Results show that for cadmium, $(\tau_1)_{max}$ is almost double the yield stress, whereas for B-ZnNi, the shear stress was only a fraction of the yield stress.

$$H \approx 3\sigma_y \tag{5.1}$$

$$(\tau_1)_{max} = 0.3p_0 \tag{5.2}$$

Differences between the mechanical properties could have led to differences observed in their fretting behaviour, as plastic flow of the coating was observed for cadmium coating, whereas for B-ZnNi, at high normal loads, only the tops of the asperities were deformed. Although from the energy ratio evolution, both coatings remained in the partial slip regime when similar loads were used, wear of Zn-Ni coating is less than Cd, especially obvious when the displacement amplitude was increased to ±150 μm the wear of Cd increased substantially as the coating material was ejected from the contact in the form of a chip, and was completely removed at some points in the contact.

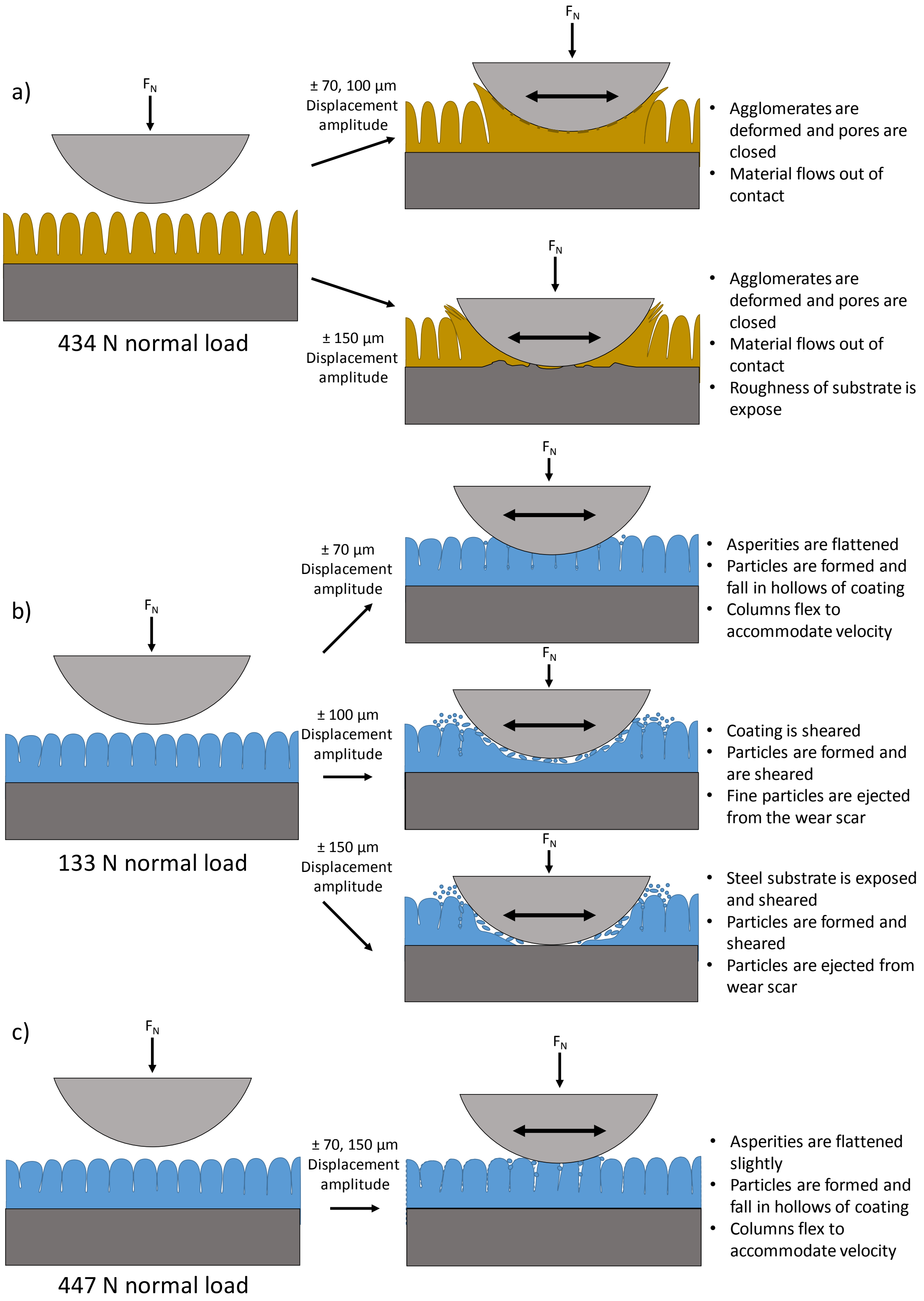

- Agglomerates are deformed and pores are closed
- Material flows out of contact

- Agglomerates are deformed and pores are closed
- Material flows out of contact
- Roughness of substrate is expose

- Asperities is flattened
- Particles are formed and fall in hollows of coating
- Columns flex to accommodate velocity

- Coating is sheared
- Particles are formed and are sheared
- Fine particles are ejected from the wear scar

- Steel substrate is exposed and sheared
- Particles are formed and sheared
- Particles are ejected from wear scar

- Asperities are flattened slightly
- Particles are formed and fall in hollows of coating
- Columns flex to accommodate velocity

Figure 5.15 Schematic representation of wear and velocity accommodation of (a) Cd under 434 N, (b) B-ZnNi under 133 N and (c) B-ZnNi under 447 N

5.6 Conclusion

The fretting wear of an electrodeposited Zn-Ni coating was compared to an electrodeposited Cd coating at a similar calculated contact stress and normal load. Displacement amplitudes which induces contact conditions in the stick, mixed slip and gross slip regimes for Zn-Ni coating was used. When the stick or partial slip regime is induced, B-ZnNi showed less wear than Cd coatings, as B-ZnNi is harder and stiffer than Cd coating, it is less likely to deform and plastically flow. Cd also showed a tendency to push material from the contact region to the side of the wear track, effectively removing the coating from the contact region. This is also more severe as the displacement amplitude increases. When slipping occurred, B-ZnNi coating showed severe wear. Since slipping was observed only in 133 N normal load for B-ZnNi, when a high load was used (447 N), a low amount of wear is observed for B-ZnNi at the same displacement amplitudes.

Acknowledgements

The authors would like to thank Dr. Sriraman Rajagopalan, Priyadarshi Behera, Salim Brahimi and Professor Stephen Yue for their continual support and inputs throughout the experiments. We would also like to thank the Natural Science and Engineering Research Center (NSERC), Boeing Canada, Pratt & Whitney Canada, Héroux Devtek, Canadian Fastener Institute and Messier-Bugatti-Dowty for their financial support. We would also like to thank Boeing, Coventya and Dipsol Inc. for providing specimens.

Chapter 6

The effect of contact stress on the sliding wear behaviour of Zn-Ni electrodeposited coatings

L. Lee, P. Behera, K. R. Sriraman & R. R. Chromik

This chapter is a manuscript intended for publication. The previous two chapters, the effects of coating morphology on the fretting behaviour and comparisons with cadmium coating was made. Fretting looks at when the displacement is small in comparison to the contact area. In the next two chapters, the sliding wear behaviour is discussed, in which the displacement is large in comparison to the contact area. In this chapter, the effect of coating morphology is again explored, but in terms or a large displacement, where the wear track can be exposed to the ambient environment.

Abstract

Zinc nickel coatings, developed in the 1980's as a replacement for zinc coatings in the automotive industry, has recently gained an interest in the aerospace industry as a replacement for cadmium as cadmium is carcinogenic and toxic. Due to different material properties of Zn-Ni and Cd, there is potential in these coatings to be used in tribological application. Sliding wear tests were performed on a reciprocating pin-on-flat tribometer using a steel countersphere on two morphologically different Zn-Ni coatings. Varying normal loads at relative humidity of 60 % were used. Wear tracks from the two coatings were analyzed and compared through wear track

morphology, chemical analysis and wear rates to see the effects of coating morphology on the sliding wear behaviour.

6.1 Introduction

Zinc-Nickel alloy coating were developed in the 1980's as a corrosion protective coating for the automotive industry [1]. Recently, they have drawn attention as a replacement for cadmium, which is also a good corrosion protection coating, but is toxic, carcinogenic and some cadmium plating baths contain cyanide [2-5, 21, 168]. Cadmium is used in the aerospace industry on landing gear components and fasteners, where both corrosion and tribological properties are important. Zn-Ni coatings, being a well utilized corrosion resistant coating for more than three decades, are a leading candidate to replace Cd coatings. However, while many studies have been made on the corrosion protection properties of Zn-Ni coatings [1, 4, 8, 9, 21, 22, 28, 29, 192], fewer studies have been made on the tribological properties of Zn-Ni coatings [3, 12, 28, 151, 186].

Recent studies on the tribology of Zn-Ni coatings include work by Sriraman *et al.* [3, 28] where the sliding wear and tribocorrosion properties of Zn-Ni and Cd were compared. They found that Zn-Ni has a better wear and corrosion resistance during sliding wear and sliding wear tests performed in 3.5 % NaCl solution. Panagopoulos *et al.* [151] conducted tribology testing of Zn-Ni and found a higher but more stable coefficient of friction for alumina counterfaces compared to steel. Increasing the load lowered the friction coefficient but an increase in wear was observed for both cases. Ghaziof and Gao [12] studied the effects of plating parameters on the Ni content, morphology and wear resistance of Zn-Ni coatings. They found that coatings that contained γ-ZnNi with a smoother nodular morphology and higher hardness exhibited better wear resistance and a lower CoF than mixed η and γ phases coatings with cauliflower like morphology and/or γ-phase coatings with larger and coarser nodular structure.

Varying the plating conditions will vary the morphology of the coating, which is one of the main differences between commercially available Zn-Ni coatings [12]. Surface morphology has an important role on the tribological properties of a system. Effects of surface morphology have been studied previously with many bulk materials, and can have a strong effect on the friction and wear behaviour, especially in the initial run-in period [13]. Surface morphology and roughness have a strong effect on the initial contact area, where a higher surface roughness results in a lower contact area. Minimizing the contact area minimizes adhesion, friction and wear [14]. Although higher surface roughness minimizes the contact area, studies have correlated greater wear with higher roughness [13, 15, 16]. Therefore, difference in the surface morphology can affect the friction and wear behaviour of the system.

Trends of friction and wear with roughness may be modified by changing the contact conditions, such as the normal load [16, 143, 147, 151, 193, 194]. Dependence of friction to the normal load in unlubricated metal-metal contacts varies with the system. In instances where the friction and wear is high, such as the case of steel-aluminum contact, the normal load did not significantly influence the friction [147]. In contrast, in metal contacts which forms an oxide layer, such as copper-copper contacts, a low COF was observed at lower loads due to the lubricating properties of the oxide layer, whereas at higher loads, the oxide layer is broken down, and a high COF is observed [147]. In some instances, when an increase in load is coupled with a rougher surface or wear debris, a decrease in COF was observed [147]. In the case of Zn-Ni, Panagopoulos *et al.* [151] found that only at the highest load they used saw a decrease in the friction, whereas lower loads used saw no significant change in steady state friction.

Tribological studies of Zn-Ni alloy coatings are sparse in the open literature and important aspects such as surface morphology and loading effects need to be understood for successful implementation of these coatings in new settings that require good tribological performance. Here, we study two commercially available Zn-Ni coating with distinctly different surface morphology. The sliding friction and wear behaviours of the coatings are explored by varying the load using a pin-on-flat reciprocating tribometer. Correlations of the surface morphology with loading conditions are made by *ex situ* examination of worn surfaces and transfer films.

6.2 Methods

6.2.1 Coating Process

Two commercially available zinc-nickel coatings were plated in industrial pilot plating tanks. The Zn-Ni alloy coating was deposited onto 100 x 160 x 0.8 mm low carbon steel sheets (SAE 1006).

C-ZnNi coatings were plated using an alkaline NaOH (120-135 g/L) based plating solution containing 7-10 g/L zinc and 1-1.8 g/L nickel. Plating was performed at 21-25 °C temperature and 10 mA/cm^2 current density. Plated samples were then passivated using a blue trivalent chrome passivate and baked at 200 °C for 24 hours. [172, 173]

D-ZnNi coatings were plated using an alkaline NaOH (135 g/L) based plating solution with the Zn:Ni ratio maintained at 10-11: 1 and the pH maintained at 12-13.5. Plating was performed at 25 °C temperature and 50 mA/cm^2 current density. Prior to plating, substrates were grit blasted and acid pickled with HCl. Plated samples were then passivated with a blue trivalent conversion coating and baked at 200 °C for 24 hours. [29]

6.2.2 Characterization

Scanning electron microscopy (SEM) was used to observe the as-received coatings, wear tracks and transfer films. An FEI Inspect F-50 microscope (US) with a field emission source was used. Selected specimens were observed in cross section which were cut with a diamond blade, mounted in conductive epoxy, grounded with SiC paper and polished using a 10% mixture of alumina and propanol.

X-ray diffraction (XRD) was used to confirm the phases present in both coatings and measure residual stress. A Bruker Discover D8-2D (US) with a Cu-Kα source was used in the standard θ-2θ mode on the as-received coatings. Biaxial residual stresses on the lateral and longitudinal directions of the coatings was measured on the peak corresponding to the (721) miller index using a standard 2θ sin^{2}ψ method [195].

Adhesion of the coating to the substrate was characterized using microscratch tester by CSM Instruments (Switzerland) with a 200 µm Rockwell C diamond tip. Incremental load scratch tests from 0 N to 30 N with a scratch length of 5 mm were performed at a rate of 5 mm/min.

Profilometry was performed using a white light profilometer (Wyko NT8000, Veeco, US) on the as-received coating in order to obtain the initial coating roughness and profiles of the wear tracks used to calculate wear rate. Wear volume of the wear tracks were calculated based on the average wear area and multiplied by the wear track length and ten profiles were made along the wear track. The average wear area is determined by the material loss below the average surface line and calculated by integrating the area below the surface. The wear rate was then calculated using the Archard and Hirst equation [136] shown in Equation (6.1).

$$K = \frac{Volume\ of\ wear}{(Normal\ Load) \times (Distance)} \tag{6.1}$$

Chemical analysis of the oxide phases on the tribofilm were performed using Raman spectroscopy (inVia Raman microscope by Renishaw, US) which has a 514.5 nm Ar^+ laser excitation source using a laser power of 2.5 mW and Olympus BH-2 microscope.

Electron probe micro analyzer (EPMA) test was previously performed in [186] to assess the composition of the coatings and C-ZnNi contained 14.63 ± 0.05 wt% Ni while D-ZnNi contained 15.65 ± 0.58 wt% Ni. Mechanical properties of the coatings were also previously performed in [186] and similar reduced moduli of $E_r = 127 \pm 15$ GPa for C-ZnNi and 137 ± 12 GPa for D-ZnNi were found. Hardness of the coatings differ (C-ZnNi: $H = 5.2 \pm 0.3$ GPa, D-ZnNi: $H = 6.6 \pm 0.3$ GPa) and may be attributed to the differences in Ni content and crystallographic orientation.

6.2.3 Wear Test

Wear tests were performed using a reciprocating pin-on-flat tribometer using 6.35 mm diameter AISI 440C steel ball counterfaces (Figure 6.1). The relative humidity and temperature were kept at 60% and 20-25 °C, respectively. A sliding speed of 14 mm/s was used. The normal loads of 3.5, 7 and 12 N were used to evaluate the effect of initial Hertzian contact stress (IHCS) on the wear behaviour of the coating. Using a Young's Modulus of 118 GPa and Poisson's ratio of 0.23 for Zn-Ni [174, 175], these normal loads correspond to an estimated maximum IHCS of 750, 940, 1130 MPa, respectively when considering a contact with no roughness. Stripe tests were performed on these coatings, where an initial track length of 20 mm was decreased by 2 mm at cycles 10, 75, 200, 500 and 850, while maintaining a constant sliding speed. A total of 2000 cycles were performed, amounting to a total sliding distance of 46.54 m.

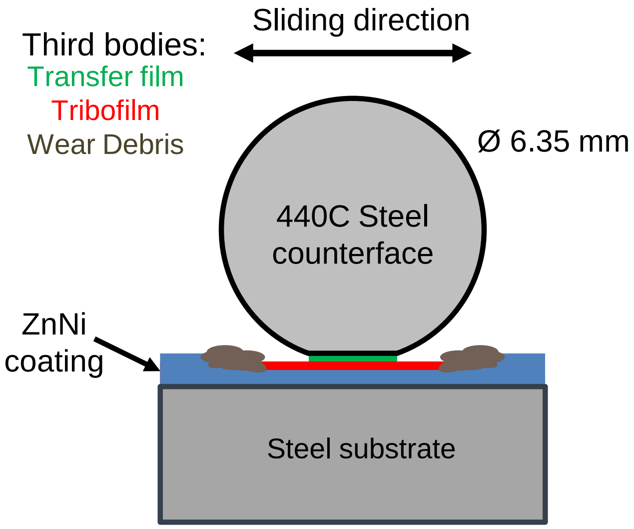

Figure 6.1 Schematic of reciprocating sliding wear test and third bodies [186]

6.3 Results

6.3.1 Characterization

Secondary electron images of the surface morphology and cross section of the as-received coatings is shown in Figure 6.2. The surface of C-ZnNi coatings shows a smooth coating formed through fine platelet agglomerations. Cross section of the coatings reveals a dense coating with through thickness vertical cracks and small porosities. The surface of D-ZnNi coating shows platelets agglomerated into hemispherical shapes, resulting in a rough coating with through coating porosity. Cross section of the coating shows cracks along the agglomerates and small porosities. Profilometry shows a higher roughness for the D-ZnNi coating ($R_a = 2.90 \pm 0.35$ µm) than C-ZnNi coating ($R_a = 1.35 \pm 0.19$ µm) [186]. XRD on the coatings shows that both as received coatings are γ-ZnNi phase and results are presented in Figure 6.3. Biaxial residual stresses measurements on the coatings shows tensile stresses for C-ZnNi, while D-ZnNi shows compressive stresses.

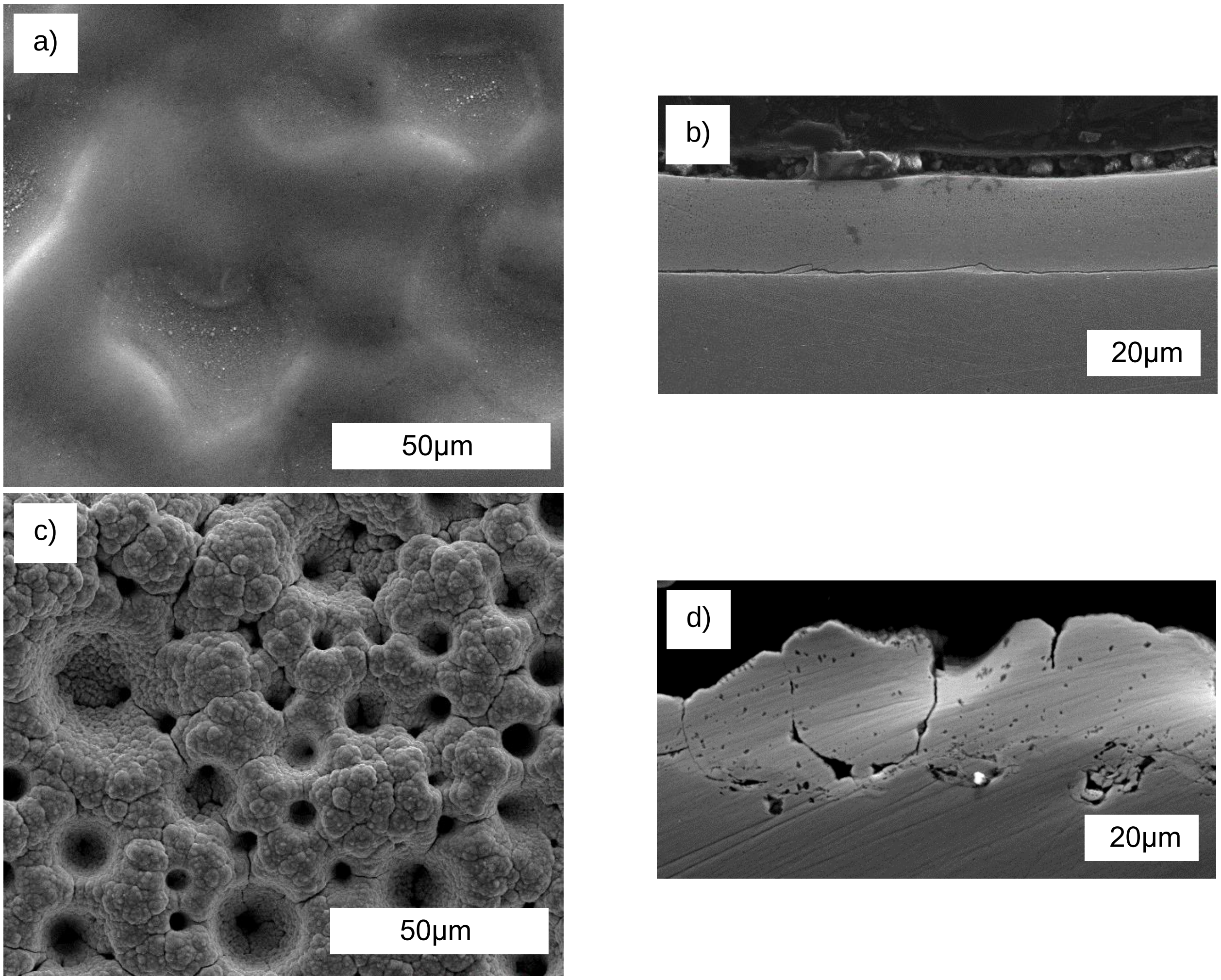

Figure 6.2. C-ZnNi a) surface morphology and b) cross section, and D-ZnNi c) surface morphology and d) cross section secondary electron images [186]

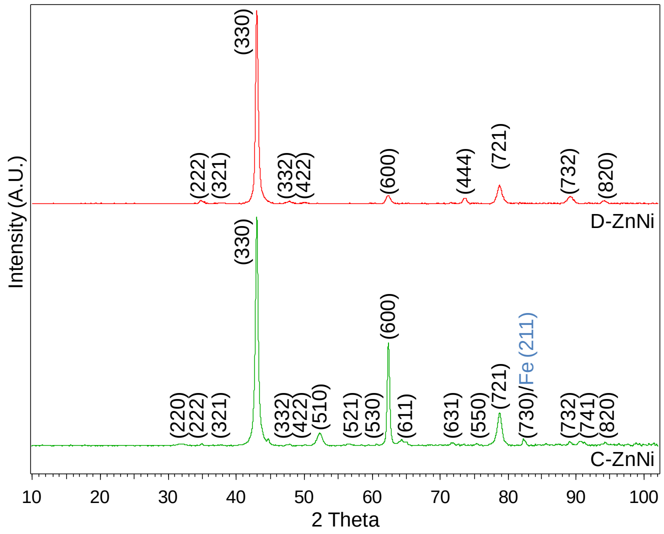

Figure 6.3. XRD diffraction pattern of C-ZnNi and D-ZnNi coatings, peaks corresponding to γ-ZnNi

6.3.2 Adhesion testing

Scratch testing was performed on the coatings to test the adhesion of the two coatings to the substrates and are shown in Figure 6.4. Both coatings showed good adhesion to the substrate. No decohesion at the interface was observed. Ductile failure modes through tensile cracking was observed for both coatings at the beginning of the scratch test, and near the end of the test, the coating is scraped off where the steel substrate is exposed [196, 197]. However, for C-ZnNi coatings, cracks were observed at the onset of the scratch and continued through the scratch as cracks and spallation at the sides of the track. Cracking and spallation at the sides of the track is not observed in tests performed on D-ZnNi coating. In addition, the scratch is accommodated by D-ZnNi coatings through deformation of the plating agglomerates. The onset of tensile cracks (indicated by the number 1) also occurred earlier in the tests for C-ZnNi coatings. The onset of continuous exposure (indicated by the number 2) also occurred earlier for C-ZnNi coatings. Also, for C-ZnNi coatings, patches of steel is also exposed as the coating is removed (indicated by number 3), which corresponds to a discontinuity observed in the tangential force. The width of the scratch tracks is also wider for C-ZnNi coatings than D-ZnNi coatings, which also corresponds to the hardness, as D-ZnNi is harder than C-ZnNi, a wider track is expected for C-ZnNi.

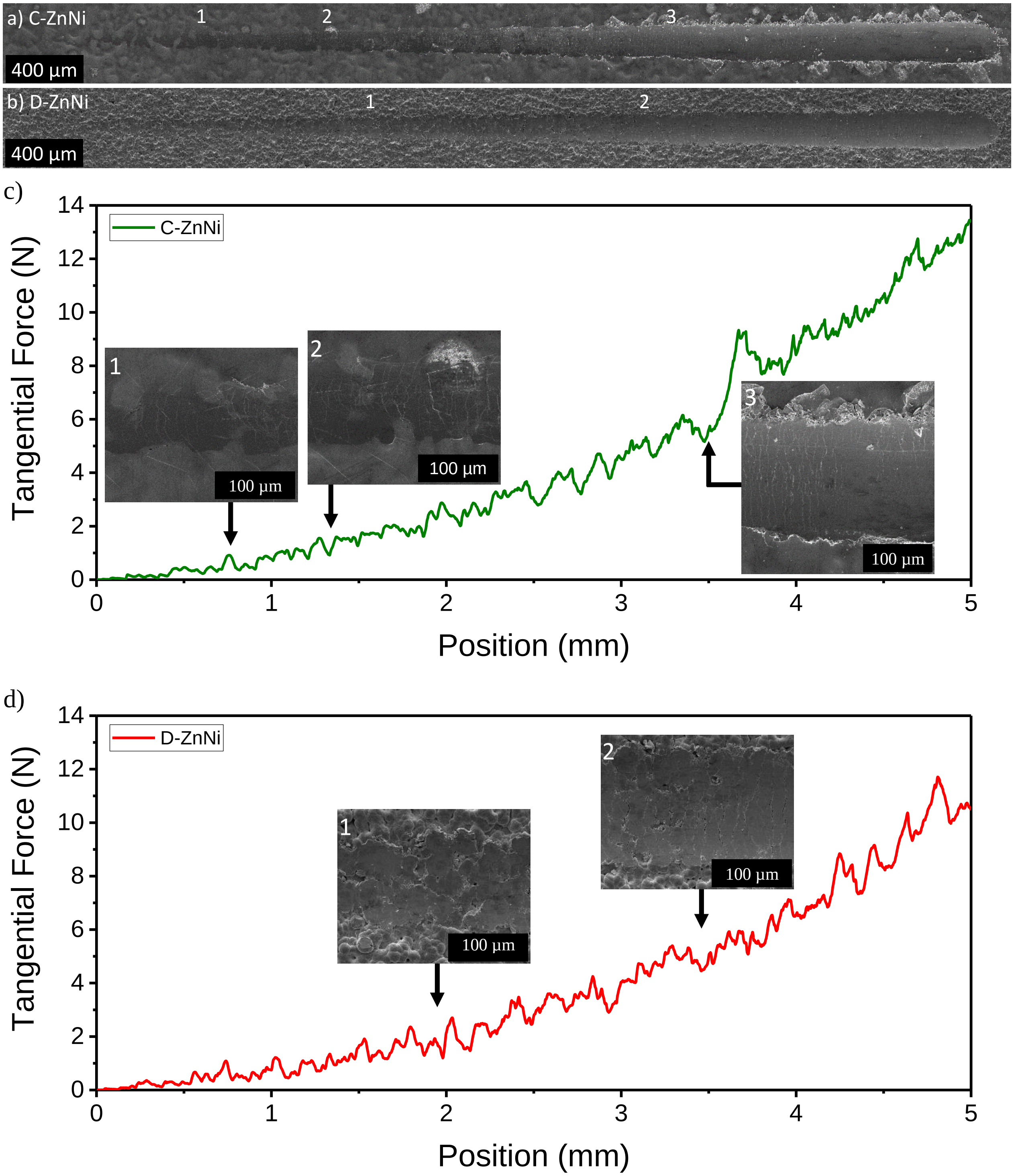

Figure 6.4 Optical images of scratch test performed on (a) C-ZnNi and (b) D-ZnNi coatings and corresponding tangential forces for (c) C-ZnNi and (d) D-ZnNi, with numbers indicating transitions

6.3.3 Wear Test

Sliding wear tests were performed on the two different coatings. Figure 6.5 shows the evolution of coefficient of friction (CoF) with the number of cycle of wear for both coatings. Both coatings show similar trends at normal loads of 3.5 and 7 N. At 3.5 N, the CoF of both coatings increases to 0.85 in the initial run-in period and stabilizes after around 250 cycles to 0.5 in the stable regime. Similarly, at 7 N for both coatings, the CoF increases to 0.85 in the initial run-in period, followed by a stable regime with a CoF of 0.55. Differences between the coatings are observed at 12 N normal load. For D-ZnNi, an increase of the CoF to 0.85 is observed in the run-in period, followed by a stable regime at a CoF of 0.7. In contrast, with C-ZnNi, the CoF rises to 0.7 and stabilizes after around 100 cycles until the end of the test.

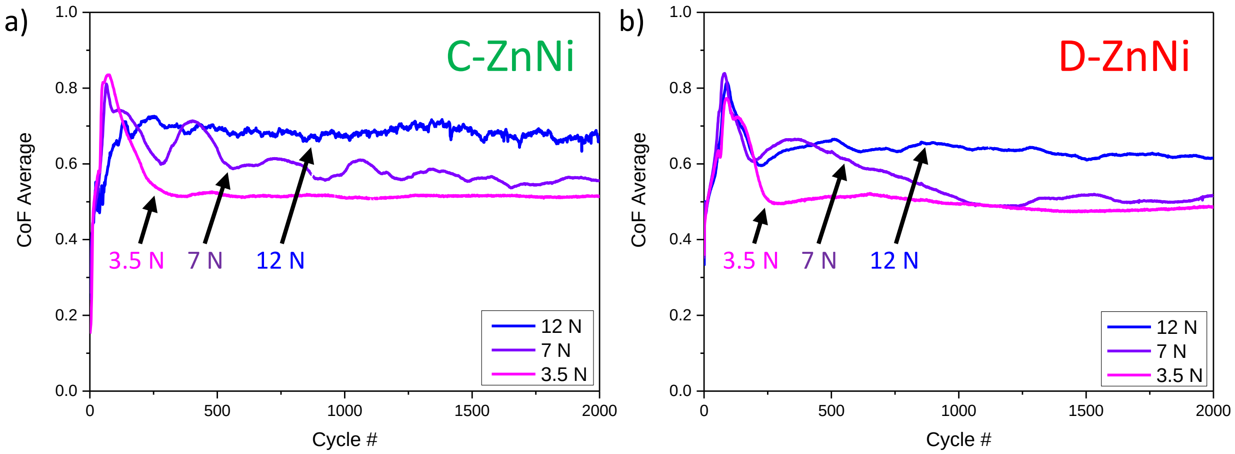

Figure 6.5 Average coefficient of friction evolution at 12, 7 and 3.5 N for (a) C-ZnNi and (b) D-ZnNi

Secondary electron images of the wear tracks are shown in Figure 6.6-6.7. Tests performed at normal loads of 3.5 and 7 N showed mild wear in both coatings, where increasing the normal load increased the severity. After 10 cycles only asperity wear is observed and after 2000 cycles a more distinguishable wear track is observed. However, the coating is still intact and unworn coating is observed within the wear tracks, shown in Figure 6.8. When the normal load was increased to 12 N, more severe wear is observed. With C-ZnNi, after 75 cycles, a clear wear track is observed with score lines running along the wear track. After 2000 cycles, deeper score lines and a wider wear track are observed. With D-ZnNi, after 75 cycles mild wear is observed. After 2000 cycles, a wider wear track and score lines are observed.

EDX analysis was performed on the wear tracks of 12 N tests and are shown in Figure 6.9. With C-ZnNi after 10 cycles of wear, iron peaks were not observed in the spectra. However, after 2000 cycles of wear, strong iron peaks are observed in the spectra, indicating the exposure of the steel substrate due to coating removal. For D-ZnNi, for both EDX taken after 10 and 2000 cycles of wear, weak iron peaks were observed. Although iron peaks are observed, valleys of unworn areas are still observed within the wear track in both cases, indication that the coating has not worn through although iron peaks are observed in the EDX analysis. Iron peaks observed in these cases may be due to large porosities induced in the coating during the plating process, or contributed by the counterface due to ball wear.

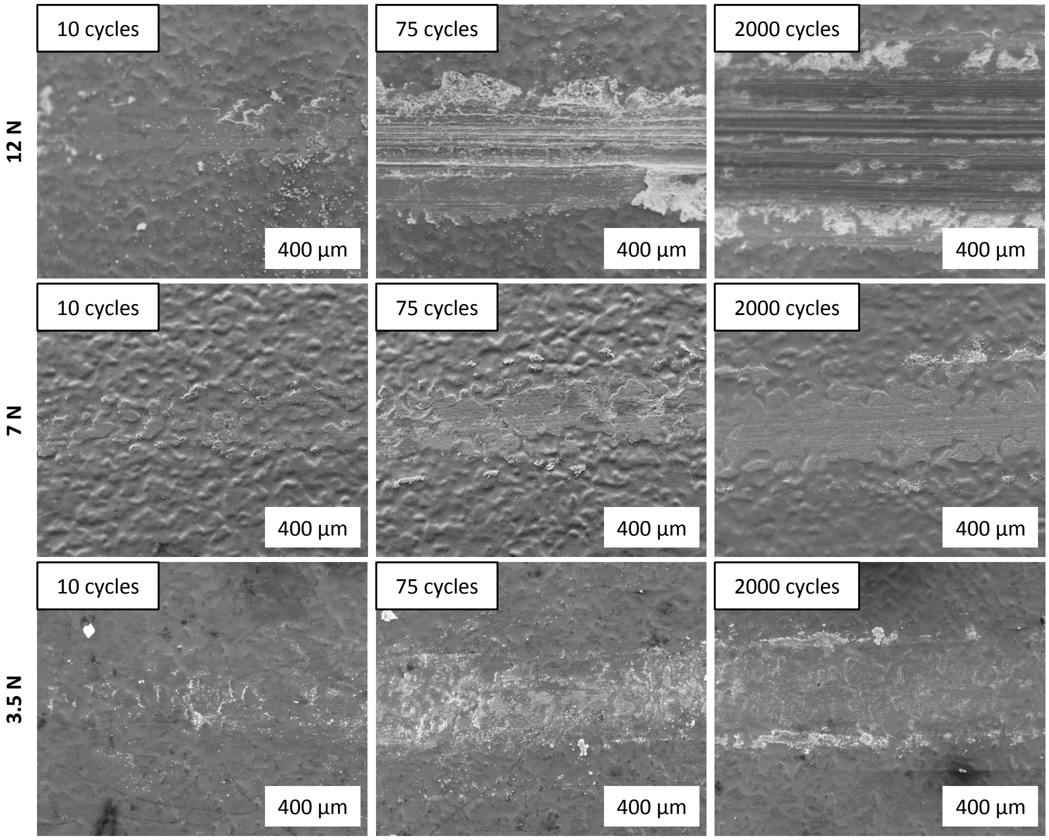

Figure 6.6 SEM images of wear tracks at 10, 75 and 2000 cycles under conditions 3.5, 7 and 12 N normal load for C-ZnNi. Sliding direction ↔

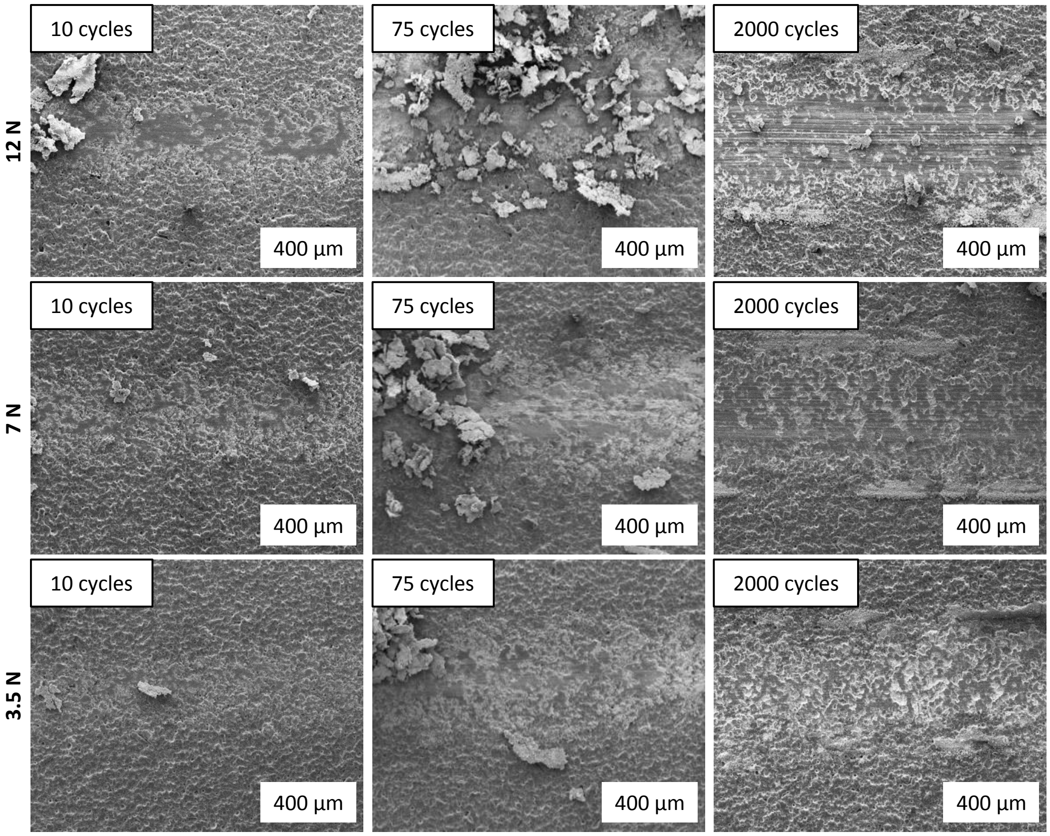

Figure 6.7 SEM images of wear tracks at 10, 75 and 2000 cycles under conditions 3.5, 7 and 12 N normal load for D-ZnNi. Sliding direction ↔

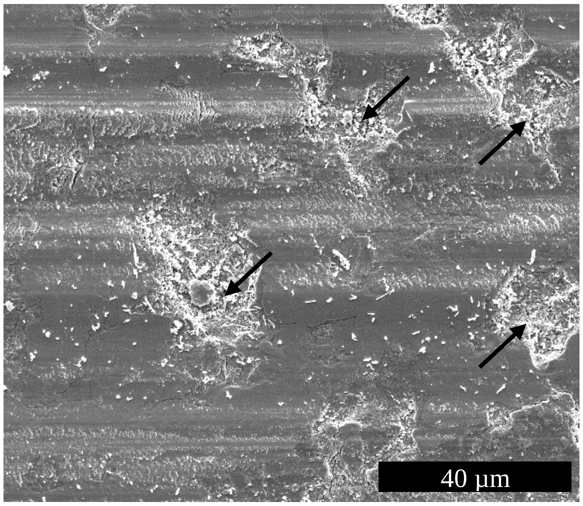

Figure 6.8 SEM image of wear track of D-ZnNi coating after 2000 cycles of wear under 12 N normal load with arrows showing pockets of coatings that have not been worn

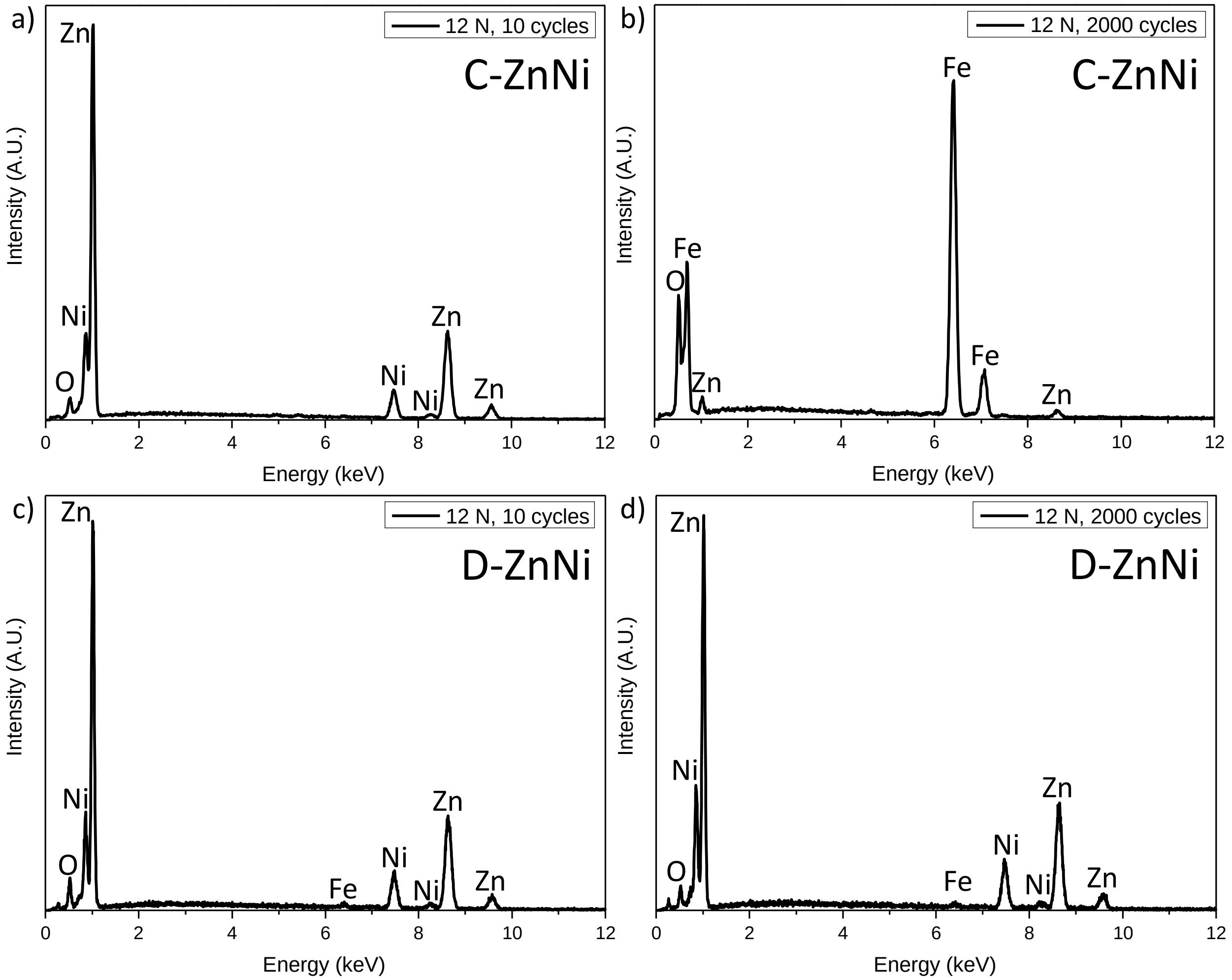

Figure 6.9 EDX of wear tracks at 12 N normal load for C-ZnNi after (a) 10 and (b) 2000 cycles and for D-ZnNi after (c) 10 and (d) 2000 cycles

6.3.4 Wear Rate

Wear volumes and wear rates were calculated for both coatings and are shown in Figure 6.10-6.11. The wear volume (Figure 6.10a) of C-ZnNi conducted at 12 N normal load condition increases throughout the test, while tests conducted at 3.5 and 7 N shows little increase in wear volume as the test progressed. This suggests that for tests conducted at lower normal loads, wear occurs mostly in the initial run in period, while for 12 N condition, wear occurs throughout the test and becomes more severe as the test progresses. A dependence of the wear volume on the normal load is observed for C-ZnNi coating, as increasing the normal load from 3.5 N to 7 N increases the wear volume slightly, while when the normal load is increased from 7 N to 12 N, a drastic increase in wear volume is observed, especially near the end of the test.

For the wear volume of D-ZnNi coatings (Figure 6.10b), higher wear volume is observed when compared to C-ZnNi under 3.5 and 7 N normal loads. However, increasing the normal load to 12 N did not change the wear volume significantly for D-ZnNi coatings. In comparison to C-ZnNi coating, there is little dependency of the wear volume to the normal load at the beginning of the test. This trend may be due to the morphological differences between the coatings. Near the end of the test, a slight dependency of the wear volume to the normal load is observed, as increasing the normal load increases the wear volume slightly.

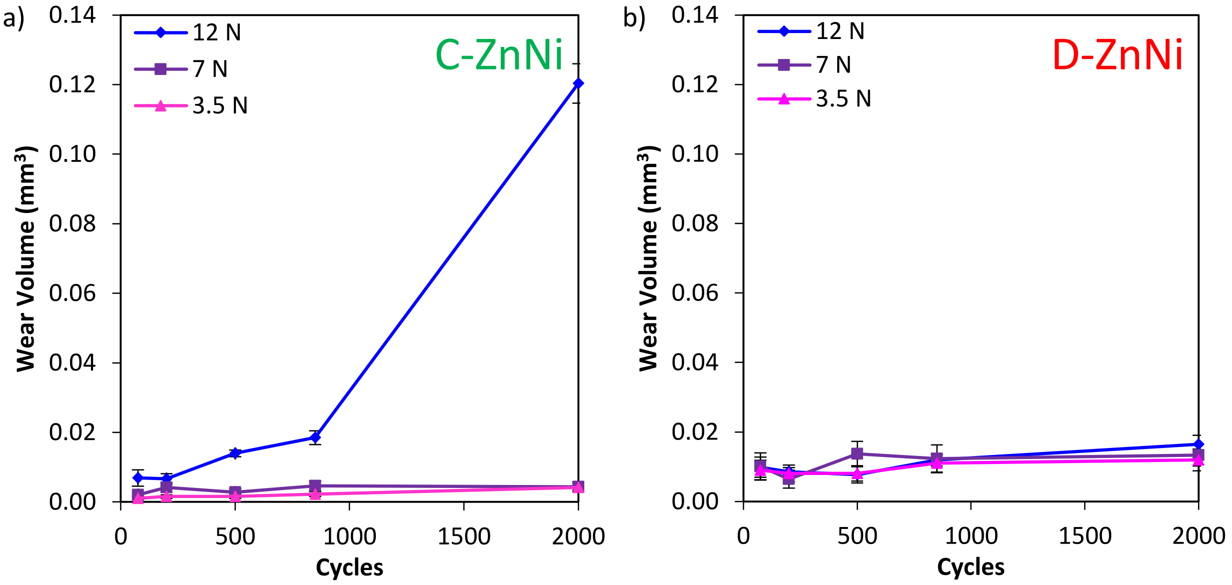

Figure 6.10 Wear volume comparison of 12, 7 and 3.5 N normal loads for (a) C-ZnNi and (b) D-ZnNi coatings

With regards to the wear rate (Figure 6.11a), for normal loads of 3.5 and 7 N, a decreasing wear rate is observed for C-ZnNi coatings, which coincides with the run-in period in the COF evolution (Figure 6.5a), indicating most of the wear occurring during the run-in period where both the wear rate and COF are high, before stabilizing to a low wear rate in the steady state regime. At 12 N normal load, a decreasing wear rate is also observed in the initial cycles. However, the wear rate is higher than the lower normal load and an increase in wear rate is observed after 850 cycles, indicating large amount of the coating is removed from the wear tracks. This trend is in agreement with the SEM images of the wear track morphologies.

A decreasing wear rate trend is also observed for D-ZnNi in all three normal load conditions (Figure 6.11b). Wear rates in the run-in period is high due to the flattening of asperities and formation of a transfer film at the initial cycles. Lower wear rates are observed at later cycles during the steady state regime. As opposed to C-ZnNi coatings, the wear rate decreases with an increasing normal load. The wear rates are also higher with D-ZnNi coatings.

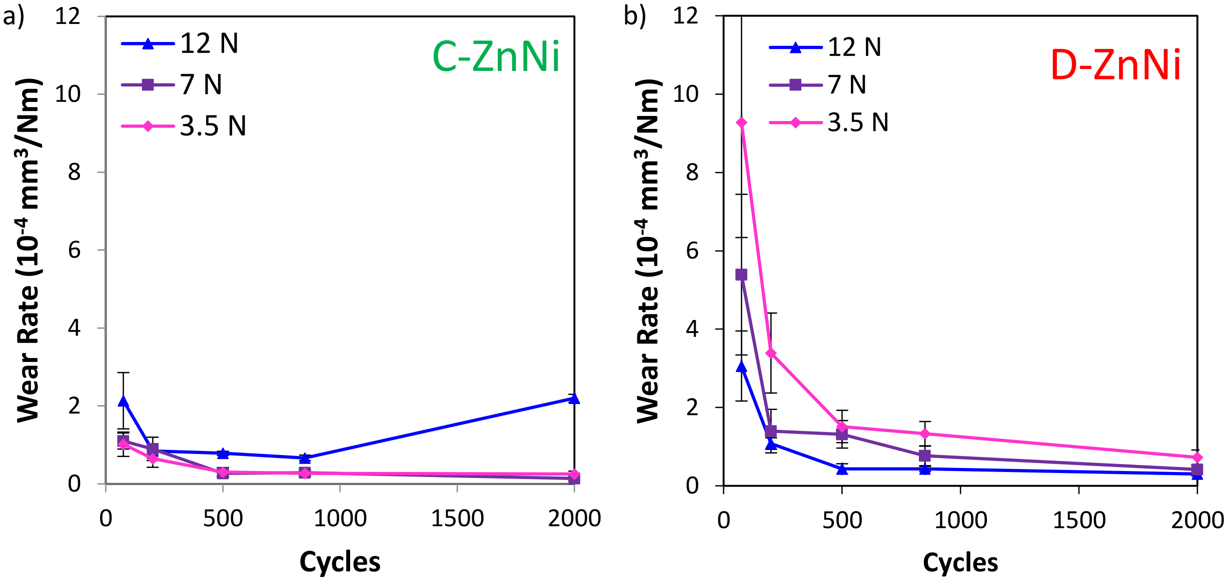

Figure 6.11 Wear rate comparison of 12, 7 and 3.5 N normal loads for (a) C-ZnNi and (b) D-ZnNi coatings

Perhaps another method of looking at wear is through the power law of wear (Eq 2) proposed by Siniawski *et al.* [137]. This equation looks at the abrasion rate, where *A(n)* is the average abrasion rate, V_n is the average wear volume at *n* cycles, *d* is the sliding distance, A_1 is the abrasion rate at the first cycle, and β is a constant of the abrasion rate. By plotting the average abrasion rate, $\overline{A(n)} = V_n/d$ to the number of cycles, A_1 and β can be obtained.

$$\overline{A(n)} = \frac{V_n}{d} = A_1 n^{\beta}, \qquad (Eq\ 2)$$

Table 6.1 Siniawski`s model parameter results

Coating	Load (N)	A_1 (mm^3/m)	β	RMS
C-ZnNi	3.5	2.5 x 10^{-3}	-0.47	0.21
	7	1.5 x 10^{-2}	-0.67	0.27
	12*	1.5 x 10^{-2} *	-0.45 *	0.27 *
D-ZnNi	3.5	7.6 x 10^{-2}	-0.76	0.18
	7	6.5 x 10^{-2}	-0.72	0.30
	12	6.1 x 10^{-2}	-0.71	0.30

* Results from 2000 cycles were not used in calculations due to substrate wear.

From the results shown in Table 6.1, β is negative for both coatings at all 3 load conditions, which is normally observed for metal-metal contacts [137]. However, it can be seen that β is more negative for D-ZnNi than C-ZnNi. β is indicative of the time dependence of the abrasive rate and when $\beta = -1$, abrasiveness is lost in a single cycle, whereas when $\beta = 0$, the abrasive rate is constant [137]. Therefore, as D-ZnNi is more negative than C-ZnNi, abrasive wear occurs and is lost earlier in the tests than for C-ZnNi coatings. This is also indicative in the A_1 values, as the abrasive wear in the first cycle is much lower for C-ZnNi than D-ZnNi. It is also interesting to note that at normal loads of 3.5 N, the wear loss due to abrasive wear is lower than at normal loads of 7 and 12 N for C-ZnNi, while it is higher for D-ZnNi. This may be due to the morphological differences between the coatings, as for a smoother and fully dense coating such as C-ZnNi, a higher amount of energy is needed to initiate wear, than for a rougher and defect ridden coating such as D-ZnNi [15]. The lowered A_1 at 7 and 12 N normal loads for D-ZnNi coatings could be due to smoothening of the coating through plastic deformation and coalescing of the asperities resulting in larger flattened areas (Figure 6.7).

6.3.5 Chemical analysis of wear track

Raman spectroscopy was performed to look at the chemical changes on the wear track and are shown in

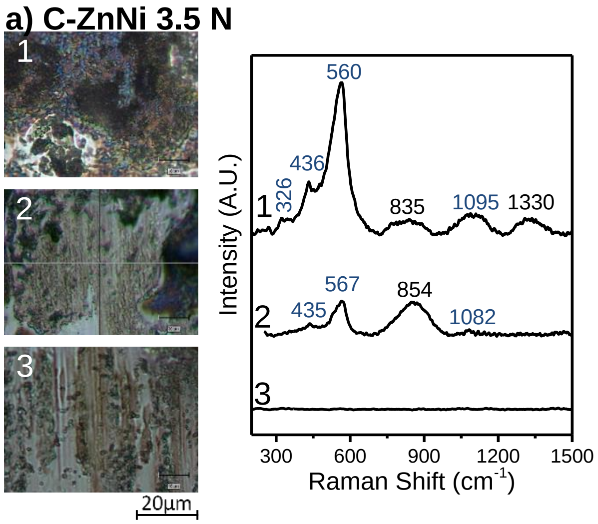
a) C-ZnNi 3.5 N

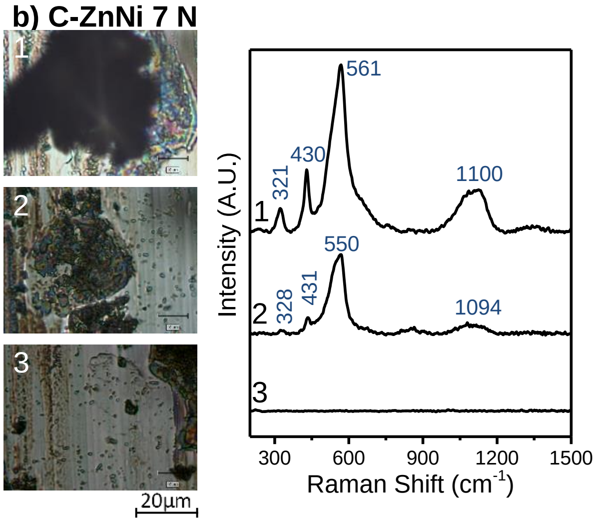
b) C-ZnNi 7 N

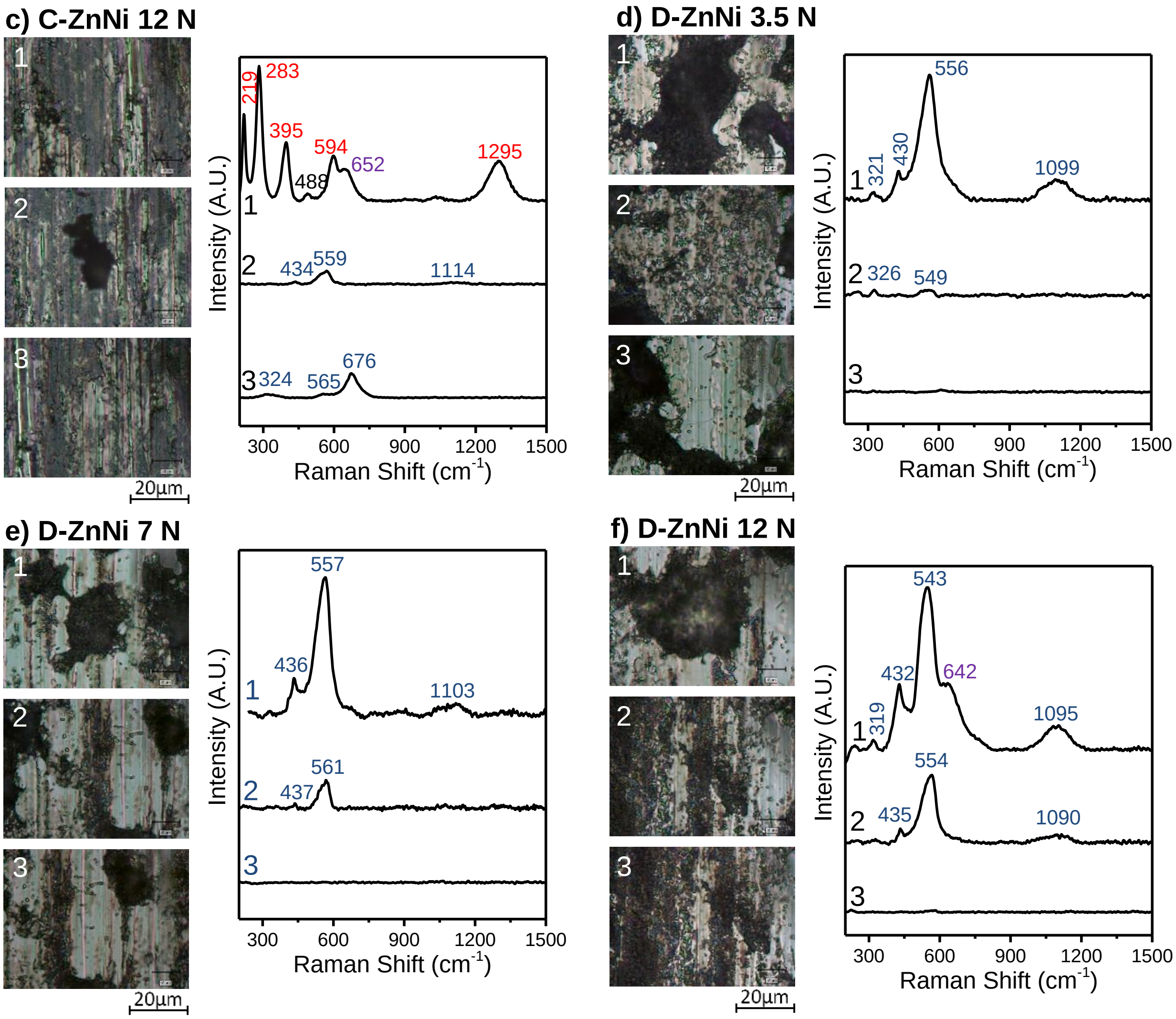

Figure 6.12. Peaks corresponding to zinc oxide [154, 198, 199] were detected on the wear tracks in all cases, which corresponded to the darker film on the surface of the wear track. However, it is evident that the wear tracks obtained using lower normal loads had more ZnO film coverage on the surface than wear tracks obtained using higher normal loads, where the film was mostly broken up. For D-ZnNi coatings, recesses of the unworn coatings are observed throughout the wear track which contained zinc oxide particles. Zinc oxide films was also detected on the surface of the wear track. In the case of C-ZnNi, at low normal load, compacted zinc oxide film is observed on the surface of the wear track. At 7 N, where the coating has not worn through yet after 2000 cycles, the compact film of zinc oxide is again observed on the surface, but at a lesser degree. At 12 N, after 2000 cycles, the coating has been worn through. Optical images of the wear track shows a grayish film on the surface of the wear track, which through Raman spectroscopy, corresponded to iron oxide peaks [200, 201] and a mixed iron and zinc oxide peak at 652 cm^{-1} [198, 200, 201].

As the coating does not contain iron, iron from the zinc and iron oxide mixed layer may have originated from either the counterface, substrate or both.

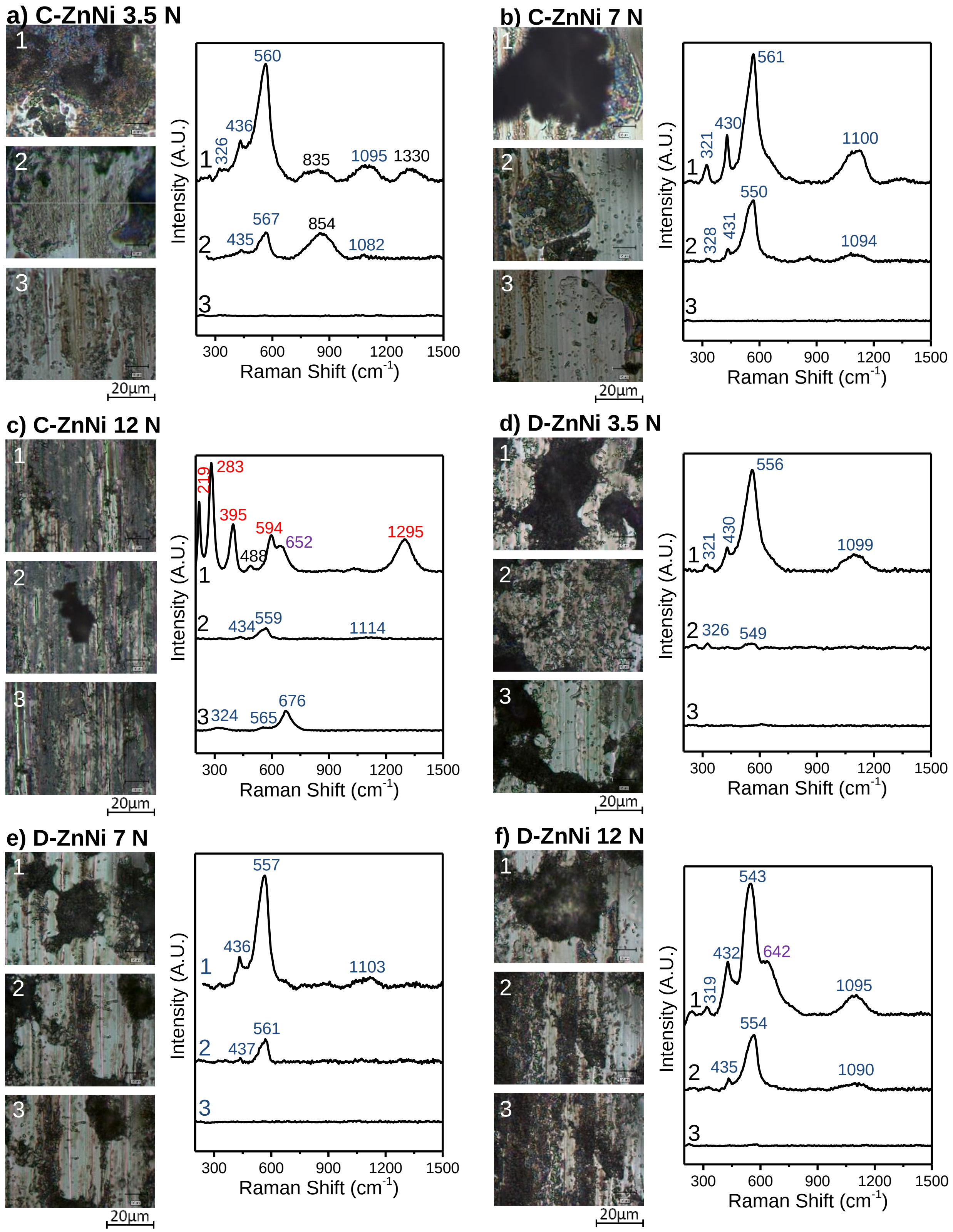

Figure 6.12 Raman Spectroscopy of wear tracks after 2000 cycles of wear for C-ZnNi (a-c) and D-ZnNi (d-f) coatings at 3.5, 7 and 12 N normal loads. ZnO [154, 198, 199], FeO [200, 201] and FeO + ZnO [198, 200, 201] peaks.

6.3.6 Counterface

Secondary electron images of the transfer film are shown in Figure 6.13. In all case coating material was transferred to the counterface as EDX on the transfer films showed Zn and Ni. The size of the area of contact corresponds to the width of the wear tracks. For C-ZnNi coatings, a small transfer film is observed at tests performed at 3.5 and 7 N tests, whereas for tests performed at 12 N, a large area of contact is observed. For D-ZnNi coating, a similar sized contact area is observed at all three normal load conditions. Although the size of the contact area for D-ZnNi coating is larger than the contact area of C-ZnNi coatings at 3.5 and 7 N conditions, at 12 N the contact area remains similar size to the lower normal load conditions.

Large amount of ball wear is observed at the center of the contact of tests performed under 12 N loads for C-ZnNi coatings. In order to calculate the volume lost at the end of the tests, 3D profiles of the transfer film were obtained using white light interferometry. With both coatings, increasing the load increased the wear volume as shown in Table 6.2, while the height of the spherical cap remained similar with the exception of C-ZnNi under 12 N normal load (around 0.8 µm for C-ZnNi coatings conducted at 3.5 and 7 N normal loads, and 2.5-3.5 µm for D-ZnNi coatings conducted at 3.5, 7 and 12 N normal loads). This may be due to increase in contact area due to increase in normal loads, resulting in an increase in wear volume, while the height of the spherical caps remained similar. A larger wear volume and spherical cap height is also observed in D-ZnNi coatings, which could be due to the rougher initial surface morphology of the coating itself or a slightly higher coating hardness of D-ZnNi coatings. For C-ZnNi coatings under 12 N normal loads, substantial of material from the counterface was removed, and the wear volume and spherical cap height (around 6 µm) is the highest among the different test conditions.

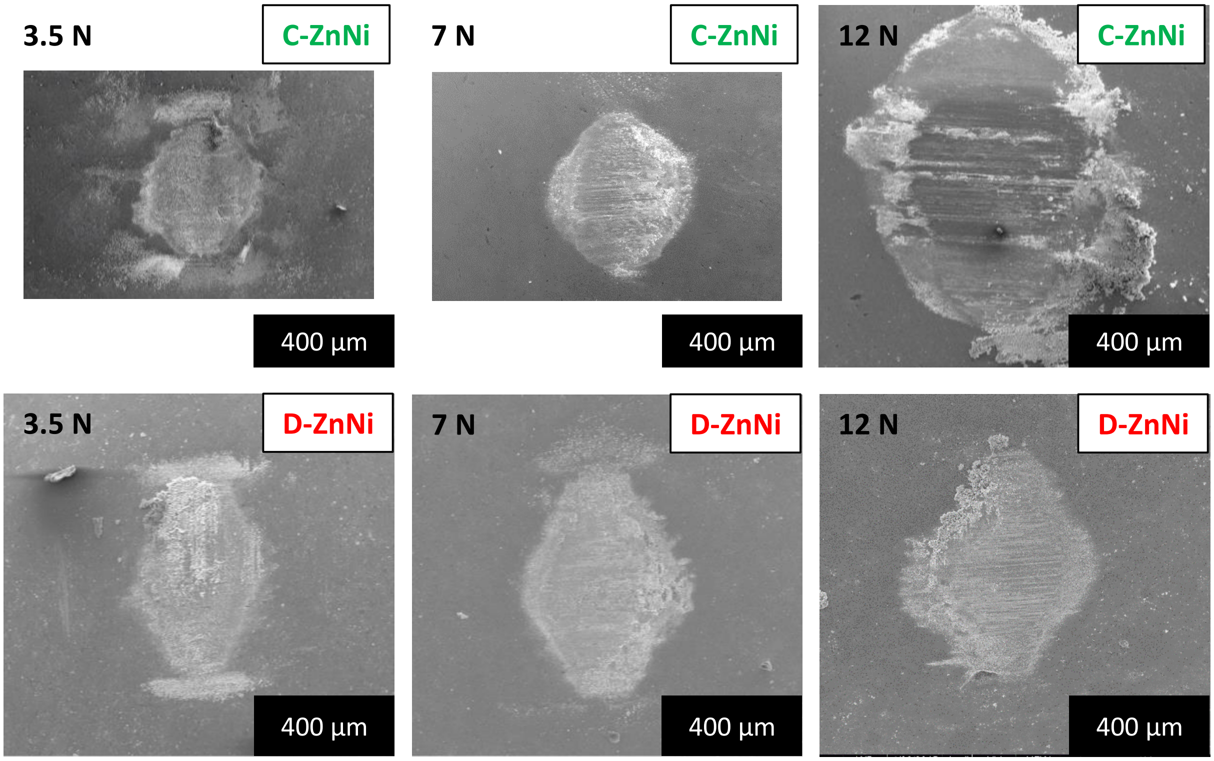

Figure 6.13 Transfer film after 2000 cycles for C-ZnNi and D-ZnNi coatings under 3.5, 7, and 12 N normal load (↔ sliding direction)

Table 6.2 Counterface wear volume

	CF wear volume (mm^3)	
	C-ZnNi	**D-ZnNi**
3.5 N	1.9 x 10^{-5}	4.1 x 10^{-5}
7 N	2.0 x 10^{-5}	10.8 x 10^{-5}
12 N	58.0 x 10^{-5}	17.9 x 10^{-5}

6.4 Discussion

Change in normal load, which consequently changed the IHCS, had a marked effect on the friction and wear behaviour of both Zn-Ni coatings. For friction, shown in Figure 6.5, similar trends are observed for all normal loads, with the exception of C-ZnNi coatings at 12 N, where a high CoF is observed in the run-in period, followed by a gradual drop to a lower steady state CoF. However, increasing the normal load, which increases the IHCS, increased the steady state CoF for both coatings. Increasing the IHCS increases the contact area [193], which is observed in the SEM images (Figure 6.6-6.7), where the worn asperity size in the run-in period and the wear track width in the steady state period is increased. Formation of a transfer film and tribofilm in the run-in period causes an increase of CoF in the run-in period due to wearing of the asperities, which also corresponds to a high wear rate. The CoF gradually decreases to a lower and stable CoF in the steady state period, which also corresponds to a low wear rate. The exception of C-ZnNi under 12 N normal load is due to a different wear mechanism. During the run-in period, flattening of the asperities through material removal occurs faster due to increased adhesion, which could be why we don't see that peak observed in the other test conditions. Score lines observed the SEM image after 75 cycles indicate that a large amount of the coating was removed from the wear track.

Although similar trends were found in the CoF for the 2 different coatings, the wear behaviour of the coatings were very different (shown in Figure 6.10-6.11). At low normal load (3.5 and 7 N) a lower wear rate and wear volume is observed in C-ZnNi coatings than in D-ZnNi coatings. However, at 12 N normal load, higher wear rate and wear volume are observed for C-ZnNi coatings. Morphological differences between the coatings contribute to the differences observed. Both coatings have through thickness defects, however, C-ZnNi is a smooth dense coating with vertical cracks, whereas D-ZnNi is a rough coating with through thickness porosities and cracks along the platelet agglomerates. At low normal loads, a higher wear rate and wear volume are observed for D-ZnNi as defects along the agglomerates allows for easier removal of the coating, resulting in a higher wear rate and wear volume. Previous fretting wear tests done with the same coatings shows more severe wear in D-ZnNi coatings as it is easier to remove coating material when sliding occurs [186]. The surface roughness affects the wear at the initial stages [13] and an increase in surface roughness is associated with an increase in wear rate [16].

At high normal load (12 N), an increasing wear rate and high wear volume is observed for C-ZnNi coatings, while the wear rates and wear volumes for D-ZnNi coatings at this condition remains similar to tests conducted at lower normal loads. Oxide formation aids in stabilizing the CoF and lowering the wear rate for these coatings at the low normal load conditions, as the oxide layer acts as a lubricant between the counterface and the coating in many cases [143, 202]. Nanocrystalline ZnO coatings have been reported to aid in reducing the CoF and wear rate [154, 156, 203]. However, when the normal load increases, the oxide layer begins to break down, as observed

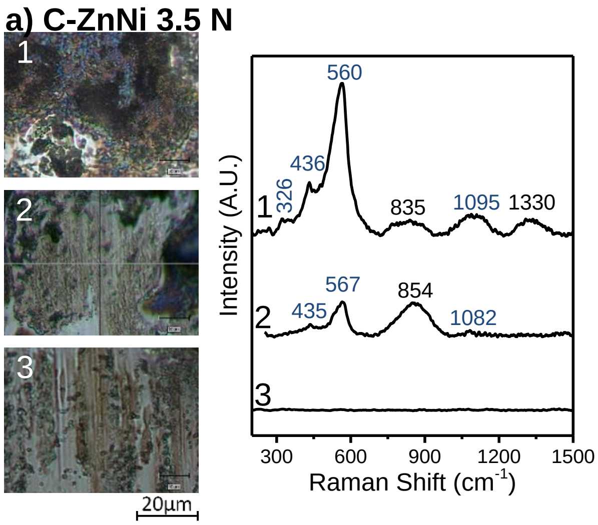

through Raman (

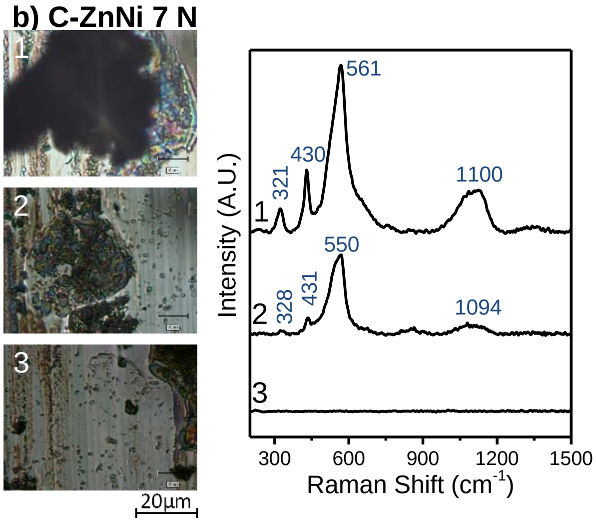

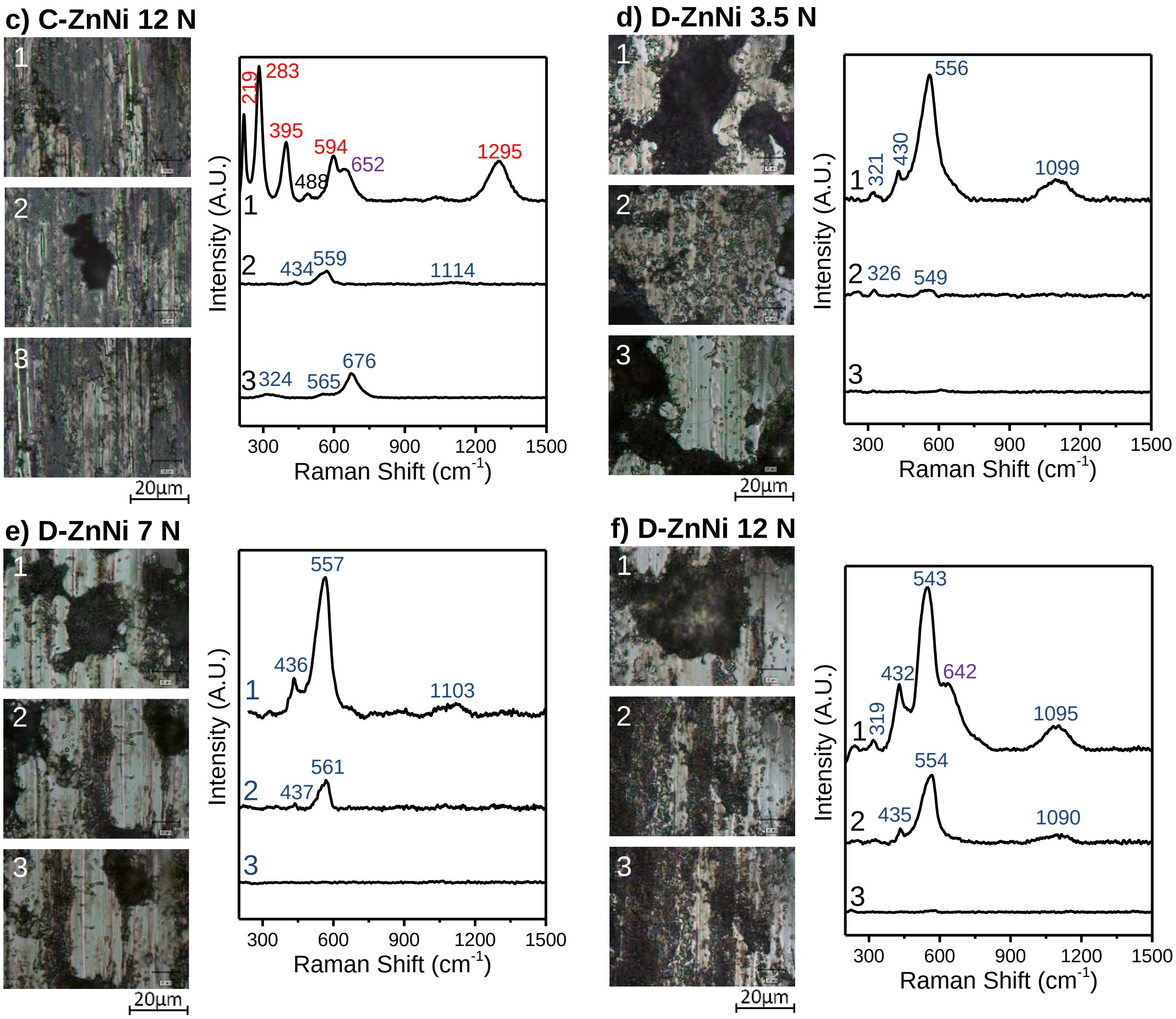

Figure 6.12), and the velocity accommodation becomes adhesive in nature, which could occur where there is an absence of the oxide [143, 202]. This mechanism is shown in Figure 6.14, where when a low normal load is used, such as 3.5 and 7 N, the tips of the asperities are flattened and a thin oxide layer is formed for both coatings during the run-in period. The velocity is accommodated through shearing the oxide layer (Figure 6.14), which resulted in stable CoFs and low wear rates in both cases. When the normal load is increased, such as to 12 N, the oxide layer is broken down. This results in adhesion between the coating and counterface (Figure 6.14). Since C-ZnNi is a denser coating and D-ZnNi has more of a columnar structure, it is easier to deform the columnar structure found in D-ZnNi in order to accommodate the motion than the fully dense C-ZnNi. Consequently, for C-ZnNi severe wear is observed in the coating and counterface (Figure 6.14a), and a higher CoF is observed. In contrast for D-ZnNi, although the CoF and wear were increased, it is less severe, as the asperities can deform plastically and elastically to accommodate the motion

(Figure 6.14b). This is also observed in a previous study from the authors using the same coatings [186], where during high load fretting tests, cracks formed in the contact area of C-ZnNi coatings, whereas for D-ZnNi coatings, asperities were plastically deformed in the stick regime, which shows that when there are high adhesion due to high load, C-ZnNi is more likely to debond than D-ZnNi coatings. This can also be attributed to the different residual stresses of the coatings as the biaxial residual stresses are tensile for C-ZnNi, but compressive for D-ZnNi coatings. Tensile residual stresses can lead to debonding of the coating when external stresses are applied to the coating.

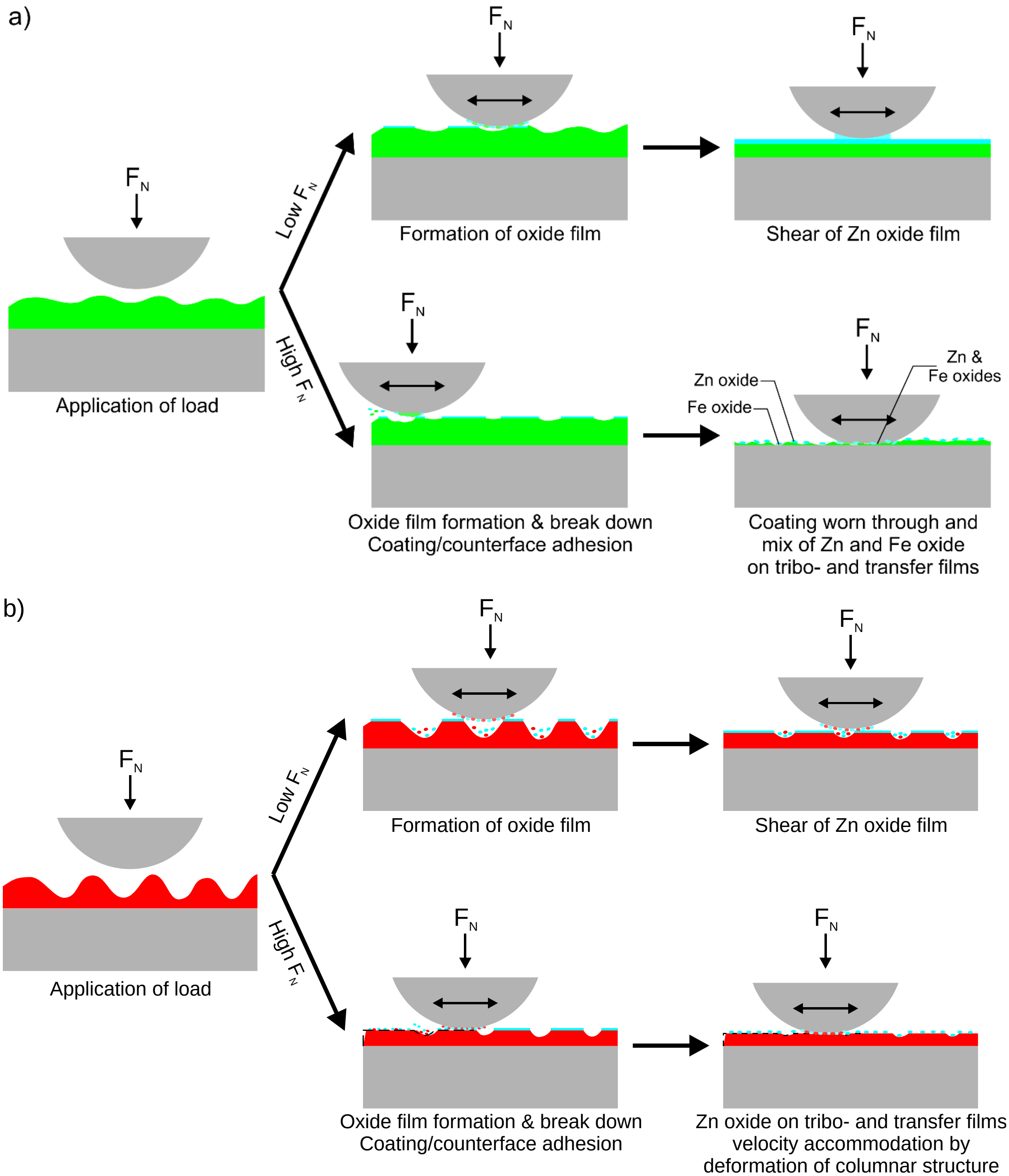

Figure 6.14 Schematic of wear and velocity accommodation mechanisms for (a) C-ZnNi and (b) D-ZnNi coatings at high (12 N) and low (3.5 and 7 N) normal loads

6.5 Conclusion

The effects of IHCS and coating morphology on the tribological behaviour were studied. Similar friction behaviour trends were observed in the 2 coatings at all contact conditions except for C-ZnNi coatings at 12 N normal load due to difference of wear mechanisms. Increase in the normal load resulted in an increase of CoF in the steady state in both coatings. Wear behaviour between the coatings were different due to the difference in coating morphology. At 3.5 and 7 N, wear rate and wear volume of D-ZnNi coatings are higher than C-ZnNi coatings due to higher coating roughness and morphology of the coating defects in D-ZnNi. At 12 N, more severe wear occurred in C-ZnNi coatings due to debonding of the coating. An increase in initial Hertzian contact stress resulted in increase in wear rate and wear volume for C-ZnNi coatings, while a decrease in wear rate and little change in wear volume is observed for D-ZnNi. This suggests that wear behaviour of C-ZnNi coatings are more sensitive to the change in IHCS than D-ZnNi due to the morphological and residual stress differences of the coatings.

Acknowledgement

The authors would like to thank Salim Brahimi for his continual support and inputs throughout the experiments. We would also like to thank Natural Science and Engineering Research Center (NSERC), Boeing Canada, Pratt & Whitney Canada, Héroux Devtek, Canadian Fastener Institute and Messier-Bugatti-Dowty for their financial support. We would also like to thank Boeing, Coventya and Dipsol Inc. for providing specimens.

Chapter 7

Effects of humidity on the sliding wear properties of Zn-Ni alloy coatings

L. Lee, P. Behera, K. R. Sriraman & R. R. Chromik

This chapter is a manuscript intended to be published. In the previous chapter, the effects of coating morphology on the sliding wear behaviour and the effect of normal load is discussed. It was found that an oxide film was formed on the surface of the wear track, and as the normal load is increased the oxide layer was broken down, which led to higher wear rate for the smoother coating. In this chapter, the effects of the oxide layer are further discussed, where the smoother coating is subjected to sliding in a series of different humidity levels.

Abstract

Zn-Ni alloy coatings were developed in the 1980’s as replacement for pure zinc coatings as a sacrificial coating for steel in the automotive industry due to their better corrosion resistance and hydrogen embrittlement properties. More recently, the aerospace industry has taken an interest in these coatings because cadmium, the sacrificial coatings used for steel in the aerospace industry, is toxic and carcinogenic in nature. Although Zn-Ni coatings are mainly used for corrosion protection, an interest in their tribological properties has arisen due to their high hardness. In this study, tribological tests were performed with a reciprocating pin-on-flat tribometer using a steel

countersphere on a commercially electrodeposited Zn-14wt%-Ni coating under relative humidity levels of 0, 20, 40 and 60% with a normal load of 3.5 N. Worn surfaces, debris and transfer films were examined for their morphology, chemistry and microstructure using electron microscopy, energy-dispersive x-ray spectroscopy, x-ray diffraction and Raman spectroscopy. Wear rates were also determined using non-contact profilometry. Tribological behaviour of the coatings under the same contact conditions but different humidity was found to differ, as an increase in humidity corresponded to a more stable coefficient of friction and lower wear rate. This is related to the formation of ZnO on the surface of the wear track which acts as a lubricating layer when humidity is present.

7.1 Introduction

Zn-Ni coatings were developed for the automotive industry in the 1980's for corrosion protection of steel coatings as a replacement for Zn coatings due to their superior corrosion properties to Zn and other Zn alloys [1]. In the past decade, the aerospace industry has developed an interest in these coatings for sacrificial corrosion protection of steel. This is because cadmium (the sacrificial corrosion protective coatings for steel used in the industry) is carcinogenic and toxic, and some cadmium plating baths contain cyanide [2-5]. As these coatings are mainly used for corrosion purposes, their corrosion properties are extensively studied, such as those found in [1, 4, 8, 9, 21, 22, 28, 29, 192]. It was found that cubic γ-ZnNi coatings have the highest corrosion resistance compared to other phases of intermetallic zinc-nickel coatings [8]. Although Zn-Ni is coveted mostly as a replacement coating for cadmium, Zn-Ni is a harder coating than cadmium coatings. This makes Zn-Ni coatings desirable for applications where tribological properties are also important. Few studies are found in the open literature regarding the tribological properties of Zn-Ni. Pangapoulos *et al.* [151] studied the effects of normal load on the coefficient of friction (CoF), and Ghaziof and Gao [204] studied the effects of morphology on the effects on their tribological properties. Interest in their tribological properties with comparison to cadmium can be seen in recent publications, such as work done by Sriraman *et al.*, where they compared the tribological and tribocorrosion properties between Zn-14 wt%-Ni alloy coatings with cadmium and Cd-Ti coatings [3, 28]. They found Zn-14 wt%-Ni to be more wear resistant than cadmium and Cd-Ti in dry sliding wear [3]. Also, Zn-14 wt%-Ni performed better than cadmium and Cd-Ti when submersed in 3.5% NaCl due to nickel surface enrichment in the coatings [28]. Differences between the tribological behaviour of Zn-Ni and cadmium opens up a potential for these coatings in purposes other than corrosion protection, such as wear resistant coatings. Tribological properties of this coating are not well represented in the open literature, and thus studies of Zn-Ni coatings in this area is needed.

Humidity is an important aspect of a tribosystem which greatly affects its friction and wear behaviour, especially in unlubricated conditions. It is well known in metals tribology, the contamination film, which is composed of adsorbed gas particles and/or oxide layer, greatly influence the tribological behaviour of a system [152]. Lancaster [202] reviewed the effects of humidity on metallic, polymer, lamellar solid lubricants, carbon and graphite, and ceramic systems, and divided the effect of humidity into 3 categories: (1) crack propagation, where water vapour or liquid water interacts with the crack tip to accelerate crack propagation; (2) surface reactions, where water vapour or liquid water reacts with the surface to either form protective oxides or reacted layers that are easy to remove; and (3) modification of the third body layer of aggregated wear debris, where liquid water prevents agglomeration of wear particles or disrupts the already agglomerated wear particles or water vapour modifies the properties of agglomerated wear particles. The last effect refers to third bodies that are developed through physical, chemical and/or microstructural changes during the sliding process and have different properties from the parent materials [140, 205]. Development of third bodies modifies the contact and influences the tribological properties [146, 206]. Studies of a steel on steel system showed an increase in humidity resulted in a decrease in CoF and total wear observed [207], while with (Ti,Al)N coatings, abrasive alumina formed and increasing the humidity lowered the abrasiveness of the alumina by forming hydrated oxides [208]. Studies on the effect of cycling of the environment between dry nitrogen and humid air was made on YSZ/Au/MoS_2 coatings showed a strong dependence on the environment as an increased CoF is observed during the humid air cycles, which reverted back to a lower CoF during the dry nitrogen cycles [153]. Further *in situ* studies were made on Pb-Mo-S coating systems, where MoS_2 is known to be sensitive to the environment [209]. *In situ* studies shows humidity changed the morphology of the transfer film, resulting in different velocity accommodation methods and CoF [209].

Studies of Zn-Ni alloy coatings are few in the open literature and does not provide a complete picture of the tribological behaviour of Zn-Ni alloy coatings. There exists extensive tribological studies of Zn and Ni in the open literature. However, Zn-14 wt%-Ni alloy is an intermetallic phase and exhibit different mechanical and tribological properties from its parent metals. It is therefore important to conduct further studies in this coating system in terms of tribology. The purpose of this study is to fill in this knowledge gap by exploring the tribological properties of Zn-Ni alloy coatings coupled with a steel (AISI 440C) counterface using a reciprocating tribometer. Change in contact conditions will be made in terms of change in relative humidity. Wear tracks and transfer film material will be studied through *ex situ* methods.

7.2 Methods

7.2.1 Coating Process

Zinc nickel alloy was electrodeposited onto a 100 x 160 x 0.8 mm low carbon steel (SAE 1006) plate through a commercially available pilot plating bath. The plating solution is an alkaline NaOH (120-135 g/L) based solution and contains zinc (7-10 g/L) and nickel (1-1.8 g/L). The plating operation was performed at 21-25 °C with a current density of 1-3 A/dm^2. The as-plated samples were then passivated using a blue trivalent chrome passivate and then baked at 200 °C for 24 hours. Electron probe micro-analyzer (EPMA) test was performed on the coating in order to determine the percentage of nickel in the coating, and the sample was composed of 14.63 wt% ± 0.05 Ni and 84.83 ± 0.21 wt% Zn.

7.2.2 Characterization

Characterization using scanning electron microscopy (SEM) and energy dispersive spectrometry (EDS) was performed on the unworn coating surface, wear track and transfer film. Surface and cross sectional morphology of the coating and the wear tracks were observed using a Philips XL30 field emission SEM at 20 kV accelerating voltage. Composition of the coatings pre-wear test and post-wear test was performed using EDS. Raman spectroscopy was also used in order to determine oxide phases on the tribofilm. Raman spectroscopy was performed with a Renishaw System InVia Raman microscope, with a low power argon-ion laser excitation (2.5 mW, 514.5 nm). Subsurface morphologies of the wear tracks were observed through a Technai G2 F20 Cryo-STEM. TEM specimens were made with focus ion beam (FIB) lift-out performed using Helios Nanolab DualBeam microscope.

7.2.3 Wear Tests

Wear tests were performed using a reciprocating pin-on-flat tribometer using 6.35 mm diameter AISI 440C steel counterfaces (Figure 7.1). A normal load of 3.5 N, which correspond to an initial Hertzian contact stress (IHCS) of 750 MPa (using an E_{ZnNi} = 118 GPa and ν_{ZnNi} = 0.23 [174, 175]), was used to evaluate the tribological properties of the coatings under relative humidity conditions of 60, 40, 20 and 0%. The relative humidity levels were controlled through the flow of wet and dry air into the chamber enclosing the tribometer. A sliding speed of 14 mm/s was used.

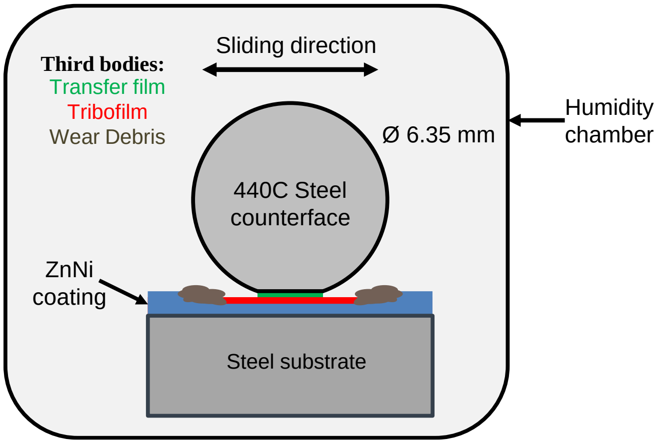

Figure 7.1 Schematic of reciprocating sliding wear test and third bodies

Stripe tests were performed on the coating. In these stripe tests, an initial track length of 20 mm is decreased by 2 mm at cycles 10, 75, 200, 500, 850 and 2000 while maintaining a constant sliding speed of 14 mm/s, amounting to a total sliding distance of 46.54 m.

Wear rates were obtained by scanning the resulting wear scars with a white light profilometer (Wyko NT8000). Wear volume of the wear tracks were calculated based on the average wear area of 10 cross sections, multiplied by the wear track length. The wear rate was then calculated using the Archard and Hirst equation [136] shown in Equation (7.1.

$$K = \frac{Volume\ of\ wear}{(Normal\ Load) \times (Distance)} \tag{7.1}$$

7.3 Results

7.3.1 Characterization

Initial characterization of the coating was performed using SEM and XRD. The electrodeposited coating is composed of fine globular platelets less than 0.5 μm in diameter and forms a smooth and slightly wavy surface (Figure 7.2). Through thickness cracks (see Figure 7.3) are present on the coating, which are induced by the baking step [186]. Cracks are induced to the coatings during the baking step to allow the escape of hydrogen introduced through the electrodeposition process [31, 176]. The coating thickness was measured on the cross sections of the SE images and was found to be around 13 ± 1 μm. The average roughness of the coating is 1.35 ± 0.19 μm, which was previously reported in [186].

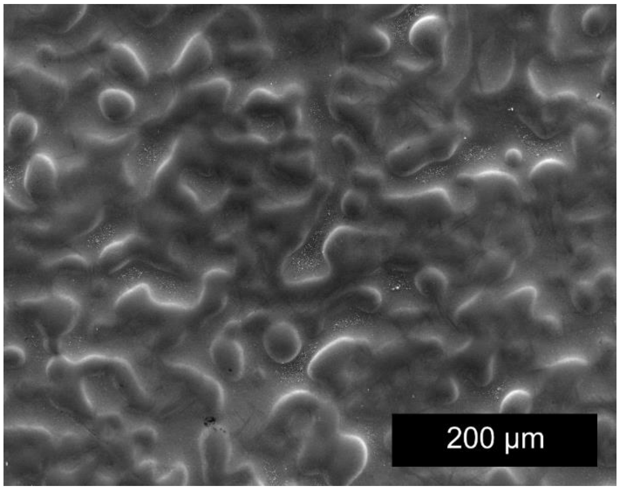

Figure 7.2 Topological SE image of Zn-14 wt%-Ni alloy coating

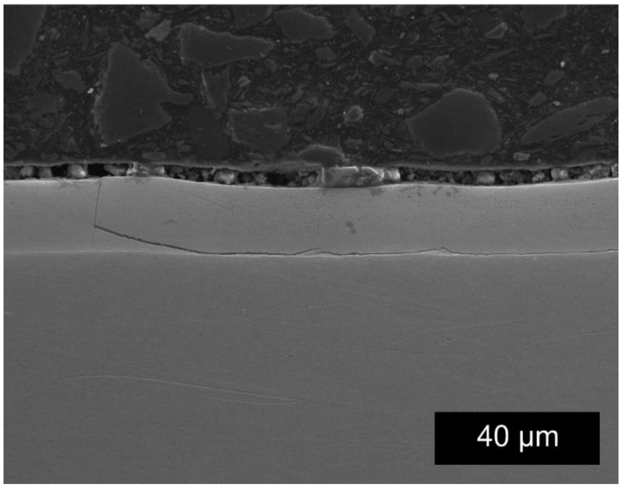

Figure 7.3 Cross section image of Zn-14 wt%-Ni alloy coating

XRD was performed on the as-received coatings in the standard θ-2θ mode with a Co-Kα source. Diffraction pattern obtained previously [186] shows peaks corresponding to the γ-ZnNi phase, which is an intermetallic phase of zinc and nickel found in the range of 12-15 wt.% nickel Zn-Ni alloys. Cubic γ-ZnNi coatings was found to have the highest corrosion resistance compared to other phases of intermetallic zinc-nickel coatings [8].

7.3.2 Wear Test

The evolution of the CoF with the number of cycles is shown in Figure 7.4a. Histograms, which plots the distribution of the CoF in steady state regime, is shown in Figure 7.4b. The steady state regime is defined based on tests performed at RH 60% and 0%, where the curves flatten out. At RH 60%, the CoF increases to 0.8 before stabilizing to 0.5. At RH 40%, the CoF increases to 0.8 and oscillates between 0.6 and 0.7 in the steady state regime. At RH 20%, the CoF increases to 0.7 before stabilizing at around 0.6. At RH 0%, the CoF increases to 0.6 and then stabilizes to 0.5. Both CoF of tests performed in RH 20 and 0% fluctuates at a high frequency in the steady state regime.

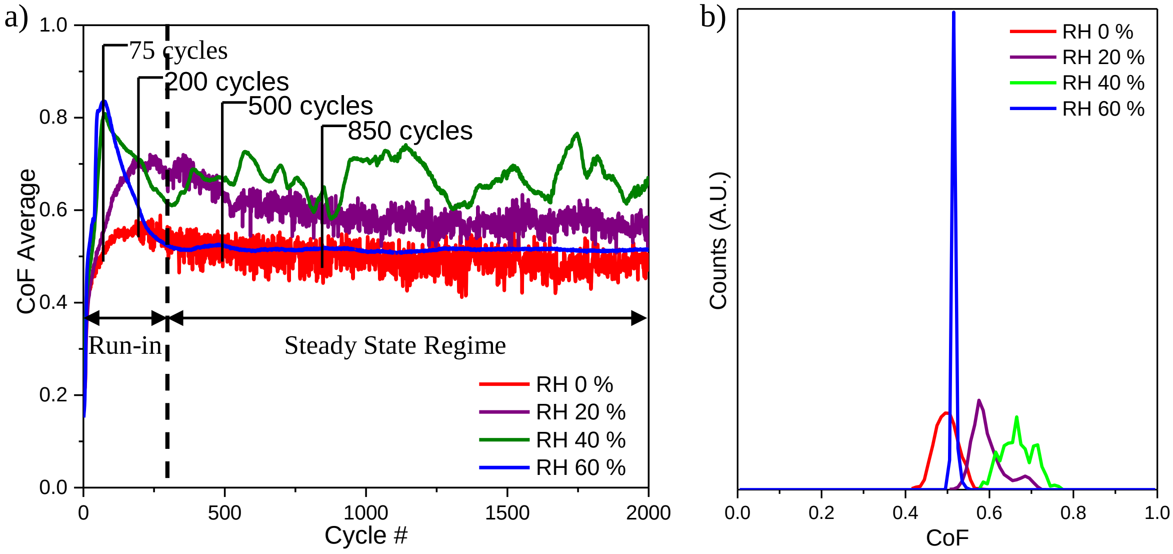

Figure 7.4 (a) CoF evolution and (b) histogram of steady state region of tests performed at RH 60, 40, 20 and 0%

The SEM micrographs of the wear tracks at 75, 200, 850 and 2000 cycles and transfer films after 2000 cycles of wear at different relative humidity levels are shown in Figure 7.5. With tests performed in RH 60%, after 75 cycles of wear, indicative of the peak CoF observed in the run-in period, asperities of the coatings are flattened through deformation and materials removal. Coating material is transferred to the counterface and dispersed in the recess of the coating as particulates.

After 200 cycles of wear, indicative of the end of the run-in period, widening of the asperities are observed. After 850 cycles, indicative of the middle of the steady state period, a distinct wear track is formed, and it appears similar to the wear track after 2000 cycles of wear. For tests performed in RH 60%, the initial increase of the CoF appears to be the result of flattening of the asperities. When a steady state is reached, further wear observed is small.

With tests performed in RH 40% (Figure 7.5), after 75 cycles, flattening of asperities are again observed, which were slightly more severe than RH 60%. After 200 cycles, a defined wear track is observed. After 850 cycles of wear, a score line is observed on the wear track. After 2000 cycles of wear, widening of the wear track is observed, along with the score line observed after 850 cycles. Also, material chip off (indicated by arrows in Figure 7.5) is observed within the wear track after 2000 cycles. Fluctuations observed in the CoF during the steady state regime may be due to the score line and material chip off observed.

With tests performed in RH 20% (Figure 7.5), after 75 cycles of wear, flattening of asperities is observed, however wear at this point is more severe than the higher humidity tests, as can be seen with the wider flattened asperities. After 200 cycles of wear, widening of the wear track is observed and a well-defined wear track is observed, although unworn areas are still observed due to the roughness of the coating. After 850 cycles of wear, the wear track is widened and wear has occurred past the roughness of the coating. Particles and a score line is also observed in the wear track. After 2000 cycles of wear, the wear track is widened. For wear tracks observed in RH 20%, the formation of a defined wear track is much quicker than the tests performed at higher humidity levels, which may account for the lack of a peak of the CoF during the run-in period. The score line and particulates within the wear track may have contributed to the high frequency fluctuations of the CoF during the steady state period.

Wear tracks obtained from RH 0% (Figure 7.5) have the most severe wear out of the 4 humidity levels tested. After 75 cycles of wear, the beginnings of a well-defined wear track is already observed. After 200 cycles of wear, wear has already gone past the roughness of the coating, as unworn coating is not observed within the wear track. After 850 cycles of wear, the wear track is widened and there is a score line present within the wear track. A lot of wear particles is present within the wear track and there appears to be abrasive wear. After 2000 cycles of wear, the wear track is widened and more particulates are observed within the wear track. Abrasive wear is also observed and the score line appears to have widened and deepened. EDS also shows a strong iron peak, which is not observed in lower cycle wear tracks and higher humidity levels, indicating that the coating has been worn through.

The transfer films were also observed and are shown in Figure 7.5. Profilometry data is shown in Table 7.1. As the humidity decreases, there is a thickening and widening of the transfer film. Counterface (CF) wear was also observed. The volume of wear is higher for humidity condition RH 20%, than for humidity conditions RH 40 and 60%, where we see a lower wear volume. Correspondingly, the height of the spherical cap increases from 1 to 3 µm with decreasing humidity. Prow formation is also observed in tests performed in RH 0% from the micrographs (Figure 7.5) and a prow thickness of around 37 µm was measured. Prow formation is defined as the build-up of a lump of transfer material through plastic shearing which separates the surfaces[210], Substantial amount of material is also transferred to the counterface for tests performed in RH 0% as can be seen from the prow formation, which suggests an adhesive nature in wear at this humidity condition.

EDX maps of the oxygen present in the wear track area are shown in Figure 7.6. At 60% relative humidity, the surface of the wear track has a high oxygen peak with exception of areas where the coating has not been worn due to the irregularity of the coating morphology. In contrast, the map for the wear track ran in RH 20%, oxygen is mostly absent from the surface of the wear track and concentrated on the debris at the sides of the wear track and on the particles present within the wear track.

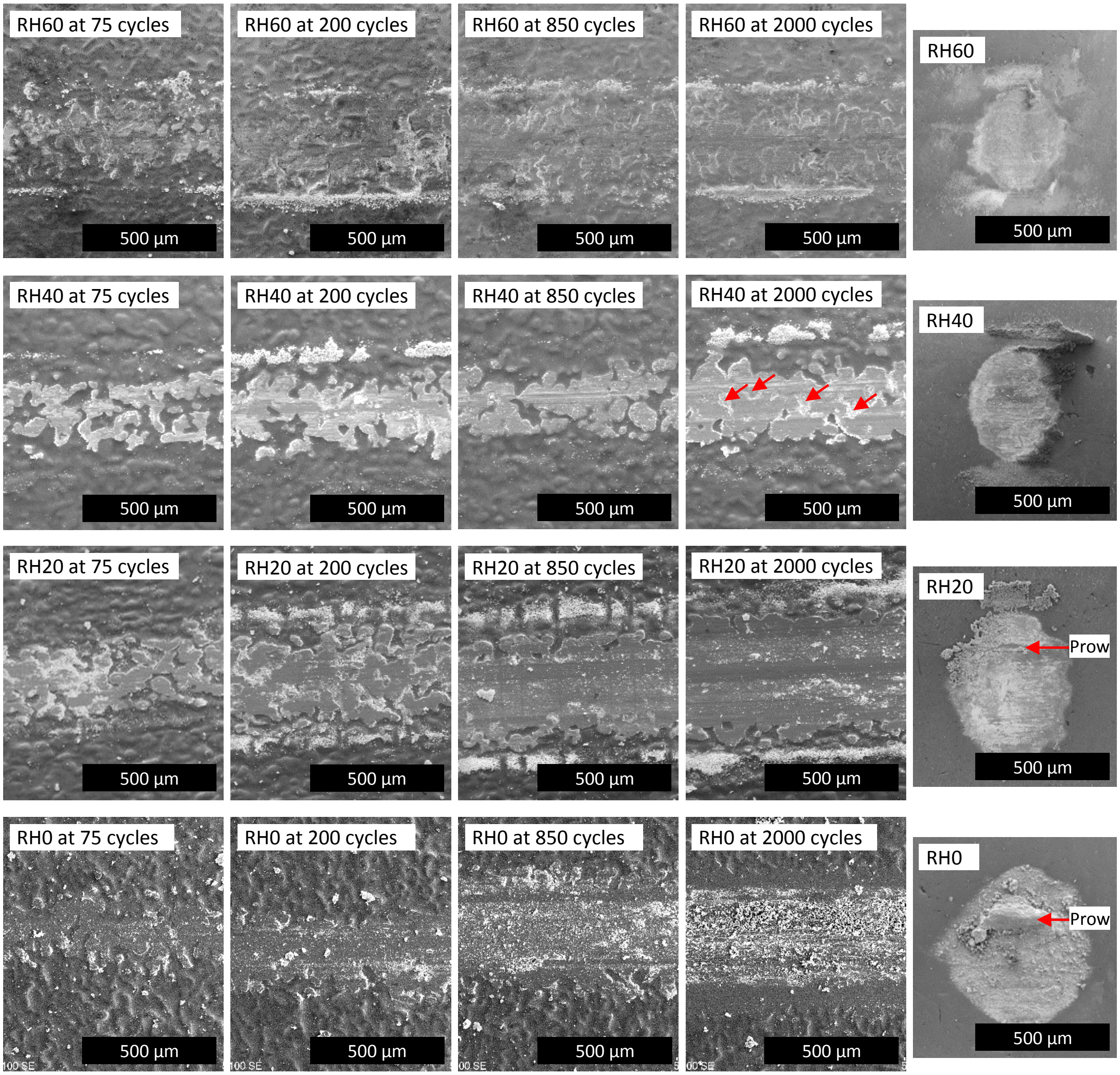

Figure 7.5 Morphologies of wear track at cycles 75, 200, 850 and 2000 (left) and transfer film after 2000 cycles of wear (right) for RH 60, 40, 20 and 0%. Sliding direction ↔

Table 7.1 Counterface wear, transfer film volume and counterface wear rate after 2000 cycles

	Wear Volume (mm^3)	**Transfer film volume (mm^3)**	**Wear rate after 2000 cycles (mm^3/Nm)**
RH0	--	145.72×10^{-5}	--
RH20	12.33×10^{-5}	--	0.075
RH40	4.37×10^{-5}	--	0.027
RH60	1.92×10^{-5}	--	0.012

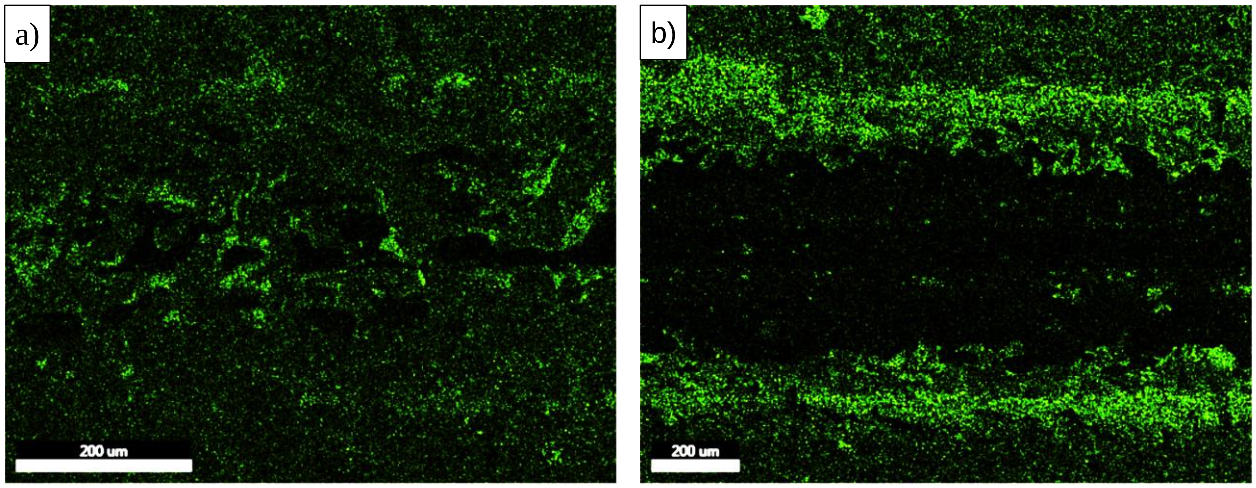

Figure 7.6 EDX map of oxygen peak at wear tracks after 2000 cycles of tests performed at (a) RH 60% and (b) RH 20%. Sliding direction ↔

7.3.3 Wear Rate

The wear rate is shown in Figure 7.7. Initial cycles of the tests show similar wear rates for 0, 20 and 40% RH levels and 60% RH shows a lower wear rate. As the test progressed, the wear rates of tests performed at RH 60 and 40% decreased and stabilized. In comparison, the wear rates of tests performed at RH 20 and 0% increased and are higher than the other humidity levels. This may be due to adhesive wear as evidence by prow formation (Figure 7.5) and subsequent ploughing or cutting of the coating by the prow. Wear rates for tests at RH 0% increased after 850 cycles while tests at RH 20% stayed constant, which may be due to more severe adhesive wear for tests performed at RH 0% due to lack of water vapour in the environment. This led to a larger prow formation and more severe ploughing of the coating, thus removing the coating material from the wear track where the prow is in contact.

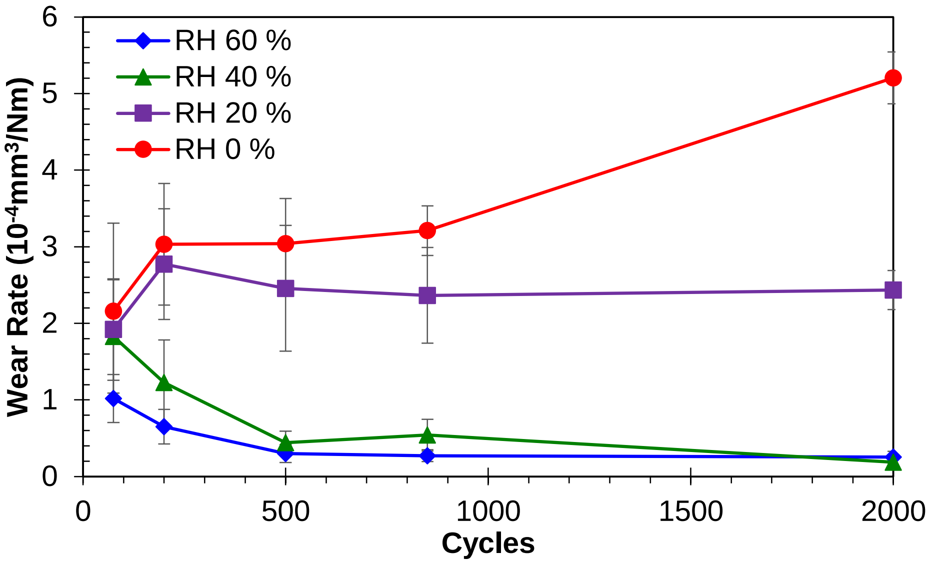

Figure 7.7 Wear rate comparison

7.3.4 Raman Spectroscopy

In order to look at the chemical changes on the wear track obtained at different humidity levels, Raman was performed on the wear tracks from RH 60 and 0%. Optical images of the wear track and location where Raman was performed are shown in Figure 7.8a-d. From the optical images shown in Figure 7.8c-d, the wear track from RH 0% is clean with dark particles scattered throughout the track, whereas the wear track from RH 60%, dark compact film throughout the surface of the wear track is observed. Raman on the dark particles and compact film (Figure 7.8e) observed in both conditions reveals peaks corresponding to ZnO [199]. Although both conditions shows ZnO, the distribution of ZnO is different in both cases. ZnO in RH 60% is more adherent to the wear track and forms a continuous film on the surface (Figure 7.8c), and the peaks corresponding to ZnO are broader. Two spectrums are taken from tracks obtained from RH 0% (Figure 7.8e). One was obtained on the cleaner area, where no peaks were observed. The other was obtained on the dark particles scattered throughout the wear tracks, which again showed peaks corresponding to ZnO (Figure 7.8d-e). The peaks were sharper than that observed from RH 60%. Differences in the peaks in the spectrums could be due to grain size or orientation of the grains [154, 198]. Raman mapping was performed on the wear tracks through mapping the 550 cm^{-1} peak. The maps showed the presence of ZnO on the dark particles and the absence in the wear tracks for those obtained from RH 0% (Figure 7.9). In contrast, for wear tracks obtained in RH 60% (Figure 7.10), presence of the peak was observed throughout the wear track, indicating the dark compact film observed throughout the wear track is ZnO.

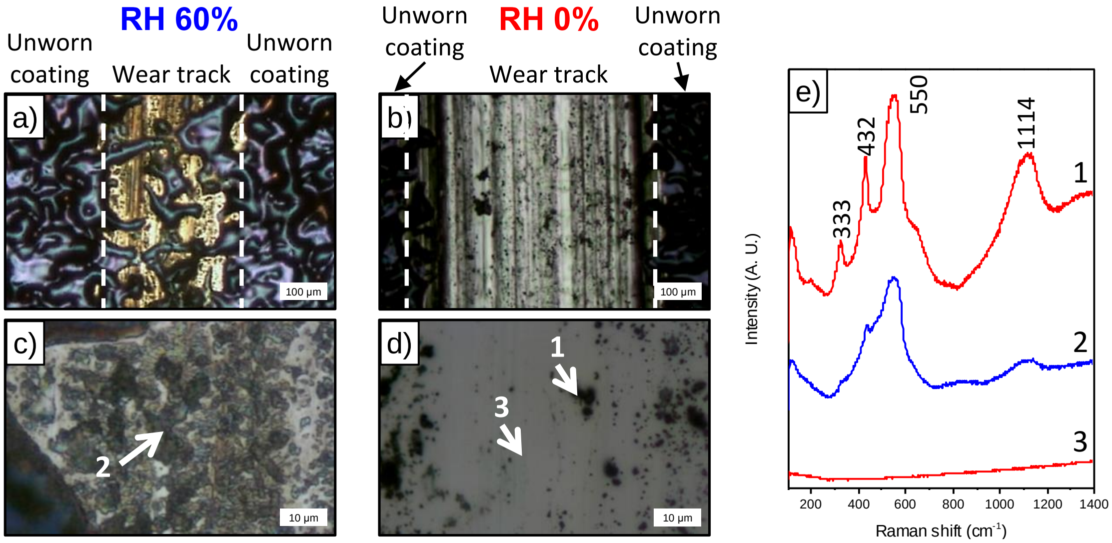

Figure 7.8 Optical images of (a) Wear track at RH 60% and (b) RH 0%. (c) Compacted ZnO patch at RH 60% and (d) dispersed ZnO particles and streak region with ZnO particles at RH 0%. (e) Raman spectra of points 1-3. Sliding direction ↕

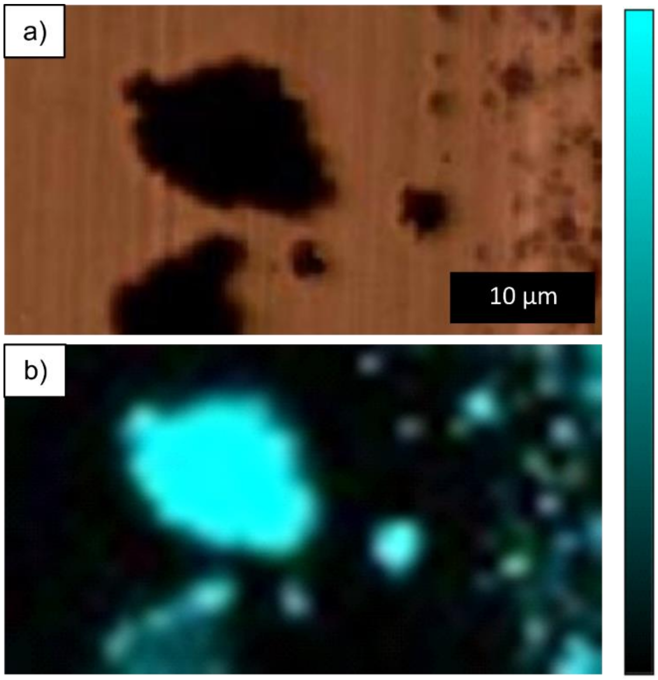

Figure 7.9 (a) Optical image of dark particle and (b) Raman map of intensity between 490-600 cm^{-1} for dark particle on wear track obtained at RH 0%

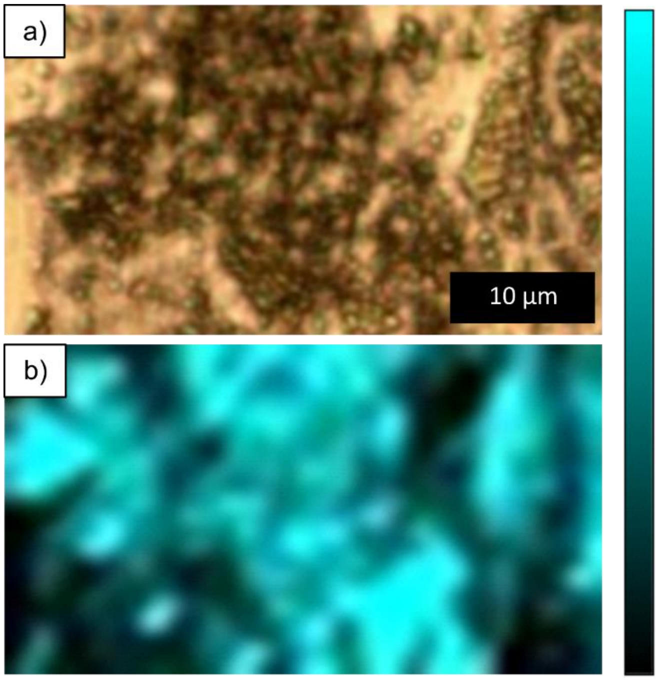

Figure 7.10 (a) Optical image of dark particle and (b) Raman map of intensity between 490-600 cm^{-1} for compact film on wear track obtained at RH 60%

7.3.5 Transmission Electron Microscopy: Selective Area Electron Diffraction

In order to see additional details on the near surface tribofilms, TEM observation and selective area electron diffraction (SAED) was performed on a cross sectional thin foil on the surface of the wear track (Figure 7.11). TEM images revealed a thin nanocrystalline layer on the surface of the wear track obtained in 60% RH with a grain size of around 10 nm (Figure 7.12a). The nanocrystalline layer was not observed on the wear track obtained at 0% RH (Figure 7.13a). Upon closer investigation (Figure 7.12c), a nanometer scale layer of mechanically transformed material is present at the subsurface of the wear track (Figure 7.13c), which is not found on the subsurface of the wear track obtained at 60% RH. Dark field images (Figure 7.13b) also show deformation of the grains into the subsurface of the wear track, which is also not observed in wear tracks obtained at 60% humidity (Figure 7.12b). SAED was performed on the different features on the wear track cross section and compared with the SAED of the unworn samples. Due to the small thickness of the nanocrystalline phase, the area of SAED included some of the larger grain size phase. In order to differentiate the two phases, the rings from the pattern were taken as the nanocrystalline phase. Table 7.2 compares the d-spacing with standard PDF card of hexagonal structured ZnO, which matched well to the d-spacing of the rings, indicating the presence of ZnO in the nanocrystalline layer.

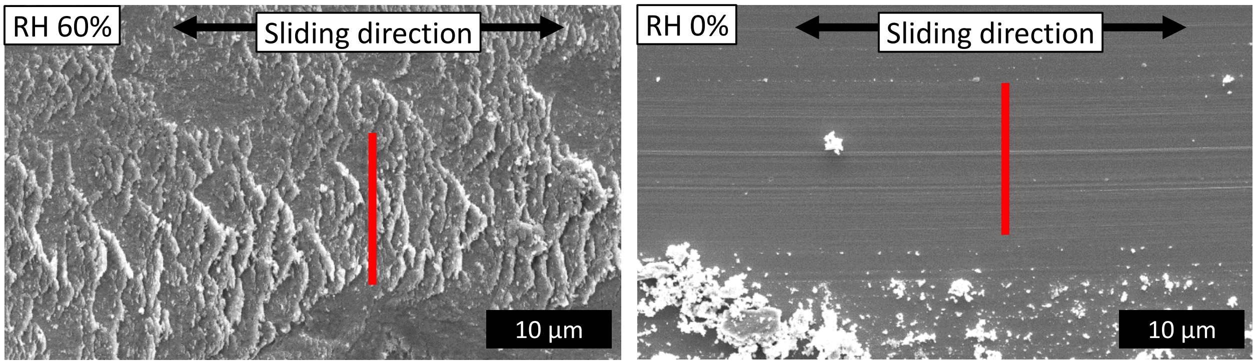

Figure 7.11 Location of TEM foil obtained through FIB cutting after 850 cycles of wear

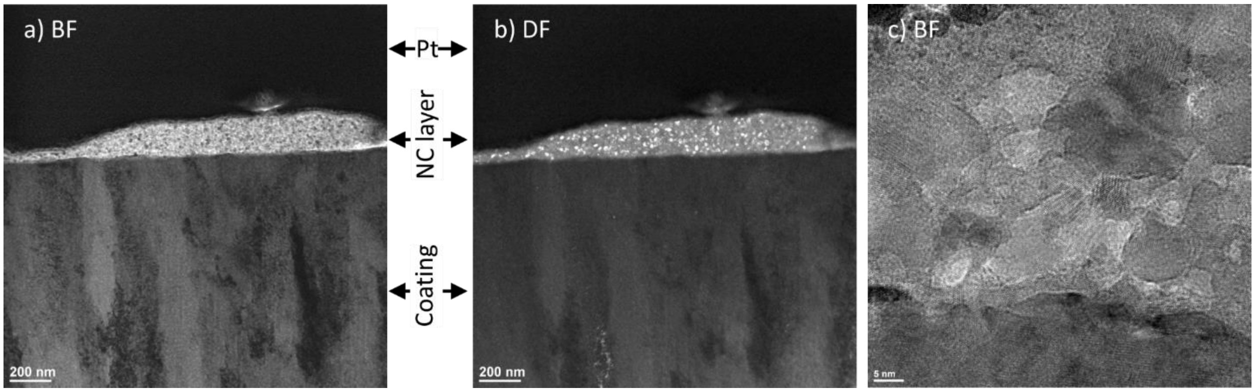

Figure 7.12 TEM images of wear track surface cross section (a) bright field, (b) dark field and (c) magnified image of the nanocrystalline layer obtained in RH 60% environment

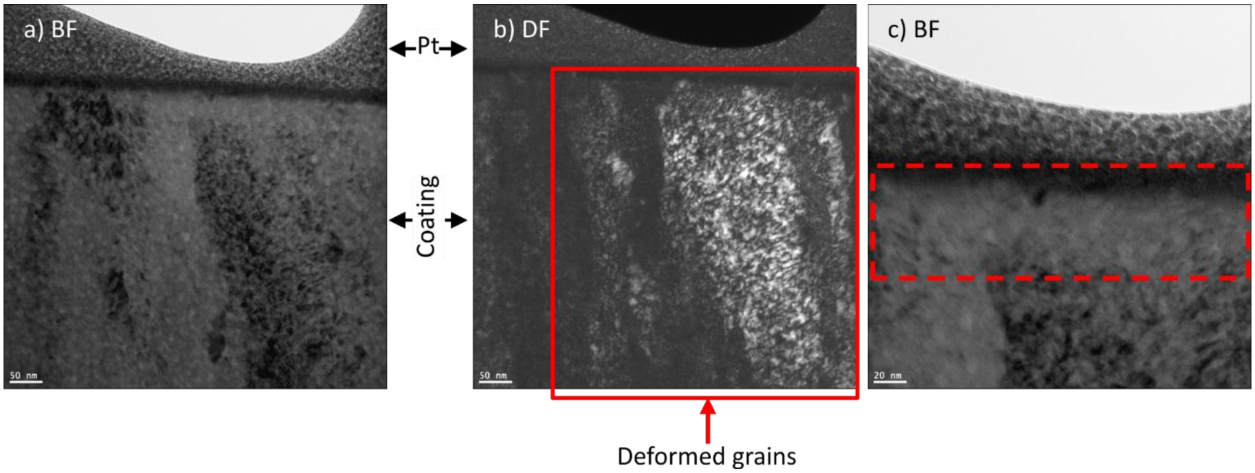

Figure 7.13 TEM image of wear track surface cross section obtained in RH 0% environment (a) bright field, (b) dark field and (c) tribologically transformed layer at subsurface of wear track

Table 7.2 d-Spacing of ring structure from RH 60% SAED patterns

Measured from rings d(Å)	PDF card reference d(Å)	Indices
2.822	2.810	$10\bar{1}0$
	2.610	0002
2.488	2.474	$10\bar{1}1$
1.919	1.912	$10\bar{1}2$
1.635	1.623	$11\bar{2}0$
1.481	1.479	$10\bar{1}3$
	1.405	$20\bar{2}0$
1.368	1.378	$11\bar{2}2$
	1.357	$20\bar{2}1$

7.4 Discussion

Humidity has a significant effect on the sliding wear behaviour of Zn-Ni alloy coatings. Coatings tested in higher humidity levels showed a high CoF during the run-in period which is due to flattening asperities and formation of third bodies (Figure 7.4a & 7.5), whereas coatings tested at lower humidity levels does not see this trend. A stable and low CoF is observed in the steady state regime for tests ran in high humidity, whereas the CoF becomes less steady as the humidity decreases. From Figure 7.4a, the average steady state CoF is summarized in Table 7.3. When the relative humidity decreases from 60 to 40%, there is an increase in the steady state CoF. However, as the relative humidity decreases from 20 to 0%, the steady state CoF also decreases. An increase of adhesive wear is observed when the relative humidity is decreased from 60 to 40%. This is probably due to reduced formation of nanocrystalline ZnO layer, as evidence by the slight coating pull-out in the wear track at RH 40%. When the relative humidity is decreased from 20 to 0%, the decrease of the steady state CoF is due to the change in velocity accommodation mechanism. When the relative humidity is decreased to 0%, an increased amount of wear particles is observed within the wear track as well as formation of a prow. This can aid in accommodating the velocity difference between the first bodies.[146] In addition, as the humidity of the test decreases, the wear increases. These differences are due to differences in the wear and velocity accommodation mechanisms at different humidity levels.

Table 7.3. Steady state coefficient of friction at different humidity levels

Relative Humidity (%)	Steady State CoF
60	0.52 ± 0.01
40	0.67 ± 0.04
20	0.60 ± 0.04
0	0.50 ± 0.03

ZnO was detected in the wear track in tests performed both in RH 60% and 0%. ZnO has been reported to reduce the CoF and wear rate when it is present in a thin nanocrystalline or amorphous form [154, 156, 203]. Although ZnO was detected in both conditions, lowered and steady CoF and wear rate was observed in RH 60%, whereas an unsteady CoF and high wear rate is observed in RH 0% in the steady state regime. In both high and low humidity cases, ZnO is observed in the Raman spectra (see Figure 7.8e). The difference of the ZnO in both wear tracks is in its formation which is reflected upon the morphology of the ZnO. At RH 0%, the oxides are in the form of agglomerated particles and very dispersed in wear track. In contrast, at RH 60%, compacted nanocrystalline oxide film layer was found on the tribolayer throughout the wear track. Therefore, the thin layer of ZnO present in the wear track contributed to a low and stable CoF and low wear rate observed in RH 60% due to shear occurring in the nanocrystalline layer (Figure 7.14). In contrast, at RH 0%, an unstable CoF and high wear rate is observed due to a lack of an adherent nanocrystalline ZnO film layer and subsequently interfacial sliding between the prow and wear track (Figure 7.15). The higher relative humidity facilitates ZnO nanocrystalline film formation, while the absence of humidity prevents a fast enough formation of ZnO nanocrystalline film. Corrosion of zinc and its alloys is well understood and documented. It is noted in atmospheric corrosion, especially in purified air, the conditions for surface condensation and atmospheric corrosion are affected by the humidity.[211-213] For zinc, it has been shown that atmospheric corrosion occurs when the relative humidity is above 60%, whereas below 60% RH, little corrosion occurs.[212, 214] In the presence of water, zinc transforms into zinc hydroxide, and then into zinc oxide in the presence of air due to dehydration, shown in the equations below.[213] The different relative humidity levels of the tests result in different atmospheric corrosion conditions, which may explain the chemical and structural differences in third bodies.

$$Zn^{2+} + 2OH^{-} \rightarrow Zn(OH)_2 \tag{Eq 7.2}$$

$$Zn(OH)_2 \rightarrow ZnO + H_2O \tag{Eq 7.3}$$

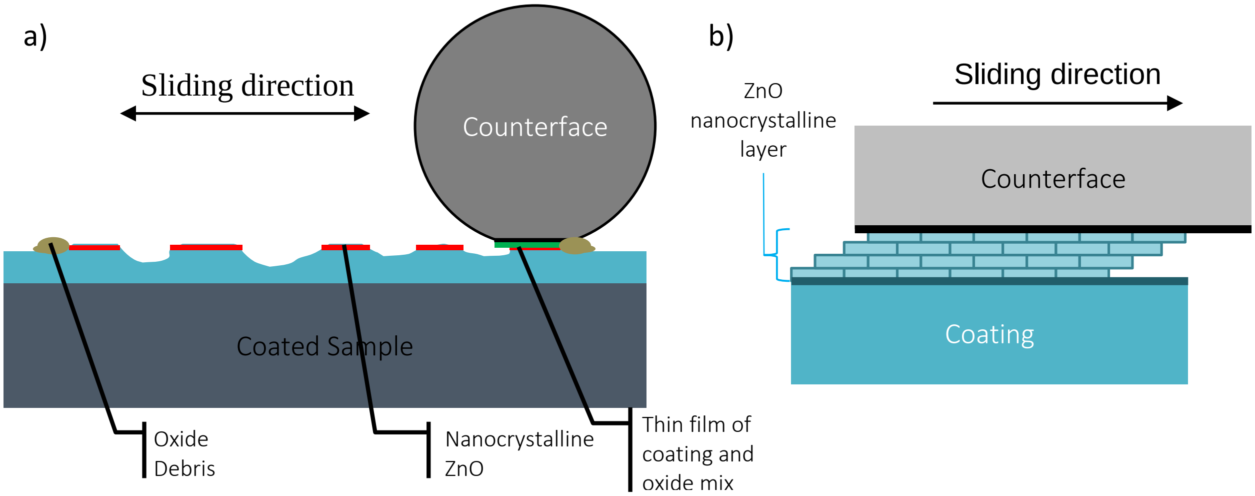

Figure 7.14 Schematic diagram of wear behaviour during steady state at high humidity levels (a) wear track during test and (b) shearing of nanocrystalline ZnO film

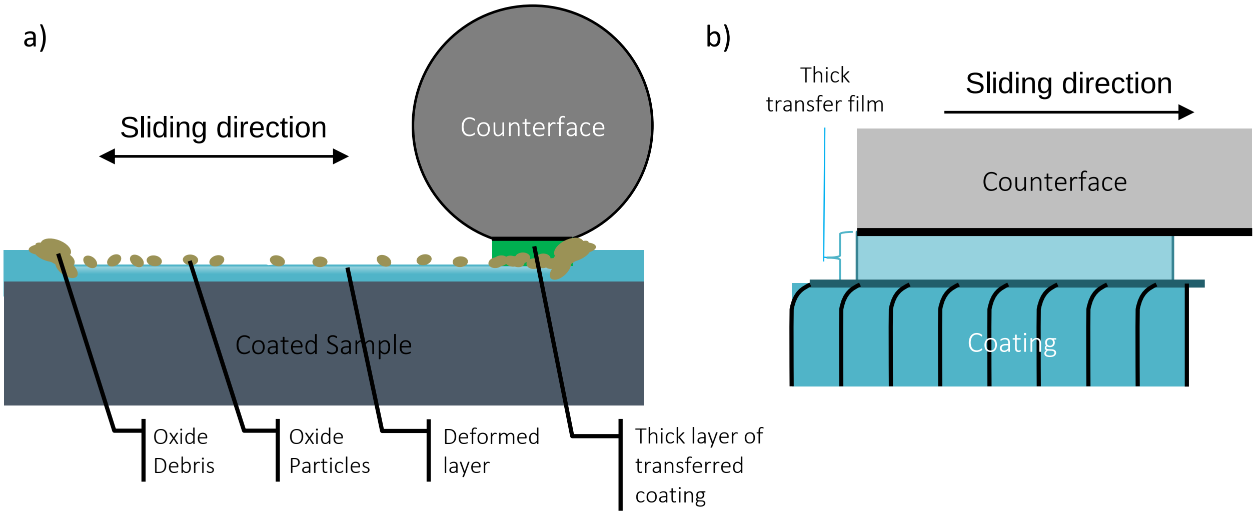

Figure 7.15 Schematic diagram of wear behaviour during steady state at low humidity levels (a) wear track during test and (b) transfer material and coating interface sliding

SEM (see Figure 7.5) shows major differences among the wear track morphologies after 2000 cycles of wear. At RH 60%, the low amount of wear may be related to the formation of a lubricating ZnO layer. At RH 40%, slightly more wear occurs in the wear track indicated by the wear rate and SEM image where slight material pull-out is observed in the wear track, which may contribute to the higher and irregular CoF. At RH 20%, the wear rate transitions from a decreasing to an increasing trend. This is due to the severe wear observed in the SEM images. Slight prow formation is observed on the transfer film and wear track which is indicative of adhesive wear. Sliding occurring between the prow/wear track interface and wear particles in the center of the wear track may contribute to an unstable yet lower CoF. At RH 0%, the large prow formation and substantial amount of wear debris in the center of the wear track may also contribute to the low but unstable CoF. Increasing adhesion of coating material to the counterface is observed with decreasing humidity in the form of prow formation due to a lack of water vapour in the environment to aid in the formation of the nanocrystalline ZnO layer. This also contributes to the higher wear rate observed due to ploughing of the coating by the prow. Grains on the near surface of the wear track is also deformed, indicating the velocity accommodated through deformation of the coating at low humidity levels.

7.5 Conclusion

A Zn-Ni coating was tested in various humidity levels in order to test the effect of humidity on the sliding wear properties of the coating. Wear rates of high humidity tests are much lower than low humidity tests due to different wear and velocity accommodation mechanisms. High humidity tests form a compacted film of nanocrystalline hexagonal ZnO on the tribolayer which is lubricious, resulting in a steady CoF and low wear rate. In contrast, at low humidity tests, ZnO particles were disperse and scattered in the wear track. Prow formation occurred for tests conducted at low humidity, which contributed to a high wear rate due to ploughing of the coating.

Acknowledgements

The authors would like to thank Salim Brahimi for his continual support and inputs throughout the experiments. We would also like to thank Natural Science and Engineering Research Center (NSERC), Boeing Canada, Pratt & Whitney Canada, Héroux Devtek, Canadian Fastener Institute and Messier-Bugatti-Dowty for their financial support. We would also like to thank Boeing, Coventya and Dipsol Inc. for providing specimens.

Chapter 8

Additional Discussion on Sliding Wear

The previous two chapters discussed the sliding wear behaviour of Zn-Ni coatings, and how varying the humidity affected the behaviour. In this chapter, comparisons of a Zn-Ni coating with roughness in between the rougher and smoother coating will be made with cadmium coating. As the author did not perform sliding wear tests on cadmium coating, all results regarding cadmium will be referenced from work done by Behera *et al.* [167], where similar studies were made.

8.1 Comparison of the effect on humidity on the sliding wear behaviour of B-ZnNi and cadmium coatings

8.1.1 Test Parameters

Reciprocating sliding wear tests were conducted on both coatings using a custom built tribometer, similar to the experimental set-up described in the previous chapter. Both tests used a 3.175 mm radius AISI 440C steel ball as the counterface. A 1.3 normal load used for cadmium, while a 1.1 N normal load was used for B-ZnNi. Similar normal loads at around 1 N were chosen for comparison purposes of the two coatings. The relative humidity was varied at humidity levels of 0, 30 and 60% relative humidity (RH). Tribological behaviours are compared in friction and wear.

8.1.2 Comparison of the as-plated samples

SEM images of the coating surface morphology and cross sections are shown in Figure 8.1 & 8.2. Both coatings show a similar surface morphology, in the sense that the coatings are formed by agglomerates of platelets into hemispherical shapes, which results in hills and valley structure, although the difference of the hills and valleys of B-ZnNi appears to be less. Through thickness defects are also present in both coating in the form of pores and cracks. A slightly thicker coating is also observed for B-ZnNi (B-ZnNi: 14 ± 2 μm, Cd: 11 ± 2 μm). XRD of the coatings showed a single γ-phase Zn-Ni for B-ZnNi coatings, while HCP structured cadmium was found for LHE Cd coatings. A list of coating properties, such as hardness and roughness can be found in Table 5.1. B-ZnNi is much stiffer and harder than cadmium coating. A lower roughness was also observed for B-ZnNi.

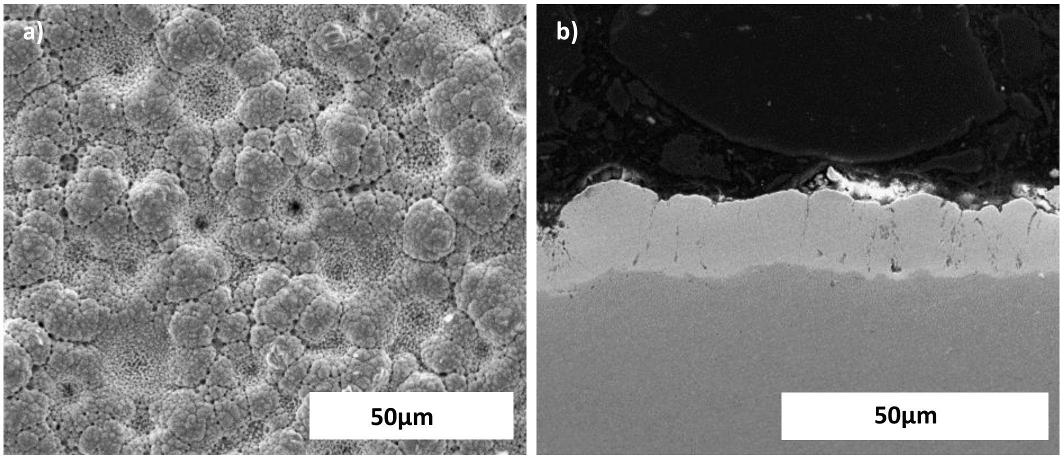

Figure 8.1 SEM characterization of B-ZnNi coating (a) Surface morphology and (b) Cross section

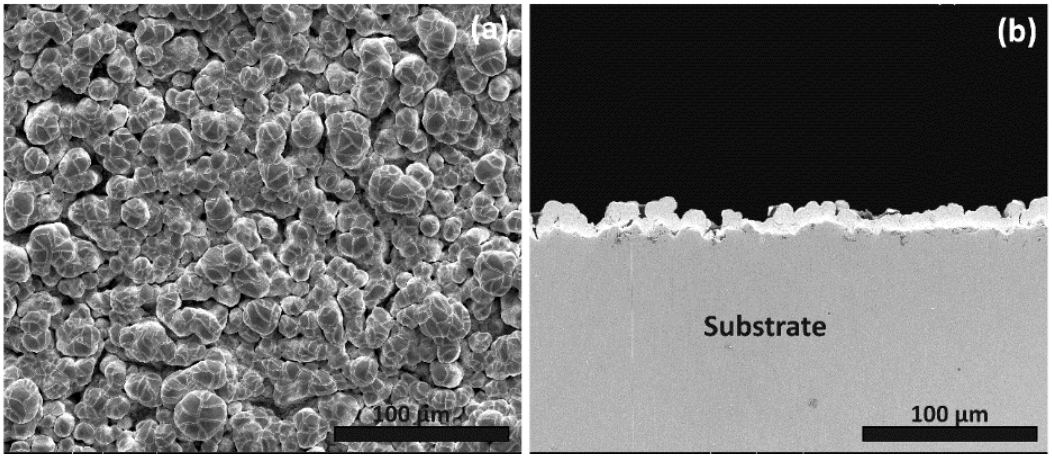

Figure 8.2 SEM characterization of LHE Cd coating (a) Surface morphology and (b) Cross section, from [167]

8.1.3 Comparison of humidity effects

Due to the vast differences in mechanical and chemical properties, the evolution of the friction for both coatings also differed greatly. Figure 8.3 shows the average CoF with the evolution of cycles at RH 60 % for Cd at 1.3 N and B-ZnNi at 1.1 N. Cadmium experiences 4 different regimes. The first regime is associated with a high CoF due to formation of the transfer film through adhesive wear processes. A lower CoF is observed in the second regime, and velocity is accommodated through shearing of the third bodies. Although steel was observed in this stage, pockets of Cd remain in the wear track. The transition regime has an increasing CoF and is associated with the depletion of the third bodies and Cd pockets. A high CoF is observed in the third regime, due to steel on steel contact [167]. In contrast, two regimes were observed for B-ZnNi, the first regime is associated with the run in period, where asperities are flattened and the area of contact is increased area of contact, and the formation of ZnO on the surface. This leads to a second regime, the steady state regime, where a more or less stable CoF is observed around 0.5. For B-ZnNi at RH 60 %, the coating remains intact, as little wear occurred in this condition.

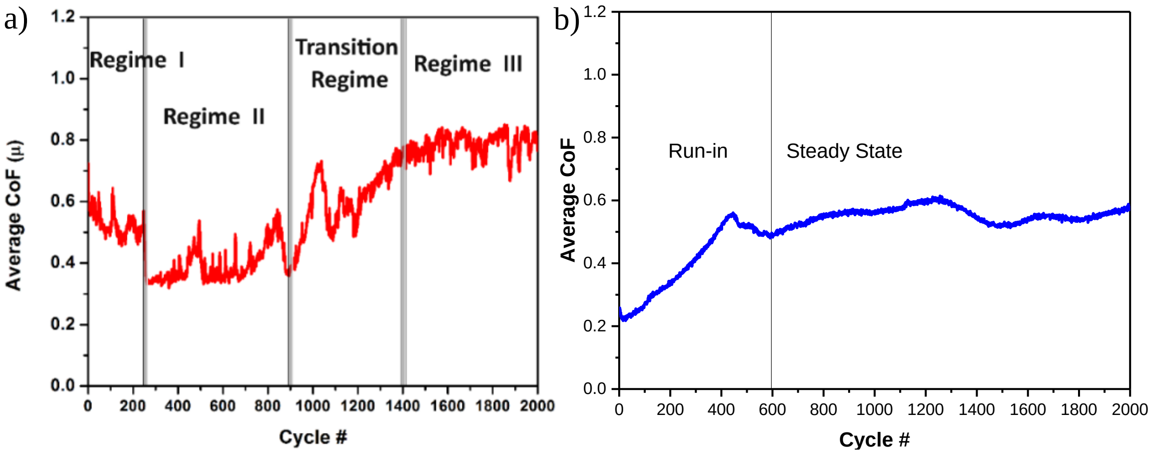

Figure 8.3 Average CoF vs cycle at RH 60% for (a) cadmium coating under 1.3 N normal load from [167] and (b) B-ZnNi under 1.1 N normal load.

Decreasing the relative humidity to 30 and 0 % resulted in change for both coatings. For Cd coating (Figure 8.4), the onset to regime II and the transition regime are increased and regime III was not observed till the end of the test [167]. An increase in CoF is also observed in the first regime and is due to formation of different Cd compounds leading to different shear strengths at the contact, due different crystal structures of the third bodies [167]. Wear rates also decreased increased [167]. It is important to note that regime II is prolonged as the relative humidity is decrease, as regime II has the lowest CoF of the four regimes. In contrast, for B-ZnNi under RH 30% (Figure 8.5a), the run in period is decreased with decrease in humidity. The peak CoF also increased from ~0.6 to ~0.75. As the humidity decreases, the time needed to form ZnO changes, resulting in higher adhesion during the run in period. When the humidity is further decrease to 0 % (Figure 8.5b), the run in regime is again shortened and the peak CoF is ~0.5. Although the CoF is relatively constant and low during the steady state regime, it is not stable. Analysis of the wear track showed complete flattening of the asperities and severe wear while the counterface showed signs of multiple prow formation. There is also a lack of nanocrystalline ZnO film formation at the wear track. Low CoF at the steady state regime could be due to the prows separating the coating and counterface, and ploughing the coating.

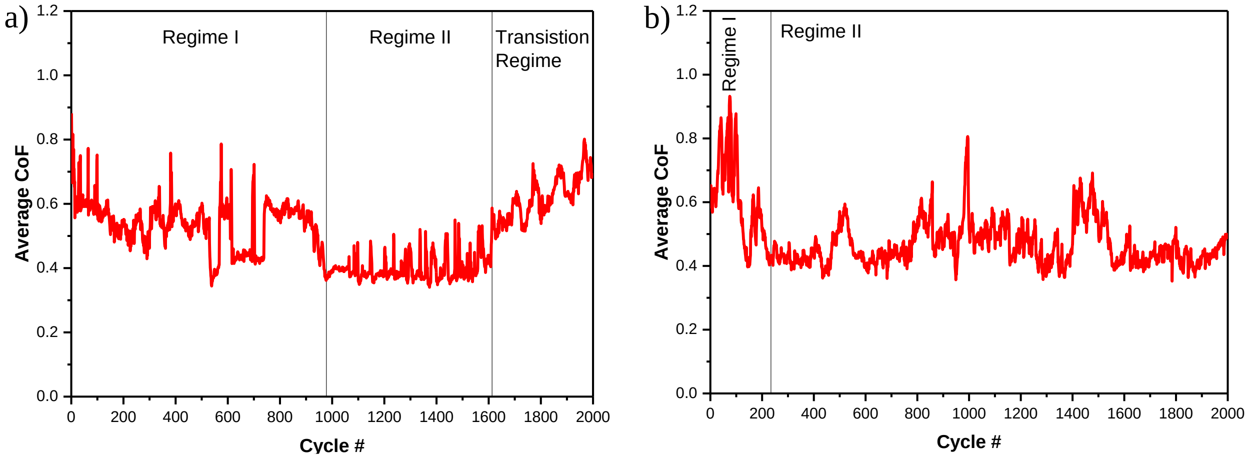

Figure 8.4 Average CoF vs cycle at (a) RH 30 % and (b) RH 0 % for Cd coating under 1.3 N normal load. Adapted from [167]

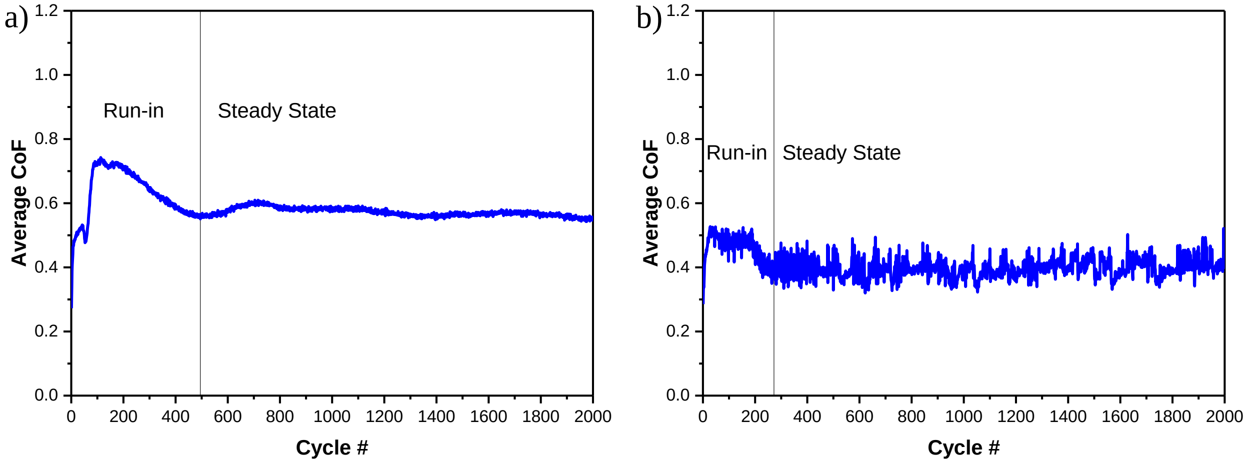

Figure 8.5 Average CoF vs cycle at (a) RH 30% and (b) RH 0 % for B-ZnNi coating under 1.1 N normal load

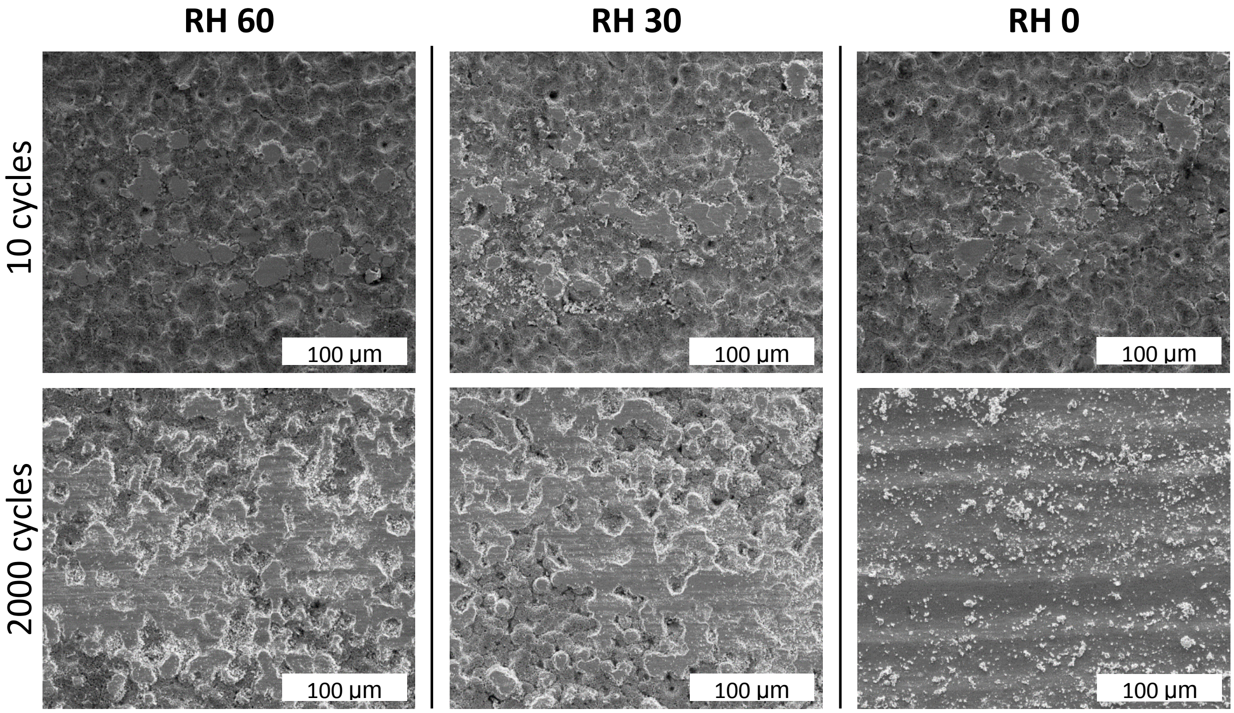

Figure 8.6 Wear track morphology of B-ZnNi coating after 10 cycles and 2000 cycles of wear at RH 60, 30 and 0 %. Mostly flattening and wearing of the asperities occurred of at RH 60 and 30 %. Severe wear is observed at RH 0 %.

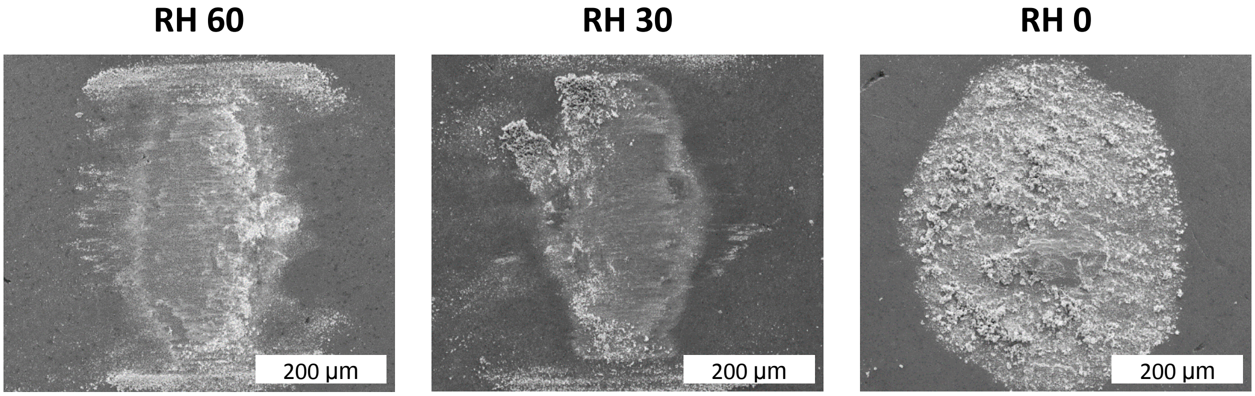

Figure 8.7 Counterface after 2000 cycles of wear. Prow formation observed at RH 0%

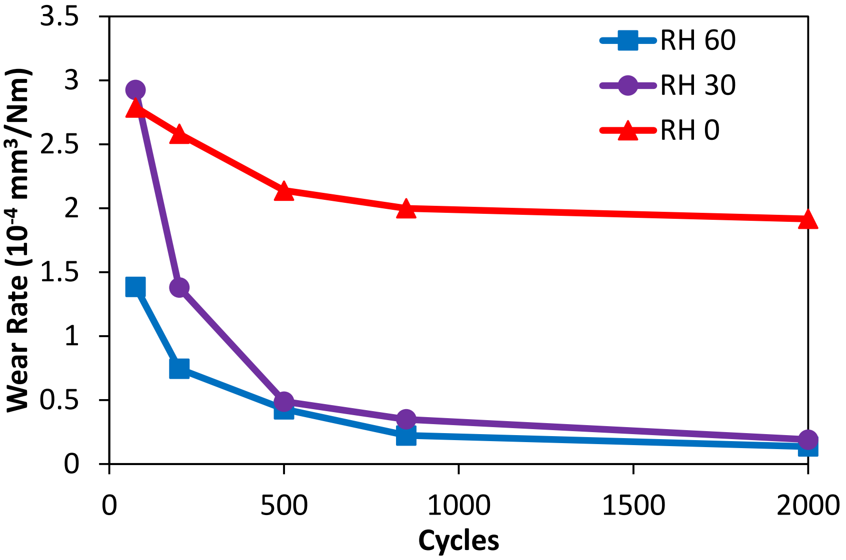

Figure 8.8 Evolution of the wear rate of B-ZnNi. Most of the wear occurs at the beginning of the test, although the wear rate of test performed at RH 0% remains high.

Table 8.1 Wear rate of Cd coating under 1.3 N normal load at the end of the test from [167]

% RH	Wear rate at end of Test ($\times 10^{-3}$ mm³/N.m)
0	0.8 ± 0.1
30	2.4 ± 1.0
60	3.2 ± 0.4

8.2 General discussion of the effects of humidity on Zn-Ni and cadmium coatings

Humidity has a strong affect on the tribological behaviour of both Cd and Zn-Ni due to chemical changes of the third bodies in the contact. For Cd, decrease in humidity was beneficial to the tribological properties as a prolonged second regime was observed, which was associated with low CoF. The wear also decreased with humidity. In contrast, decrease in humidity is detrimental to Zn-Ni coatings. Chapter 7 shows that at 60% relative humidity, there is a film of nanocrystalline ZnO which formed on the surface of the wear track, which acts as a lubricating layer. When the humidity is low, the lubricious ZnO layer does not form. The wear track is ploughed by the prow formed on the counterface, which is observed for both B-ZnNi in Chapter 8 and C-ZnNi in Chapter 7. Prow formation is indicative of wear adhesive in nature. Wear also increased with the decrease in humidity.

Although opposing behaviour is observed, the wear of Zn-Ni coating remains 1 order lower than Cd coating in all wear conditions, which could be attributed to the mechanical properties of Zn-Ni, allowing the coating to be more wear resistant. Comparison of the fretting behaviour in chapter 5 shows that when similar normal loads are used, the shear stress for cadmium is much higher than its yield stress, whereas the shear stress is only a fraction of the yield stress for Zn-Ni coatings due to the higher hardness and stiffness of Zn-Ni coatings. Although the wear is higher for Cd than Zn-Ni, the CoF during the second regime for Cd is lower than the steady state regime for B-ZnNi coating. This can again be attributed to the difference in mechanical properties and crystal structure of the two materials and the third bodies. For Zn-Ni coating at 60% the CoF is stable in the steady state regime, as seen in chapter 7 and 8 for C-ZnNi and B-ZnNi respectively. Decreasing the relative humidity resulting in unstable CoF for both coatings. This could be due to the difference in the wear and velocity accommodation mechanisms. In contrast, for Cd coating, decreasing the relative humidity resulted in a prolonged second regime, due to difference in third bodies formation. Comparing the sliding wear behaviour of the two types of coating, Zn-Ni has better wear resistance, while Cd has a lower CoF due to the inherent properties of the coatings.

Chapter 9

Synopsis

9.1 Summary and conclusions

Studies of the tribological behaviours of γ-phase Zn-Ni coatings were made in terms of fretting and reciprocating sliding wear. In these studies, three Zn-Ni coatings (C-ZnNi, D-ZnNi and B-ZnNi) with different surface morphologies were studied. C-ZnNi has the lowest roughness and a smooth and dense surface morphology, whereas D-ZnNi has the highest roughness and through thickness defects resulting in a surface morphology with high hills and low valleys formed by hemispherical platelet agglomerates, and a porous structure. B-ZnNi acted as an intermediate between the two coatings, and although it had through thickness defects and is porous, the hills and valleys were smoother. Differences between these coatings greatly affected their tribological properties. Cadmium coatings were also briefly compared to B-ZnNi coatings, as these coatings are intended to be used in the aerospace industry to replace cadmium.

Fretting behaviour was compared with the smoother coating (C-ZnNi) the roughest coating (D-ZnNi) in terms of the contact conditions, fretting regimes and velocity accommodation mechanisms by varying the displacement amplitude, such that the tests fell in the stick or partial slip regime, mixed slip regime or gross slip regime. Analyses were made by comparison of the energy ratios, SEM and EDX analysis and wear scar depth measurements. In the stick regime, cracks were formed in the contact area of C-ZnNi in order to accommodate the motion through elastic deformation of the formed columns. In contrast, D-ZnNi showed little wear, other than flattening of the asperities where they were in contact with the counterface. Velocity was most likely accommodated through elastic deformation of the agglomerates, as pre-existing defects already formed columns in the coating. Both coatings showed very little wear in this regime. In the mixed slip regime, significant increase in wear was observed for both coatings, as substantial amount of wear particles were ejected from the contact and plastic deformation of the coating and sheering of flat particles within the contact accommodated the motion. In the gross slip regime, even more severe wear occurred as substantial amount of wear debris was ejected from the contact and sheering of the particles and in the case of D-ZnNi plastic deformation of the steel substrate occurred to accommodate the motion. It was interesting to note that the wear of D-ZnNi coatings increased much more due to the coating morphology allowing the coating to wear more easily. Increasing the normal load allowed both coatings to remain in the stick regime, where little wear was observed.

Comparisons of the fretting behaviour of B-ZnNi coating was made with cadmium coating. Normal loads were chosen such that a similar initial Hertzian contact stress and a similar load were achieved. Fretting behaviour was discussed in terms of contact conditions, fretting regimes and velocity accommodation mechanisms. Displacement amplitude were chosen such that Zn-Ni coating fell in the stick or partial slip, mixed slip and gross slip regimes. The material properties of the coatings played an important role in the differences in the fretting behaviours as Zn-Ni is harder and stiffer, and also is cubic structured, while cadmium has a hexagonal crystal structure. B-ZnNi exhibited similar fretting behaviour as D-ZnNi. Although cadmium remained in the stick and partial slip regime in all tests, substantial amount of plastic flow occurred in order to accommodate the motion. It is interesting to note that wear debris of B-ZnNi coatings occurred as particles, while for cadmium it appeared as a continuous chip. Wear increased as the displacement amplitude increased, although when similar normal load was used, the wear of B-ZnNi remained low.

When the displacement amplitude is increased to much larger than the contact radius, reciprocating sliding wear occurs. As increasing the normal load during fretting resulted in low wear during fretting, the effect of normal load on the sliding wear behaviour was studied. This was achieved through varying the load from 3.5 to 7 to 12 N. C-ZnNi (smoother) was also compared with D-ZnNi (rougher) in order to study the effects of surface morphology. Both coatings showed similar friction trends with the exception of tests conducted at 12 N. Generally increasing the load resulted in increase in the steady state friction in both coatings. Wear on the other hand was influenced by the coating morphology, as at 3.5 and 7 N normal load, the rougher coating showed more wear. However, at 12 N, C-ZnNi showed severe wear due to debonding of the coating as the increased load broke the oxide layer formed on the surface, resulting in adhesion and severe wear.

Since the oxide film formed during sliding appeared to affect the sliding wear behaviour of Zn-Ni coatings, especially for the smoother coating, humidity tests were conducted on C-ZnNi by varying the humidity level of the chamber from 0 to 60 % relative humidity. Although the steady state friction appears to remain similar for the humidity test, the wear behaviour differed. As the humidity decreased, the wear rate increased. This is because at high humidity, a nanocrystalline ZnO layer formed on the surface of the wear track which contributed to a stable friction and low wear rate, as deformation occurred at the nanocrystalline ZnO layer. In contrast, when the humidity was low, a prow was formed due to adhesion between the coating and counterface. The prow then ploughed the wear track, causing severe wear.

The effects of humidity were compared between B-ZnNi and cadmium coating. Both coatings were affected by humidity, as humidity changed the composition of the third bodies within the contact in both cases. Wear of cadmium showed four distinct regimes, with the second regime having the lowest CoF. Decreasing the humidity showed beneficial to friction and wear, as the second regime was prolonged and the wear rate decreased with the decrease in humidity. In contrast, B-ZnNi coatings showed the opposite trend, where decreasing the humidity was detrimental to the coating as the wear was increased, similar to C-ZnNi coatings. Due to mechanical properties of these coatings, a lower CoF was obtained by Cd, while a higher wear resistance was obtained with Zn-Ni coatings.

9.2 Suggestion for future work

1. In general, as these coatings are used as a corrosion protection coating, studies regarding the synergistic effects of wear and corrosion should be made and how the surface morphology may affect this behaviour.

2. For fretting wear, analysis of the fretting wear behaviour was not very complete, as only superficial analysis of the coatings was made. More work can go towards characterizing the wear rate, finding the number of cycles needed to activate wear, analysis of the coefficient of friction, proposal of a fretting map, analyzing the tribologically transformed structures, etc. These work can increase the knowledge on Zn-Ni coatings and help in the design of their application to make it safer and more reliable.

3. Only point on flat geometry tests were used in the various tests performed to compare the effects of coating morphology, contact stress and humidity on the sliding wear and fretting behaviours. In application, such as landing gear and fastener applications, the geometry is not point on flat. Therefore, more types of geometry or more complex geometry should be studied, as the geometry also significantly affects the third bodies.

4. Electroplating Zn-Ni is still a developing technology, and there are always new improvements to plating baths to improve properties such as corrosion resistance and hydrogen embrittlement properties. Such as adding additives to refine grains and modify structure, creating composites with ceramic particles, adding a ternary metal to the system or creating multi layered coatings, Tribological behaviours of these systems should also be considered.

5. In terms of sliding wear, more can be done in terms of studying why and how the ZnO layer forms, proposing mechanisms, in order to better understand this phenomenon as a self lubricating coating is very attractive in many cases.

9.3 Contributions to original knowledge

1. The fretting wear behaviour of Zn-Ni and Cd coatings were studied for the first time in terms of contact conditions, fretting regimes and velocity accommodation mechanisms.

2. The effects of surface morphology on the fretting behaviour was discussed with regards to Zn-Ni coatings for the first time. It was found that for Zn-Ni coatings, smoother and denser coatings formed cracks in the stick or partial slip regime in order to accommodate motion,

while the morphology of the rougher and porous coating allowed some degree of elastic deformation. Rougher coatings also showed more wear when slipping occurred in the contact region due to the surface morphology.

3. For the first time, the fretting wear behaviour of cadmium was studied using the third body approach and was compared with Zn-Ni coatings systematically.

4. Effects of surface morphology on the sliding behaviour was discussed using the third body approach for the first time.

5. Effects of humidity on the sliding wear behaviour of Zn-Ni coating was analyzed for the first time. Extensive analysis of the third bodies were made which showed the formation of nanocrystalline ZnO at high humidity conditions, and is to some degree self-lubricating. Studies also showed that decreasing the humidity is detrimental to Zn-Ni coatings due to increased adhesion.

6. Direct comparison of sliding wear behaviour when using a steel counterface was made with Zn-Ni and Cd for the first time.

References

1. Wilcox, G.D. and D.R. Gabe, *Electrodeposited zinc alloy coatings.* Corrosion Science, 1993. **35**(5–8): p. 1251-1258.

2. British Defence Standards, *Guidance to the Use of Cadmium Alternatives in the Protective Coating of Defence Equipment,* in *Defence Standard 03-36* 2010, Crown: Glasgow, UK.

3. Sriraman, K.R., et al., *Tribological behavior of electrodeposited Zn, Zn-Ni, Cd and Cd-Ti coatings on low carbon steel substrates.* Tribology International, 2012. **56**: p. 107-120.

4. Bielawski, M., *Alternative technologies and coatings for electroplated cadmium and hard chromium.* Canadian Aeronautics and Space Journal, 2010. **56**(3): p. 67-80.

5. Legg, K., *Cadmium Replacement Options* 2003, Rowan Technology Group.

6. Guo, C., et al., *Microstructure and tribological properties of TiCu2Al intermetallic compound coating.* Applied Surface Science, 2011. **257**(13): p. 5885-5892.

7. Russell, A.M., *Ductility in Intermetallic Compounds.* Advanced Engineering Materials, 2003. **5**(9): p. 629-639.

8. Byk, T.V., T.V. Gaevskaya, and L.S. Tsybulskaya, *Effect of electrodeposition conditions on the composition, microstructure, and corrosion resistance of Zn-Ni alloy coatings.* Surface and Coatings Technology, 2008. **202**(24): p. 5817-5823.

9. Conde, A., M.A. Arenas, and J.J. de Damborenea, *Electrodeposition of Zn-Ni coatings as Cd replacement for corrosion protection of high strength steel.* Corrosion Science, 2011. **53**(4): p. 1489-1497.

10. Holmberg, K., H. Ronkainen, and A. Matthews, *Tribology of thin coatings.* Ceramics International, 2000. **26**(7): p. 787-795.

11. Singer, I.L., *Solid Lubrication Processes*, in *Fundamentals of Friction: Macroscopic and Microscopic Processes*, I.L. Singer and H.M. Pollock, Editors. 1992, Springer Netherlands: Dordrecht. p. 237-261.

12. Ghaziof, S. and W. Gao, *Electrodeposition of single gamma phased Zn-Ni alloy coatings from additive-free acidic bath.* Applied Surface Science, 2014. **311**: p. 635-642.

13. Jahanmir, S. and N.P. Suh, *Surface topography and integrity effects on sliding wear.* Wear, 1977. **44**(1): p. 87-99.

14. Bhushan, B., *Nanotribology: Friction, wear and lubrication at the atomic scale.* Nature, 1995. **374**(6523): p. 607-616.

15. Kubiak, K.J., T.W. Liskiewicz, and T.G. Mathia, *Surface morphology in engineering applications: influence of roughness on sliding and wear in dry fretting.* Tribology International, 2011. **44**(11): p. 1427-1432.

16. Riyadh, A., A. Khairel Rafezi, and Y. Al-Douri, *Evaluate the effects of various surface roughness on the tribological characteristics under dry and lubricated conditions for Al-Si alloy.* Journal of Surface Engineered Materials and Advanced Technology, 2012. **2012**.

17. Waterhouse, R.B., *Fretting Corrosion*. 1972, Oxford; New York: Pergamon Press.

18. Paatsch, W., W. Kautek, and M. Sahre, *Corrosion behaviour and mechanical properties of plated Zn-alloys.* Transactions of the Institute of Metal Finishing, 1997. **75**(6): p. 216-218.

19. Baldwin, K.R., M.J. Robinson, and C.J.E. Smith, *The corrosion resistance of electrodeposited zinc-nickel alloy coatings.* Corrosion Science, 1993. **35**(5-8): p. 1267-1272.

20. Baldwin, K.R., M.J. Robinson, and C.J.E. Smith, *Corrosion rate measurements of electrodeposited zinc-nickel alloy coatings.* Corrosion Science, 1994. **36**(7): p. 1115-1131.

21. Baldwin, K.R. and C.J.E. Smith, *Advances in replacements for cadmium plating in aerospace applications.* Transactions of the Institute of Metal Finishing, 1996. **74**(6): p. 202-209.

22. Bates, J.A., *Comparison of alkaline Zn-Ni & acid Zn-Ni as a replacement coating for cadmium.* Plating and Surface Finishing, 1994. **81**(4): p. 36-40.

23. El-Sayed, A.R., H.M. Abd El-Lateef, and H.S. Mohran, *Effect of nickel content on the anodic dissolution and passivation of zinc-nickel alloys in alkaline solutions by*

potentiodynamic and potentiostatic techniques. Bulletin of Materials Science, 2015. **38**(2): p. 379-391.

24. Gavrila, M., et al., *Corrosion behaviour of zinc–nickel coatings, electrodeposited on steel.* Surface and Coatings Technology, 2000. **123**(2–3): p. 164-172.

25. Goodwin, F.E., *Corrosion of zinc and its alloys,* in *Shreir's Corrosion*. 2010. p. 2078-2093.

26. Siitari, D.W., M. Sagiyama, and T. Hara, *CORROSION OF Ni-Zn ELECTRODEPOSITED ALLOY.* Transactions of the Iron and Steel Institute of Japan, 1983. **23**(11): p. 959-966.

27. Silva, L.A.S. and L. Sathler, *The corrosion behavior of cadmium, zinc, zinc-nickel & nickel-phosphorus/zinc commercial coatings in chloride solutions.* Plating and Surface Finishing, 2003. **90**(12): p. 38-42.

28. Sriraman, K.R., et al., *Tribocorrosion behavior of Zn, Zn-Ni, Cd and Cd-Ti electrodeposited on low carbon steel substrates.* Surface and Coatings Technology, 2013. **224**: p. 126-137.

29. Sriraman, K.R., et al., *Characterization of corrosion resistance of electrodeposited Zn-Ni, Zn and Cd coatings.* Electrochimica Acta, 2013. **105**: p. 314-323.

30. Fratesi, R. and G. Roventi, *Corrosion resistance of Zn-Ni alloy coatings in industrial production.* Surface and Coatings Technology, 1996. **82**(1-2): p. 158-164.

31. Sriraman, K.R., et al., *Hydrogen embrittlement of Zn-, Zn-Ni-, and Cd-coated high strength steel.* Journal of Applied Electrochemistry, 2013: p. 1-11.

32. Addi, Y. and A. Khouider. *Electrodeposition of Ni-Zn alloys on steel from acidic solution in presence of boric acid*. 2013.

33. Ando, S., *Electrodeposition behavior of Zn-Ni alloys produced from sulfate solutions at high current densities.* Nippon Kinzoku Gakkaishi/Journal of the Japan Institute of Metals, 2015. **79**(8): p. 398-403.

34. Berman, E., et al. *Chromium-free conversion coatings for zinc-nickel plating lines*. 2012.

35. Boonyongmaneerat, Y., et al., *Corrosion behavior of reverse-pulse electrodeposited Zn-Ni alloys in saline environment.* Journal of Materials Engineering and Performance, 2014. **23**(1): p. 302-307.

36. Chang, L.M., et al., *Pulse plated Zn transition layer in electroplating Zn-Ni coatings on magnesium alloys.* Surface Engineering, 2012. **28**(10): p. 725-730.

37. Chira, M., et al., *Corrosion behavior of Zn-Ni coatings electrodeposited in pulsed current and magnetic field on different substrates by electrochemical impedance spectroscopy techniques.* Studia Universitatis Babes-Bolyai Chemia, 2014. **59**(1): p. 63-78.

38. Conrad, H.A., et al., *Improved corrosion resistant properties of electrochemically deposited zinc-nickel alloys utilizing a borate electrolytic alkaline solution.* Surface and Coatings Technology, 2015. **272**: p. 50-57.

39. Darband, G.B., A. Afshar, and A. Aliabadi, *Zn-Ni Electrophosphating on galvanized steel using cathodic and anodic electrochemical methods.* Surface and Coatings Technology, 2015.

40. Darband, G.B., A. Afshar, and M. Rabani, *Effect of treatment time and temperature on microstructure and corrosion behavior of Zn-Ni electrophosphate coating.* Journal of Alloys and Compounds, 2016. **688**: p. 596-604.

41. Diaddario Jr, L.L. *Plating bath parameters affecting the performance of zinc-nickel alloys for post-plate fabrication*. 2012.

42. Dingwerth, B.O., *High performance corrosion protection for brake components: Direct zinc-nickel application and post-treatment.* 2012. **7**.

43. Fashu, S., et al., *Influence of electrodeposition conditions on the microstructure and corrosion resistance of Zn-Ni alloy coatings from a deep eutectic solvent.* Surface and Coatings Technology, 2014. **242**: p. 34-41.

44. Fashu, S., et al., *Effect of EDTA and NH<inf>4</inf>Cl additives on electrodeposition of Zn-Ni films from choline chloride-based ionic liquid.* Transactions of Nonferrous Metals Society of China (English Edition), 2015. **25**(6): p. 2054-2064.

45. Feng, Z., et al., *Corrosion mechanism of nanocrystalline Zn-Ni alloys obtained from a new DMH-based bath as a replacement for Zn and Cd coatings.* RSC Advances, 2016. **6**(69): p. 64726-64740.

46. Feng, Z., et al., *Electrochemical behaviors and properties of Zn-Ni alloys obtained from alkaline non-cyanide bath using 5,5 ´-Dimethylhydantoin as complexing agent.* Journal of the Electrochemical Society, 2015. **162**(9): p. D412-D422.

47. Feng, Z., et al., *Studies on the enhanced properties of nanocrystalline Zn-Ni coatings from a new alkaline bath due to electrolyte additives.* RSC Advances, 2015. **5**(72): p. 58199-58210.

48. Feng, Z., et al., *Electrodeposition of nanocrystalline Zn-Ni coatings with single gamma phase from an alkaline bath.* Surface and Coatings Technology, 2015. **270**: p. 47-56.

49. Feng, Z., et al., *Effect of additives on the corrosion mechanism of nanocrystalline zinc-nickel alloys in an alkaline bath.* RSC Advances, 2016. **6**(91): p. 88469-88485.

50. Feng, Z., et al., *Influence of additives on microstructure, mechanical and tribological properties of nanocrystalline Zn-Ni coatings in a novel alkaline bath.* RSC Advances, 2016. **6**(48): p. 42029-42040.

51. Feng, Z., et al., *Theoretical calculations and electrochemical behaviors of additives in DMH-based alkaline bath for nanocrystalline Zn-Ni electrodeposition.* Journal of the Electrochemical Society, 2016. **163**(9): p. D544-D553.

52. Hammami, O., et al., *Effect of diethanolamine and triethanolamine on the properties of electroplated Zn-Ni alloy coatings from acid bath.* Canadian Journal of Chemical Engineering, 2013. **91**(1): p. 19-26.

53. Ieffa, S., et al., *Direct and pulse plating of metastable Zn-Ni alloys.* Transactions of the Institute of Metal Finishing, 2014. **92**(6): p. 321-324.

54. Kamel, M.M., et al., *Electrodeposition of nanocrystalline Zn-Ni alloys from sulphate bath containing lactic acid.* Metall, 2015. **69**(7-8): p. 286-291.

55. Katirci, R., *Effects of ZnO and NaOH in Zn-Ni bath.* Surface Engineering, 2015. **31**(1): p. 11-16.

56. Katirci, R., *Statistical approach to optimizing a zn-ni bath containing ed and tea.* Surface Review and Letters, 2015. **22**(1).

57. Klingenberg, M., et al. *Chromium-free conversion coating for electroplated Zinc-Nickel plating lines*. 2014.

58. Lin, Z.F., X.B. Li, and L.K. Xu, *Electrodeposition and corrosion behavior of zinc-nickel films obtained from acid solutions: Effects of teos as additive.* International Journal of Electrochemical Science, 2012. **7**(12): p. 12507-12517.

59. Long, J.M., X. Zhang, and H.Z. Pei, *Effect of triethanolamine addition in alkaline bath on the electroplating behavior, composition and corrosion resistance of Zn-Ni alloy coatings*. 2013. p. 87-91.

60. Maciej, A., et al., *Anodic treatment of Zn-Ni alloy in alkaline solutions*. 2015. p. 139-142.

61. Magagnin, L. and L. Nobili. *Electrodeposition and pulse plating of high performance Zinc-Nickel coatings*. 2014.

62. Magagnin, L., L. Nobili, and P.L. Cavallotti, *Metastable zinc-nickel alloys deposited from an alkaline electrolyte.* Journal of Alloys and Compounds, 2014. **615**(S1): p. S663-S666.

63. Nakano, H., et al., *Electrodeposition behavior of Zn-Ni alloys from an alkaline zincate solution containing ethylenediamine.* ISIJ International, 2013. **53**(10): p. 1864-1870.

64. Nakano, H., et al., *Electrodeposition behavior of Zn-Ni alloy from alkaline zincate solution containing ethylenediamine.* Tetsu-To-Hagane/Journal of the Iron and Steel Institute of Japan, 2013. **99**(6): p. 35-41.

65. Nakano, H., et al., *Electrodeposition behavior of a Zn-Ni alloy in an alkaline zincate solution.* Materials Transactions, 2012. **53**(11): p. 1946-1951.

66. Nayana, K.O. and T.V. Venkatesha, *Effect of ethyl vanillin on ZnNi alloy electrodeposition and its properties.* Bulletin of Materials Science, 2014. **37**(5): p. 1137-1146.

67. Oriti, T. *High performance acid zinc nickel systems*. 2013.

68. Oriti, T. *A comparative study of alkaline and acid zinc nickel alloy systems and their deposits*. 2014.

69. Panzeri, G., et al. *Electrodeposition of ZnNi alloys from ethylene glycol/choline chloride based ionic liquid*. 2016.

70. Pereira, N.M., et al., *Influence of amines on the electrodeposition of Zn-Ni alloy from a eutectic-type ionic liquid.* Journal of the Electrochemical Society, 2015. **162**(8): p. D325-D330.

71. Popczyk, M., et al., *Influence of thermal treatment on the structure and the corrosion resistance of Zn-Ni alloy coatings*. 2013. p. 224-227.

72. Qiao, X., et al., *Effects of deposition temperature on electrodeposition of zinc-nickel alloy coatings.* Electrochimica Acta, 2013. **89**: p. 771-777.

73. Ramazan, K. and Y. Uɟur, *Statistical studies of Zn-Ni alloy coatings using Non-cyanide alkaline baths containing polyethyleneimine complexing agents.* Transactions of the Institute of Metal Finishing, 2014. **92**(5): p. 245-252.

74. Rao, V.R., K.V. Bangera, and A.C. Hegde, *Magnetically induced electrodeposition of Zn-Ni alloy coatings and their corrosion behaviors.* Journal of Magnetism and Magnetic Materials, 2013. **345**: p. 48-54.

75. Rao, V.R. and A.C. Hegde, *Synergistic effect of gelatin and glycerol on electrodeposition of Zn-Ni alloy.* Metallurgical and Materials Transactions B: Process Metallurgy and Materials Processing Science, 2013. **44**(5): p. 1236-1242.

76. Rao, V.R. and A.C. Hegde, *Effect of induced magnetic field on electrocrystallization of Zn-Ni alloy and their corrosion study.* Journal of Materials Engineering and Performance, 2014. **23**(6): p. 2067-2074.

77. Su, X., et al., *Effects of heat treatment on microstructure and electrochemical performance of cold sprayed Zn-Ni coating.* Jinshu Rechuli/Heat Treatment of Metals, 2015. **40**(3): p. 96-99.

78. Sundaramali, G., P.A. Jeeva, and S. Karthikeyan, *Surface properties of pressure die cast(PDC) AL 7075 using laser texturing and electrodeposition zinc-nickel alloy coatings.* International Journal of ChemTech Research, 2016. **9**(4): p. 707-711.

79. Yu, Y.D., et al., *Magnetic electrodeposition of ZnNi alloy films.* Materials Research Innovations, 2014. **18**(4): p. 314-319.

80. Yu, Y.D., et al., *Preparation of ZnNi alloy films by electrodeposition.* Surface Engineering, 2013. **29**(10): p. 743-748.

81. Zheng, K., et al., *Preparing γ-crystalline controlling thickness's Zn-Ni coating and studying corrosion performance*, in *Advanced Materials Research*. 2014. p. 337-342.

82. Abd El-Lateef, H.M., A.R. El-Sayed, and H.S. Mohran, *Role of Ni content in improvement of corrosion resistance of Zn-Ni alloy in 3.5% NaCl solution. Part I: Polarization and impedance studies.* Transactions of Nonferrous Metals Society of China (English Edition), 2015. **25**(8): p. 2807-2816.

83. Álló, Š., et al., *Detection of corrosion resistance of components in cyclic salt spray.* Acta Universitatis Agriculturae et Silviculturae Mendelianae Brunensis, 2015. **63**(1): p. 9-13.

84. Astuty, A., et al., *Evaluation of corrosion performance of zinc-plated underhood automotive fasteners using salt spray test*. 2015. p. 560-564.

85. Diafi, M., et al., *Effect of Ni doping on some properties of electrodeposited zinc alloy coatings.* Acta Metallurgica Slovaca, 2015. **21**(3): p. 226-235.

86. El-Lateef, H.M.A., A.R. El-Sayed, and H.S. Mohran, *Role of nickel alloying on anodic dissolution behavior of zinc in 3.5% NaCl solution. Part II: Potentiodynamic, potentiostatic and galvanostatic studies.* Transactions of Nonferrous Metals Society of China (English Edition), 2015. **25**(9): p. 3152-3164.

87. He-Zhong, P., et al., *Research to the corrosion resistance of the alkaline zinc-nickel alloy plates*. 2013. p. 1756-1761.

88. Kwon, M., et al., *Characterization of the influence of Ni content on the corrosion resistance of electrodeposited Zn-Ni alloy coatings.* Surface and Coatings Technology, 2016. **288**: p. 163-170.

89. Møller, P.P. *Evaluation of atmospheric corrosion on electroplated zinc and zinc nickel coatings by Electrical Resistance (ER) Monitoring*. 2013.

90. Rao, V.R. and A.C. Hegde, *Role of cadmium on corrosion resistance of Zn-Ni alloy coatings.* Surface Engineering and Applied Electrochemistry, 2014. **50**(1): p. 63-71.

91. Sheu, H.H., et al., *Investigation on the corrosion resistance of trivalent chromium conversion passivate on electroplated Zn–Ni alloy.* Surface and Coatings Technology, 2016. **305**: p. 241-248.

92. Sriraman, K.R., et al., *Characterization of corrosion resistance of electrodeposited Zn-Ni Zn and Cd coatings.* Electrochimica Acta, 2013. **105**: p. 314-323.

93. Tanaka, H., et al., *Simulating study of atmospheric corrosion of Zn-Ni alloy coating on steels in marine zone: Structure and properties of artificially synthesized Ni(II)-doped zinc hydroxychloride rust particles.* Advanced Powder Technology, 2015. **26**(2): p. 612-617.

94. Tozar, A. and I.H. Karahan, *Structural and corrosion protection properties of electrochemically deposited nano-sized Zn-Ni alloy coatings.* Applied Surface Science, 2014. **318**: p. 15-23.

95. Zhang, X., et al., *Structure and corrosion resistance of Zn-Ni alloy coatings electrodeposited from alkaline binary complexes bath.* Cailiao Kexue yu Gongyi/Material Science and Technology, 2015. **23**(1): p. 83-88.

96. Abou-Krisha, M., et al., *Electrochemical behavior and corrosion resistance of electrodeposited nano-particles Zn-Co-Fe alloy.* Anti-Corrosion Methods and Materials, 2016. **63**(1): p. 29-35.

97. Abou-Krisha, M.M., et al., *Deposition Potential Influence on the Electrodeposition of Zn–Ni–Mn Alloy.* Transactions of the Indian Institute of Metals, 2016: p. 1-10.

98. Abou-Krisha, M.M., et al., *Influence of pH on the composition, morphology and corrosion resistance of Zn-Ni-Mn alloy films synthesized by electrodeposition.* International Journal of Electrochemical Science, 2015. **10**(4): p. 2972-2987.

99. Assaf, F.H., et al., *The effect manganese concentration on the corrosion resistance and physical properties of Zn-Ni-Mn alloy films produced by electrodeposition.* International Journal of Electrochemical Science, 2015. **10**(8): p. 6273-6287.

100. Assaf, F.H., et al., *Electrodeposition and characterization of Zn-Ni-Mn alloy from sulfate bath: Influence of current density.* International Journal of Electrochemical Science, 2015. **10**(7): p. 5465-5478.

101. Bachvarov, V.D., et al., *Corrosion properties of Zn-Ni-P alloys in neutral model medium.* Central European Journal of Chemistry, 2014. **12**(11): p. 1183-1193.

102. Choudhary, R.K., P. Mishra, and V. Kain, *Pulse DC electrodeposition of Zn–Ni–Co coatings.* Surface Engineering, 2015: p. 1-4.

103. Constantin, I. and P. Moldovan, *Microstructure and corrosion resistance of electrodeposited Zn-Ni-P thin films.* UPB Scientific Bulletin, Series B: Chemistry and Materials Science, 2016. **78**(1): p. 185-192.

104. Fashu, S. and R. Khan, *Electrodeposition of ternary Zn–Ni–Sn alloys from an ionic liquid based on choline chloride and their characterisation.* Transactions of the Institute of Metal Finishing, 2016. **94**(5): p. 237-245.

105. Hammami, O., et al., *Effect of phosphorus doping on some properties of electroplated Zn-Ni alloy coatings.* Surface and Coatings Technology, 2013. **219**: p. 119-125.

106. Kamimoto, Y., et al., *Preparation of Zn-Ni-P alloys with high Zn content using electrochemical processes.* Science of Advanced Materials, 2014. **6**(10): p. 2269-2274.

107. Sakai, T., Y. Kamimoto, and R. Ichino, *Preparation of electrodeposited Zn-Ni-B alloy coatings.* Japanese Journal of Applied Physics, 2016. **55**(1).

108. Soare, V., et al., *Synthesis and performance of Zn-Ni-P thin films.* Chinese Physics B, 2015. **24**(3).

109. Tomić, M.V., et al., *Ternary Zn-Ni-Co alloy: Anomalous codeposition and corrosion stability.* Journal of the Serbian Chemical Society, 2014. **79**(11): p. 1-21.

110. Tomić, M.V., et al., *Ternary Zn-Ni-Co alloy: Anomalous codeposition and corrosion stability.* Journal of the Serbian Chemical Society, 2015. **80**(1): p. 73-86.

111. Winiarski, J., A. Laszczyńska, and B. Szczygieł, *An electrochemical study on the influence of sodium molybdate on electrodeposition process and phase composition of ternary Zn-Ni-Mo alloy coatings.* Transactions of the Institute of Metal Finishing, 2015. **93**(5): p. 267-274.

112. Wu, C.J., et al., *Microstructure and corrosion resistance of hot-dipped Zn-Ni-Ti coatings.* Cailiao Rechuli Xuebao/Transactions of Materials and Heat Treatment, 2015. **36**(9): p. 156-160.

113. Wykpis, K., *Influence of Co2+ ions concentration in a galvanic bath on properties of electrolytic Zn-Ni-Co coatings.* Surface and Interface Analysis, 2014. **46**(10-11): p. 746-749.

114. Zhang, L., Y. Zhang, and Z. Ma, *Effects of aging on microstructure and shear strength of Cu-Zn-Ni alloy.* Jinshu Rechuli/Heat Treatment of Metals, 2015. **40**(6): p. 132-134.

115. Ataie, S.A. and A. Zakeri, *Improving tribological properties of (Zn-Ni)/nano Al2O3 composite coatings produced by ultrasonic assisted pulse plating.* Journal of Alloys and Compounds, 2016. **674**: p. 315-322.

116. Blejan, D. and L.M. Muresan, *Corrosion behavior of Zn-Ni-Al2O3 nanocomposite coatings obtained by electrodeposition from alkaline electrolytes.* Materials and Corrosion, 2013. **64**(5): p. 433-438.

117. Diafi, M., et al., *Study of Zn-Ni alloy coatingsmodified by nano-AL2O3particles incorporation.* Acta Metallurgica Slovaca, 2016. **22**(3): p. 171-180.

118. Fayomi, O.S.I., M. Abdulwahab, and A.P.I. Popoola, *Properties evaluation of ternary surfactant-induced Zn-Ni-Al2O3 films on mild steel by electrolytic chemical deposition.* Journal of Ovonic Research, 2013. **9**(5): p. 123-132.

119. Ghaziof, S. and W. Gao, *The effect of pulse electroplating on Zn-Ni alloy and Zn-Ni-Al2O3 composite coatings.* Journal of Alloys and Compounds, 2014. **622**: p. 918-924.

120. Ghaziof, S. and W. Gao, *Zn-Ni-Al2O3 nano-composite coatings prepared by sol-enhanced electroplating.* Applied Surface Science, 2015. **351**: p. 869-879.

121. Ghaziof, S., P.A. Kilmartin, and W. Gao, *Electrochemical studies of sol-enhanced Zn-Ni-Al<inf>2</inf>O<inf>3</inf> composite and Zn-Ni alloy coatings.* Journal of Electroanalytical Chemistry, 2015. **755**: p. 63-70.

122. Hammami, O., et al., *Zn-Ni/nano-TiO2 composite electrodeposits: Surface modifications and protective properties.* Journal of Applied Electrochemistry, 2014. **44**(1): p. 115-121.

123. Hino, M., et al., *Influence of SiO2 nanoparticle codeposition on homogeneity of zinc-nickel alloy plating from an acid sulphate bath*. 2014. p. 1420-1425.

124. Hino, M., et al., *Effects of silica nanoparticle co-deposition on macrothrowing power of zinc-nickel alloy plating from an acid sulfate bath.* Nippon Kinzoku Gakkaishi/Journal of the Japan Institute of Metals, 2014. **78**(1): p. 31-36.

125. Hino, M., et al., *Effects of silica nanoparticle Co-deposition on macrothrowing power of zinc-nickel alloy plating from an acid sulfate bath.* Materials Transactions, 2014. **56**(1): p. 85-90.

126. Liu, J.H., et al., *Fabrication of Zn-Ni/Ni-P compositionally modulated multilayer coatings.* Materials and Corrosion, 2013. **64**(4): p. 335-340.

127. Momeni, M.M., et al., *Preparation, characterisation, hardness and antibacterial properties of Zn–Ni–TiO2 nanocomposites coatings.* Surface Engineering, 2016. **32**(7): p. 490-494.

128. Nagrabia, A., et al., *Galvanic formation of Zn-Ni/Zn-Co type multilayer alloy coatings on steel substrate*. 2015. p. 147-150.

129. Ullal, Y. and A. Chitharanjan Hegde, *Corrosion protection of electrodeposited multilayer nanocomposite Zn-Ni-SiO2 coatings.* Surface Engineering and Applied Electrochemistry, 2013. **49**(2): p. 161-167.

130. Ullal, Y. and A.C. Hegde, *Multilayer Zn-Ni-Al2O3 coatings for corrosion protection.* International Journal of Materials Engineering Innovation, 2014. **5**(3): p. 247-260.

131. Wykpis, K., et al., *Influence of thermal treatment on the corrosion resistance of electrolytic Zn-Ni+Ni composite coatings.* Advanced Composite Materials, 2015. **24**(5): p. 431-438.

132. Lee, L., et al., *Fretting wear behavior of Zn-Ni alloy coatings.* Wear, 2015. **330-331**: p. 112-121.

133. Williams, J., *Engineering Tribology*. 1994: Cambridge University Press.

134. Stachowiak, G.W. and A.W. Batchelor, *Engineering Tribology*. 2013, [S.l.]: Butterworth-Heinemann.

135. Holmberg, K. and A. Matthews, *Coatings tribology : properties, mechanisms, techniques and applications in surface engineering*. 2009, Amsterdam; Boston: Elsevier Science.

136. Archard, J.F. and W. Hirst, *The Wear of Metals under Unlubricated Conditions.* Proceedings of the Royal Society of London. Series A, Mathematical and Physical Sciences, 1956. **236**(1206): p. 397-410.

137. Siniawski, M.T., S.J. Harris, and Q. Wang, *A universal wear law for abrasion.* Wear, 2007. **262**(7-8): p. 883-888.

138. Singer, I.L., et al., *Third body processes and friction of solid lubricants studied by in situ optical and raman tribometry*, in *Tribology Series*, M.P.G.D. D. Dowson and A.A. Lubrecht, Editors. 2002, Elsevier. p. 327-336.

139. Ko, C.H., et al., *A Comparison of Cadmium Electroplate and Some Alternatives.* Plating and Surface Finishing, 1991. **78**(10): p. 46-50.

140. Godet, M., *The third-body approach: A mechanical view of wear.* Wear, 1984. **100**(1-3): p. 437-452.

141. Berthier, Y., L. Vincent, and M. Godet, *Fretting fatigue and fretting wear.* Tribology International, 1989. **22**(4): p. 235-242.

142. Zum Gahr, K.-H., *Microstructure and wear of materials*. 1987, Amsterdam; New York: Elsevier.

143. Bowden, F.P. and D. Tabor, *The friction and lubrication of solids*. 2001, Oxford; New York: Clarendon Press ; Oxford University Press.

144. Berthier, Y., *Experimental evidence for friction and wear modelling.* Wear, 1990. **139**(1): p. 77-92.

145. Denape, J., Y. Berthier, and L. Vincent, *Wear Particle Life in a Sliding Contact Under Dry Conditions : Third Body Approach*, in *Fundamentals of Tribology and Bridging the Gap Between the Macro- and Micro/Nanoscales*, B. Bhushan, Editor. 2001, Springer Netherlands. p. 393-411.

146. Berthier, Y., L. Vincent, and M. Godet, *Velocity accommodation in fretting.* Wear, 1988. **125**(1-2): p. 25-38.

147. Bhushan, B., *Introduction to tribology*. 2013, New York: John Wiley & Sons Inc.

148. Kapsa, P., S. Fouvry, and L. Vincent, *Basic principles of fretting.* Wear–Mechanisms, Materials and Practice, 2005: p. 317-338.

149. Vingsbo, O. and S. Söderberg, *On fretting maps.* Wear, 1988. **126**(2): p. 131-147.

150. Fouvry, S., P. Kapsa, and L. Vincent, *Analysis of sliding behaviour for fretting loadings: determination of transition criteria*. Wear, 1995. **185**(1–2): p. 35-46.

151. Panagopoulos, C.N., K.G. Georgarakis, and P.E. Agathocleous, *Sliding wear behaviour of zinc-nickel alloy electrodeposits.* Tribology International, 2003. **36**(8): p. 619-623.

152. Bowden, F.P. and D. Tabor, *The friction and lubrication of solids*. 1954, Oxford: Clarendon Press.

153. Baker, C.C., et al., *Preparation of chameleon coatings for space and ambient environments.* Thin Solid Films, 2007. **515**(17): p. 6737-6743.

154. Zabinski, J.S., et al., *Lubricious zinc oxide films: Synthesis, characterization and tribological behaviour*. Journal of Materials Science, 1997. **32**(20): p. 5313-5319.

155. Prasad, S.V., S.D. Walck, and J.S. Zabinski, *Microstructural evolution in lubricious ZnO films grown by pulsed laser deposition.* Thin Solid Films, 2000. **360**(1-2): p. 107-117.

156. Prasad, S.V. and J.S. Zabinski, *Tribological behavior of nanocrystalline zinc oxide films.* Wear, 1997. **203–204**(0): p. 498-506.

157. Ruggeri, O., et al., *Dry lubrication with soft metals: The tribological behaviour of a thin film of cadmium rubbing on carbon steel.* Wear, 1980. **59**(2): p. 433-446.

158. Cooper, R., *Ubi 1 User Manual*. 2007, Hysitron Inc.: Minneapolis USA.

159. Oliver, W.C. and G.M. Pharr, *An improved technique for determining hardness and elastic modulus using load and displacement sensing indentation experiments.* Journal of Materials Research, 1992. **7**(06): p. 1564-1583.

160. Sasaki, T. and Y. Hirose, *Residual stress distribution in electroplated ZnNi alloy layer determined by X-ray diffraction.* Thin Solid Films, 1994. **253**(1-2): p. 356-361.

161. Automations Creations Inc. *MatWeb: The online materials information resource*. 1997; Available from: http://www.matweb.com/search/DataSheet.aspx?MatGUID=09c2c08077404267873186a35107a0b5.

162. Ireman, T., *Three-dimensional stress analysis of bolted single-lap composite joints.* Composite Structures, 1998. **43**(3): p. 195-216.

163. McCarthy, M.A., et al., *Bolt-hole clearance effects and strength criteria in single-bolt, single-lap, composite bolted joints.* Composites Science and Technology, 2002. **62**(10–11): p. 1415-1431.

164. Wagle, S. and H. Kato, *Ultrasonic detection of fretting fatigue damage at bolt joints of aluminum alloy plates.* International Journal of Fatigue, 2009. **31**(8–9): p. 1378-1385.

165. Strauss, H.W., et al., *In situ tribology of nanocomposite Ti–Si–C–H coatings prepared by PE-CVD.* Wear, 2011. **272**(1): p. 133-148.

166. Chromik, R., H. Strauss, and T. Scharf, *Materials phenomena revealed by in situ tribometry.* JOM, 2012. **64**(1): p. 35-43.

167. P. Behera, et al., *Effect of relative humidity on third bodies evolution of LHE Cd coating*. 2016, McGill.

168. Cadmium REACH Consortium. Cadmium REACH [cited 2013; Available from: http://www.reach-cadmium.eu/.

169. Stachowiak, G.W., *Wear: Materials, Mechanisms and Practice*. 2006: John Wiley & Sons.

170. Ramalho, A., L.M. Correia, and J.D. Costa, *Fretting fatigue of zinc coated low carbon steel EN H320 M.* Tribology International, 2000. **33**(11): p. 761-768.

171. Gao, H., H. Gu, and H. Zhou, *Sliding wear and fretting fatigue resistance of amorphous Ni-P coatings.* Wear, 1991. **142**(2): p. 291-301.

172. Thiery, L., L. Moui, and J.J. Duprat, *Performa 280.5*. 2004, Coventya: UK.

173. Coventya. *Protection : technical sheets and documentation*. 2013 [cited 2014; Available from: http://www.coventya.com/technical-information/protection/technical-sheets-and-documentation/.

174. Lin, C.S., H.B. Lee, and S.H. Hsieh, *Microstructure and formability of ZnNi alloy electrodeposited sheet steel.* Metallurgical and Materials Transactions A: Physical Metallurgy and Materials Science, 2000. **31**(2): p. 475-485.

175. Sasaki, T. and Y. Hirose, *Residual stress distribution in electroplated Zn ・ Ni alloy layer determined by X-ray diffraction.* Thin solid films, 1994. **253**(1): p. 356-361.

176. ASTM International, *Standard Test Method for Mechanical Hydrogen Embrittlement Evaluation of Plating/Coating Processes and Service Environments*, in *F519-10*. 2011, ASTM International: Pennsylvania, USA.

177. Fouvry, S., P. Kapsa, and L. Vincent, *Quantification of fretting damage.* Wear, 1996. **200**(1–2): p. 186-205.

178. Vincent, L., et al., *Mechanics and materials in fretting.* Wear, 1992. **153**(1): p. 135-148.

179. Kurita, H. and H. Yamagata, *Effect of hardness on fretting wear characteristics of AC9B and AC8A aluminum alloys.* Nippon Kinzoku Gakkaishi/Journal of the Japan Institute of Metals, 1998. **62**(1): p. 50-55.

180. Ramesh, R. and R. Gnanamoorthy, *Effect of hardness on fretting wear behaviour of structural steel, En 24, against bearing steel, En 31.* Materials and Design, 2007. **28**(5): p. 1447-1452.

181. Zhang, X., H. Liu, and X.s. Wang, *On the effects of hardness on the fretting wear behavior and on the wear debris composition of carbon steel.* Mocaxue Xuebao/Tribology, 1995. **15**(4): p. 300-305.

182. Vincent, L., et al., *Mechanics and materials in fretting.* Wear, 1992. **153**(1): p. 135-148.

183. Kapsa, P., S. Fouvry, and L. Vincent, *Basic Principles of Fretting*, in *Wear: materials, mechanisms and practice*, G.W. Stachowiak, Editor. 2006, John Wiley & Sons. p. 317-338.

184. Carton, J.F., A.B. Vannes, and L. Vincent, *Basis of a coating choice methodology in fretting.* Wear, 1995. **185**(1): p. 47-57.

185. Carton, J.F., et al., *An investigation of the fretting behaviour of low friction coatings on steel.* Tribology International, 1996. **29**(6): p. 445-455.

186. Lee, L., et al., *Fretting wear behavior of Zn–Ni alloy coatings.* Wear, 2015. **330–331**(0): p. 112-121.

187. Tran, L.M., P.M. Matthias, and J.H. Jones, *Low Hydrogen Embrittlement Zinc/nickel Plating for High Strength Steels*. 2011: United States.

188. Department of Defence Standard Practice, *MIL-STD-870C, U.S. Military Standard (USAF) on Cadmium plating, Low embrittlement, Electrodeposition*. 27 April 2009.

189. Automations Creations Inc. *Cadmium, Cd*. 1997; Available from: http://www.matweb.com/search/DataSheet.aspx?MatGUID=ca862f5c59594be3b9a2d250460d2dba.

190. Behera, P., et al., *Combining in situ tribometry and triboscopy to understand third body behavior of a Cd coating*. 2016, McGill University.

191. Ashby, M.F. and D.R.H. Jones. *Engineering materials 1 : an introduction to properties, applications, and design*. 2012; Available from: http://www.dawsonera.com/depp/reader/protected/external/AbstractView/S9780080966663.

192. Bruet, H., et al., *Structure of zinc-nickel alloy electrodeposits.* Journal of Materials Science, 1999. **34**(4): p. 881-886.

193. Bowden, F. and D. Tabor, *Friction, lubrication and wear: a survey of work during the last decade.* British Journal of Applied Physics, 1966. **17**(12): p. 1521.

194. Rigney, D. and J. Hirth, *Plastic deformation and sliding friction of metals.* Wear, 1979. **53**(2): p. 345-370.

195. He, B.B., *Two-dimensional x-ray diffraction*. 2009, Hoboken, N.J.: Wiley.

196. Bull, S.J., *Failure mode maps in the thin film scratch adhesion test.* Tribology International, 1997. **30**(7): p. 491-498.

197. Bull, S.J. and E.G. Berasetegui, *An overview of the potential of quantitative coating adhesion measurement by scratch testing.* Tribology International, 2006. **39**(2): p. 99-114.

198. Sriraman, K.R., et al., *Effect of crystallographic orientation on the tribological behavior of electrodeposited Zn coatings.* RSC Advances, 2016. **6**(21): p. 17360-17372.

199. Damen, T.C., S.P.S. Porto, and B. Tell, *Raman effect in zinc oxide.* Physical Review, 1966. **142**(2): p. 570-574.

200. Oh, S.J., D.C. Cook, and H.E. Townsend, *Characterization of Iron Oxides Commonly Formed as Corrosion Products on Steel.* Hyperfine Interactions. **112**(1): p. 59-66.

201. Shim, S.H. and T.S. Duffy, *Raman spectroscopy of Fe2O3 to 62 GPa.* American Mineralogist, 2002. **87**(2-3): p. 318-326.

202. Lancaster, J.K., *A review of the influence of environmental humidity and water on friction, lubrication and wear.* Tribology International, 1990. **23**(6): p. 371-389.

203. Zhang, J. and J. Zheng, *Surfactant inducing phase change of ZnO nanorods to low friction.* Tribology Letters, 2013. **49**(1): p. 77-83.

204. Ghaziof, S. and W. Gao, *Electrodeposition of single gamma phased Zn–Ni alloy coatings from additive-free acidic bath.* Applied Surface Science, 2014. **311**(0): p. 635-642.

205. Godet, M., *Third-bodies in tribology*. Wear, 1990. **136**(1): p. 29-45.

206. Berthier, Y., *Maurice Godet's Third Body*, in *Tribology Series*, D. Dowson, et al., Editors. 1996, Elsevier. p. 21-30.

207. Klaffke, D., *On the repeatability of friction and wear results and on the influence of humidity in oscillating sliding tests of steel-steel pairings.* Wear, 1995. **189**(1–2): p. 117-121.

208. Huq, M.Z. and J.P. Celis, *Fretting wear of multilayered (Ti,Al)N/TiN coatings in air of different relative humidity.* Wear, 1999. **225–229, Part 1**(0): p. 53-64.

209. Dvorak, S.D., K.J. Wahl, and I.L. Singer, *In situ analysis of third body contributions to sliding friction of a Pb-Mo-S coating in dry and humid air.* Tribology Letters, 2007. **28**(3): p. 263-274.

210. Antler, M., *Processes of metal transfer and wear.* Wear, 1964. **7**(2): p. 181-203.

211. Porter, F.C., *Resistance to Atmospheric Corrosion*, in *Corrosion resistance of zinc and zinc alloys*. 1994, CRC Press.

212. Vernon, W.H.J., *A laboratory study of the atmospheric corrosion of metals. Part II.-Iron: the primary oxide film. Part III.-The secondary product or rust (influence of sulphur dioxide, carbon dioxide, and suspended particles on the rusting of iron).* Transactions of the Faraday Society, 1935. **31**(0): p. 1668-1700.

213. Zhang, X.G., *Atmospheric Corrosion*, in *Corrosion and electrochemistry of zinc*. 1996, Springer US. p. 241-281.

214. Suzumura, K. and S.I. Nakamura, *Environmental factors affecting corrosion of galvanized steel wires.* Journal of Materials in Civil Engineering, 2004. **16**(1): p. 1-7.

Appendix A

Matlab code for calculation of energy ratio, friction and fretting log

```
%% Import data from text file.

%% Initialize variables.
[filename,pathname]=uigetfile('*.txt','Select the text
file','C:\Users\Lisa Lee\Documents\PhD
Research\Experiments\Fretting Wear\Impact II\');
delimiter = '\t';
startRow = 25;

%% Read columns of data as text:
% For more information, see the TEXTSCAN documentation.
formatSpec = '%q%q%q%q%q%q%q%[^\n\r]';

%% Open the text file.
fileID = fopen(strcat(pathname,filename),'r');

%% Read columns of data according to the format.
% This call is based on the structure of the file used to
generate this
% code. If an error occurs for a different file, try
regenerating the code
% from the Import Tool.
dataArray = textscan(fileID, formatSpec, 'Delimiter', delimiter,
'HeaderLines' ,startRow-1, 'ReturnOnError', false, 'EndOfLine',
'\r\n');
```

```
%% Close the text file.
fclose(fileID);

%% Convert the contents of columns containing numeric text to
numbers.
% Replace non-numeric text with NaN.
raw = repmat({''},length(dataArray{1}),length(dataArray)-1);
for col=1:length(dataArray)-1
    raw(1:length(dataArray{col}),col) = dataArray{col};
end
numericData = NaN(size(dataArray{1},1),size(dataArray,2));

for col=[1,2,3,4,5,6,7]
    % Converts text in the input cell array to numbers. Replaced
non-numeric
    % text with NaN.
    rawData = dataArray{col};
    for row=1:size(rawData, 1);
        % Create a regular expression to detect and remove non-
numeric prefixes and
        % suffixes.
        regexstr =
'(?<prefix>.*?)(?<numbers>([-]*(\d+[\.]*)+[\,]{0,1}\d*[eEdD]{0,1
}[-+]*\d*[i]{0,1})|([-]*(\d+[\.]*)*[\,]{1,1}\d+[eEdD]{0,1}[-
+]*\d*[i]{0,1}))(?<suffix>.*)';
        try
            result = regexp(rawData{row}, regexstr, 'names');
            numbers = result.numbers;

            % Detected commas in non-thousand locations.
            invalidThousandsSeparator = false;
            if any(numbers=='.');
                thousandsRegExp = '^\d+?(\.\d{3})*\,{0,1}\d*$';
                if isempty(regexp(numbers, thousandsRegExp,
'once'));
                    numbers = NaN;
                    invalidThousandsSeparator = true;
                end
            end
            % Convert numeric text to numbers.
            if ~invalidThousandsSeparator;
                numbers = strrep(numbers, '.', '');
                numbers = strrep(numbers, ',', '.');
                numbers = textscan(numbers, '%f');
                numericData(row, col) = numbers{1};
                raw{row, col} = numbers{1};
            end
```

```
        catch me
        end
    end
end


%% Replace non-numeric cells with NaN
R = cellfun(@(x) ~isnumeric(x) && ~islogical(x),raw); % Find
non-numeric cells
raw(R) = {NaN}; % Replace non-numeric cells

%% Allocate imported array to column variable names
X_value = cell2mat(raw(:, 1));
Fz = cell2mat(raw(:, 2));
Fy = cell2mat(raw(:, 3));
Fx = cell2mat(raw(:, 4));
Temp = cell2mat(raw(:, 5));
Dy = cell2mat(raw(:, 6));
Dz = cell2mat(raw(:, 7));


%% Clear temporary variables
clearvars filename delimiter startRow formatSpec fileID
dataArray ans raw col numericData rawData row regexstr result
numbers invalidThousandsSeparator thousandsRegExp me R;



%Calculate COF
Ntotal=size(Dy,1);
COF=zeros(Ntotal,1);
for i=1:Ntotal
    COF(i,1)=Fy(i,1)/Fz(i,1);
end
COF=abs(COF);

%set parameters
AcquisitionPoints=1000;
Timegap=15;
NAcquisition=Ntotal/AcquisitionPoints;
Frequency=15;
Totaltime=NAcquisition*Timegap;
Npointscycle=floor(AcquisitionPoints/Frequency)+1;

Cycles=zeros(Ntotal,1);
%Assign Cycle Numbers
for i=1:AcquisitionPoints:Ntotal
    m=(i-1)/AcquisitionPoints*Frequency*Timegap+1;
```

```
    for n=i:Npointscycle:i+AcquisitionPoints
        for j=n:n+Npointscycle-1
           Cycles(j,1)=m;
        end
        m=m+1;
    end
end
Cycles(Ntotal+1:end,:)=[];

%Fretting log and CoF matrix
Frettinglog=[Cycles,Dy,Fy];
CoFplot=[Cycles,COF];

%CoF average, note, last cycle of each acquisition dropped
i=1;
j=1;
m=1;
%COFA column 1 = Cycle number
%COFA column 2 = Average CoF
%COFA column 3 = Maximum CoF
%COFA column 4 = Minimum CoF
%Area column 1 = Total Energy (ET)
%Area column 2 = Dissipated Energy (Ed)
%Area column 3 = Energy Ratio (Ed/ET)

for i=1:AcquisitionPoints:Ntotal
    for j=i:Npointscycle:i+AcquisitionPoints-66
        COFA(m,1)=Cycles(j,1);
        COFA(m,2)=mean(COF(j:j+Npointscycle-1,1));
        COFA(m,3)=max(COF(j:j+Npointscycle-1,1));
        COFA(m,4)=min(COF(j:j+Npointscycle-1,1));
        [M1,I1]=max(Dy(j:j+Npointscycle-1,1));
        [M2,I2]=min(Dy(j:j+Npointscycle-1,1));
        D1=Fy(I1+j-1,1);
        D2=Fy(I2+j-1,1);
        Area(m,1)=abs(M1-M2)*abs(D1-D2);
        Area(m,2)=polyarea(Dy(j:j+Npointscycle-
1,1),Fy(j:j+Npointscycle-1,1));
        Area(m,3)=Area(m,2)/Area(m,1);
        m=m+1;
    end
end

clearvars i j D1 D2 I I1 I2 m n M1 M2

figure
```

```
%Plot Fretting log matrix
subplot(3,1,1)
plot3(Frettinglog(:,1),Frettinglog(:,2),Frettinglog(:,3));
xlabel('Cycles')
ylabel('Dy')
zlabel('Fy')
title('Fretting log')

%Plot CoF
subplot(3,1,2)
plot(CoFplot(:,1),CoFplot(:,2));
hold on
plot(COFA(:,1),COFA(:,2))
plot(COFA(:,1),COFA(:,3))
plot(COFA(:,1),COFA(:,4))
xlabel('Cycles')
ylabel('CoF')
title('Coefficient of Friction')

%Plot Ed/ET
subplot(3,1,3)
plot(COFA(10:end,1),Area(10:end,3))
xlabel('Cycles')
ylabel('Ed/ET')
title('Energy Ratio')


%Saving cleaned data file (commas to decimals and cycle number)
fileID = fopen(strcat(pathname,'alldata.txt'),'w');
fprintf(fileID,'%s\t%s\t%s\t%s\t%s\t%s\t%s\t%s\t%s\n','X_Value',
'Cycles','Fx','Fy','Fz','Temp','Dy','Dz','COF');
Matrix=[X_value,Cycles,Fx,Fy,Fz,Temp,Dy,Dz,COF];
for i=1:Ntotal

fprintf(fileID,'%.6f\t%i\t%.6f\t%.6f\t%.6f\t%.6f\t%.6f\t%.6f\t%.
6f\n',Matrix(i,:));
end
fclose(fileID);
clearvars Matrix

%Saving frettinglog file
fileID = fopen(strcat(pathname,'frettinglog.txt'),'w');
fprintf(fileID,'%s\t%s\t%s\n','Cycles','Dy','Fy');
for i=1:Ntotal
    fprintf(fileID,'%i\t%.6f\t%.6f\n',Frettinglog(i,:));
end
fclose(fileID);
```

```
Ncycles=size(COFA,1);

%Saving COF file
fileID = fopen(strcat(pathname,'COFfile.txt'),'w');
fprintf(fileID,'%s\t%s\t%s\t%s\n','Cycles','CoF Avg','CoF
Max','CoF Min');
for i=1:Ncycles
    fprintf(fileID,'%i\t%.6f\t%.6f\t%.6f\n',COFA(i,:));
end
fclose(fileID);

%Saving energy ratio file
fileID = fopen(strcat(pathname,'Energy_Ratio.txt'),'w');
fprintf(fileID,'%s\t%s\t%s\t%s\n','Cycles','ET','Ed','Ed/ET');
for i=1:Ncycles

fprintf(fileID,'%i\t%.6f\t%.6f\t%.6f\n',COFA(i,1),Area(i,:));
end
fclose(fileID);

clearvars -except filename foldername
```

Appendix B

Fretting logs

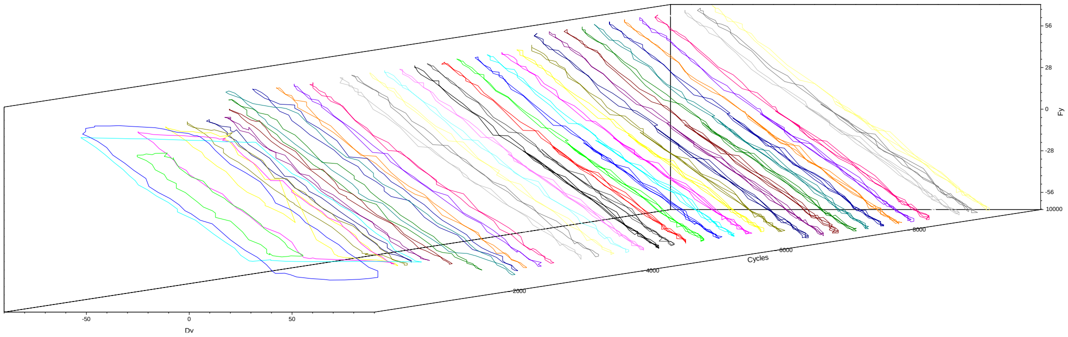

Figure B.1 Fretting log of C-ZnNi coating under 133 N at ±70 µm displacement

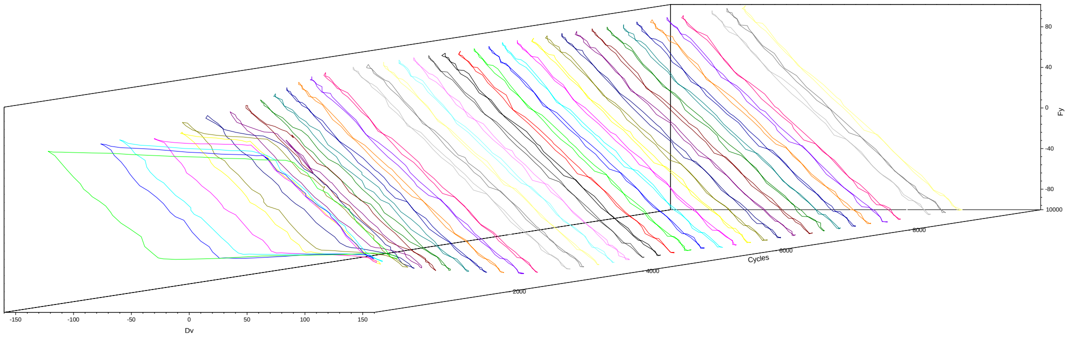

Figure B.2 Fretting log of C-ZnNi coating under 133 N at ±100 µm displacement

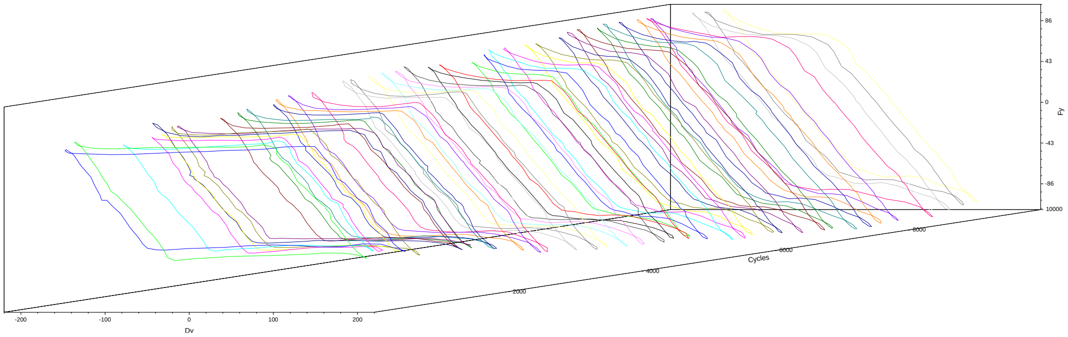

Figure B.3 Fretting log of C-ZnNi coating under 133 N at ±150 μm displacement

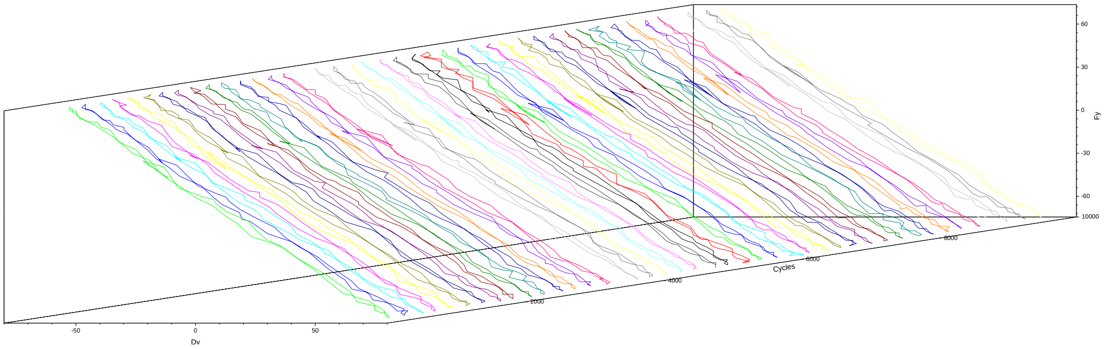

Figure B.4 Fretting log of C-ZnNi coating under 447 N at ±70 μm displacement

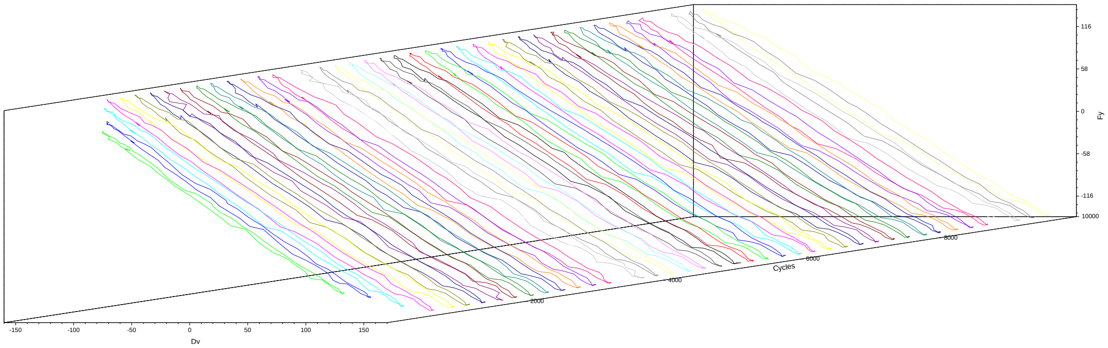

Figure B.5 Fretting log of C-ZnNi coating under 447 N at ±150 μm displacement

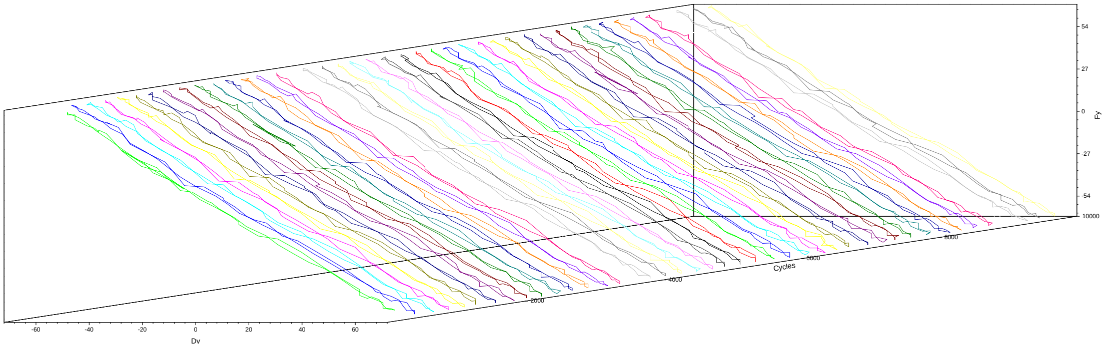

Figure B.6 Fretting log of D-ZnNi coating under 133 N at ±70 μm displacement

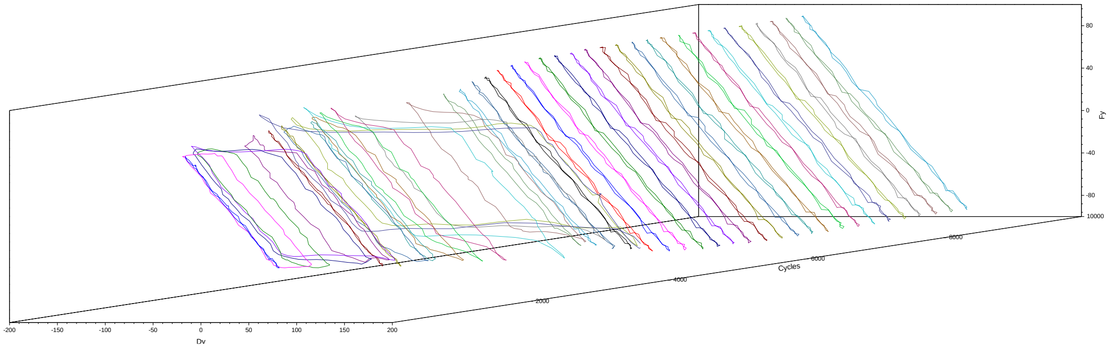

Figure B.7 Fretting log of D-ZnNi coating under 133 N at ±100 µm displacement

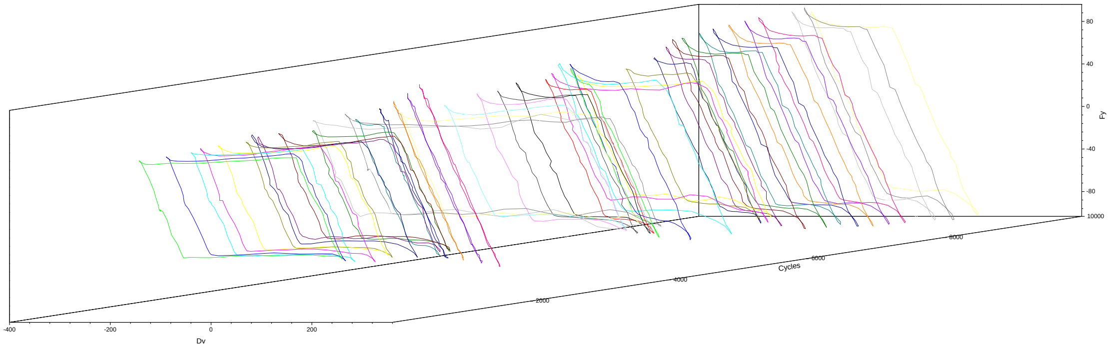

Figure B.8 Fretting log of D-ZnNi coating under 133 N at ±150 µm displacement

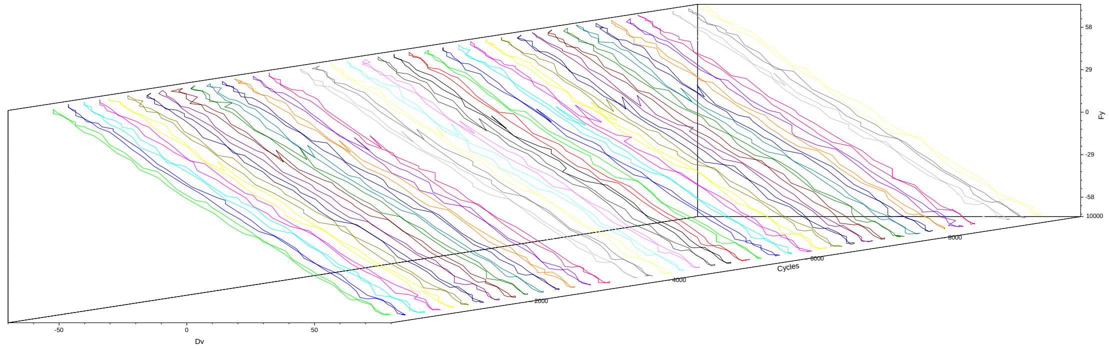

Figure B.9 Fretting log of D-ZnNi coating under 447 N at ±70 µm displacement

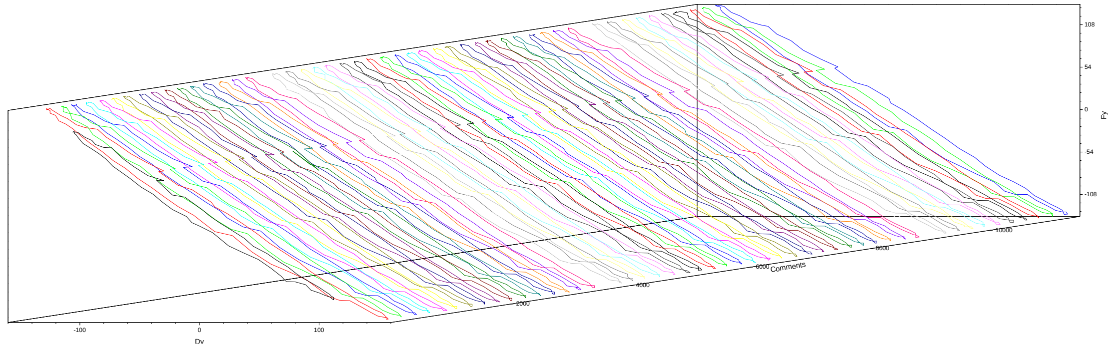

Figure B.10 Fretting log of D-ZnNi coating under 447 N at ±150 µm displacement

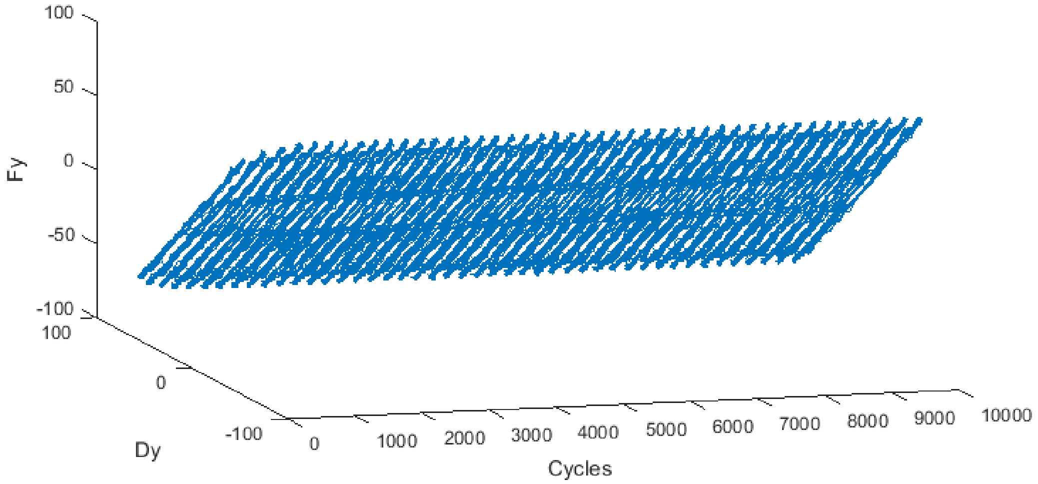

Figure B.11 Fretting log of cadmium coating under 434 N at ±70 µm displacement

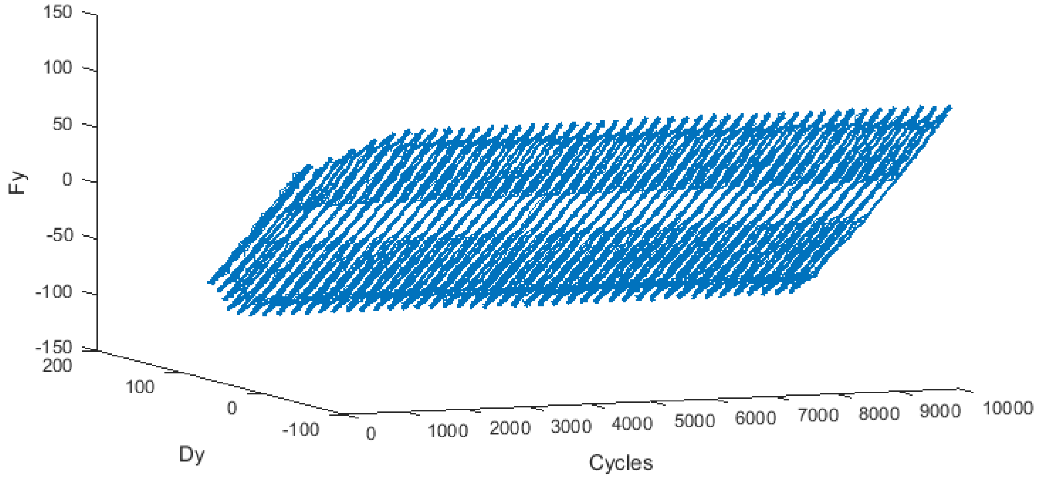

Figure B.12 Fretting log of cadmium coating under 434 N at ±100 µm displacement

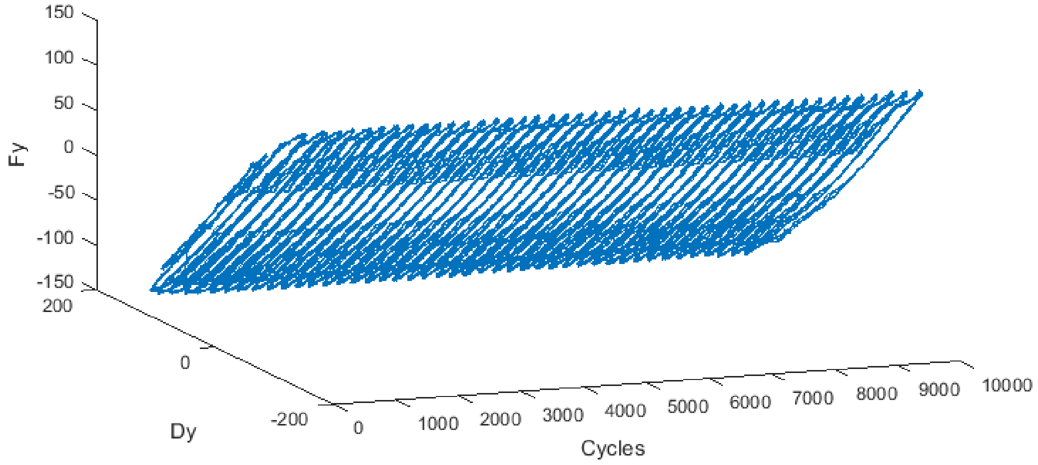

Figure B.13 Fretting log of cadmium coating under 434 N at ±150 µm displacement

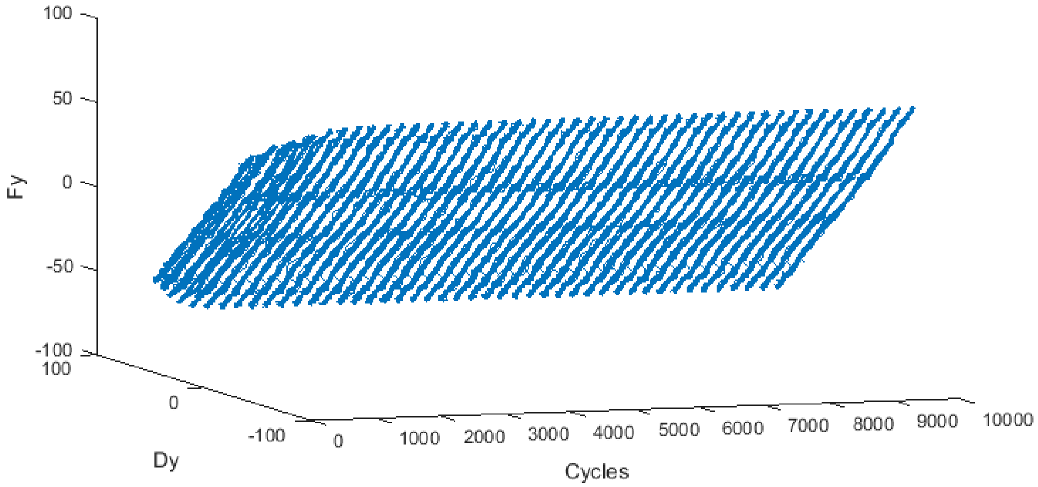

Figure B.14 Fretting log of B-ZnNi coating under 133 N at ±70 µm displacement

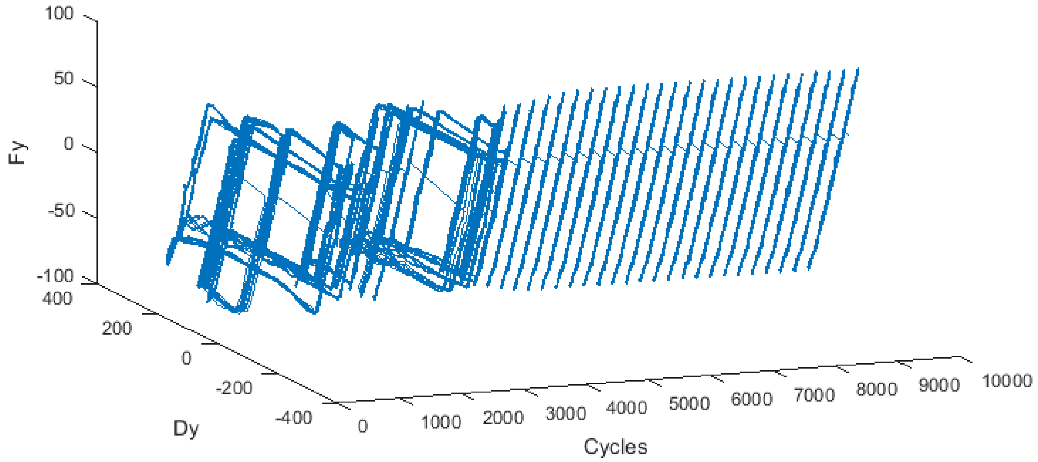

Figure B.15 Fretting log of B-ZnNi coating under 133 N at ±100 µm displacement

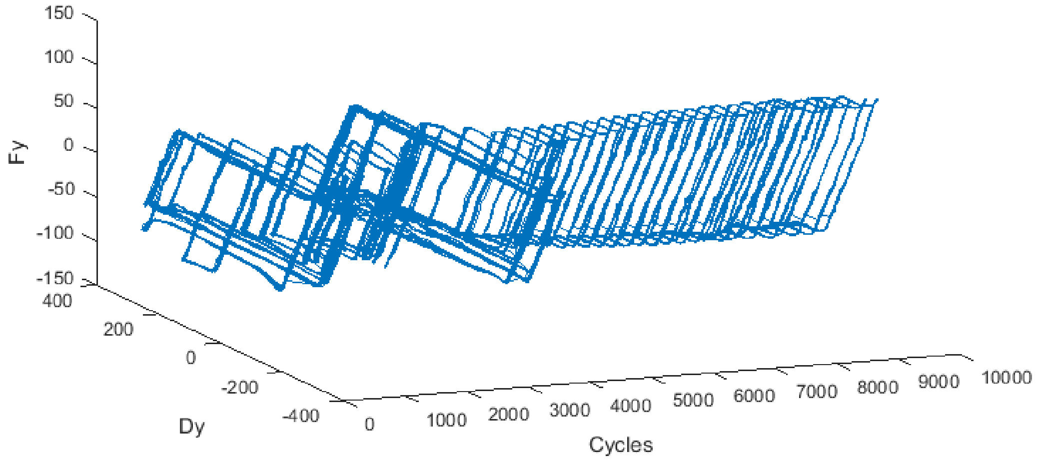

Figure B.16 Fretting log of B-ZnNi coating under 133 N at ±150 µm displacement

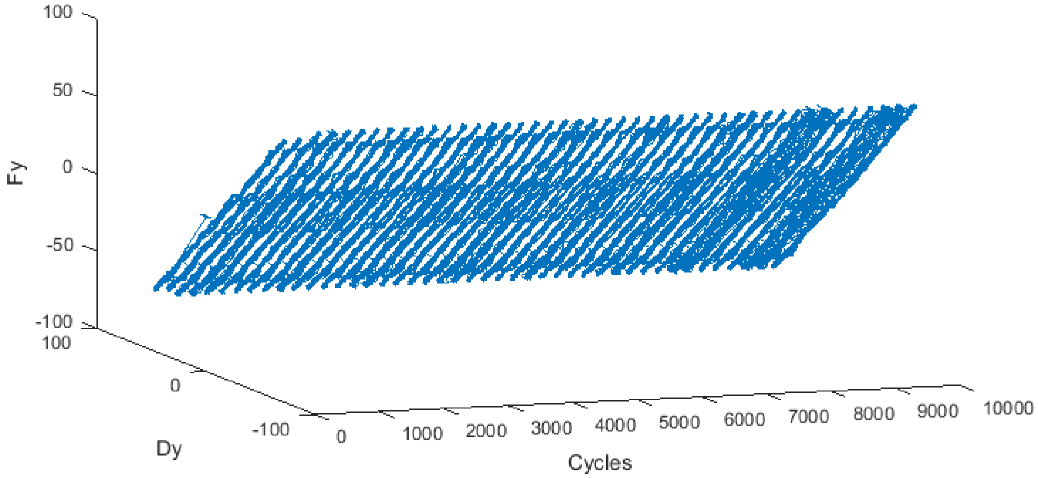

Figure B.17 Fretting log of B-ZnNi coating under 447 N at ±70 µm displacement

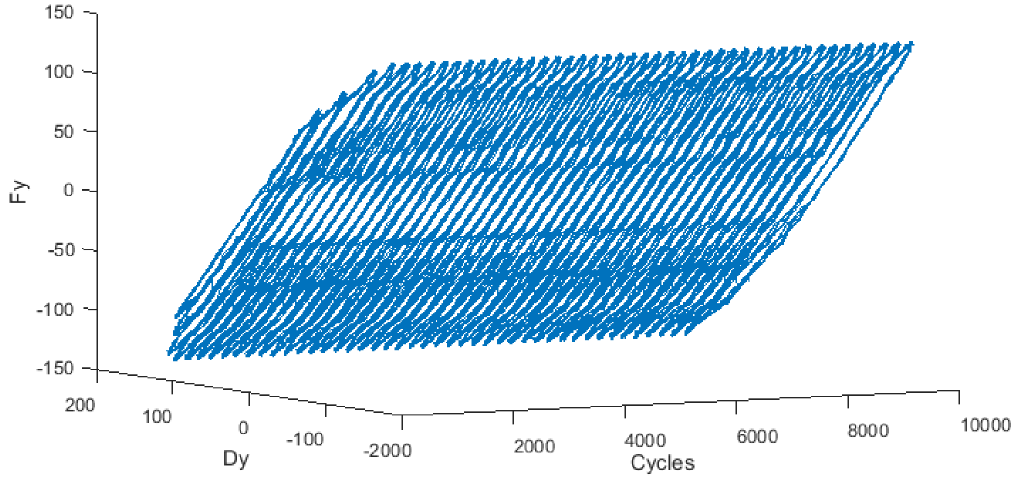

Figure B.18 Fretting log of B-ZnNi coating under 447 N at ±150 µm displacement

Appendix C

TEM SAED patterns

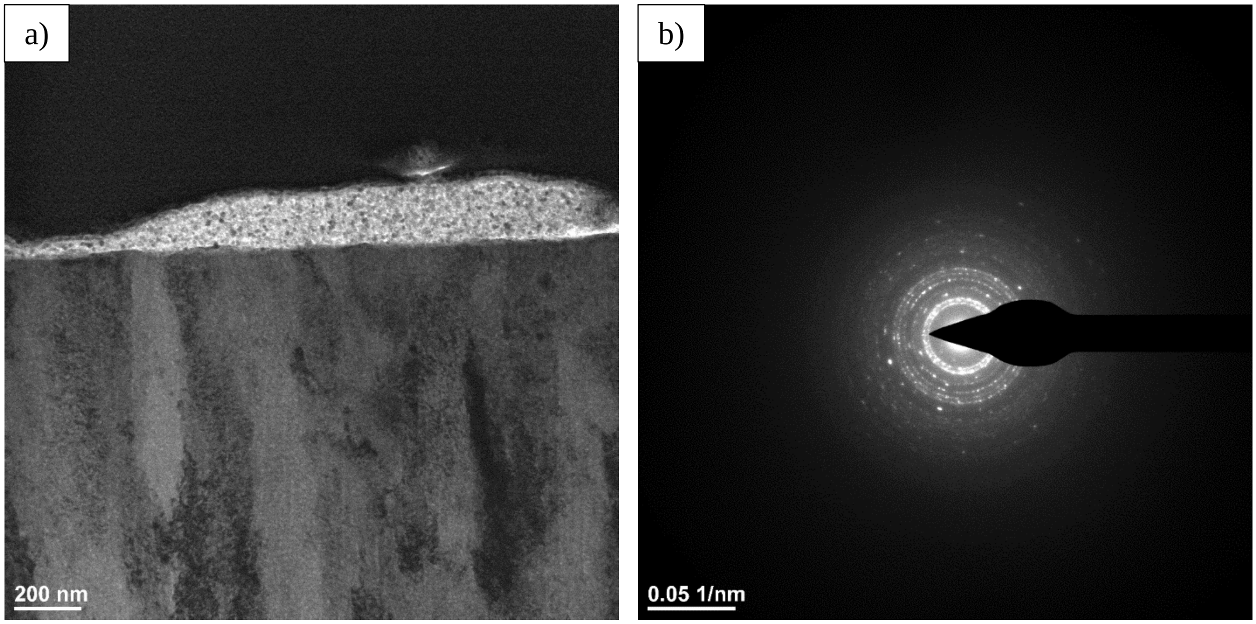

Figure C.1 TEM of wear track cross section for RH 60% condition. (a) Image of SAED location and (b) SAED pattern showing rings corresponding to nanocrystalline ZnO

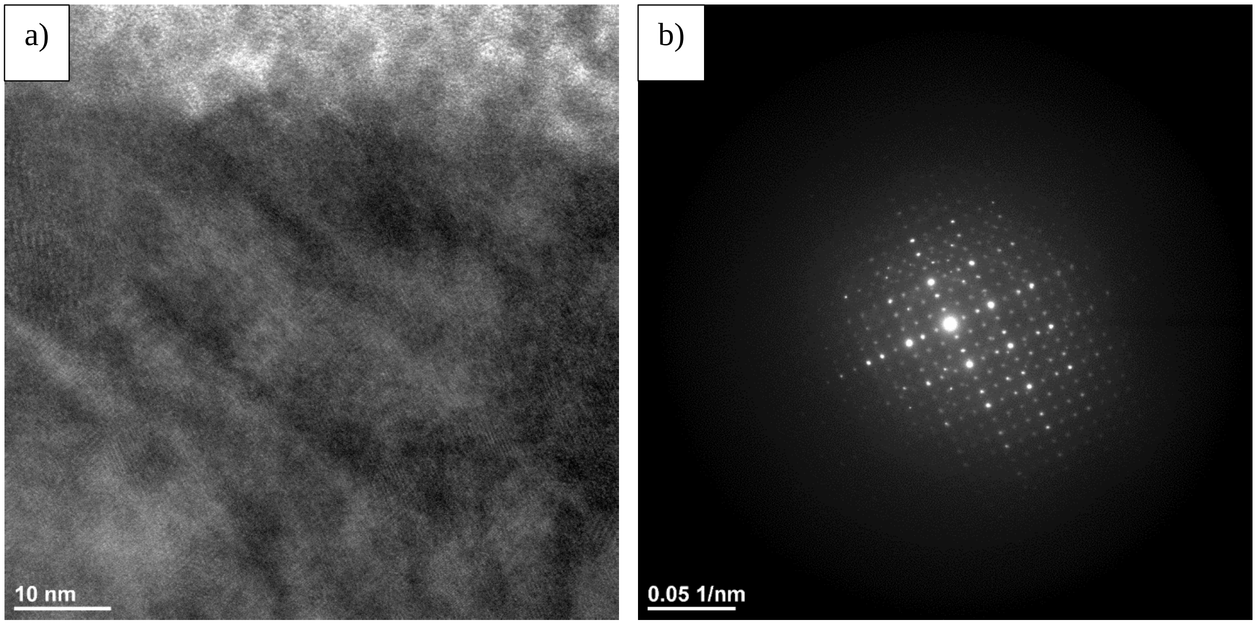

Figure C.2 TEM of wear track cross section for RH 0% condition. (a) Image of SAED location and (b) SAED pattern showing rings corresponding to nanocrystalline ZnO